INTERNATIONAL CONFERENCE

MEĐUNARODNA KONFERENCIJA

MEETING POINT OF THE SCIENCE AND PRACTICE IN THE FIELDS OF CORROSION, MATERIALS AND ENVIRONMENTAL PROTECTION

STECIŠTE NAUKE I PRAKSE U OBLASTIMA KOROZIJE, ZAŠTITE MATERIJALA I ŽIVOTNE SREDINE

PROCEEDINGS

KNJIGA RADOVA

Under the auspicies of the
MINISTRY OF SCIENCE, TECHNOLOGICAL DEVELOPMENT AND INNOVATION OF THE REPUBLIC OF SERBIA

Pod pokroviteljstvom
MINISTARSTVO NAUKE, TEHNOLOŠKOG RAZVOJA I INOVACIJA REPUBLIKE SRBIJE

May 28-31, 2023 : : Divčibare, Serbia

CIP - Каталогизација у публикацији
Народна библиотека Србије, Београд

620.193/.197(082)(0.034.2)
621.793/.795(082)(0.034.2)
667.6(082)(0.034.2)
502/504(082)(0.034.2)
66.017/.018(082)(0.034.2)

INTERNATIONAL Conference YUCORR (24 ; 2023 ; Divčibare)
Meeting point of the science and practice in the fields of corrosion, materials and environmental protection [Elektronski izvor] : proceedings = Stecište nauke i prakse u oblastima korozije, zaštite materijala i životne sredine : knjiga radova / XXIV YuCorr International Conference, May 28-31, 2023, Divčibare, Serbia = XXIV YuCorr [Jugoslovenska korozija] Međunarodna konferencija = [organized by] Serbian Society of Corrosion and Materials Protection ... [et al.]] ; [organizatori Udruženje inženjera Srbije za koroziju i zaštitu materijala ... [et al.] ; [editors, urednici Miroslav Pavlović, Marijana Pantović Pavlović, Miomir Pavlović]. - Beograd : Serbian Society of Corrosion and Materials Protection UISKOZAM = Udruženje inženjera Srbije za koroziju i zaštitu materijala UISKOZAM, 2023 (Beograd : Serbian Society of Corrosion and Materials Protection UISKOZAM = Udruženje inženjera Srbije za koroziju i zaštitu materijala UISKOZAM). - 1 elektronski optički disk (CD-ROM) ; 12 cm
Sistemski zahtevi: Nisu navedeni. - Nasl. sa naslovne strane dokumenta. - Radovi na engl. i srp. jeziku. - Tiraž 200. - Bibliografija uz većinu radova. - Abstracts.

ISBN 978-86-82343-30-1

a) Премази, антикорозиони -- Зборници b) Превлаке, антикорозионе -- Зборници v) Антикорозиона заштита -- Зборници g) Животна средина -- Заштита -- Зборници d) Наука о материјалима -- Зборници

COBISS.SR-ID 119553545

XXIV YUCORR – International Conference | *Međunarodna konferencija*

PUBLISHED BY | *IZDAVAČ*
SERBIAN SOCIETY OF CORROSION AND MATERIALS PROTECTION (UISKOZAM)
UDRUŽENJE INŽENJERA SRBIJE ZA KORZIJU I ZAŠTITU MATERIJALA (UISKOZAM),
Kneza Miloša 7a/II, 11000 Beograd, Srbija, tel/fax: +381 11 3230 028, *office@sitzam.org.rs; www.sitzam.org.rs*

FOR PUBLISHER | *ZA IZDAVAČA* *Prof. dr MIOMIR PAVLOVIĆ, predsednik UISKOZAM*

CIRCULATION | *TIRAŽ:* **200** copies **|** *primeraka*
PUBLICATION YEAR | *GODINA IZDANJA:* **2023**
ISBN 978-86-82343-30-1

Synthesis : : Materials : : Corrosion : : Environment : : Energy

YuCorr

Analyse : : Discover : : Coat : : Green : : Protect : : Save : : Sustain

May 28-31, 2023, Divčibare, Serbia

Ovaj PDF fajl sadrži elektronsku Knjigu radova prezentovanih u okviru Međunarodne konferencije **XXIV YuCorr.** U knjizi su **plavom bojom** obeleženi aktivni linkovi ka pojedinim njenim delovima, iz Sadržaja do naznačenih stranica.

This PDF file contains Proceedings presented on the **XXIV YuCorr** International Conference. It can be easily navigated through the book contents by a single click on the appropriate links in Contents (**showed in blue**).

Autori snose punu odgovornost za sadržaj, originalnost, jezik i gramatičku korektnost sopstvenih radova.

Authors bear full responsibility for the content, originality, language and grammatical correctness of their own works.

XXIV YUCORR IS ORGANIZED BY
ORGANIZATORI XXIV YUCORR-a

SERBIAN SOCIETY OF CORROSION AND MATERIALS PROTECTION

Udruženje Inženjera Srbije za Koroziju i Zaštitu Materijala

INSTITUTE OF CHEMISTRY, TECHNOLOGY AND METALLURGY, UNIVERSITY OF BELGRADE

Institut za Hemiju, Tehnologiju i Metalurgiju, Univerzitet u Beogradu

INSTITUTE OF GENERAL AND PHYSICAL CHEMISTRY, BELGRADE

Institut za Opštu i Fizičku Hemiju

UNION OF ENGINEERS AND TEHNICIANS OF SERBIA, BELGRADE

Savez Inženjera i Tehničara Srbije

ENGINEERING ACADEMY OF SERBIA

Inženjerska Akademija Srbije

XXIV YUCORR IS ORGANIZED UNDER THE AUSPICIES OF THE

MINISTRY OF SCIENCE, TECHNOLOGICAL DEVELOPMENT AND INNOVATION OF THE REPUBLIC OF SERBIA

XXIV YUCORR JE FINANSIJSKI POMOGLO

MINISTARSTVO NAUKE, TEHNOLOŠKOG RAZVOJA I INOVACIJA REPUBLIKE SRBIJE

SPONSORS | *SPONZORI*

INTERNATIONAL SOCIETY OF ELECTROCHEMISTRY, Switzerland
SAVEZ INŽENJERA I TEHNIČARA SRBIJE, Beograd
INŽENJERSKA KOMORA SRBIJE, Beograd
HELIOS SRBIJA a.d., Gornji Milanovac
MIKROLUX d.o.o., Zaprešić, Hrvatska
TESCAN
FIRESTOP INTERNACIONAL d.o.o., Nova Pazova
SURTEC ČAČAK d.o.o., Čačak
INSTITUT ZA PREVENTIVU d.o.o., Novi Sad
EKP ELKER a.d., Prijedor, Republika Srpska, B&H
EKO ZAŠTITA d.o.o., Bijeljina, Republika Srpska, B&H
IPIN d.o.o., Bijeljina, Republika Srpska, B&H
HEMIPRODUKT d.o.o., Novi Sad
INSTITUT ZA OPŠTU I FIZIČKU HEMIJU, Beograd
SZR "GALVA", Kragujevac
EPS OGRANAK DRINSKO-LIMSKE HIDROELEKTRANE, Bajina Bašta
NOVOHEM d.o.o., Šabac

Table of Contents

PLENARY LECTURES
PLENARNA PREDAVANJA

Strong Metal-Support Interaction - a Tool Towards Enhanced Electrocatalytic Materials

Milutin Smiljanić[1*], Marjan Bele[1], Luka Pavko[1], Armin Hrnjić[1], Lea Gašparič[2], Anton Kokalj[2], Miran Gaberšček[1], Nejc Hodnik[1]

[1]*Department of Materials Chemistry, National Institute of Chemistry, Hajdrihova 19, 1000 Ljubljana, Slovenia*

[2]*Department of Physical and Organic Chemistry, „Jožef Stefan" Institute, Jamova cesta 39, 1000 Ljubljana, Slovenia*

[*]*milutin.smiljanic@ki.si*

Abstract

Modern society is facing a variety of problems caused by the usage of fossil fuels as the main energy source. Hydrogen is regarded as the most convenient energy carrier to replace fossils, and the whole concept of hydrogen energy and the economy around it was envisioned half a century ago.[1] *Electrocatalysis is the cornerstone of the transition to a sustainable energy cycle, as it offers means to produce and utilize hydrogen as a green energy vector. Water electrolysis (WE) has been considered the most convenient way to produce hydrogen, while hydrogen's chemical energy can be converted into electricity in fuel cells (FC). The efficient running of the electrochemical processes in these energy conversion devices demands the usage of efficient and durable electrocatalytic materials. The core of the electrocatalytic composites used in WEs and FCs are metal nanoparticles (usually platinum group metals (PGM) or their alloys with transition metals) which act as the active sites, and high surface area support materials (most commonly carbon) whose role is to effectively disperse the nanoparticles and to maximize their utilization. A common strategy for obtaining enhanced catalytic materials is to focus on the engineering and tailoring of specific active sites. For instance, alloying has been adopted as the general strategy to enhance catalytic performance, while it is also beneficial for the decrease of the share of expensive PGMs in the catalyst.*[2] *Another option is to focus on the support's effect on the catalytic composite's overall performance. Carbon materials are used in electrocatalysis thanks to their high surface area, electrical conductivity, and relatively good (electro)chemical stability. However, carbon itself does not offer the possibility to affect the intrinsic activity of supported metallic active sites due to the only weak interactions.*

In this talk, I will present a strategy to modify electrocatalytic composites' activity, stability, and selectivity by substituting carbon with novel support materials. By using an organic matrix tris(aza)pentacene (TAP) to support Pt particles in FCs, one can obtain a smart anode catalyst that can selectively catalyze fuel cell reactions, which is beneficial for the overall durability of these devices.[3,4] *In the case of WEs, a significant boost of activity and stability of the catalysts can be obtained by using conductive titanium oxynitride ($TiON_x$) as the support.*[5] *Unlike carbon, $TiON_x$ is able to induce strong metal-support interaction with metallic nanoparticles, which affects their catalytic performance.*

Keywords: *electrocatalysis; hydrogen energy; fuell cells; water electrolysis; support effect; strong metal-support interaction;*

Izvod

Moderno društvo se suočava sa brojnim posledicama masovne upotrebe fosilnih goriva kao glavnog izvora energije. Vodonik se smatra najprikladnijom zamenom za fosilna goriva, a cela ideja o širokoj upotrebi vodonične energije je osmišljena još pre pola veka.[1] *U ovom konceptu, elektrohemija i elektrokataliza igraju značajnu ulogu, jer nude mogućnost proizvodnje i korišćenja vodonika kao*

zelenog energenta. Elektroliza vode je tehnologija za održivu proizvodnju vodonika, dok gorivne ćelije omogućavaju konverziju hemijske energije vodonika u električnu energiju. Efikasno funkcionisanje elektrohemijskih procesa u ovim uređajima zahteva upotrebu efikasnih i stabilnih elektrokatalitičkih materijala. Glavne komponente elektrokatalitičkih kompozita koji se koriste u gorivnim ćelijama i elektrolizerima su nanočestice metala i materijali koji se koriste kao njihovi nosači. Kao aktivni centri za elektrohemijske reakcije, najčešće se koriste metali iz platinske grupe (eng. platnium group metals, PGM) ili njihove legure sa prelaznim metalima. Kao nosači, upotrebljavaju se materijali sa velikom specifičnom površinom (najčešće ugljenik) čija je uloga da efikasno disperguju nanočestice metala i tako povećaju njihovu iskorišćenost. Uobičajena strategija za poboljšavanje katalitičkih svojstava materijala je fokusiranje na dizajn specifičnih aktivnih mesta. Na primer, legiranje PGM sa prelaznim metalima se koristi kao generalna strategija za poboljšanje katalitičkih performansi, koja je istovremeno korisna i za smanjenje udela skupih PGM u katalizatoru.[2] Druga mogućnost je proučavanje efekta nosača na performanse katalitičkih kompozita, odnosno aktivnih mesta za odvijanje elektrohemijskih reakcija. Ugljenični materijali se često koriste kao nosači u (elektro)katalizi zahvaljujući njihovoj visokoj specifičnoj površini, električnoj provodljivosti i relativno dobroj (elektro)hemijskoj stabilnosti. Međutim, ugljenik sam po sebi ne može uticati na intrinzičnu aktivnosti katalitičkih kompozita zbog slabe interakcije sa metalnim aktivnim centrima.

U ovom predavanju, predstaviću strategiju da se modifikuje aktivnost, stabilnost i selektivnost elektrokatalitičkih kompozita korišćenjem alternativnih nosača umesto ugljenika. Upotrebom organskog materijala tris(aza)pentacena (TAP) kao nosača za Pt nanočestice u gorivnim ćelijama, može se dobiti „pametan" anodni katalizator koji selektivno katališe reakcije u gorivnim ćelijama, što može značajno uticati na njihovu stabilnost.[2,3] U slučaju elektrolize vode, značajno poboljšanje aktivnosti i stabilnosti može se postići korišćenjem provodljivog titanijum oksinitrida ($TiON_x$) kao nosača.[4] Za razliku od ugljeničnih nosača, $TiON_x$ indukuje metal-nosač interakcije sa nanetim nanočesticama (eng. strong metal-support interaction), i tako utiče na njihovu katalitičku aktivnost i stabilnost.

Ključne reči: *elektrokataliza; vodonična energija; gorivne ćelije; elektroliza vode; uticaj nosača; metal-nosač interakcije;*

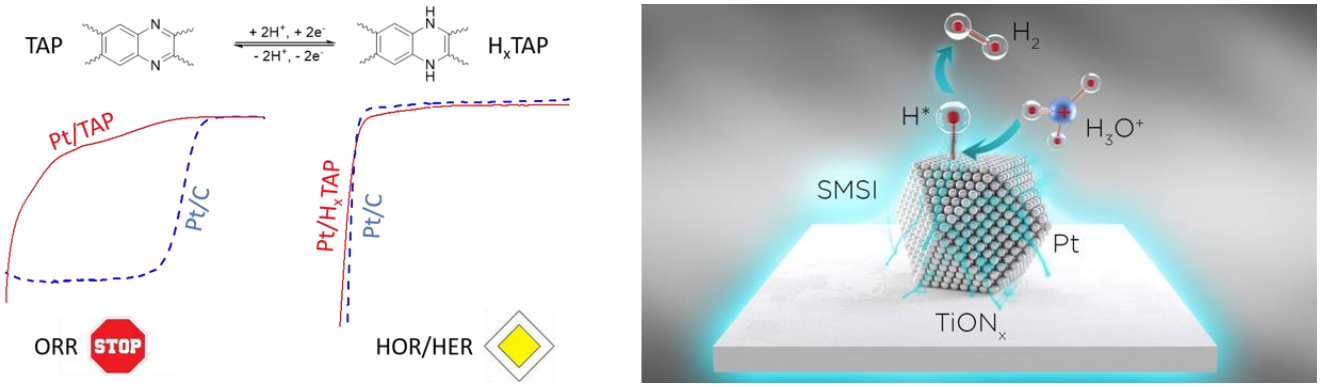

Figure 1. *Tuning the activity, selectivity, and stability of the electrocatalysts via the effect of the support material.*

Acknowledgments

This work was financially supported by the Slovenian Ministry of Education Science and Sport & EU─European Regional Development Fund (project Raziskovalci-2.1-KI-952007); the Slovenian Research Agency through the research programs/projects I0-0003 and P2-0393, NC-0007, NC-0016, N2-0248, and N2-0155; European Research Council (ERC) Starting Grant 123STABLE (Grant agreement ID: 852208); and NATO Science for Peace and Security Program under Grant G5729.

Reference

1. Bockris, J. O. M. The Hydrogen Economy: Its History. Int J Hydrogen Energy, 38 (6), 2579–2588, 2013.
2. Gatalo, M.; Bele, M.; Ruiz-Zepeda, F.; Šest, E.; Šala, M.; Kamšek, A. R.; Maselj, N.; Galun, T.; Jovanovič, P.; Hodnik, N.; Gaberšček, M. A Double-Passivation Water-Based Galvanic Displacement Method for Reproducible Gram-Scale Production of High-Performance Platinum-Alloy Electrocatalysts. Angewandte Chemie International Edition 58 (38), 13266–13270, 2019.
3. Vélez Santa, J. F.; Menart, S.; Bele, M.; Ruiz-Zepeda, F.; Jovanovič, P.; Jovanovski, V.; Šala, M.; Smiljanić, M.; Hodnik, N. High-Surface-Area Organic Matrix Tris(Aza)Pentacene Supported Platinum Nanostructures as Selective Electrocatalyst for Hydrogen Oxidation/Evolution Reaction and Suppressive for Oxygen Reduction Reaction. Int J Hydrogen Energy 46 (49), 25039–25049, 2021.
4. Smiljanić, M.; Bele, M.; Moriau, L.; Vélez Santa, J.; Menart, S.; Šala, M.; Hrnjić, A.; Jovanovič, P.; Ruiz-Zepeda, F.; Gaberšček, M.; Hodnik, N. Suppressing Platinum Electrocatalyst Degradation via a High-Surface-Area Organic Matrix Support. ACS Omega 7 (4), 3540–3548, 2022.
5. Smiljanić, M.; Panić, S.; Bele, M.; Ruiz-Zepeda, F.; Pavko, L.; Gašparič, L.; Kokalj, A.; Gaberšček, M.; Hodnik, N. Improving the HER Activity and Stability of Pt Nanoparticles by Titanium Oxynitride Support. ACS Catal, 12 (20), 13021–13033, 2022.

Enzymatic Electrochemical Bisoensors

Enzimske elektrhemijski biosenzori

Milica Gvozdenović

Faculty of Technology and Metallurgy, University of Belgrade, Karnegijeva 4, 11120 Belgrade Serbia

popovic@tmf.bg.ac.rs

Abstract

An electrochemical biosensor, as recommended by the Commission of Physical Chemistry and Analytical Chemistry of the International Union of Pure and Applied Chemistry (IUPAC), can be defined as a self-contained integrated device that provides specific quantitative or semi-quantitative analytical information using a biological recognition element, i.e. a biochemical receptor, which is spatially connected to the electrochemical transducer and detector. In this way, an electrochemical biosensor inherits high specificity from a biological receptor combined with high accuracy and precision from electrochemical detection techniques. Among a large group of electrochemical biosensors, enzymatic electrochemical biosensors are the most investigated and commercially available.

The development of this multidisciplinary field began in the sixties of the last century with the introduction of the so-called "enzyme electrode" constructed by Clark and Lyons by immobilizing the enzyme glucose-oxidase inside the membrane of an oxygen electrode. This enzyme electrode was then used to clinically determine blood glucose levels. This first successful attempt resulted in the accelerated development of this multidisciplinary field. Today, electrochemical biosensors are used in many fields: medicine, the food industry, the pharmaceutical industry, and environmental protection. The development of enzyme immobilization techniques and the abundance of newly developed enzymes together with the development of electrode materials especially by nano structurization make the field of enzymatic electrochemical biosensors constantly attractive in a both theoretical and practical manner.

Keywords: *biological recognition element; enyzmes; electrochemicl detector; enyzme electrode, immobolization*

Izvod

Kao što je to preporučeno od strane Komisije za Fizičku hemiju i Analitičku hemiju Međunarodne unije za čistu i primenjenu hemiju (IUPAC), elektrohemijski biosenzor može da se definiše kao samostalni integrisani uređaj koji pruža specifične kvantitativne ili polu-kvantitativne analitičke informacije pomoću biološkog elementa prepoznavanja, odnosno biohemijskog receptora, koji je prostorno povezan sa elektrohemijskim pretvaračem i detektorom. Dakle, elektrohemisjki biosenzori su uređaji koji kombinuju veliku specifičnost koja je poreklom od bioloških receptora i veliku tačnost i preciznost zahvaljujući upotrebi elektrohemijskih tehnika detekcije. Od velikog broja elektrohemijskih biosenzora, enzimski su najrasprostranjeniji i komercijalno dostupni.

Razvoj i komercijalizacija u ovoj oblsasti vezuju se za šezdesete godine prošlog veka kada su su Klark (Clark) i Lajons (Lyons) konstruisali „enzimsku elektrodu" imobilizacijom enzima glukoza-oksidaze unutar membrane kiseonične elektrode i uspešno je primenili u određivanju nivoa glukoze u krvi pacijenata obolelih od dijabeteasa. Danas se elektrohemijski bisenzori primenjuju u velikom broju oblasti: dijagnostici u kliničkim i kućnim uslovima, industriji hrane, farmaceutskoj industriji, analiyi zagađenja životne sredine. Razvoj tehnika imobilizacije i obilje enzima ceptora kao razvoj elektrodnih materrijala prvenstveno nanostrukturizacijom uz mogućnost miniturizacije čini oblast elektrohemijskih biosenzora stalno atraktivnom kako u teorijskom tako i u praktičnom slislu.

Ključne reči: *biološki element prepoznavanja; enzimi; elektrohemijska detekcija; enzimska elektrode; imobilizacija*

Introduction

After more than sixty years of the enzyme electrode concept, used for the determination of blood glucose and introduced by Clark and Lyons [1,2], enzymatic electrochemical biosensors (EEBSs) are the most studied and commercially available sensors used in everyday life. The enzyme electrode concept involves immobilized enzymes into electrode material while the operation principle of an EEBS is fully electrochemical, meaning that the signal is formed due to a charge transfer reaction originating from the interaction of substrate in an enzyme-catalyzed reaction. Bearing in mind that oxidation and reduction are required for the formation of the sensor signal, oxydoreductases are enzymes used as recognition elements in EEBS. Nowadays, EEBSs are successfully used in many fields beyond the well-known and first introduced determination of glucose, such as monitoring of the course of diagnostic treatments, clinical and home diagnostics, the food industry, environmental monitoring, forensics, etc. [2-4]. Having in mind the fact that enzymes are the most powerful natural catalyst with high selectivity and the fact that electrochemical transduction methods enable increased selectivity since different molecules can be oxidized or reduced at different potentials together with the simplicity, reproducibility, and high accuracy of electrochemical detection, EEBSs offers immense inspiration for both theoretical and practical grounds. Current research EEBSs is moved from its conventional ground to the field of nanomaterials (nanomaterials based on metals and metal oxides, carbon-based nanomaterials, and nanomaterials based on conducting polymers) [5-8]that can enable the construction of sensors for specific analytes and offer not just the possibility of device miniaturization but also lower the detection limit enable direct analysis of simple, in vivo usage, etc.[6,8-10]. This work is a short overview of EEBSs their advantages, construction, and operational principles together with future perspectives in various fields.

Deffinition and clasification

Sensors are devices that detect or react to events from the environment and create some type of response. A chemical sensor uses the chemical or physical properties of the analyte to produce a signal proportional to the concentration of the desired analyte. A chemical sensor is usually composed of two major parts receptor and transducer. The receptor is a part that is directly exposed to the analyte and therefore interacts with it, whilst the transducer is used for converting the chemical event to a measurable signal using various detection techniques. A biosensor is a special case of a chemical sensor that has a biochemical receptor or biochemical recognition element. On the other hand, an electrochemical biosensor is a special case of a biosensor that has an electrochemical transducing part i.e. modified electrode, with an output signal from an electrochemical reaction detected by various electrochemical techniques. According to IUPAC definition electrochemical biosensor is considered a „*self-contained integrated device, which is capable of providing specific quantitative or semi-quantitative analytical information using a biological recognition element which is retained in direct spatial contact with an electrochemical transduction element*“ [11]. EEBSs are a special class of electrochemical biosensors whose biological recognition elements are enzymes [2-4,12].

EEBSs can be classified according to electrochemical detection techniques as potentiometric, voltammetric, amperometric, impedimetric, and conductometric and those using striping techniques [2].

The potentiometric EEBSs use a potentiometric technique which is static and so-called zero-current technique. The signal is based on the measurement of the potential difference that is freely established most often on the membrane that contains immobilized enzyme. This technique uses ion-selective electrodes, modified electrodes, and recently field effect transistors. Also, it provides simple instrumentation [13].

Amperometric EEBSs are the most frequent in practical applications, their principle relays to the application of the constant potential imposed on the working electrode which results in an electrochemical reaction with an output signal in the form of current [2,14]. The selection of the working potential is necessary for the functioning of amperometric EEBS that can allow charge transfer to take place under diffusion control, enabling registered stationary current to be directly proportional to the activity of the analyte. The characteristics of amperometric electrochemical biosensors largely depend on the material of the working electrode.
Voltammetric EEBSs are also very popular since the amount of voltammetric detection techniques is huge. The common feature of voltammetric EEBSs is that the controlled potential is imposed on the working electrode and a complex current-potential function known as a voltammogram is recorded with current peaks whose intensity is proportional to the amount of analyte [2].
Impedimetric EEBSs are based on the electrochemical impedance spectroscopy technique. This technique refers to the input signal in the form of a low-amplitude sinusoidal potential, that results in a low-amplitude current output signal. Given the character of the input and output signals, impedance represents a sinusoidal transfer function that can most easily be understood as generalized resistance, which hides information related to changes in resistance and capacitance caused by biochemical reactions[9,14].
The principle of conductometric sensors is based on the fact that during biochemical reactions catalyzed by enzymes, a change in the ionic strength i.e. conductivity of the solution occurs. Although they have not been commercialized to a large extent, recently the development of nanostructured materials has increased the interest in this type of biosensor [5].
Stripping techniques are newly developed and involve an analyte preconcentration step enabling trace analysis [15].

Enzyme electrode concept and the generation of EEBSs

As stated before the concept of an enzyme electrode was introduced by Clark and Lyons. This „first“ enzyme electrode construction referred to a thin layer of enzyme glucose oxidase introduced to the membrane of an oxygen electrode. The electrode measured oxygen consumption, in an enzyme-catalyzed reaction of glucose oxidation, by its reduction on the platinum electrode [16].
Since oxygen is also needed for the regeneration of the reduced enzyme and therefore the data were not accurate, the possible solution was seen in tracing some other electrochemically active compounds. This was a starting point in creating the first generation of EEBSs that relays on the electrochemical oxidation of hydrogen peroxide originating from the second step of the reaction in which the reduced form of the enzyme reacts with oxygen. The potential required for oxidation of H_2O_2 is relatively high, so it can be expected that other electroactive compounds in the testing simple can be co-oxidized such as uric or ascorbic acid. Moreover, there is a fluctuation in the amount of dissolved oxygen [1,10]. The improvement of the selectivity and stability can be overcome by introducing ion-exchange membranes and electrochemically polymerized films to inhibit the diffusion of interfering compounds [10].
The second generation of EEBSs involves the usage of electron mediators to overtake oxygen as an electron acceptor in the enzyme-catalyzed reaction [1]. The limiting factor in mediators' usage is potential toxicity, competition with dissolved oxygen, and conduction efficiency due to nondirect charge transfer [10].
The third generation of EEBSs is based on direct electron transfer between the enzyme active center and the electrode and therefore is not dependent on oxygen nor a mediator [1]. Although progress was made in the research of direct electron transfer the fact that most enzymes have an inaccessible active center so this approach is limited to a small number of enzymes. The possible solution is enzyme wiring and the application of so-called bi-enzyme electrodes [10,17].

Enzymes and immobilization

Enzymes are the most efficient catalyst in nature. Unlike other catalysts, enzymes are more specific to the so-called substrate. However, their activity is strongly dependent on temperature or pH or the presence of other molecules that can either decrease (inhibitors) or increase (activators) activity. In other to fabricate efficient enzyme electrode immobilization of the enzymes into electrode material is crucial. The immobilization techniques involve entrapment in a thin layer of solution in contact with the electrode behind the membrane; covalent attachment into a nylon membrane in direct contact with the electrode; cross-linking via glutaraldehyde; entrapment in a polymer film directly polymerized on the electrode; incorporation into carbon material with carbon paste and covalent attachment to a thiol linked to self-assembled monolayers [18].
Since oxidation/reduction is necessary for EEBSs, as mentioned before, oxydoreductases are used for the fabrication of enzyme electrodes. The electrochemical activity of oxydoreductases is related to their active centers capable of charge transfer. The most common redox-active centers in oxydoreductases are nicotinamide adenine dinucleotide (NAD^+/NADH) and its phosphorylated form ($NADP^+$/NADPH) that undergoes one proton and two-electron transfer and flavin adenine dinucleotide (FAD^{++}/$FADH_2$) that undergoes two protons and two electron exchange [1].

Conclusions

EEBSs combine the high selectivity of enzymes as biological receptors and the analytical power of electrochemical detection techniques. The working principle of EEBSs is electrochemical, meaning that the sensor signal is due to oxidation/reduction. The field of EEBSs is highly commercialized and covers a broad range of practical applications in diagnostics, prevention, food and pharmaceutic industries, forensics, and environmental monitoring. The EEBSs market is projected to rapidly grow due to technological advancement in novel materials motivated by the demand for miniaturization to produce wearable, portable end implantable devices.
Research in this area of EHBS is focused on the development of immobilization techniques and new electrode materials

Acknowledgments

The work is supported by the Ministry of Education, Science and Technological Development and Innovation of the Republic of Serbia under Contract No. 451-03-68/2023-14/200135.

References

1. J. Wang, Electrochemical Glucose Biosensors, *Chem. Rew*. **108**, 814-825, 2008.
2. N. J. Ronkainen, H. B. Halsall, and W. R. Heineman, Electrochemical biosensors, *Chem.Soc. Rev*. **39(5)**, 1747-1763, 2010.
3. F. W. Scheller, U. Wollenberger, A. Warsinke, and F. Lisdat, Research, and development in biosensors, *Curr.Opin.Biotechnol*.**12(1)**,35-40, 2001.
4. J. D. Newman and S. J. Setford, Enzymatic Biosensors, *Mol.Biotechnol.* **32**, 249-268, 2006.
5. N. Wongkaew, M. Simsek, C. Griesche, and A. J. Baeumner, Functional Nanomaterials and Nanostructures Enhancing Electrochemical Biosensors and Lab-on-a-Chip Performances: Recent Progress, Applications, and Future Perspective, *Chem.Rev.* **119(1)**, 120-194, 2019.
6. K. Nemčeková and J. Labuda, Advanced materials-integrated electrochemical sensors as promising medical diagnostics tools: A review, *Mater. Sci. Eng. C*, **120**, 2021
7. S. K. Krishnan, E. Singh, P. Singh, M. Meyyappan, and H. S. Nalwa, A review on graphene-based nanocomposites for electrochemical and fluorescent biosensors, *RSC Adv.* **9(16)**, 8778-8781, 2019.
8. I. H. Cho, D. H. Kim, and S. Park, Electrochemical biosensors: Perspective on functional nanomaterials for on-site analysis, *Biomater. Res.* **24(1)**, 1-12, 2020.

9. J. Wu, H. Liu, W. Chen, B. Ma, and H. Ju, Device integration of electrochemical biosensors, *Nat. Rev. Bioeng.* **1**, 346-360, 2023.
10. S. Wang, Y. Liu, A. Zhu, and Y. Tian, In Vivo Electrochemical Biosensors: Recent Advances in Molecular Design, Electrode Materials, and Electrochemical Devices, *Anal. Chem.* **95(1)**, 388-406, 2023.
11. D. R. The, "ELECTROCHEMICAL BIOSENSORS : RECOMMENDED Electrochemical biosensors : Recommendations and classification (Technical Report)," *IUPAC*, **71(12)**, 2333-2348, 1999.
12. M. Pohanka and P. Skladal, Electrochemical biosensors – principles and applications, *A. Appl. Biomed.* **6(2)**, 57-64, 2008.
13. C. S. Lee, S. Kyu Kim, and M. Kim, Ion-sensitive field-effect transistor for biological sensing, *Sensors*, **9(9)**, 7111-7131, 2009.
14. D. Grieshaber, R. MacKenzie, J. Vörös, and E. Reimhult, Electrochemical biosensors - Sensor principles and architectures, *Sensors*, **8(3)**, 1400-1458, 2008.
15. J. M. Pingarrón *et al.*, "Terminology of electrochemical methods of analysis (IUPAC Recommendations 2019), *Pure Appl. Chem.* **92(4)**, 641-694, 2020.
16. J. Wang, Glucose Biosensors : 40 Years of Advances and Challenges, *Electroanalysis*, **13(12)**, 983-988, 2001.
17. R. Paper, "Electrochemical Biosensors - Sensor Principles and Architectures, *Sensors*, **8(3)**, 1400-1458, 2008.
18. L. Gorton and P. Bartlett, "NADP-Based Biosensors," in *Bioelectrochemistry*, *Fundamentals, Experimental Techniques and Applications*, 2008, p. 158.

Renewable Energy Potentials of the Republic of Serbia for Green Hydrogen Production and Applications

Potencijali Obnovljive Energije Republike Srbije za Proizvodnju i Primenu Zelenog Vodonika

Branimir N. Grgur

Faculty of Technology and Metallurgy University of Belgrade,

Karnegijeva 4, 11020 Belgrade, Serbia

**BNGrgur@tmf.bg.ac.rs*

Abstract

The paper treated the possibility of green hydrogen production in the Republic of Serbia using some renewable energy sources by alkaline water electrolysis. The mass and volume of green hydrogen are estimated for the usage of 5%, 10%, and 15% of wind, solar, and hydro technically available potentials. The possibility of natural gas substitution with green hydrogen and the number of fuel cell-based electric cars are estimated. Also, the principles of cogeneration of electric and heat energy by biomass gasification as a fuel for solid oxide fuel cells are considered.
Keywords: *electrolysis; natural gas; fuel cells, biomass; gasification*

Izvod

U radu je obrađena mogućnost proizvodnje zelenog vodonika u Republici Srbiji korišćenjem nekih obnovljivih izvora energije elektrolizom vode. Masa i zapremina zelenog vodonika su procenjeni za korišćenje 5%, 10% i 15% tehnički raspoloživih potencijala vetra, sunca i hidro energije. Procenjuje se mogućnost zamene prirodnog gasa zelenim vodonikom i broj električnih automobila sa gorivim ćelijama. Takođe, razmatrani su principi kogeneracije električne i toplotne energije gasifikacijom biomase kao goriva za čvrste oksidne gorivne ćelije.
Ključne reči: *elektroliza; prirodni gas; gorivne ćelije, biomasa; gasifikacija*

Why green hydrogen

Enormous usage of fossil fuels (oil and oil derivate, coal, natural gas) mainly by burning, produces numerous greenhouse gases that lead to unpredictable climate changes [1]. Among other efforts, the possibility to use hydrogen as an energy source or energy carrier starting to become a reality. The advantage of hydrogen is the simple fact that during burning pure water and energy is produced:

$$2H_2 + O_2 = 2H_2O + 572 \text{ kJ mol}^{-1}$$

Also, the specific electric capacity of 1 kg of hydrogen is 26.8 kAh, while for metallic lithium is 3.83 kAh. In addition, 1 kg of hydrogen releases approximately 140 MJ of heat energy, methane 50 MJ, natural gas 47 MJ, or biogas 27 MJ. Hydrogen can be used as an energy carrier (like electric energy), where produced hydrogen at one place could be transported via pipelines or by track tank to the places of usage. Many different chemical plants use hydrogen as row material for producing valuable chemicals (ammonia, different fertilizers, methanol, in petroleum refining, etc.) [2].

Technologies for hydrogen production

Nowadays, nearly all hydrogen is produced from natural methane or coal and water steam. This procedure is environmentally very unfavorable because it leads to significant CO_2 emissions [3,4]. Both reactions are highly endothermic:

$$2CH_4 + 2H_2O \rightarrow 2CO + 3H_2$$
$$3C + O_2 + H_2O \rightarrow 3CO + H_2$$

Released carbon monoxide in water gas shift reaction can be converted into more hydrogen and carbon dioxide:

$$CO + H_2O \rightarrow CO_2 + H_2$$

Today, about 76% of hydrogen is produced from methane, and 23% from coal gasification. Stoichiometrically, for one ton of hydrogen obtained from fossil raw materials, at least 11 tons of CO_2 are generated. It is estimated by International Energy Agency (IEA), that in 2019, ~830 million tons (Mt) of CO_2 are released into the Earth's atmosphere from the fossil fuels hydrogen production [5]. Because, such hydrogen (grey or brown hydrogen) is not environmentally friendly, replacements with green hydrogen are of enormous importance.

On the other hand, hydrogen produced by electrolysis of water using electricity obtained from renewable energy sources (RES) could be considered environmentally friendly. But there is some obstacles. Small home wind turbines that are 5 kW in size and massive utility-scale wind turbines that are 5 MW in size are both commercially available. Wind energy is converted into electricity by wind turbines with a 20% to 40% efficiency. A wind turbine has a 20-year average lifespan and needs regular maintenance every six months. Because of the variation in wind speed, wind turbine power output is variable; however, when combined with an energy storage device, wind power can give a stable power output. [6]. The necessity for more land to sustain a wind turbine and the challenge of finding a place with enough wind to provide optimal efficiency and power are drawbacks of deploying wind turbines. Noise and aesthetic issues may also result from the deployment of turbines in densely populated regions. Death of birds and bats from collisions with rotating turbine blades and turbine interference in their flight routes are two additional downsides.

In recent years, silicon-based semiconductor-based solar energy conversion systems have been widely used throughout the world, while photovoltaic and artificial photosynthetic systems employing conventional materials and architectures have also become more advanced. Laboratory energy conversion efficiency for single-crystal and polycrystalline silicon photovoltaic cells are over 25% and over 20%, respectively. Nevertheless, under typical test conditions, industrially made solar modules now have efficiency between 18% and 22%. of [7].

The potential energy of water, hydropower, flowing from higher to lower elevations is used to generate electricity, which is a renewable energy source known as hydroelectric power. It is a technology that is well developed, reliable, predictable, and inexpensive. Hydroelectric power has the highest conversion rates of all known energy sources (about 90% efficiency, water to wire). It has a long lifespan and very low operation and maintenance costs, but it does require a rather large initial investment. [8]

The reactions that take place during the electrolysis of water are:

anode (+): $4OH^- = O_2 + 2H_20 + 4e$
cathode (-): $2H_20 + 2e = H_2 + 2OH^-$
Overall reaction: $2H_2O = 2H_2 + O_2$

Today, there are four main technologies for water electrolysis: Alkaline electrolyzes (AE); Polymer Electrolyte Membrane electrolyzes (PEM); Solid oxide electrolysis (SOEC), and Anion Exchange Membrane electrolysis (AEM) [9]. Of these, alkaline electrolyzers are among the most common [10], while the other three are partially used but are still in the R&D phase. The principle of operation of these electrolyzers is very similar, except that alkalis have a liquid electrolyte based on KOH or NaOH and a separator or diaphragm, while the other three types perform electrolysis of pure water and ionic conductors are membranes or solid electrolyte that has the ability to conduct ions. The theoretical energy for obtaining 1 kg of H_2 is 33 kWh, while the real ones are, taking the whole system of electrolyzes, in the order of 40-100 kWh per 1 kg of H_2 [**Error! Bookmark not defined.**]**Error! Reference source not found.**. It should be noted that significant amounts of pure oxygen are also obtained by electrolysis of water, e.g. electrolysis of 1 t of water yielded ~ 110 kg H_2 and ~ 890 kg O_2. Such large amounts of oxygen can be used after compression to improve the operation of blast furnaces, and thermal power plants, and after additional purification for medical purposes.
Therefore, many western European countries, the USA, China, Japan, etc. have brought "Hydrogen strategy" documents, that deal with the production and application of hydrogen produced by renewable sources.

Hence, this paper attempt to roughly estimate the potentials of the Republic of Serbia in green hydrogen production and some applications.

RES potentials in the Republic of Serbia

Table 1 provides an overview of the available technical potential of renewable energy sources in the Republic of Serbia [11].

Table 1. Overview of the potential of renewable energy sources in the Republic of Serbia for 2020. [**Error! Bookmark not defined.**].

Type of RES	Available used technical potentials Mteo	Unused available technical potential Mteo	Total RES technical potentials Mteo	Share %
Biomass	1.054	2.394	3.448	61
Hydro	0.909	0.770	1.679	30
Geothermal	≈0.08	0.1	0.180	3
Solar	≈0	0.240	0.240	4.2
Wind	?*	?*	0.103	1.8
Total RES	1.968	3.682	5.65	

*In the Republic of Serbia ~430 MW wind generators are installed but without precise data about yearly electric energy production.

According to Table 1, the total estimated technical potential (after conversion) is around 5.65 Mteo. It should be mentioned that the newest investigations suggest that potentials are much higher, around 12 Mteo, but data is still not published and the methodology is uncertain.

Estimation of RES green hydrogen possible production and application

Considering the above given data estimated maximum values of electricity from RES, the share of electricity when using 5%, 10% and 15% of the potential from the maximum can be calculated, Table 2. Also, the percentage share based on the energy balance, and the total yearly electricity consumption of ~44.5 TWh is given.

Table 2. Estimated share of the electricity when using 5%, 10%, and 15% of RES potential from the maximum technically available potentials.

Source	100%	5%	10%	15%
Solar, TWh	2.79	0.14	0.28	0.42
Wind, TWh	1.20	0.06	0.12	0.18
Hydro energy, TWh	19.5	0.97	1.95	2.92
Total, TWh	23.5	1.17	2.35	3.52
% of 44.5 TWh	53	2.6	5.3	7.9

Based on the estimated electric energy production given in Table 2, the mass of the hydrogen can be estimated, using the data that 1 kg of hydrogen consumes 50 kWh of electricity using an optimistic value for an optimized alkaline electrolyzer [**Error! Bookmark not defined.**]. The estimated data a re shown in Table 3, and graphically in Fig. 1. It is obvious that hydrogen obtained using electricity from hydropower is dominant, with practically 83% of the total share. The mass of hydrogen depends on the usage of RES potentials and ranges from 23.5 kt to 70.5 kt.

Table 3. The estimated mass of the hydrogen in kt that could be obtained by using 5%, 10%, and 15% of technical RES potentials.

Source	5%	10%	15%
Solar, kt H_2	2.8	5.6	8.4
Wind, kt H_2	1.2	2.4	3.6
Hydro, kt H_2	19.5	39.0	58.6
Total, , kt H_2	23.5	47.0	70.5

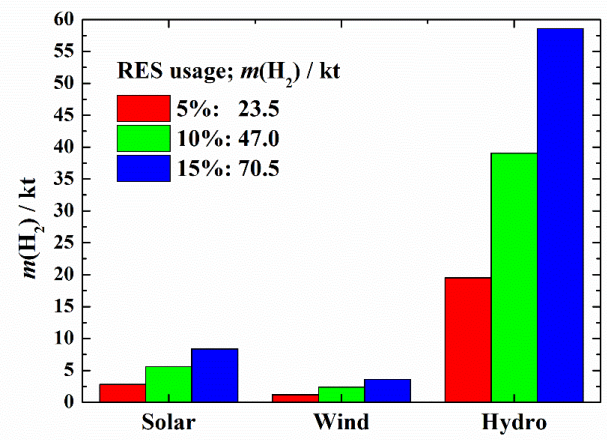

Figure 1. *Graphical presentation of the estimated mass of the hydrogen in kt that could be obtained by using 5%, 10%, and 15% of technical RES potentials.*

It is also possible to calculate the volume of hydrogen from the mass of hydrogen (the conversion factor from kg to m^3 (0°C) is 11.13). The estimated data are shown in Table 4, and graphically in Fig. 2. The total volume of hydrogen range from 259 Mm^3 for using 5% of RES to 776 Mm^3 for 15%.

Table 4. The estimated volume of the hydrogen from the mass of hydrogen.

RES	5%	10%	15%
Solar, Mm^3 H_2	30.7	61.4	92.1
Wind, Mm^3 H_2	13.18	26.3	39.5
Hydro, Mm^3 H_2	214.8	429.6	644.4
Total, Mm^3 H_2	258.7	517.3	776.0

The possible substitution of hydrogen in the total consumption of natural gas, 98% of methane, which in 2020 is amounted to 2665 Mm^3, is also calculated, and shown as the inset in Fig. 2. It can be seen that substitutions of natural gas with hydrogen vary between 10 to ~30%.

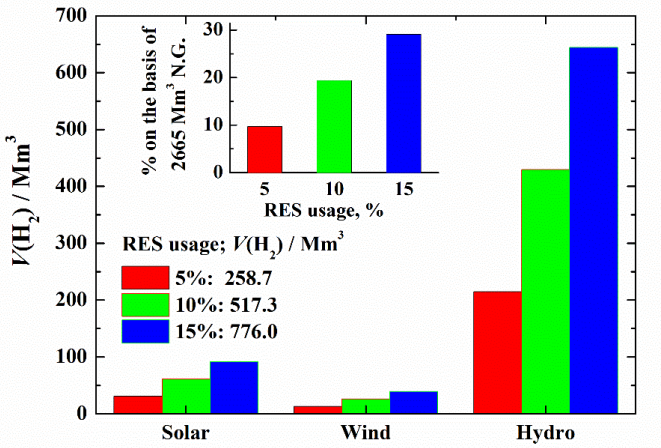

Figure 2. *The estimated volume of the hydrogen from the mass of hydrogen. Inset: The possible substitution in the total yearly consumption of natural gas (2665 Mm^3) by hydrogen.*

Considering the enormous rise of the natural gas price due to the situation in Ukraine from the beginning of 2022, these are very important observations. Commercial burners designed for natural gas can only sustain limited hydrogen concentrations, typically 5 to 20 vol.% in the fuel mixture [12]. Based on calculations of Carlanescu et al. [13], the lower calorific value of the hydrogen-methane mixture significantly increase above 40 vol.% of hydrogen in the mixture, as can be seen in Fig. 3, which is drowning from the tabular data. Consequently, below 20% energetic effects are minor, but considering the price, it could have a favorable effect.

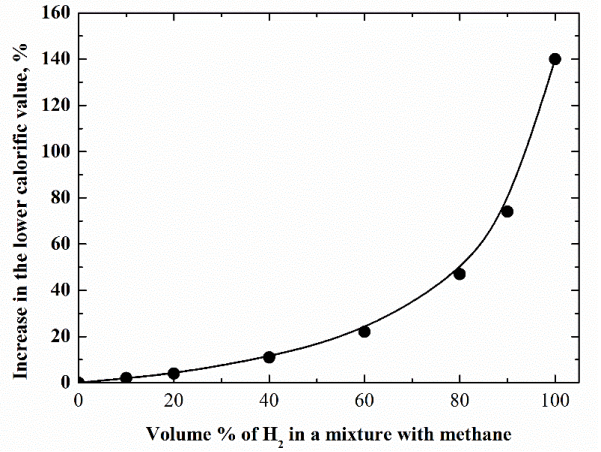

Figure 3. The relative increase of the lower calorific value of hydrogen-methane mixtures [adapted from ref. **Error! Bookmark not defined.**]

To evaluate the application of hydrogen for the fuel cell electric vehicles (FCEV) with polymer electrolyte fuel cells (PEFC) [**Error! Bookmark not defined.**], the data from Table 3 are applied. E

stimation is very dificult due to the some of uncertain parameters. For exapmle, in the first aproximation, the data from the study given by Candelaresi [14] is used; H_2 consumption of 0.76 kg per 100 km, lifespan of 190.000 km travelled, electric motor power 80 kW. From the given data of an average European driving performance of 12.000–15.000 km year^{-1} it can be estimated that FCEV can operate 16 to 12 years, or in average 14 years. Consequently, the yearly consumption of hydrogen could be roughly estimated to ~100 kg per car. But other report, suggests that average mileages are ~23.000 km per year that gives average spanlife of ~8 year (~65 km daily) that is more realistic. This is in agreement of DOE (USA Department of Energy) target for 2020, of 5000 h of FC operations, or for 8 years, approximately ~2 h of driving per day [15]. Also, hydrogen consumption vary depending on speed, vehicle mass *etc.* from 0.8 to 1.33 kg per 100 km [16]. Therefore, for the estimation it is used that hydrogen consumption is 1 kg per 100 km, spanlife of 8 years, and ~23.000 km per year. Consequently the average yearly consumption of hydrogen per car is assumed to be ~230 kg. From Fig. 4, it can be seen that the number of FCEV ranges from ~100.000 for 5% to ~300.000 units for 15% of the usage of RES potentials.

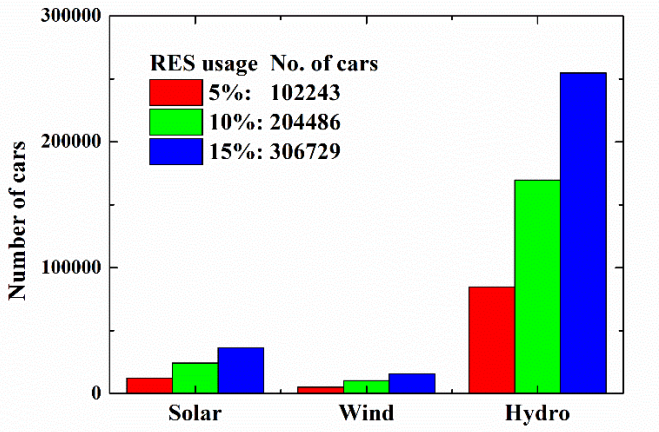

Figure 4. The rough estimation of numbers of fuel cells electric vehicles per year.

One other technology will be of interest in the future-biomass gasification combined with steam reforming [17,18 ,19 ,20]. A simplified example of a gasification reaction by partial oxidation of cellulose and lignocellulose is given by the following equation [**Error! Bookmark not defined.**]:

$$(C_6H_{10}O_5)_n + 2.5nO_2 \rightarrow 3nCO + 3nCO_2 + 5nH_2 + \text{other compounds}$$

Carbon monoxide can further reacts with water vapor (WGS-*water gas shift reaction*) and converts into more hydrogen and carbon dioxide:

$$CO + H_2O \rightarrow CO_2 + H_2 + \text{small amount of heat}$$

Actual biomass has a very variable composition and complexity with cellulose as one of the main components, so the reaction products can also differ significantly [**Error! Bookmark not defined.**]. S uch processes do not produce pure hydrogen, but in combination with solid oxide fuel cells [**Error! Bookmark not defined.**], which operate above 650^{o}C, could be used for the simultaneous generation of electricity and heat with high efficiency [21], as schematically shown in Fig. 5. Avaiable biomass resurces in Republic of Serbia could be found at [22]

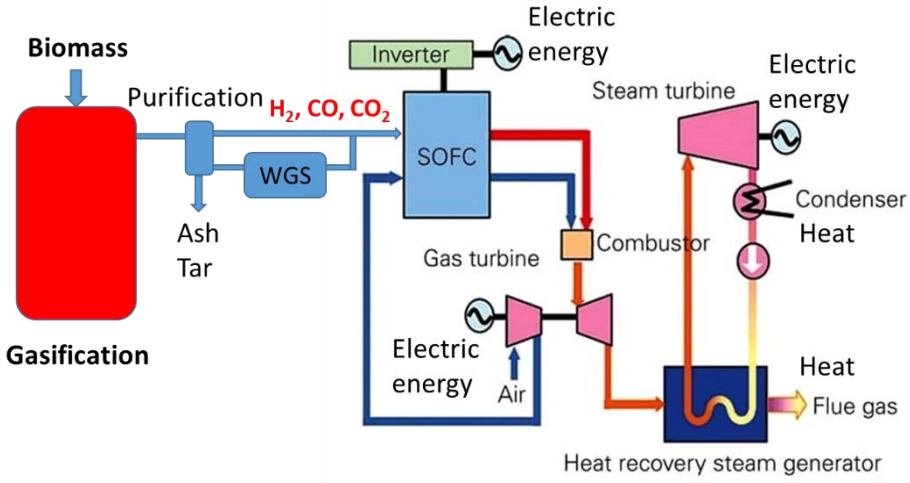

Figure 5. *Schematic principles of simultaneous production electric and heat energy by the combination of biomass gasification and solid oxide fuel cell.*

Conclusions

Based on the publicly available technical potentials of renewable energy sources in the Republic of Serbia, the possibility of green hydrogen production from solar, wind, and hydro potentials are roughly estimated. It is shown that using 5%, 10% and 15% of total available technical RES potentials the mass of hydrogen produced by water alkaline electrolysis varies from 23.5 kt to 70.5 kt. The mass of hydrogen is converted to volume and the substitution of natural gas (methane) by hydrogen ranging from 10% to 30% is estimated. Also, it is estimated that on a yearly basis the number of FCEV ranges from ~100.000 for 5% to ~300.000 units for 15% of the usage of RES potentials. It should be noted that the presented results are only rough estimations, and with the furthermore studious determination of the real technical available potentials of the renewable energy sources in the Republic of Serbia, this data can be much higher. It is also noticed that in the future hydrogen obtained from biomass by different technological processes should be intensified.

Acknowledgment

This work was supported by the Ministry of Education, Science and Technological Development of the Republic of Serbia (Contract No. 451-03-47/2023-01/200135)

References

1. LJ. R Nunes, M. F. Dias, Perception of climate change effects over time and the contribution of different areas of knowledge to Its understanding and mitigation, *Climate*, **10(1)**, 7, 2022.
2. C. Stiller, H. Hochrinner, "Use of conventional and green hydrogen in the chemical industry,“ in *Hydrogen and Fuel Cell*, J. Töpler, J. Lehmann, Eds. Berlin, Heidelberg, Springer, 2016, 173–186,
3. B. Parkinson, M. Tabatabaei, D.C. Upham, B. Ballinger, C. Greig, S. Smart, E. McFarland, Hydrogen production using methane: Techno-economics of decarbonizing fuels and chemicals, *Int J Hydrog Energy*, **43(5)**, 2540-2555, 2018.
4. A. Midilli, H Kucuk, M. E. Topal, U. Akbulut, I. Dincer, A comprehensive review on hydrogen production from coal gasification: Challenges and opportunities, *Int J Hydrog Energy*, **46(50)**, 25385-25412, 2021.
5. The Future of Hydrogen Report prepared by the IEA, for the G20, Japan, Seizing today’s opportunities, (2019). [Online] Available: https://www.iea.org/reports/the-future-of-hydrogen
6. K. A. Adeyeye, N. Ijumba, J. Colton, The effect of the number of blades on the efficiency of a wind turbine, *IOP Conf. Ser.: Earth Environ. Sci*., **801**, 012020, 2021.
7. N. S. Lewis, Introduction: Solar Energy Conversion, *Chem. Rev.*, **115(23)**, 12631–12632, 2015.

8. Å. Killingtveit. "Hydroelectric Power,"- Chapter 21 in: Future Energy (Second Edition), T. M. Letcher, Ed. Elsevier BV, 2014, 453-470.
9. IRENA, Green hydrogen cost reduction: Scaling up electrolysers to meet the 1.5^{0}C climate goal. International Renewable Energy Agency, Abu Dhabi. (2020). [Online] Available: https://www.irena.org/publications/2020/Dec/Green-hydrogen-cost-reduction
10. B. Lee, H. Lee, H.-S. Cho, W.-C. Cho, C.-H Kim, H. Lim, Projected economic outlook and scenario analysis for H_2 production by alkaline water electrolysis on the basis of the unit electricity price, the learning rate, and the automation level, *Sustain. Energy Fuels*, **3**, 1799-1807, 2019.
11. Serbian Chamber of Commerce, Green Energy. [Online] Available: http://www.zelenaenergija.pks.rs/ZelenaEnergija.aspx?idjezik=3
12. A. Aniello, T. Poinsot, L. Selle, T. Schuller, Hydrogen substitution of natural-gas in premixed burners and implications for blow-off and flashback limits, *Int. J. Hydrog. Energy*. **47(77)**, 33067-33081, 2022.
13. R. Carlanescu, M. Enache, R. Maier, A. Alcea, R. Condruz, C. Stoica, M. Ghilvacs, Calculation of the main parameters involved in the combustion process of CH_4-H_2 mixtures at different proportions, 9th International Conference on Thermal Equipments, Renewable Energy and Rural Development (TE-RE-RD 2020), E3S Web Conf., **180**, 01013, 2020. https://doi.org/10.1051/e3sconf/202018001013
14. D. Candelaresi, A. Valente, D. Iribarren, J. Dufour, G. Spazzafumo, Comparative life cycle assessment of hydrogen-fuelled passenger cars, *Int. J. Hydrog. Energy*. **46(72)**, 35961-35973, 2021.
15. DOE Technical Targets for Fuel Cell Systems and Stacks for Transportation Applications. [Online] Available: https://www.energy.gov/eere/fuelcells/doe-technical-targets-fuel-cell-systems-and-stacks-transportation-applications
16. T. Selmi, A. Khadhraoui, A. Cherif, A. Fuel cell–based electric vehicles technologies and challenges. *Environ. Sci. Pollut. Res.*, **29**, 78121–78131, 2022.
17. T. Lepage, M. Kammoun, Q. Schmetz, A. Richel. Biomass-to-hydrogen: A review of main routes production, processes evaluation and techno-economical assessment, Biomass Bioenerg; **144**, 105920, 2021.
18. M. Binder, M. Kraussler, M. Kuba, M. Luisser (2019. Jan), Hydrogen from biomass gasification, Edited by R. Rauch Ed. 2018. *IEA Bioenergy*. [Online] Available: https://www.ieabioenergy.com/wp-content/uploads/2019/01/Wasserstoffstudie_IEA-final.pdf
19. Office of Energy Efficiency & Renewable Energy, Hydrogen Production: Biomass Gasification, Washington, DC, 2022. [Online] Available: https://www.energy.gov/eere/fuelcells/hydrogen-production-biomass-gasification
20. C. Ciliberti, A. Biundo, R. Albergo, G. Agrimi, G. Braccio, I. de Bari, I. Pisano. Syngas derived from lignocellulosic biomass gasification as an alternative resource for innovative bioprocesses. *Processes*, **8(12)**, 1567, 2020.
21. D. Oryshchyn, N. F. Harun, D. Tucker, K. M. Bryden, L. Shadle, Fuel utilization effects on system efficiency in solid oxide fuel cell gas turbine hybrid systems, *App. Energy*, **228**, 1953-1965, 2018.
22. Serbian Chamber of Commerce, Green Energy. [Online] Available: http://www.zelenaenergija.pks.rs/ZelenaEnergija.aspx?id=3&p=0&

Development and optimization of photoreactor prototype for the treatment of wastewater loaded with organic effluents

Nemanja Banić*

*University of Novi Sad Faculty of Sciences, Department of Chemistry, Biochemistry and Environmental Protection, Trg D. Obradovića 3, 21000 Novi Sad, Serbia, nemanja.banic@dh.uns.ac.rs**

Abstract

As a process for water purification, photochemical oxidation has numerous advantages over many existing technologies. The technique can result in the mineralization of pollutants rather than transferring them to an alternative phase, as with activated carbon adsorption. Since artificial radiation sources require much energy delivery, this method is recommended for toxic contaminants in a specific concentration range below the recommended levels for recovery and above the levels for conventional biological treatment. Selecting a radiation source and an oxidation system and determining key parameters are essential to treatment efficiency. Sufficient UV penetration into the radiated liquid/suspension is crucial, especially for an opaque environment; the UV radiation is only available very close to the UV lamp surface. High mass transfer rates for efficient interaction between the pollutant and the photocatalyst and for high oxygen uptake at the gas-liquid interface is another requirement for practical application. In the present study, a new batch-recirculated cascade reactor was used to investigate the degradation of thiacloprid from Calypso 480-SC commercial formulation by UVC radiation. This patent-protected photoreactor design combines the positive features of step and shallow pond photoreactors and can operate in batch or continuous mode. The degradation kinetics were monitored by HPLC–DAD. The photochemical degradation of thiacloprid (0.32 mM) was studied under various solution conditions by varying the initial concentrations of H_2O_2 from 0 to 162 mM and the pH from 2.8 to 10.0. In the UVC/H_2O_2 system, thiacloprid reacted rapidly, with maximum degradation efficiency observed at the H_2O_2/thiacloprid molar ratio of 141 and pH 2.8. Under these conditions, 82% of the thiacloprid was removed in about 30 min. Also, the influence of the type of catalyst (TiO_2, ZnO) in the presence/absence of H_2O_2 on the thiacloprid photodegradation efficiency was investigated. Finally, a comparison of the efficiency of different AOPs (UVC, UVC/H_2O_2, UVC/TiO_2, UVC/ZnO, UVC/H_2O_2/TiO_2, UVC/H_2O_2/ZnO, UVC/Fe^{2+}/H_2O_2, and Fe^{2+}/H_2O_2) in the photodegradation and mineralization of thiacloprid was revised. UVC/H_2O_2 at pH 7.2 proved the most efficient, wherein 100% thiacloprid was photodegraded and mineralized. In the cascade photoreactor, electrical energy consumption was 3.22 kWh.

Acknowledgements*: The author acknowledges the financial support of the Provincial Secretariat for Higher Education, Scientific and Research Activity of Vojvodina, Republic of Serbia (Project No. 142-451-2227/2022-01/01).*

Uranium - *Magnum Crimen*

Radomir Kovačević

Institut za medicinu rada Srbije "Dr Dragomir Karajović" Beograd, Deligradska 29

Abstract

In aggression against Federal Republic of Yugoslavia from March 24 to June 10, 1999, NATO Alliance used, along with various kinds of weapons, depleted-uranium (U238) ammunition with alpha radiation emission.

Contamination of environment by depleted uranium and its consequences will be long-standing and numerous, as the human health is being affected in the way that depleted uranium particles, brought into body, may cause varying harmful effects.

Detection and identification of these effects in population living adjacent to contaminated regions was the subject of our study.

The examined region was the south-east part of Serbia below 44th parallel, in broader region of Vranje, where high contamination levels of the soil, water, air and biosphere by depleted uranium and other radionuclides were detected as presented in UNEP Report, April 2002. The subjects consisted of 29 inhabitants from that region with mean age of 39.5 years.

High-specific tests were used to investigate internal contamination of subjects (alpha spectrometry as exposure marker) and characteristic sequels (biodosimetry as effect marker). The results obtained by gamma spectrometry of 24-hour urine revealed no higher activity what suggested the internal radionuclide contamination with gamma emission.

Alpha spectrometry of uranium isotope content in 24-hour urine was performed in 19 subjects (10 subjects failed to provide enough urine volumes). All tested urine samples showed the uranium concentrations ranging from 36 ng/L to 231 ng/L, except in one case in which the concentration was 3759 ng/L, i.e. 3.7 μg/L. U-234/U-238 isotope ratio in this person's urine was 0.21, what indicated the presence of depleted uranium in the urine. One more subject had the isotope ratio of 0.6, but due to high measurement uncertainty (40%) it could not be definitely concluded that depleted uranium was present in the urine. Typical U-234/U-238 isotope ratio in drinking water is 0.8-1.0, and levels deviating from such ratio suggest the presence of depleted uranium.

The analysis of genetic material of peripheral blood lymphocytes in 6 (20.7%) subjects revealed higher incidence of chromosome aberrations, and specific changes such as dicentric, ring chromosome and acentric fragments were noted. Non-specific changes were manifested in 10 (34.5%) subjects and the results were considered tolerable, since these changes are generally common even in people who are not exposed at all and they are considered reparable aberrations. Lower mitotic index was reported in 6 (20.7%) of subjects.

Based on the analysis of results of tested parameters, it may be concluded that examined environment has been contaminated by depleted uranium for a long time, and that internal contamination of population as well as early consequences to human population were determined using the specific effect markers. Accordingly, it is necessary to continue the initiated decontamination of the examined region and continual monitoring of environmental contamination level and health condition of an overall population.

***Key words**: NATO Alliance, aggression, depleted-uranium (U238), contamination, detection, alpha spectrometry, biodosimetry, chromosome aberrations, environment, population, health condition.*

Towards sustainable rare earth elements recovery

Ka održivom recikliranju elemenata retkih zemalja

Vesna S. Cvetković*

Department of Electrochemistry, Institute of Chemistry, Technology and Metallurgy, National Institute, University of Belgrade, Njegoševa 12, 11000 Belgrade, Serbia

*v.cvetkovic@ihtm.bg.ac.rs

Rare-earth elements (REEs) have become extremely important to our world of technology and their sustainable supply is necessary for the transition to the clean energy economy [1,2]. As a result, the push to increase REEs availability is necessary to manage the gap between demand and supply. To supplement the REEs production slated for electronic/electrical industrial sectors and to further help the protection of the environment, recycling of Nd and other REEs will have to become a significant source of these critical metals [3–5]. Consequently, considerable efforts have been invested in different approaches toward the recovery of these critical elements from REE-containing end-of-life (EOL) products [6]. Obstacles to reprocessing the complex scrap material left behind from end-of-life resources are the absence of infrastructure, and the lack of cost-effective recycling technologies for Nd, Pr and Dy metals recovery from recycled feedstock [3,4,7]. It is understandable then that, for the time being, the strategy which is required to complete complex REE recovery processes from EOL materials must be a combination of the known methods and adaptations of the available techniques. Efforts have been made to develop a complete recycling process for NdFeB magnets, producing raw materials for remanufacturing similar magnets and closing the recycling loop. To date, the feasibility and technical aspects of REE recycling still have not been systematically evaluated [5]. However, even with considerable efforts, REE recycling processes are still not commercially viable [3].

Thus, from the viewpoint of sustainability in the coming decades, an inexpensive and environmentally friendly recycling process of REEs will certainly play an important role. Numerous papers and conference proceedings have been published focusing on the features and conditions for the possible recycling facilities of RE elements from EOL magnets [6].

So far, various approaches to the REE separation technologies have been suggested: hydrometallurgical processing [1], liquid metal extraction [8], pyrometallurgical processing [9], molten salt electrolysis (MSE) [7,10–12]. The most promising method with a strong potential to satisfy the demands is the combination of pyrometallurgical processing of the EOL materials and subsequent molten salt electrolysis of the obtained products. One of the notable advantages of electrolysis is that the process itself and especially the purity of the final products can be well controlled.

Our contribution, made in joint research efforts of ICTM Institute, University of Belgrade with IME Institute, Aachen University, to the molten salt electrolysis within the field of recycling rare earth metals from end-of-life NdFeB magnets containing significant amounts of rare earth elements, was focused on the Nd-Pr alloy formation that could be fed directly back to the vacuum alloying step in the production of the new NdFeB magnets. In order to make extracting of individual rare earth metals for reuse in magnets or other materials economically viable, additional knowledge onto the electrodeposition of Nd and Pr from molten fluoride electrolyte had to be acquired. We started the investigation with the reaction mechanism of Nd electrodeposition, Fig. 1. [12,13], and continued with simultaneous electrodeposition processes of neodymium and praseodymium [10,11,14].

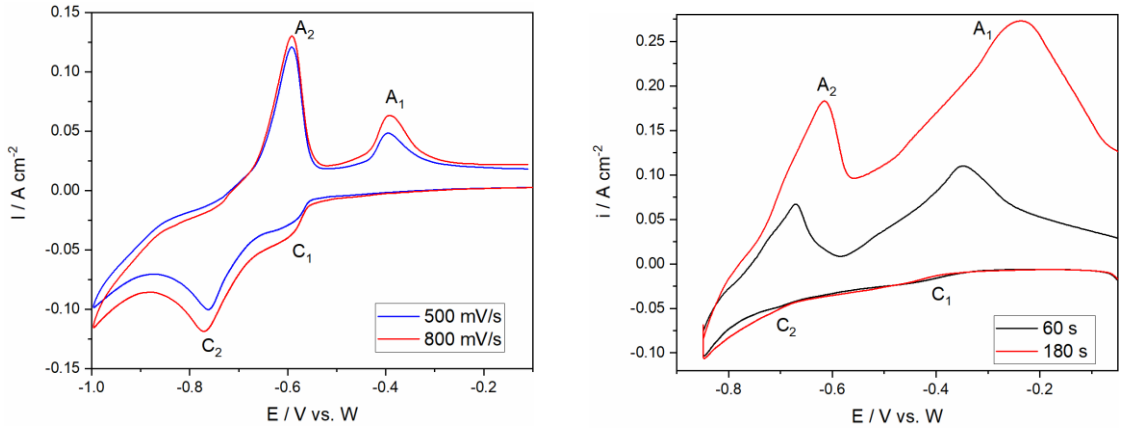

a) b)

Figure 1. *Cyclic voltammograms recorded on Mo cathode in 87.5 wt.% NdF_3 + 12.5 wt.% LiF + 2 wt.% Nd_2O_3 molten salt electrolyte, at 1323 K: (**a**) potential range from −0.100 V to −1.000 V vs. W scanned with different sweep rates; (b) Voltammograms obtained with different "holding times" (t = 60 and 180 s) at the cathodic end potential of the cycle E_F = −0.850 V vs. W, sweep rate = 100 mVs^{-1}.*

Our study was focused on the fundamentals underlying the electrochemical reduction of both Nd(III)/Nd(0) and Pr(III)/Pr(0) in the oxide-fluoride melt using tungsten (W) or molybdenum (Mo) working electrode, glassy carbon counter electrode (GC anode) and W reference electrode. The electrochemical reduction process of Nd(III) ions in the systems investigated has been identified as a two-step process via Nd(II). Actually, neodymium Nd(III) ions were electrochemically reduced in two consecutive steps: $Nd(III) + e^- \rightarrow Nd(II)$ (reflected by the cathodic current wave C_1 on CV, Fig.1. a) and b)) and $Nd(II) + 2e^- \rightarrow Nd(0)$, (ascribed to the cathodic current wave C_2 on the CV from Fig. 1. a) and b)). As soon as the first amounts of Nd metal were electrodeposited on the working electrode, the following disproportionation (comproportionation) reaction takes place with the electrolyte and leads to [10–13]:

$$2Nd(III) + Nd \rightarrow 3Nd(II) \quad (1)$$

Under the same conditions, praseodymium electrodeposition is a single step process $Pr(III) + 3e^- \rightarrow Pr(0)$ (ascribed to the cathodic current wave C_3 on the CV, Fig.2.) following the neodymium deposition [10,11]. Detailed studies of the Nd and Pr cations redox transitions to their metal forms during electrodeposition from fluoride based molten salt enriched with REO revealed that electrochemical steps are under mixed control: by ion mass transfer and charge transfer rate involving the decomposition of their ligand shells.

After initial results, our aim was to achieve better deposition efficiency by increasing the quantity of neodymium and praseodymium metal remaining on the working electrode surface after the deposition, to improve control of the electrodeposition process and to reduce the greenhouse gas emission during electrolysis. To make this possible, a ternary phase diagram was constructed for the liquidus temperatures of the chosen fluoride based molten salts, NdF_3 + PrF_3 + LiF [11]. This step was necessary to obtain an improved prediction of the optimal electrolyte constitution, and to avoid issues related to inappropriate composition and high melting temperatures of the mixture required for the process realization.

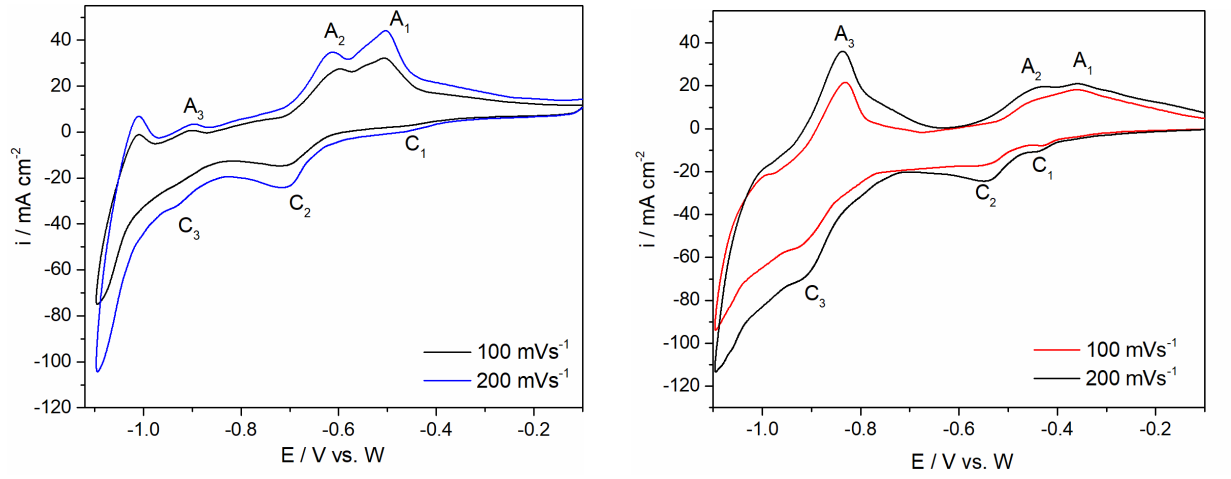

a) b)

Figure 2. *Cyclic voltammograms recorded on W working substrate starting from initial potential E_I = −0.100 V to final cathodic end potential E_F = −1.100 V vs. W. Voltammograms were obtained with different sweep rates at 1323 K in 45.5 wt.% NdF_3 + 45.5 wt.% PrF_3 + 9 wt.% LiF electrolyte containing different RE oxide concentrations added: (a) 1 wt.% Nd_2O_3 + 1 wt.% Pr_6O_{11}; (b) 2 wt.% Nd_2O_3 + 2 wt.% Pr_6O_{11}.*

To address the suitability of the chosen electrolyte, system chemical composition and optimal process conditions, the concentration of the REO added to the fluoride based NdF_3 + PrF_3 + LiF electrolyte was varied in order to precisely determine the adjustable parameters, Table 1.
Obtained results were encouraging. The electrodeposition mechanism for each RE (Nd and Pr) was identified, and the deposition efficiency of each element was improved, Figures 3. and 4.

Table 1. Electrolyte composition

Electrolyte	Components	Weigh percentage (wt.%)	REO content (wt%)		Literature
			Nd_2O_3	Pr_6O_{11}	
E-1	NdF_3	87.5	2	-	
	LiF	12.5			[12,13]
E-2	NdF_3	63.17	1	1	
	LiF	12.02	2	2	[10]
	PrF_3	20.96			
E-3	NdF_3	45.5	0.5	0.5	[11]
	LiF	9.0	1	1	
	PrF_3	45.5	2	2	

EPMA mapping of the sample's cross-section after Nd and Pr co-deposition revealed that most of neodymium and praseodymium metals were distributed in the area next to the working electrode substrate, Figs. 3.a) and b).
This area represents a thin layer of Nd and Pr metals, approximately 40 mas % neodymium and 40 mass % Pr, deposited on the electrode surface. In these areas, oxygen and fluoride were present in the lowest recorded concentrations, Fig. 3.c).

Continuing the series of fundamental studies on Nd and Pr co-deposition from the fluoride melts, allowed us to build experimental and theoretical knowledge, which would allow to forecast the viability of extracting rare earth metals from end-of-life NdFeB magnets.

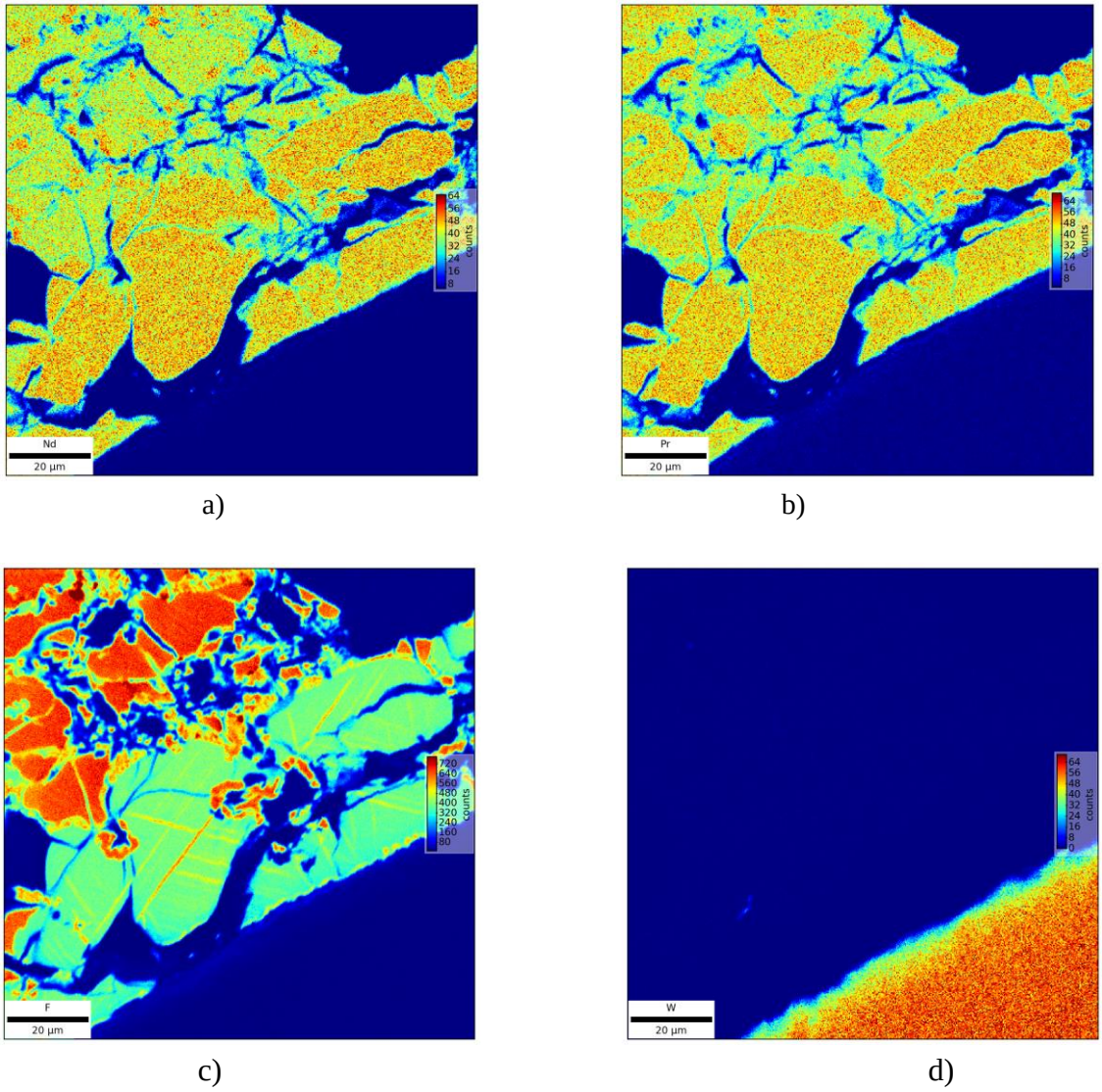

a) b)

c) d)

Figure 3. *EPMA mapping of the sample after deposition at – 0.900 V vs. W on a W cathode from molten 45.5 wt.% NdF_3 + 45.5 wt.% PrF_3 + 9 wt.% LiF + 0.5 wt.% Nd_2O3 + 0.5 wt. %Pr_6O_{11} electrolyte for 240 min. at 1323 K, showing distribution: (a) Pr; (b) Nd; (c) F; (d) W.*

Additionally, scanning electron microscopy (SEM) revealed insight into the deposited material and energy dispersive spectroscopy (EDS) confirmed the presence of Nd and Pr metals on the working electrode substrate. The weight % of all elements in the deposit detected by EDS analysis are summarized in Table 2.

Table 2. Elemental analysis (in weight %) of the electrodeposits obtained.

Elements in weight %						
	O	F	Pr	Nd	W	Total
Spectrum 1	4.77	25.51	28.78	29.72	11.21	100
Spectrum 2	5.48	24.78	34.30	35.45	-	100

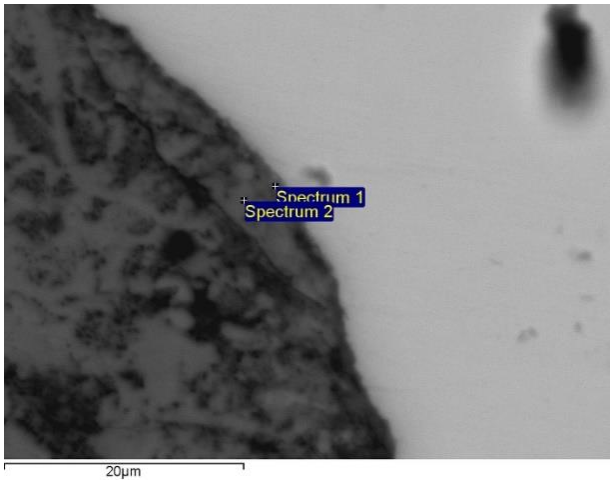

a)

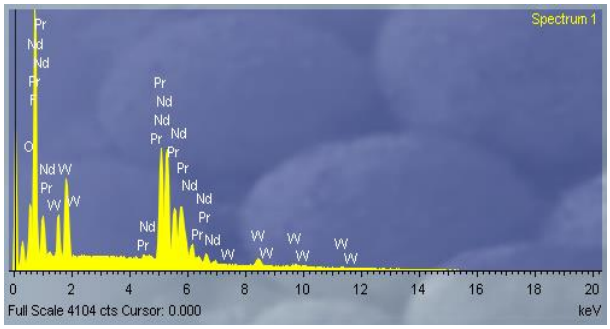

b)

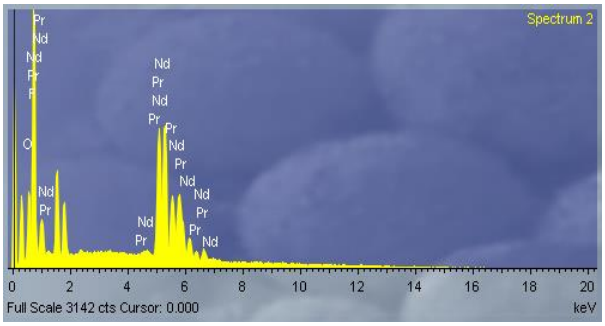

c)

Figure 4. *a) SEM micrographs of deposits obtained by electrodeposition at – 0.900 V vs. W on a W cathode from molten 45.5 wt.% NdF_3 + 45.5 wt.% PrF_3 + 9 wt.% LiF + 0.5 wt.% Nd_2O_3+0.5 wt.% Pr_6O_{11} electrolyte, for 240 min. at 1323 K; b) and c) EDS spectra of the deposit obtained.*

Two general steps in this process of recycling rare earth metals are, the production of magnet recycling-derived oxide (MRDO) followed by molten salt electrolysis. It is important to note that these two steps are integrated. The proposed process uses the advantage of the obtained REE alloy metallic phase which consists of the REE and iron ready to be further used directly in the NdFeB magnet production.

We prepared MRDO from the spent NdFeB-magnets in two steps [9,15]. First step was oxidation of the spent NdFeB magnets into mixed rare earth, iron, boron… oxide containing form [15]. In the second step, by using the reductive smelting process, a substantial amount of iron present in the metal phase was removed from the oxidized magnets [9]. At the end of reductive smelting step, the ICE-OES and XRD analysis were conducted on both phases. According to those analyses, the metal phase showed a maximum Fe content of 92.3 wt.%, while the slag phase (MRDO) showed a maximum total REE (Nd, Pr, and Dy) content of 47.47 wt.%, both obtained at a smelting temperature of 1773 K [9].

To complete the process of recycling the NdFeB magnet, MRDO was used as a source of the rare earth oxides in fluoride-based baths during the molten salt electrolysis process [16]. Under the applied conditions, Nd and Pr were electrodeposited in metal form from the electrolyte composed of rare earth oxides present in the MRDO dissolved in the corresponding rare earth fluoride salts [16].

Although there are many parameters that should be addressed for a direct implementation of this method on an industrial scale, with this particular approach we confirmed the viability of using

MRDO in the electrolysis as a part of fluoride molten salt electrolyte and finally established the route for recycling rare earth elements from used magnet scrap.

Finally, in an effort to develop a more efficient electrochemical deposition process, we chose low-deposition overpotential to suppress greenhouse gas emissions and to achieve high-purity Nd and Pr metal production on the working substrate [10–13].

Acknowledgements: Most of the results achieved and the results presented here would be difficult to produce without the cooperation of my colleagues: ICTM - Prof. Jovan Jovićević and Dr Nataša Petrović, and IME Institute - Prof. Bernd Friedrich, Dr Ksenija Milicevic Neumman and MSc Dominic Feldhaus. The author acknowledges the financial support via the bilateral research projects (ID: 451-03-01971/2018-09/4; ID: 451-03-01344/2020-09/8 and ID: 337-00-19/2023-01/5), supported by the Ministry of Education, Science and Technological Development of the Republic of Serbia and German Academic Exchange Service (DAAD). Dr Vesna S. Cvetković acknowledges the financial support for the investigation received from Ministry of Science, Technological Development and Innovation of Republic of Serbia (Contract No: 451-03-47/2023-01/200026).

References

1. I. Makarava, A. Kasach, D. Kharytonau, I. Kurilo, M. Laatikainen, E. Repo, Enhanced acid leaching of rare earths from NdCeFeB magnets, *Miner. Eng.*, **179,** 107446, 2022. https://doi.org/10.1016/j.mineng.2022.107446.
2. K. Binnemans, P. T. Jones, B. Blanpain, T. Van Gerven, Y. Yang, A. Walton, M. Buchert, Recycling of rare earths: a critical review, *J. Clean. Prod.*, **51**, 1-22, 2013. https://doi.org/10.1016/j.jclepro.2012.12.037.
3. Y. Fujita, S. K. McCall, D. Ginosar, Recycling rare earths: Perspectives and recent advances, MRS Bull., **47**, 283–288, 2022. https://doi.org/10.1557/s43577-022-00301-w.
4. V. Balaram, Rare earth elements: A review of applications, occurrence, exploration, analysis, recycling, and environmental impact, *Geosci. Front.*, **10,** 1285–1303, 2019. https://doi.org/10.1016/j.gsf.2018.12.005.
5. Y. Yang, A. Walton, R. Sheridan, K. Güth, R. Gauß, O. Gutfleisch, M. Buchert, B.-M. Steenari, T. Van Gerven, P.T. Jones, K. Binnemans, REE Recovery from End-of-Life NdFeB Permanent Magnet Scrap: A Critical Review, *J. Sustain. Metall.*, **3,** 122–149, 2017. https://doi.org/10.1007/s40831-016-0090-4.
6. M. Firdaus, M. A. Rhamdhani, Y. Durandet, W. J. Rankin, K. McGregor, Review of High-Temperature Recovery of Rare Earth (Nd/Dy) from Magnet Waste, *J. Sustain. Metall.*, **2,** 276–295, 2016. https://doi.org/10.1007/s40831-016-0045-9.
7. Y. Yang, C. Lan, L. Guo, Z. An, Z. Zhao, B. Li, Recovery of rare-earth element from rare-earth permanent magnet waste by electro-refining in molten fluorides, *Sep. Purif. Technol.*, **233**, 116030, 2020. https://doi.org/10.1016/j.seppur.2019.116030.
8. T. Akahori, Y. Miyamoto, T. Saeki, M. Okamoto, T. H. Okabe, Optimum conditions for extracting rare earth metals from waste magnets by using molten magnesium, *J. Alloys Compd.*, **703**, 337–343, 2017. https://doi.org/10.1016/j.jallcom.2017.01.211.
9. H. Chung, S. Stopic, E. Emil-Kaya, S. Gürmen, B. Friedrich, Recovery of Rare Earth Elements from Spent NdFeB-Magnets: Separation of Iron through Reductive Smelting of the Oxidized Material (Second Part), *Metals*, **12,** 1615, 2022. https://doi.org/10.3390/met12101615.
10. V. S. Cvetković, D. Feldhaus, N. M. Vukićević, T. S. Barudžija, B. Friedrich, J. N. Jovićević, Electrochemical Study of Nd and Pr Co-Deposition onto Mo and W from Molten Oxyfluorides, *Metals*, **11,** 1494, 2021. https://doi.org/10.3390/met11091494.
11. V. S. Cvetković, D. Feldhaus, N. M. Vukićević, K. Milicevic-Neumann, T. S. Barudžija, B. Friedrich, J. N. Jovićević, Influence of Rare Earth Oxide Concentration on Electrochemical Co-Deposition of Nd and Pr from NdF_3-PrF_3-LiF Based Melts, *Metals*, **12**, 1204, 2022. https://doi.org/10.3390/met12071204.
12. V. S. Cvetković, N. M. Vukićević, D. Feldhaus, T. S. Barudžija, J. Stevanović, B. Friedrich, J. N. Jovićević, Study of Nd Deposition onto W and Mo Cathodes from Molten Oxide-Fluoride Electrolyte,

Int. J. Electrochem. Sci., **15,** 7039–7052, 2020. https://doi.org/10.20964/2020.07.82.

13. V.S. Cvetković, D. Feldhaus, N.M. Vukićević, T.S. Barudžija, B. Friedrich, J.N. Jovićević, Investigation on the electrochemical behaviour and deposition mechanism of neodymium in NdF3–LiF–Nd_2O_3 melt on Mo electrode, *Metals*, **10**, 576, 2020. https://doi.org/10.3390/met10050576.
14. V. S. Cvetković, D. Feldhaus, N. M.Vukićević, N. D. Nikolić, B. Friedrich, J. N. Jovićević, Electrodeposition of Nd and Pr onto W from fluoride based melts, *Proceedings of the XXII YuCorr International Conference on Meeting Point of the Science and Practice in the Fields of Corrosion, Materials and Environmental Protection*, Tara, Serbia, 2021, 157–160.
15. S. Stopic, B. Polat, H. Chung, E. Emil-Kaya, S. Smiljanić, S. Gürmen, B. Friedrich, Recovery of Rare Earth Elements through Spent NdFeB Magnet Oxidation (First Part), *Metals*, **12**, 1464, 2022. https://doi.org/10.3390/met12091464.
16. H. Chung, L. Prasakti, S. Stopic, D. Feldhaus, V. S. Cvetković, B. Friedrich, Recovery of Rare Earth Elements from Spent NdFeB Magnets: Metal Extraction by Molten Salt Electrolysis (Third Part), *Metals*, **13**, 559, 2023. https://doi.org/10.3390/met13030559.

INVITED LECTURES
PREDAVANJA PO POZIVU

Review of the Anticorrosive Contribution of Nanotechnologies and Nanostructured Materials Based on LHO

Prikaz antikorozivnog doprinosa nanotehnologija i nanostrukturnih materijala na bazi LHO

Jovan P. Šetrajčić*

Academy of Sciences and Arts of the Republic of Srpska, Bana dr T. Lazarevića 1, Banja Luka, Republic of Srpska – B&H

*jovan.setrajcic@gmail.com

Abstract

In the last few years, layered double hydroxide (LDH) has been highly developed in the field of corrosion protection of materials, based on its special characteristics, which include extraordinary anion exchange ability, increased anion capacitance, as well as barrier resistance and an evident structural memory effect. This paper includes a review of very recent works on the properties of LDH in powder and film form and preparations based on LDH for applications in the protection of materials from corrosion in various environments.

Keywords: *nanotechnology; nanomaterials; corrosion protection; LDH; ultrathin film-coating; anion exchange*

Izvod

U nekoliko poslednjih godina slojeviti dvostruki hidroksid (LDH) je veoma razvijen u oblasti zaštite materijala od korozije, a na osnovu njegovih posebnih karakteristika, koje uključuju vanrednu sposobnost razmene anjona, povećanom anjonskom kapacitivnošću, te i barijernom otpornošću i evidentnim efektom strukturne memorije. Ovaj rad obuhvata pregled sasvim nedavnih radova o svojstvima LDH u obliku praha i filma i preparatima na bazi LDH za primenu u zaštiti materijala od korozije u različitim sredinama.

Ključne reči: *nanomaterijali; zaštita od korozije; LDH; ultratanki film-prevlaka; anjonska razmena*

Uvod

Nedavna nanotehnološka dostignuća omogućila su nove inovacije u zaštitnim nanokompozitima – premazima za antikorozivne, anti-obrastajuće i samozarastajuće nasluge na materijalnim površima. Nanotehnologija obuhvata istraživanje, proizvodnju i primenu arhitekture nanočestica, cevastih struktura, listova ili ploča veličine ispod 100 nm u barem jednoj dimenziji [1]. Uključivanje nano-čestica u organske celine pokazalo je poboljšana svojstva neophodna za postizanje estetike, antikorozije, termičku stabilnost za performanse na visokim temperaturama, mehaničku čvrstoću koja je neophodna za otpornost na starenje i eroziju premaza u teškim uslovima, nano-arhitektonsko umrežavanje sposobno da efikasno ometa prodiranje korozivnih i biološki obraštajućih entiteta. Sve ovo je vrlo obećavajuće za nastajanje ključnih napredaka u inoviranim tehnikama u razvoju nanoskopski tankih premaza za primenu u ambalažnoj, vazduhoplovnoj i automobilskoj industriji, biomedicini, pomorskoj i naftnoj i gasnoj industriji za postizanje superiorne zaštite od obrastanja, antikorozije, sa efektima ponašanja samoizlečenja na kritičnim materijalnim površima. Dakle, nanomaterijali su omogućili modifikaciju (nano)prevlaka za efikasno suzbijanje korozije, prljanja i grebanja metalnih materijala, pored postizanja samozalečenja (nano)premaza u različitim arhitekturama i različitim uslovima iz okruženja, sa svim pratećim prednostima.

Nanomaterijali se javljaju kao bezdimenzioni entiteti – nanočestice, jednodimenzioni entiteti – nanožice, nanošipke i nanocevi ili kao dvodimenzioni entiteti u obliku nanoslojeva, nanofilmova, nanolimova i nanopločica. Nanomaterijali pokazuju poboljšana fizičko-hemijskog ponašanja i osobina, posebno elektronskih, optičkih, mehaničkih, termičkih i magnetnih [2]. Ova ponašanja se uglavnom pripisuju njihovim veoma malim dimenzijama koje omogućavaju višu površinsku jedinicu zapremine, a radi povećanja efektivne interakcije. Nanomaterijali pokazuju izvanredne izglede za minimiziranje stepena korozije na metalnim površima putem površinske modifikacije – korišćenjem nanokristalnih strukturnih premaza. Slika 1 šematski objašnjava dimenzionu klasifikaciju nanomaterijala, dok slika 2 šematski objašnjava primene nanomaterijala u različitim vitalnim oblastima.

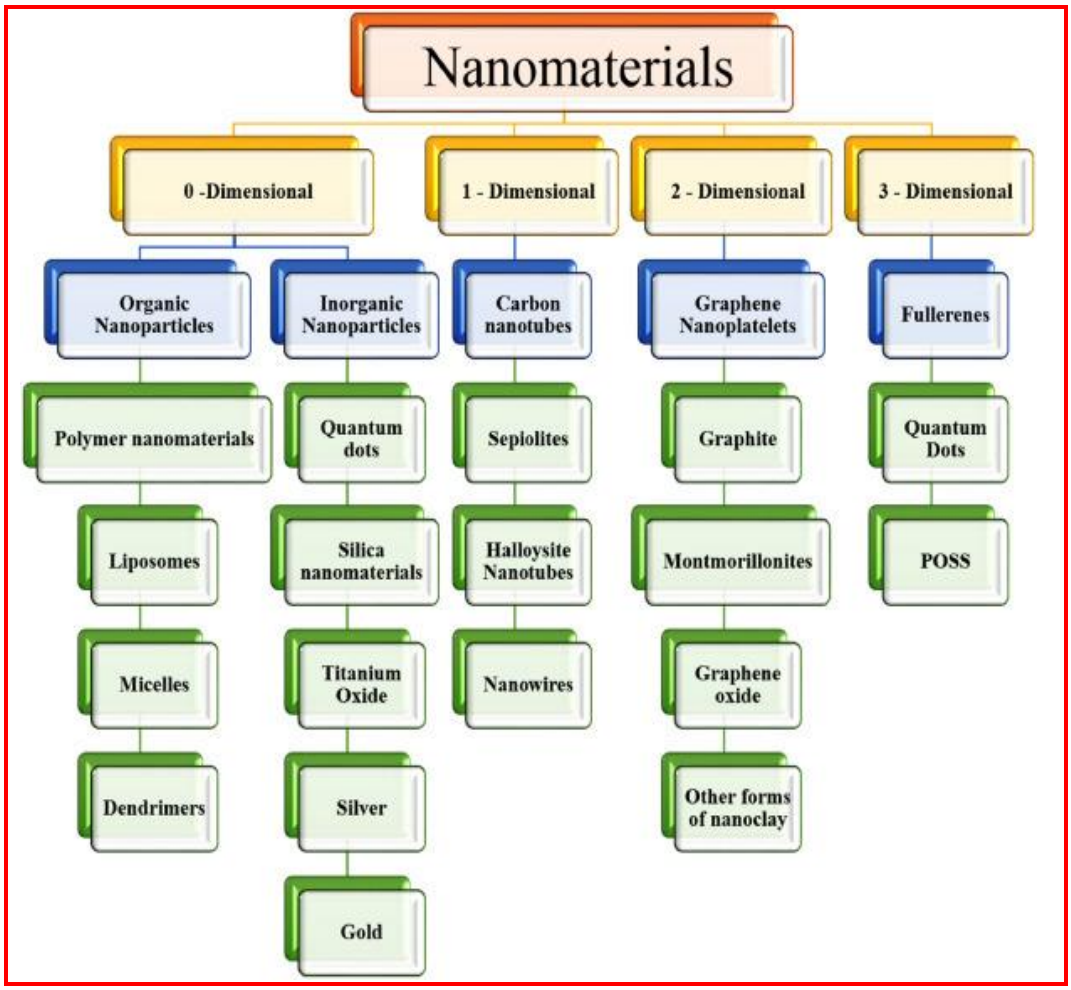

Slika 1. *Klasifikacija vrsta nanomaterijala (iz [3])*

Različiti nanopremazi su se pokazali vrlo efikasnim u smanjenju negativnih efekata korozije. Najčešće se koriste nanopremazi-prevlake koji sadrže sastojke bilo na nanoskopskom nivou, ili čija se konstitucija sastoji od listova ili slojeva debljine ispod 100 nm. Dimenzije ili veličine nanomaterijala, pored njihove veoma velike slojne gustine, pojačavaju vezivanje i fizičko pokrivanje obložene površi. Nanopremazi se mogu naneti na unutrašnje i spoljašnje površi datog materijala u različitim temperaturskim opsezima, uključujući čak i ako su veoma glatke. Značajno je da uspešno korišćenje nanoprevlaka za sprečavanje ili ublažavanje prljanja, korozije i grebanja ili habanja, usled sposobnosti samozalečenja (koja se ostvaruje preko inherentne mikroarhitektonske poroznosti), koja pokazuje ometanje prodiranja stranih entiteta štetnih za datu površ. Uključivanje nanomaterijala u zaštitne premaze značajno poboljšava njihove performanse od barijerne zaštite.

Nanočestice koje ulaze u sastav nanoslojeva za zaštitu materijala izučavaju se više od dve decenije i postoji mnoštvo različith proizvoda. Međutim, tek u poslednjih par godina istraživački napori su krunisani adekvatnim rezultatima, izdvojene samo neke koje cenom i svojstvima zadovoljavaju svoju namenu. Među njima je svakako slojeviti dvostruki hidroksid (LHD) [4], kome će ovde biti usredsređena sva pažnja.

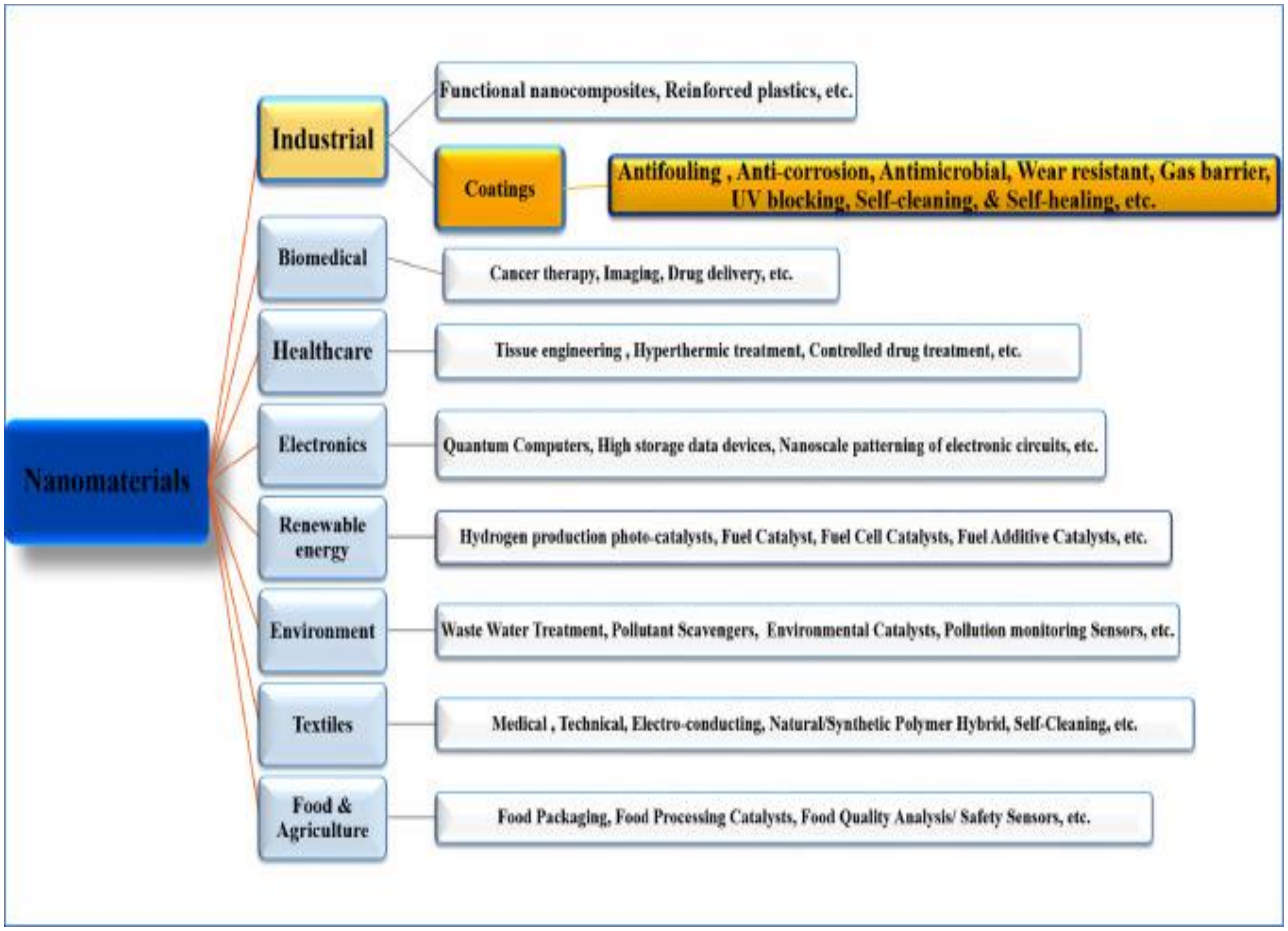

Slika 2. *Klasifikacija oblasti primene nanomaterijala (iz [3])*

Slojeviti dvostruki hidroksidi uspešno se primenjuju u površinskoj zaštiti i funkcionalizaciji metalnih materijala zahvaljujući svojoj posebnoj strukturi, sastavu, kontrolisanosti, anjonskoj razmeni i drugim izuzetnim svojstvima. Ovaj pregled fokusirao se na najčešće metode pripreme LDH na legurama magnezijuma sumirajući rezultate iz preko 50 istraživačkih radova. Istovremeno, na osnovu mehanizma zaštite od korozije pomoću LDH materijala, ukratko su predstavljene performanse LDH filmova i LDH kao punila na metalnim podlogama. Površ LDH materijala je hemijski modifikovana da bi se poboljšala njihova kompatibilnost sa rastvaračima, a njihova funkcija otpornosti na koroziju je razvijena kao aditiv. Konačno, razmatrani su kompozitni premazi zasnovani na LDH na legurama Mg prethodnom površinskom obradom i hemijskom modifikacijom.

Magnezijum (Mg) i njegove legure, poznate kao najlakši metalni konstrukcijski materijali, imaju široku primenu u računarskoj, elektronskoj, automobilskoj i vazduhoplovnoj industriji zbog svojih prednosti (uključujući nisku specifičnu težinu, visoku specifičnu čvrstoću i krutost, laku obradu i jednostavnu reciklažu) [5]. Korišćenjem legura magnezijuma ukupna masa automobila je smanjena za 10%, a gorivo je štedeno za oko 20% – 30% bez značajnih promena dizajna. Pored toga, modul elastičnosti legura magnezijuma je sličan onom kod ljudskog skeleta, koji može da ublaži spoljašnji stres i predstavlja glavnu komponentu veštačkih skeleta. Stoga, kao medicinski materijal, legure magnezijuma su idealni materijali za popravku hrskavice i za metalne implante. Iako legure magnezijuma imaju mnoga odlična svojstva, njihova lošija otpornost na koroziju zbog niskog

standardnog potencijala (−2,36 V) ograničila im je dalji razvoj i širu primenu [4]. U istraživanjima ovog problema, korišćeno je mnogo pristupa, uključujući legiranje, poboljšani proces toplotne obrade i naprednu tehnologiju površinske obrade. Među njima, tehnologija površinske obrade je najopsežnija i najefikasnija metoda, uključujući prevlake za hemijsku konverziju, polimerne premaze, mikrolučnu oksidaciju, filmove sloj po sloj i LDH premaze [6]. Poslednjih godina, LDH su zauzeli ključnu poziciju ne samo zbog ekološke prihvatljivosti i niske cene, već zbog njihove visoke sposobnosti anjonske razmene [7]. Kao rezultat toga, interkalirani materijali su pokazali široke izglede za primenu kao premazi otporni na koroziju.

Šta je LDH?

LDH je vrsta materijala sličnih hidrotalcitu, sastavljena od dva ili više metalnih elemenata, sa slojevitom strukturom hidroksida [8]. LDH se sastoji od pozitivno naelektrisanih mešanih slojeva jona metala $M^{3+}/(M^{2+}+M^{3+})$ hidroksida, anjona sa molekulima vode između slojeva. Kao što je prikazano na slici 3, opšta kristalna struktura LDH filmova je $[M^{2+}_{1-x}\,M^{3+}_{x}\,(OH)_2]^{x+}(A^{m-})_{x/m}\cdot nH_2O$, gde se M^{2+} odnosi na katjone metala (npr. Mg^{2+}, Zn^{2+}, Cu^{2+}, Ni^{2+}), M^{3+} označava trovalentni katjon (npr. Al^{3+}, Fe^{3+}, Cr^{3+}), x je molski odnos $M^{3+}/(M^{2+}+M^{3+})$, a A^{m-} je anjon sa m− valencijom [9]; dok su slojevi hidroksida prepuni molekula vode tokom sinteze. U osnovi, kristalna struktura, jačina veze i kapacitet izmene anjona LDH zavise od veličine i naelektrisanja metalnog katjona, naelektrisanja anjona i relativne količine kristalne vode [10].

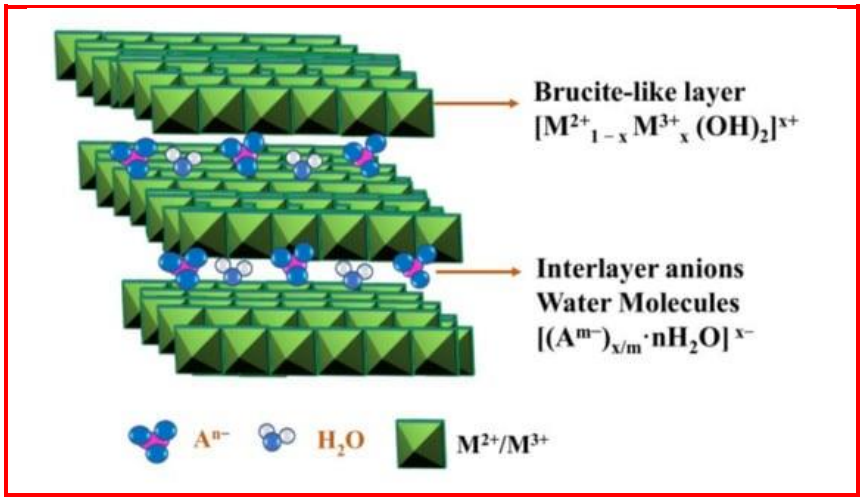

Slika 3. *Šematska ilustracija LDH strukture i njenih komponenti (iz [3])*

LDH imaju potencijalnu primenu u katalizi, funkcionalnim materijalima, zaštiti životne sredine i biomedicini zbog svog jedinstvenog memorijskog efekta i međuslojnog kapaciteta izmene anjona [10]. U poslednje vreme široko se koriste pripremljeni LDH premazi na legurama zbog širokog resursa sirovina, jednostavnih metoda sinteze i u velikim količinama, posebno na legurama magnezijuma i različitim tipovima LDH materijala, na dvostrukim jedinjenjenjima koje se sastoji od Mg–Al LDH i karbonata.

Sinteza LDH

Ko-precipitacija

Koprecipitacija (CPT) znači da se dve ili više vrsta rastvorljivih soli sa slojevitom strukturom metalnih jona ravnomerno mešaju u atmosferi azota, a odgovarajuće čvrste čestice se dobijaju reakcijom precipitacije sa odgovarajućem pH. CPT pristup je jedna od najatraktivnijih tehnika za pripremu LDH interkalacionih materijala od Mg, Al, Zn i drugih metala. Kombinacija CPT i hidrotermalne reakcije može da formira LDH prevlake različitih sistema, bez obzira na to kakav je

hemijski sastav supstrata, laminata i vrste anjona među slojevima [11]. Kao što je prikazano na slici 4, slojevi LDH su dobro kombinovani jedni sa drugima, a na interfejsu nisu pronađeni defekti. Primećeno je da su celi Mg–Al LDH premazi glatki i kompaktni, što poboljšava prijanjanje materijala podloge i prevlake/premaza.

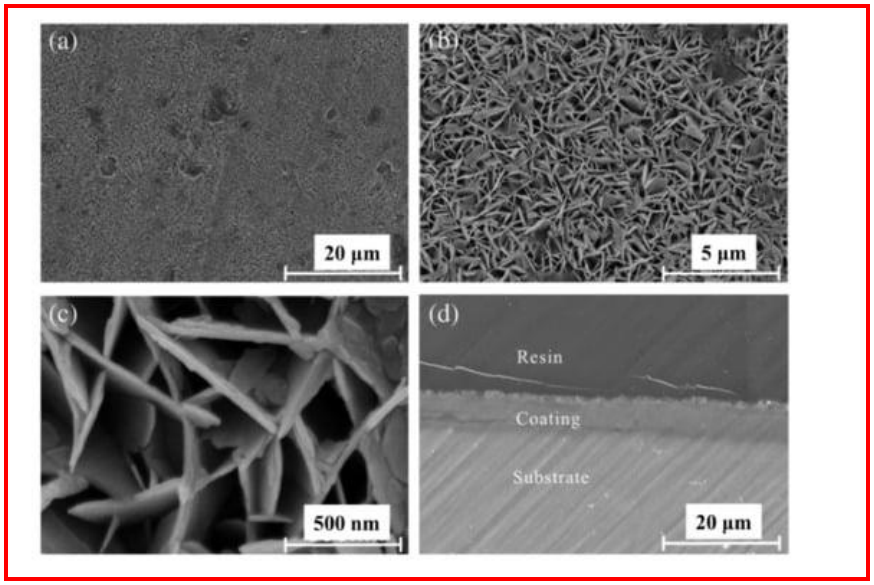

Slika 4. *(a–c) SEM slike LDH prevlake na Mg leguri sa različitim uvećanjima; (d) slike poprečnog preseka SEM (iz [4])*

U radu [12] predstavljena je priprema Mg–Al LDH prevlake sa poroznim organskim površinskim slojem integracijom tehnike koprecipitacije i metode hidrotermalne sinteze za proširenu primenu legura Mg. Pokazano je da se odgovarajućim dodavanjem poliglutaminske kiseline (PGA) može produžiti vreme korozije kompozitnog premaza kada pH dostigne minimalnu vrednost, tako da je otpornost na koroziju legure AZ31 poboljšana opisanim kompozitnim premazom na površi.
Generalno, istaloženi materijal treba da se zagreva nekoliko sati na 60–80 °C da bi se poboljšala kristalnost LDH. Međutim, metoda CPT se široko koristi u pripremi LDH praha zbog dugotrajnosti i loše adhezije između podloge i premaza, što nije pogodno za prevlake na metalnoj podlozi [13].

In-Situ metodi rasta

Metod rasta na licu mesta se odnosi na izbor specijalnog površinskog tretmana metalne ploče, koji direktno učestvuje u reakciji i katjonski obezbeđuje metal na metalnoj podlozi za tehnologiju formiranja filma. Smatra se da je ovo metod koja najviše obećava zbog dobre adhezije između LDH filmova i supstrata formiranog hemijskim vezama. Trenutno postoji pet metoda za *in-situ* sintezu rasta LDH filmova na Mg legurama.

Metod rasta na licu mesta u jednom koraku

Tehnika rasta in-situ u jednom koraku je obećavajući metod, jer može direktno sintetizovati LDH filmove na podlozi i značajno poboljšati mehanička svojstva i adheziju premaza na podlogu. U [14] je referisano da su Mg–Al LDH filmovi prvo fosforilisani na celuloznim mikrosferama (CM), a zatim pripremljeni in situ nano-rastom. Ovaj nalaz nudi novi pristup koji ne samo da može poboljšati proizvodnju i kristalnost Mg–Al LDH, već i poboljšati opterećenje Mg–Al LDH i poroznu strukturu CM. Na taj način Mg–Al LDH @CM su pogodni za superhidrofobni tretman. Kompozitni premaz: inhibitor (2-merkapto benzotiazol, MBT) u kombinaciji sa Mg–Al LDH premazima (Mg–Al LDH/MBT) na podlozi od legure AZ31 na relativno niskoj temperaturi (95 °C) i pritisku okoline, ispitan je [15] u jednom koraku tehnike rasta na licu mesta. Zatim je procenjena zaštita od korozije ovog premaza. Kao što je prikazano na slici 5, gustina struje korozije LDH/MBT kompozitnih

premaza je veoma niska, pa čak i nema korozionog ponašanja izloženog rastvoru NaCl ili okruženju slanog spreja tokom 15 dana, što ukazuje na vrlo dobru korozionu otpornost.

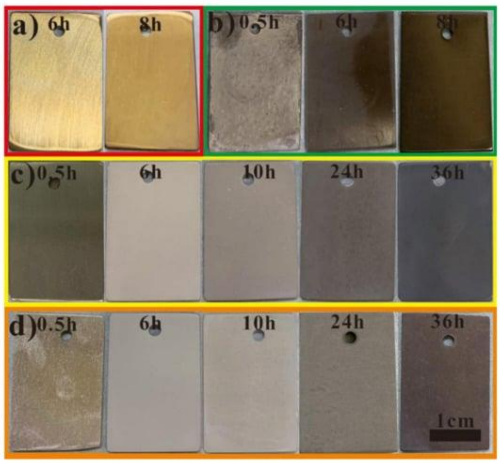

Slika 5. *Digitalne slike (a) prazne; (b) MBT; (c) Mg–Al LDH; i (d) Mg–Al LDHs/MBT filmovi sintetisani sa različitim vremenima reakcije na 95 °C i pritisku od 1 bara (iz [15])*

Mg–Al LDH premazi proizvedeni tehnikom rasta u jednom koraku na Mg legurama u stanju su da reše štetne efekte koje hidrotermalni metod izaziva na višim temperaturama i pod višim pritiscima.

Metod rasta na licu mesta u dva koraka

Metod rasta in-situ u dva koraka čine: *prethodni tretman* ugradnje jona u LDH prevlake i *naknadni tretman* za održavanje poravnanja dodavanjem rastvora NaOH. U [16] je zaključeno je da je ovaj pristup veoma pogodan i za druge legure Mg bez obzira da li sadrže Al elemente ili ne, sve dok su parametri procesa pravilno podešeni. Zbog toga se otpornost na koroziju većine legura Mg može poboljšati metodom rasta na licu mesta u dva koraka. Prema tome, ovim metodom može se dobiti gusta prevlaka pod uslovom kontrolisanja pH vrednosti, ali je proces oprilično komplikovan. U tehnici se supstrat uranja u rastvor soli metala, alkalije rastvora se dodaju da bi se kontrolisala pH vrednost, a metalni supstrat efektivno postaje metalni izvor reakcije, na kome raste film uz žrtvovanje dela supstrata. Stoga je ovaj metod pogodan samo za pripremu LDH filmova direktno na metalnoj matrici, ali ne i za pripremu LDH praha/čestica.

Hidrotermalni tretman

Metod hidrotermalne obrade odnosi se na LDH dobijen mešanjem metalnih oksida ili metalnih hidroksida sa alkalnim rastvorom u reaktoru visokog pritiska tokom određenog vremenskog perioda i pod određenim uslovima temperature i pritiska. Kao što je prikazano na slici 6, zatvorena poroznost LDH sloja i kapacitet apsorpcije hloridnih jona ograničavaju prodiranje korozivnog Cl^- i obezbeđuju efikasnu zaštitu od korozije za oksidni film premaza.

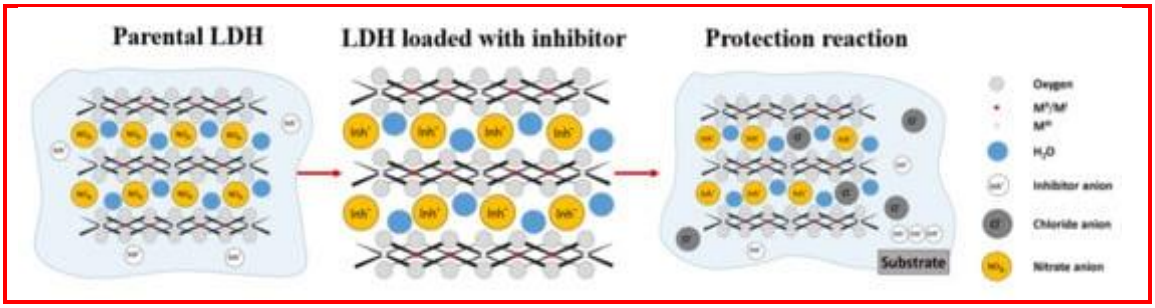

Slika 6. *Šematski prikaz strukture LDH, anjonske razmene sa inhibitornim jonom i njihovog aktiviranog oslobađanja radi zaštite od korozije (iz [17])*

LDH se ovde obično priprema stavljanjem dva mešana oksida u autoklav sa dejonizovanom vodom na 140 °C tokom nekoliko dana [17]. Shodno tome, prednosti hidrotermalne sinteze su potpuno kristalna struktura, očigledno slojevita struktura i ujednačena distribucija veličine zrna LDH.

Hidroliza uree

Urea je vrsta baze sa visokom rastvorljivošću u vodi; lako je kontrolisati brzinu hidrolize. Može da generiše amonijum hidroksid hidrolizom u vodi, dok CO_3^{2-} dobijen hidrolizom može da se koristi kao međuslojni anjon za sintezu LDH u alkalnoj sredini [18]. Kontrolom hidrotermalnih uslova sintetizovan je Mg–Al LDH na leguri Mg primenom reakcije hidrolize uree. Prednost ove metode je u tome što sintetisani LDH ima visoku kristalizaciju i veliku zapreminu. Utvrđeno je da nanostruktura i kapacitet izmene jona LDH mogu dramatično poboljšati zaštitu od korozije legure AZ31, ali da ima i tendenciju da proizvodi nusproizvode, a M^{2+} ili M^{3+} mogu da se konzumiraju tokom procesa formiranja nusproizvoda, smanjajući broj LDH u sledećim formacijama.

Naparavanje

Naparavanje je metoda pripreme antikorozivnog premaza od legure magnezijuma bez hemijske pare koristeći ultra čistu vodu kao izvor pare. Zaštitni Mg–Al LDH proizveden je na legurama magnezijuma putem hemijskog naparavanja, što je jednostavan, ekološki prihvatljiv i jeftin metod. Kao što je prikazano na slici 6, KSRD analiza pokazuje da su Mg–Al LDH filmovi uspešno pripremljeni. Eksperimenti sa korozijom takođe pokazuju da film ima dobar efekat zaštite podloge.

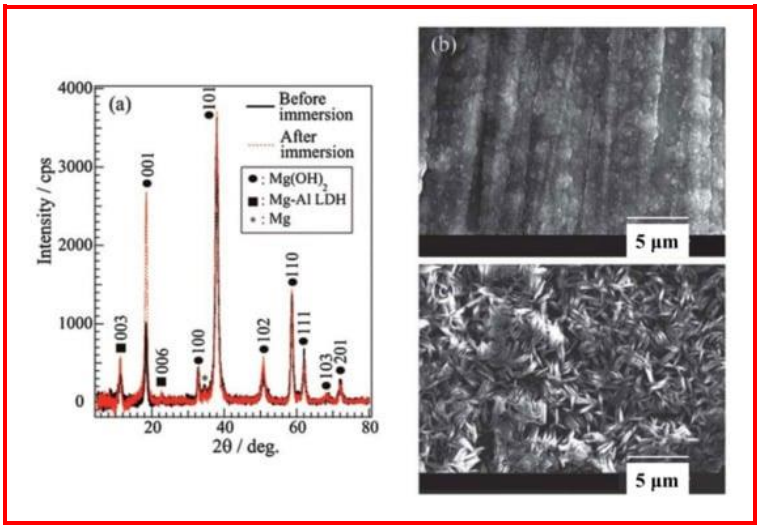

Slika 6. *(a) XRD uzorci sa različitim tretmanima, SEM grafika filmom obloženog AZ31 (b) pre i (c) posle potapanja (iz [4])*

Elektrohemijsko taloženje / depozicija

Elektrohemijsko taloženje se može posmatrati kao validan metod za proizvodnju LDH filmova, koji ima prednosti visoke čistoće, velike brzine taloženja i jednostavne opreme. Mg–Al LDH film sa nitratom je homogen i čvrst, tanji od Li-Al LDH filma, ali ima nekih malih nedostataka – pukotina [19]. Potenciodinamička polarizacija i EIS merenja su pokazala da je zaštita od korozije magnezijumske legure obložene LDH bolja od one legure magnezijuma bez prevlake.

Spining / Upredena prevlaka

Upredeni premaz je još jedan način pripreme regenerativnog glatkog filma, a prednosti ove metode su što je ekološki prihvatljiv, obezbeđuje odličnu adheziju između filma i podloge, ujednačeno formiranje filma i postiže dobru mikro-konkavnu i konveksnu strukturu na površi. LDH folije sa dobrom zaštitom od korozije i lepljenjem mogu se pripremiti jednostavnim postupkom. U [20] su kombinovali LDH filmove na leguri AZ31 Mg metodom rotacionog premaza koristeći vodeni rastvor kao izvor pare. Dobijena površina filma je ujednačena, a kriva elektrohemijske polarizacije filma

nakon nanošenja premaza u trajanju od 7 h pokazuje veoma nisku gustinu struje korozije, koja je mnogo niža od one kod legure magnezijuma AZ31 bez prevlake.

Anjonska izmena

Metoda izmene anjona potiče od intracelularne izmene anjona LDH, koja ne samo da održava originalnu lamelarnu strukturu LDH, već i bira tip intracelularnih anjona. Anjoni inhibicije korozije mogu se sporo isporučivati, a korozivni medijum se može adsorbovati, zahvaljujući ovako proizvedenim LDH, tako da je matriks dvostruko zaštićen. Kao što je prikazano na slici 7, može se videti da je površina matrice potpuno prekrivena zategnutom i iskrivljenom lamelom, premaz je gust, gladak i skoro da nema mikro-pukotina [21]. Ipak, ovaj metod je zahtevan i stepen kristalnosti LDH je manji nego kod prethodno navedenih metoda.

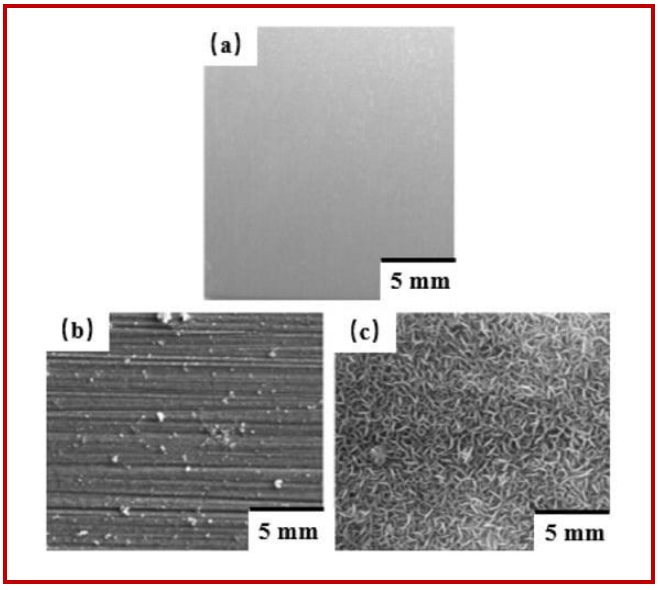

Slika 7. *Slike LDH filma: (a) optička mikrostruktura; (b) SEM slike sa malim uvećanjem i (c) velikim uvećanjem (iz [4])*

Anti-korozivni mehanizmi

Poslednjih nekoliko godina, LDH filmovi se smatraju sledećim potencijalnim premazima za legure magnezijuma zbog svoje stabilne lamelarne strukture i podesivih međuslojnih anjona, koji ne samo da mogu da obezbede zaštitu za metalnu matricu već i da apsorbuju korozivne jone. U [4] su veoma intenzivno istražena svojstva korozije i mehanizam otpornosti na koroziju LDH materijala.

Međuslojni mehanizam anjonske razmene

LDH su najbolje nanocevi za inhibitore korozije zbog svoje stabilne slojevite strukture, visoke efikasnosti, niske cene i jednostavnog rada. Dodavanje samo manjih količina hemijskih supstancija u tragovima korozivnom medijumu putem fizičke ili hemijske reakcije, može usporiti brzinu korozije metala i zadržati nepromenjena fizička, hemijska svojstva metala. Interlamelarna zamena anjona je važno svojstvo LDH, a njegovi anjoni mogu da se zamene različitim anjonima za dobijanje materijala sa različitim funkcijama.

Zahvaljujući sposobnosti izmene anjona između LDH slojeva, to postaje efikasan način za interkalaciju inhibitora korozije u zaštitni sloj sa lamelarnom strukturom kako bi se dobila visoka zaštita od korozije podloge. U [22] je objavljena priprema inhibitor korozije na leguri AZ31 Mg ubacivanjem asparaginske kiseline (ASP) u Mg–Al LDH hidrotermalnom metodom u jednom koraku. U rezultatu velike pokrivenosti poroznošću i lamelarne nanostrukture, Mg–Al–ASP LDH poprima vrlo-dobre performanse inhibicije korozije i dosta veću specifičnu površ za ubacivanje invazivnih

anjonskih vrsta kao što je Cl^-. Dakle, to je efikasan antikorozivni i ekološki premaz za konverziju lakih metala i legura.

Kompozitni sinergistički mehanizmi otpornosti na koroziju

Poslednjih godina, epoksidne smole na bazi vode izdvajaju se kao efikasni lepkovi i premazi na složenim podlogama zbog njihove dobre adhezije, stabilnih hemijskih svojstava i vrle korozione otpornosti. Međutim, u procesu očvršćavanja na visokim temperaturama, ove smole mogu da generišu brojne mikro-pore, što će omogućiti spoljnom korozivnom medijumu da prodre u materijal zaštitnog matriksa, što im ozbiljno ograničava širu primenu. Međutim, primećeno je da dodavanje LDH nanokontejnera u ZRE film može zahvatiti korozivni Cl^- i osloboditi odgovarajuće supstancije, tako da matrica od ugljeničnog čelika ima jače performanse inhibicije korozije. Drugo, zbog dvodimenzione slojevite strukture LDH, njihova struktura može blokirati neke šupljine u premazu, kako bi efikasno ograničila prodiranje korozivnih jona u film i poboljšala otpornost na koroziju materijala matrice.

Grafen može efikasno da spreči difuziju molekula kiseonika i vode na površinu metala zahvaljujući posebnoj slojevitoj strukturi. Sinergistički efekat dodavanja drugih nanomaterijala i jona inhibitora međusloja LDH u grafitne kompozite može poboljšati zaštitu od korozije LDH filmova. U [22] je referisano deponovanje grafenom modifikovanje LDH nanocefalnih filmova na površi legure Mg koristeći in situ metod u dva koraka. Ovi eksperimentalni rezultati su pokazali da modifikovani sloj grafena može zatvoriti pore LDH filmova u obliku gnezda, čineći da LDH filmovi imaju hidrofobnost (CA 127,8°) i time poboljšanu korozionu otpornost.

Trenutno je organski premaz jedan od najčešćih i najefikasnijih metoda za zaštitu metala. Inhibitor korozije se direktno meša sa organskim premazom koji dozvoljava korozivnim jonima spolja da uđu u metalnu matricu, pa čak i uzrokuju gubitak aktivnosti inhibitora korozije. Zbog specifičnosti slojevite strukture LDH i njegovih performansi izmene anjona, direktan kontakt između inhibitora i organske prevlake može se efikasno izbeći. Stoga, dodavanje inhibitora korozije kao što je LDH u organski premaz može efikasno povećati zaštitu premaza na površi metalnih materijala.

LDH modifikovani premaz na leguri magnezijuma

LDH rastu direktno na metalnoj podlozi formiranjem hemijskih veza kroz in situ tehnologiju rasta, tako da postoji jaka adhezija između LDH filmova i metalne matrice. S druge strane, upotreba in-situ rasta dovodi do poravnanja LDH okomito na supstrat, što uzrokuje različite kristalne orijentacije. Ova orijentacija filma je generalno povezana sa defektima kristalizacije i, sledbeno – formiranjem korozionih kanala. Zbog toga, da bi se maksimizirao vek trajanja otpornosti LDH filmova na koroziju, često se koriste anjonska razmena i modifikacija površine [23] da bi se dobila bolja koroziona otpornost i superhidrofobna svojstva.

Antikorozivna interkalirana struktura

LDH filmovi imaju dobru zaštitu od korozije zahvaljujući svom kapacitetu izmene anjona i posebnoj slojevitoj strukturi, koja usporava brzinu korozije legure Mg. U poređenju sa uobičajenim premazima, nanoploče LDH obično rastu okomito na površinu supstrata, a između slojeva ima mnogo pora, obezbeđujući puteve difuzije za razmenu anjona. Pored toga, različite anjonske interkalacione strukture mogu dati različite zaštite. Npr. u [24] je korišćen in situ hidrotermalni metod za rast Mg–Al LDH na površi legure AZ31, praćen reakcijama interkalacije vanadata za proizvodnju Mg–Al–$V_2O_7^{4-}$ LDH premaza, dok je u [25] proučavan Mg–Al LDH interkaliran sa CO_3^{2-} kao višestruki adsorbent sa kapacitetom izmene anjona, koji je korišćen za uklanjanje HCl, SO_2 i NO_x. Tabela 1 ilustruje karakteristične vrednosti antikorozionih parametara.

Tabela 1. *Potencijal korozije (E_{corr}), gustina struje korozije (I_{corr}) uzoraka u rastvorima NaCl (iz [25])*

Uzorak	Elektrolit	E_{corr} (V/SCE)	I_{corr} (μAcm^{-2})
CO_3·Mg–Al LDH	3.5 wt.% NaCl	− 0.805	1.13×10^{-7}
Cl·Mg–Al LDH		− 1.300	2.52×10^{-7}
NO_3·Mg–Al LDH		− 1.357	5.58×10^{-7}
V_2O_7·Mg–Al LDH		− 0.920	0.13×10^{-7}

Generalno, veći E_{corr} i manji I_{corr} mogu sprečiti koroziju u okviru termodinamičkih i kinetičkih uslova. Kao što tabela pokazuje, zaštita od korozije je sukcesivna u istom rastvoru natrijum hlorida: CO_3^{2-} > $V_2O_7^{4-}$ > Cl^- > NO_3^-. Među ovim premazima, primećeno je da je I_{corr} prevlaka MgAl–CO_3^{2-} LDH četiri reda veličine niža od MgAl–NO_3^- LDH premaza i do dva reda veličine niži od ostalih LDH premaza. Vredi napomenuti da u nekim visokotemperaturskim superprovodnim materijalima [26–28], tanki filmovi imaju jaču sposobnost prihvatanja hloridnih jona u korozionom rastvoru i time poboljšavaju zaštitu od korozije. Stoga su debljina i gustina premaza takođe ključni faktori koji utiču na otpornost na koroziju, jer mogu ograničiti direktan kontakt između matrice i korozivnog medija. Stoga, na osnovu odlične sposobnosti izmene anjona i posebne lamelarne strukture LDH, ovaj proces interkalacije je efikasan i štedi vreme u zaštiti od korozije. Iz perspektive primene LDH filmova na Mg legurama, učitavanje neorganskih anjona u LDH filmove je optimalan i efikasan metod zaštite od korozije.

Super-hidrofobna modifikacija

Biolozi su otkrili da je lotos biljka koja se samočisti i povezali su svoj mehanizam samočišćenja sa mikroskopskom morfologijom njegove superhidrofobne površi. Otkrili su da su superhidrofobne osobine površine lotosovog lista posledica određene hrapavosti na nanoskopskoj površi [29]. Inspirisani „efektom lotosa“, naučnici su počeli da pripremaju veštački hidrofobni premaz na metalnoj površini kako bi dobili neravne površinske materijale sa malom površinskom energijom.
Tako su proizvedeni inhibitori korozije interkalirani Mg–Al LDH filmovi na legurama magnezijuma metodom rasta na licu mesta, a proučavan je efekat višekomponentnih sinergističkih efekata, kao što su interkalacija molibdata i niska modifikacija površine laurinske kiseline za zaštitu filmova od korozije. Elektrohemijsko merenje je pokazalo da superhidrofobni LDH premazi značajno smanjuju gustinu struje korozije, što dokazuje da se antikorozivna zaštita legure Mg može poboljšati zbog kombinovanog dejstva molibdata i laurinske kiseline. Stoga se zaključuje da površinu superhidrofobnog filma nije lako infiltrirati, što može sprečiti da molekuli vode, Cl^- i drugi korozivni joni dođu na površinu matrice kako bi se metal bolje štitio od korozije.

Biokompatibilni premazi

Poslednjih godina, biokompatibilni materijali su veoma potrebni zbog njihovih posebnih izuzetnih svojstava, a modifikacija površine na legurama magnezijuma privlači sve više pažnje, posebno zbog njihove bolje biokompatibilnosti. Postoje dve vrste biokompatibilnih materijala: jedni su originalni biokompatibilni materijali, a drugi su oni kojima treba nametnuti biokompatibilnost modifikacijom površine i drugim sredstvima.
PVA je jedan od trenutno najčešće korišćenih polimernih materijala, koji je biorazgradivi polimer sa finom biokompatibilnošću, stabilnošću i hemijskom otpornošću. Modifikovani Mg-Al-CO_3 LDH sa organskom kiselinom metodom ko-precipitacije može podstaći interkalaciju LDH u polimernu matricu, čime se može dobiti odgovarajući stepen disperzije. U cilju promovisanja interkalacije u LDH polimernoj matrici i poboljšanja idealne disperzije, organska dikiselina je pripremljena od

tetrabromoftalnih anhidrida i L-asparaginske kiseline u refleksnoj sirćetnoj kiselini sa piridinom [30]. Pod ultrazvučnim zračenjem, međuslojni bazni razmak laktat dehidrogenaze je modifikovan metodom ko-precipitacije organske dikiseline, što je efikasno smanjilo vreme polimerizacije i nano koheziju. Proces modifikacije je prikazan na slici 9, zatezna čvrstoća i modul PVA/mLDH NC su poboljšani zbog vodonične veze i dobre disperzije mLDH u polimernoj matrici.

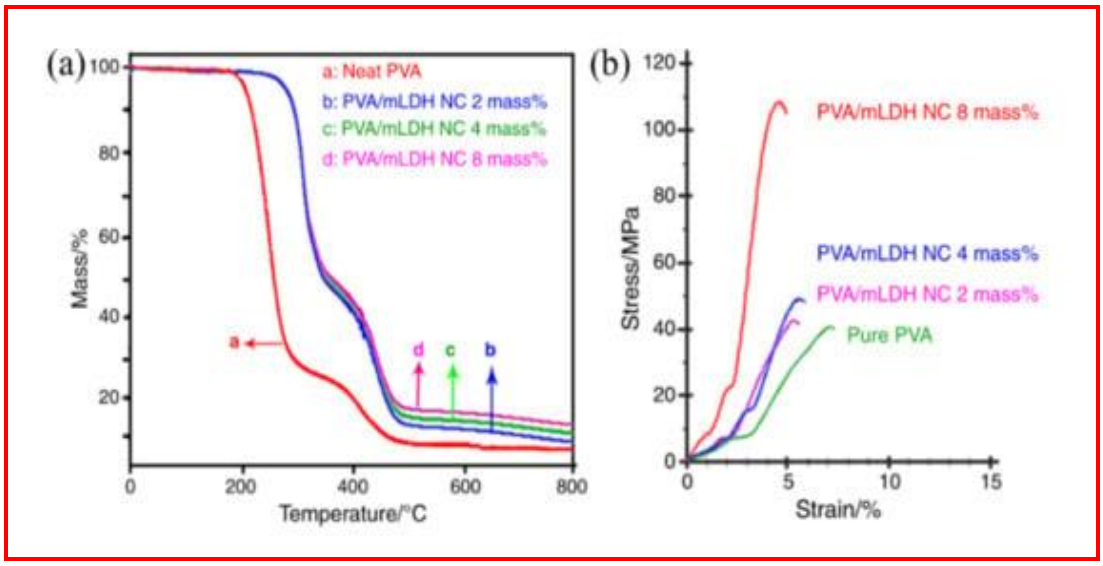

Slika 8. *Grafici PVA i PVA/mLDH NCs (a) TG krive; (b) tipični dijagrami napon-deformacija (iz [4])*

Radi daljeg proširenja dugog dometa zaštitnog efekta upijajuće legure magnezijuma, u [12] je prikazana priprema PGA (vrsta sintetičkog peptida sa dobrom hidrofilnošću i biorazgradljivošću) zapečaćene Mg–Al LDH prevlakom na leguri magnezijuma AZ31 kombinovanjem hidrotermalnog i metoda vakuumskog sušenja zamrzavanjem, čime je sintetisana kompozitna prevlaka LDH i PGA premaza. Elektrohemijska polarizacija, impedansna spektroskopija i testovi evolucije vodonika pokazali su da ove kompozitne prevlake efikasno obezbeđuju zaštitu od korozije za leguru AZ31. Kompozitni premaz deluje kao fizička barijera za zaptivanje poroznog LDH premaza, što poboljšava zaštitu filma od korozije i pruža dugoročnu zaštitu AZ31 podlozi. Autori [31] sintetizovali su PGA i konjugat bengalske ruže (PGA–RB), što je poboljšalo farmakokinetiku i antitumorsko dejstvo. Pored toga, hidrofobni polikaprolakton (PCL) i PGA su korišćeni kao sirovine za sintetizaciju tkivno projektovanih meniskusa sa dobrim biomehaničkim i biorazgradivim svojstvima. Na osnovu toga u [32] su hidrotermalnom obradom uspešno primenili PGA premaz na Mg–Al LDH, a rezultati pokazuju da LDH ima dobru otpornost na koroziju. Studija ćelijske adhezije matičnih ćelija koštane srži pacova je takođe pokazala da PGA/LDH kompozitni premazi mogu značajno poboljšati ćelijsku kompatibilnost supstrata i da imaju široku perspektivu primene u ortopedskoj hirurgiji [33–36].

Zaključni rezime i perspective

LDH materijali se široko koriste u oblasti zaštite metala zbog brzog razvoja LDH u razmeni anjona, tehnologiji pripreme, metodima modifikacije i mehanizmu korozije. Međutim, premalo je studija o mehanizmu razmene anjona između slojeva LDH i mehanizmu rekombinacije slojevite strukture sa mikroskopske tačke gledišta. U ovom pregledu sumirane su metode sinteze LDH prevlaka. Ukratko je razmotren mehanizam otpornosti na koroziju LDH materijala na leguri magnezijuma. Površina LDH materijala je hemijski modifikovana da bi se poboljšala kompatibilnost sa rastvaračem, a funkcija otpornosti na koroziju je razvijena u obliku aditiva, koji su kulminirali kompozitnim premazima sa posebnim funkcijama.

Zaključno, LDH prevlake ili premazi imaju dobar zaštitni efekat na leguru magnezijuma, ali još uvek postoje problemi koje treba dalje proučavati. In-situ rast je najčešće korišćen metod, ali stepen i debljina LDH premaza su ponekad neadekvatni. Ovo ukazuje na važnost višestrukih metoda sinteze za LDH premaze. Sila vezivanja između LDH i supstrata može se promeniti izmenom odnosa metalnih katjona, a otpornost na koroziju se može poboljšati kako bi se produžio radni vek filma. Da bi se postigao ovaj cilj i drugi funkcionalni efekti legure Mg, neophodno je proučiti mehanizam rekombinacije strukture LDH interlaminacije, koji može maksimizirati oslobađanje inhibitornih jona i apsorpciju jona korozije. Hemijska modifikacija ili inkorporacija sinergističkih jona može poboljšati kompatibilnost između LDH i organskih polimera, čime se povećava kompaktnost kompozitne prevlake i poboljšava njegova otpornost na koroziju.

Uz istraživanje pripreme Mg–Al LDH sistema prevlaka na površini legure Mg radi poboljšanja njene anti-korozivnosti, posebno je važno bolje razumeti kako odabrati odgovarajuće ključne parametre i proces sinteze. Kako LDH film ima glavne karakteristike pozitivne antikorozivne funkcije, neophodno je pronaći nove regulatorne parametre za realizaciju pripreme multifunkcionog LDH filma sa kontrolisanim veličinama graničnih parametara na specifičnim graničnim površima i dodatno poboljšati zaštitne performanse kompozitnih filmova na Mg legurama. Prema tome, kompozitni filmovi Mg–Al LDH pripremljeni na površi legure Mg imaju velike izglede za široku primenu u korozivnoj zaštiti.

Zahvalnica

Ovaj rad je finanskijski podržalo Ministarstvo za naučnotehnološki razvoj, visoko obrazovanje i informaciono društvo Republike Srpske (Projekti br. 19.032/961-36/19 i 19.032/961-42/19).

Reference

1. D. Abdeen, et. al. A Review on the corrosion behaviour of nanocoatings on metallic substrates, *Materials*, **12**, 210, 2019.
2. Y. Ahmadi, S. Ahmad, "Polymeric nanocomposite coatings", ch. 19, in: *Micro and Nano Technologies, Corrosion Protection at the Nanoscale*, S. Rajendran, et. al. Eds. London, Elsevier, 2020.
3. C.I. Idumah, et al. Recently emerging nanotechnological advancements in polymer nanocomposite coatings for anti-corrosion, anti-fouling and self-healing, *Surf. Interfaces* **21**, 100734, 2020
4. C. Yanhui, et al. Layered double hydroxide (LDH) for multi-functionalized corrosion protection of metals: A review, *J. Mater. Sci. Technol.* **102** , 232-263, 2022.
5. L.-X. Li, et al. Development of a thiophene derivative modified LDH coating for Mg alloy corrosion protection, *Electrochim. Acta* **330**, 135186, 2020.
6. J.I. Chen, et al. Comparison of corrosion resistance of MgAl-LDH and ZnAl-LDH films intercalated with organic anions ASP on AZ31 Mg alloys, *Trans. Nonferrous Met. Soc. China* **30**, 2424–2434, 2020.
7. C. Yanhui, et al. Layered double hydroxide (LDH) for multi-functionalized corrosion protection of metals: A review, *J. Mater. Sci. Technol.* **102** , 232-263, 2022.
8. W. Jin, D.-H. Park, Functional layered double hydroxide nanohybrids for biomedical imaging, *Nanomaterials* **9**, 1404, 2019.
9. J.-C. Liu, B. Qi, Y.-F. Song, Engineering polyoxometalate-intercalated layered double hydroxides for catalytic applications, *Dalton Trans.* **49**, 3934–3941, 2020.
10. X. Wang, C. Jing, Y.X. Chen, Active corrosion protection of super-hydrophobic corrosion inhibitor intercalated Mg–Al layered double hydroxide coating on AZ31 magnesium alloy. *J. Alloys Compd.* **8**, 291–300, 2021.
11. J. Li, et al. Enhanced corrosion protection property of Li–Al layered double hydroxides (LDHs) film modified by 2-guanidinosuccinic acid with excellent self-repairing and self-antibacterial properties, *Appl. Surf. Sci.* **480**, 384–394, 2019.
12. W. Wu, et al, Biocorrosion resistance and biocompatibility of Mg–Al layered double hydroxide/poly-L-glutamic acid hybrid coating on magnesium alloy AZ31, *Prog. Org. Coat.* **147**, 426–441, 2020.

13. M. T abish, et. Reviewing the current status of layered double hydroxide-based smart nanocontainers for corrosion inhibiting applications, *J. Mater. Res. Technol.* **10**, 390–421, 2021.
14. C. Yang, et al. In situ nano-assembly of Mg/Al LDH embedded on phosphorylated cellulose microspheres for tetracycline hydrochloride removal, *Cellulose* **28**, 301–316, 2020.
15. T. Hu, et al. One-pot scalable in situ growth of highly corrosion-resistant MgAl-LDH/MBT composite coating on magnesium alloy under mild conditions. *J. Mater. Sci. Technol.* **92**, 225–235, 2021.
16. M.J. Anjum, et al. In-situ intercalation of 8-hydroxyquinoline in Mg–Al LDH coating to improve the corrosion resistance of AZ31, *Corros. Sci.* **157**, 1–10, 2019.
17. A. Bouali, et al. Layered double hydroxides (LDHs) as functional materials for the corrosion protection of aluminum alloys: A review, *Appl. Mater. Today* **21**, 100857, 2020.
18. H. Wu, et al. Corrosion behavior of Mg–Al LDH film in-situ assembled with graphene on Mg alloy pre-sprayed Al layer, *J. Alloy. Compd.* **834**, 155107, 2020.
19. L. Wu, et al. Fabrication and characterization of an actively protective Mg–Al LDHs/Al_2O_3 composite coating on magnesium alloy AZ31, *Appl. Surf. Sci.* **487**, 558–568, 2019.
20. J.-M. Zhang, et al. Effect of hydrothermal treatment time on microstructure and corrosion behavior of micro-arc oxidation/layered double hydroxide composite coatings on LA103Z Mg–Li Alloy in 3.5 wt.% NaCl solution, *J. Mater. Eng. Perform.* **29**, 4032–4039, 2020.
21. M. Kaseem, et al. A Review on LDH-smart functionalization of anodic films of Mg alloys, *Nanomaterials* **11**, 536, 2021.
22. Y. Chen, et al. One-step in situ synthesis of graphene oxide/MgAl-layered double hydroxide coating on a micro-arc oxidation coating for enhanced corrosion protection of magnesium alloys, *Surf. Coat. Technol.* **413**, 127083, 2021.
23. D. Mashtalyar, et al. Composite coatings formed on Ti by PEO and fluoropolymer treatment. *Appl. Surf. Sci.* **536**, 147976, 2021.
24. Y. Wu, et al. MgAl-V2O74- LDHs/(PEI/MXene)10 composite film for magnesium alloy corrosion protection, *J. Mater. Sci. Technol.* **91**, 28–39, 2021.
25. T. Kameda, Uchidaet al. Regeneration of car-bonate-intercalated Mg–Al layered double hydroxides (CO_3·Mg–Al LDHs) by CO_2-induced desorption of anions (X) from X·Mg–Al LDH (X = Cl, SO_4, or NO_3): A kinetic study, *Chem. Eng. Res. Des.* **165**, 207–213, 2021.
26. J.P. Šetrajčić, et al. "Phonon participation in thermodynamics and superconductive properties of thin ceramic films", in: *Thermodynamics*, M. Tadashi, ed. (ISBN: 978-953-307-544-0), Vienna, InTech, 2011, ch. 15, 317-348.
27. J.P. Šetrajčić, S.M. Vučenović, S.K. Jaćimovski, Possible states of charge carriers in thin multilayered superconductive ceramics, *Zaštita Materijala* **57**/2, 239-243, 2016.
28. J.P. Šetrajčić, et al. Impact of surface conditions changes on changes in thermodynamic properties of quasi 2D crystals, *Physica* A **566**, 125650, 2021.
29. L. Wu, et al. Corrosion resistance of fatty acid and fluoroalkylsilane-modified hydrophobic Mg–Al LDH films on anodized magnesium alloy, *Appl. Surf. Sci.* **487**, 569–580, 2019.
30. S. Zhang, et al. Enhanced antitumor effect of poly(L-glutamic acid)-rose bengal conjugate nanoparticle, *J. Control. Release* **259**, e122–e123, 2017.
31. M. Laipan, et al. Layered intercalation compounds: Mechanisms, new methodologies, and advanced applications, *Prog. Mater. Sci.* **109**, 100631, 2020.
32. M. Kaseem, Y.G. Ko, A novel hybrid composite composed of albumin, WO_3, and LDHs film for smart corrosion protection of Mg alloy. *Compos. Part. B Eng.* **204**, 108490, 2021.
33. F. Peng, et al.. PEO/Mg–Zn–Al LDH Composite Coating on Mg Alloy as a Zn/Mg Ion-Release Platform with Multifunctions: Enhanced Corrosion Resistance, Osteogenic, and Antibacterial Activities, *ACS Biomater. Sci. Eng.* **4**, 4112–4121, 2018.
34. "Nanomedicina: Stanje i perspektiva", u: *Biomaterijali*, D. Uskoković, D. Raković, urednici, Beograd, Institut tehničkih nauka SANU i Društvo za istraživanje materijala, 2010. gl.27.
35. J.P. Šetrajčić, Nanostrukturni materijali u biomedicini (pozivno predavanje), *Zbornik radova 57. ETRAN,* NE-MO **2**.1, 1-6, 2013.
36. A.J. Šetrajčić-Tomić, et al. Review of core-multishell nanostructured models for nano-biomedical and nano-biopharmaceutical application, *Bio-Med.Mater.Eng.* **29**/4, 451-471, 2018.

The Impact of Ultrasound Waves on Polyphenol Yield and Antioxidant Capacity of *Aloe vera* L. Extracts

Uticaj ultrazvučnih talasa na prinos polifenola i antioksidativni kapacitet Aloe vera L. ekstrakata

Aleksandra A. Jovanović[1,*]

[1] *University of Belgrade, Institute for the Application of Nuclear Energy INEP, Banatska 31b, 11080 Zemun Belgrade, Serbia*

[*] *ajovanovic@inep.co.rs*

Abstract

Aloe vera L. is a tropical, drought-resistant, and perennial succulent native to Africa that later spread to other parts of the world. It contains anthraquinones, flavonoids, tannins, terpenoids, saponins, resins, polysaccharides, sterols, polypeptides, lectins, enzymes, chromones, fatty, amino and organic acids, vitamins, and minerals. Aloe and its extracts are widely used as active ingredients in laxative and antiobesity preparations and as a moisturizer, emollient, or wound-healing agent in pharmaceuticals, sunscreen, and other cosmetic formulations. Modern extraction procedures, such as ultrasound-assisted extraction, provide numerous benefits, including reduced solvent consumption, short extraction time, and a higher extraction yield, while operation and device are simple. Thus, in this study, A. vera extracts were prepared using dried and grinded leaves, 50% ethanol as the extraction medium, a solid-to-solvent ratio of 1:30, and an ultrasound probe at three different amplitude values, 20, 40, and 60% for 10 min. The impact of different amplitudes on the total polyphenol content and antioxidant capacity of the extracts (ABTS, DPPH, and CUPRAC assays) was investigated. There were no statistically significant differences between the polyphenol yield of the extracts obtained at various amplitudes (6.45±0.51, 6.83±0.32, and 6.95±0.23 mg gallic acid equivalents (GAE)/g of plant material). Anti-ABTS activity was significantly different between 20 and 40 or 60% of amplitude (1.20±0.05, 1.43±0.10, and 1.40±0.07 mmol Trolox/g). DPPH radical scavenging activity also increased (i.e. IC_{50} value decreased) at higher amplitudes (43.9±0.9, 41.6±1.1, and 39.4±1.0 mg/mL). According to the results of the CUPRAC assay, the antioxidant potential was the same for all prepared extracts (0.130±0.003, 0.131±0.002, and 0.125±0.004 mmol Trolox/g). Therefore, it can be concluded that radical scavenging ability did not correlate with the polyphenol yield of A. vera extracts, whereas cupric ion-reducing potential depended on the concentration of polyphenols.

Keywords: *Aloe vera; antioxidants; polyphenols; ultrasound probe*

Izvod

Aloe vera L. je tropski, višegodišnji sukulent otporan na sušu, poreklom iz Afrike, koji se kasnije proširio na druge delove sveta. Sadrži antrahinone, flavonoide, tanine, terpenoide, saponine, smole, polisaharide, sterole, polipeptide, lektine, enzime, hromone, masne, amino i organske kiseline, vitamine i minerale. Aloja i njeni ekstrakti se široko koriste kao aktivni sastojci u preparatima za laksaciju i protiv gojaznosti i kao hidratant, emolijens ili agens za zarastanje rana u farmaceutskim proizvodima, kremama za sunčanje i drugim kozmetičkim formulacijama. Savremeni postupci ekstrakcije, kao što je ultrazvučna ekstrakcija, imaju brojne prednosti, uključujući smanjenu potrošnju rastvarača, kratko vreme ekstrakcije i veći prinos, dok su izvođenje procesa i uređaj jednostavni. U ovoj studiji su A. vera ekstrakti pripremljeni korišćenjem osušenog i usitnjenog lišća biljke, 50% etanola kao medijuma za ekstrakciju, pri odnosu biljnog materijala i rastvarača od 1:30 i ultrazvučne sonde sa tri različite vrednosti amplitude, 20, 40 i 60%, tokom 10 minuta. Ispitan je uticaj različitih amplituda na ukupan sadržaj polifenola i antioksidativni kapacitet ekstrakata

(primenom ABTS, DPPH i CUPRAC testova). Nije bilo statistički značajnih razlika između prinosa polifenola dobijenih ekstrakata pri različitim amplitudama (6,45±0,51, 6,83±0,32 i 6,95±0,23 mg ekvivalenta galne kiseline (GAE)/g biljnog materijala). Anti-ABTS aktivnost se značajno razlikovala između 20 i 40 ili 60% amplitude (1,20±0,05, 1,43±0,10 i 1,40±0,07 mmol Trolox/g). Aktivnost uklanjanja DPPH radikala takođe je porasla (tj. vrednost IC_{50} se smanjivala) pri većim amplitudama (43,9±0,9, 41,6±1,1 i 39,4±1,0 mg/mL). Prema rezultatima CUPRAC testa, antioksidativni potencijal je bio isti za sve pripremljene ekstrakte (0,130±0,003, 0,131±0,002 i 0,125±0,004 mmol Trolox/g). Stoga se može zaključiti da sposobnost uklanjanja radikala nije bila u korelaciji sa prinosom polifenola u A. vera ekstraktima, dok je potencijal ekstrakata da redukuju jone bakra zavisio od koncentracije polifenola.
Ključne reči: *Aloe vera; antioksidansi; polifenoli; ultrazvučna sonda*

Introduction

Aloe vera (L.) Burm. f. (Asphodelaceae) is a tropical, drought-resistant, and perennial succulent native to Africa that later spread to other parts of the world. The plant contains anthraquinones, flavonoids, tannins, terpenoids, saponins, resins, polysaccharides, sterols, polypeptides, lectins, enzymes, chromones, fatty, amino and organic acids, vitamins, and minerals. Aloe and its extracts are widely used as active ingredients in laxative and antiobesity preparations and as a moisturizer, emollient, or wound-healing agent in pharmaceuticals, sunscreen, and other cosmetic formulations [1,2].

Novel extraction methods, such as ultrasound-assisted extraction, provide various benefits: reduced solvent consumption, short extraction time, a higher extraction yield, and simple operation [3]. Additionally, novel procedures support the concept of "green" solvents, aimed to minimize the negative environmental impact of the utilization of large amounts of the extraction solvents. Namely, simple alcohols (e.g. ethanol) and their mixtures with water are more environmentally favorable solvents [4].

Therefore, in the present study, *A. vera* extracts were prepared using leaves, 50% ethanol as the extraction solvent, and an ultrasound probe at various amplitudes. The impact of different amplitude values on the polyphenol yield and antioxidant potential of the extracts (ABTS, DPPH, and CUPRAC assays) was investigated.

Materials and Methods

Reagents and plant material

The following reagents were used: Folin-Ciocalteu reagent and gallic acid (Merck, Germany), ethanol (Fisher Scientific, UK), 2,2'-azino-bis(3-ethylbenzothiazoline-6-sulphonic acid) - ABTS, 6-hydroxy-2,5,7,8-tetramethylchroman-2-carboxylic acid - Trolox, 2,2-diphenyl-1-picrylhydrazyl - DPPH iron(III) chloride, potassium ferricyanide, methanol, ammonium acetate, and iron(II) sulfate (Sigma-Aldrich, USA), neocuproin (Acros Organics, Belgium), cupric chloride (Fluka, Germany).

A. vera was purchased at ASC Garden d.o.o., Belgrade, Serbia.

Ultrasound-assisted extraction

A. vera extracts were prepared using dried leaves (1 g), 50% ethanol as the extraction medium (30 mL), and an ultrasound probe (Sonoplus, Bandelin, Germany), at three various amplitude values (20, 40, and 60%) for 10 min. All extracts were filtered through a cellulose filter (fine pore, 0.45 µm) and stored at 4°C until further analyses.

Total polyphenol content

The polyphenol yield of *A. vera* extracts was determined spectrophotometrically using the modified Folin-Ciocalteu method [5]. The results are expressed as milligrams of gallic acid equivalents per gram of plant material (mg GAE/g).

ABTS test

The ABTS assay was based on the procedure described by Re et al. [6] with a slight modification and the absorbance was measured at 734 nm. The antioxidant activity was expressed as mmol Trolox per g of plant material (mmol Trolox/g).

DPPH test

The DPPH assay was based on the procedure described by [7] with a slight modification and the absorbance was measured at 517 nm. The results were expressed as IC_{50} (mg/mL), defined as the concentration of the extract required to scavenge 50% of DPPH free radicals.

CUPRAC test

The cupric ion-reducing antioxidant ability of *A. vera* extracts was also measured [8]. The absorbance was read at 450 nm and the results were expressed as mmol Trolox per g of plant material (mmol Trolox/g).
All spectrophotometric measurements were performed in a UV-1800 spectrophotometer (Shimadzu, Japan).

Statistical analysis

The statistical analysis was done by using analysis of variance (one-way ANOVA) and Duncan's *post hoc* test in STATISTICA 7.0. The differences were considered statistically significant at $p<0.05$.

Results and Discussion

The impact of three various amplitudes of the ultrasound probe on polyphenol yield and antioxidant capacity (ABTS and DPPH radical scavenging activities and cupric ion-reducing antioxidant potential) of ethanol *A. vera* extracts was investigated. The obtained results are presented in Figure 1 (for polyphenol yield) and Figure 2 (for antioxidant potential).
According to the results from Figure 1, it can be seen that there was no statistically significant difference between the polyphenol yield of the extracts obtained at different values of amplitude. Hence, the polyphenol concentration amounted to 6.45±0.51, 6.83±0.32, and 6.95±0.23 mg GAE/g. Deng et al. [9] and Horžić et al. [10] have reported that the mechanical and thermal effects of ultrasound-assisted extraction cause the degradation of plant cell walls, the release of cell contents, higher penetration of extraction solvent into the plant material, the increase in mass transfer, and consequently the enhancement of polyphenols yield even at lower values of amplitude. Therefore, it can explain the absence of statistically significant differences in polyphenol yield between the extracts prepared using various amplitudes.

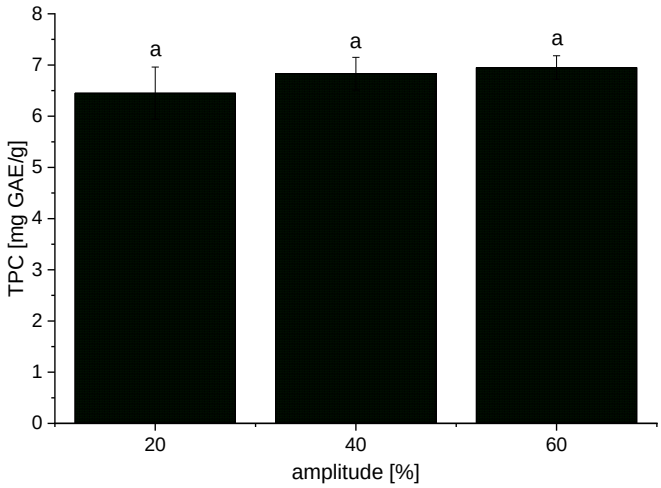

Figure 1. *Total polyphenol content of Aloe vera extracts prepared using ultrasound probe and different amplitudes; GAE, gallic acid equivalents; the letters above bars showed statistically significant differences (p<0.05; n=3; analysis of variance, Duncan's post-hoc test).*

Anti-ABTS activity was significantly different between the extracts prepared at 20% of amplitude and the other two used amplitude values (1.20±0.05, 1.43±0.10, and 1.40±0.07 mmol Trolox/g, Figure 2A). It can be noticed that the antioxidant activity of ethanol *A. vera* extracts showed in the ABTS assay did not follow the trend of polyphenol yield, where there was no statistically significant difference. The obtained phenomenon can be explained by the fact that non-phenolic compounds, such as ascorbic acid, uric acid, triterpenoid saponins, thiols, and synergism of the active compounds have an important role in the overall antioxidant activity of plant extracts [11,12].
According to the results of the DPPH assay, the antioxidant activity of ethanol *A. vera* extracts also increased with the increase of amplitude (i.e. IC_{50} value decreased, 43.9±0.9, 41.6±1.1, and 39.4±1.0 mg/mL, Figure 2B). Hirano et al. [13] have reported that the anti- DPPH potential of extracts was correlated with the flavonoid yield.

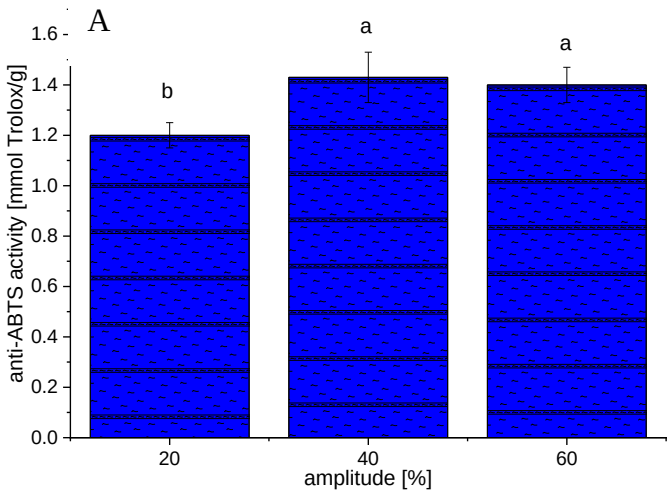

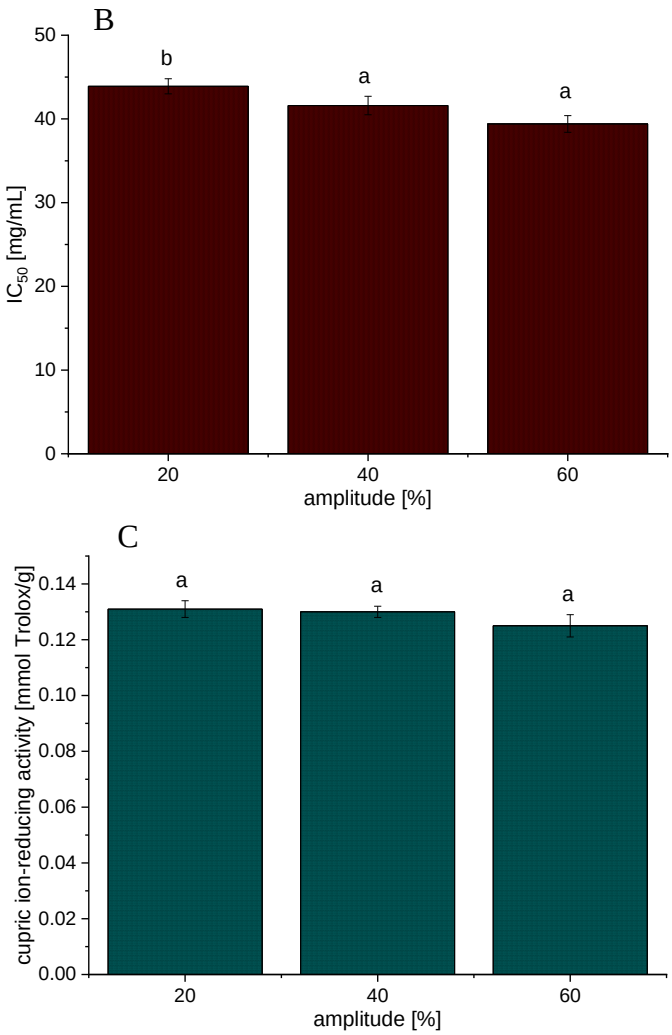

Figure 2. *Antioxidant capacity of Aloe vera extracts prepared using ultrasound probe and different amplitudes: (A) ABTS, (B) DPPH, and (C) CUPRAC assays; IC_{50}, the concentration of the extract required to scavenge 50% of DPPH radicals; the letters above bars showed statistically significant differences ($p<0.05$; $n=3$; analysis of variance, Duncan's post-hoc test).*

As can be seen from Figure 2C, there were no statistically significant differences in cupric-ion reducing antioxidant capacity between the extracts prepared using various amplitudes of the ultrasound probe (0.130±0.003, 0.131±0.002, and 0.125±0.004 mmol Trolox/g), which is in accordance with the obtained results of polyphenol content and literature data as well. Namely, Apak et al. study [14] showed that there was a correlation between the polyphenol yield determined in the Folin-Ciocalteu assay and the antioxidant capacity obtained in the CUPRAC method. According to the literature data, polyphenol compounds that possess the highest cupric ion-reducing capacity include catechin, epicatechin, epicatechin gallate, epigallocatechin, epigallocatechin gallate, quercetin, rutin, caffeic, gallic, and chlorogenic acids [14]. On the other hand, thiols, D-ascorbic acid, mannitol, and glucose have an important role in the reduction of cupric ions as well [15].

Conclusion

In the present study, *A. vera* extracts were prepared using ultrasound-assisted extraction and various amplitudes of the ultrasound probe. The influence of different amplitude values was investigated via the determination of polyphenol yield and antioxidant capacity of the extracts. Different amplitudes

did not have a statically significant impact on polyphenol yield and cupric ion-reducing antioxidant capacity of the extracts. However, the extracts prepared using higher values of the amplitude possessed statistically significantly better ABTS and DPPH radical scavenging capacity. Thus, it can be concluded that radical scavenging activity did not correlate with the polyphenol yield of *A. vera* extracts, while cupric ion-reducing ability depended on the concentration of polyphenols. Future experiments should be focused on the biological potential of the extracts (antimicrobial, anti-inflammatory, skin regeneration, and enzyme inhibition potential), as well as their potential use in industry as textile dyes or anticorrosive agents.

Acknowledgements

The authors acknowledge their gratitude to the Ministry of Education, Science and Technological Development of Serbia, contract numbers 451-03-47/2023-01/200019, 451-03-47/2023-01/200135, 451-03-47/2023-01/200026, 451-03-47/2023-01/200023, and 451-03-47/2023-01/200017.

References

1. M. Hęś, K. Dziedzic, D. Górecka, A. Jędrusek-Golińska, E. Gujska, *Aloe vera* (L.) Webb.: Natural sources of antioxidants - a review, *Plant Foods Hum. Nutr.*, **74**, 255-265, 2019. https://doi.org/10.1007/s11130-019-00747-5
2. I. A. Khan, E. A. Abourashed, *Leung's encyclopedia of common natural ingredients: used in food, drugs and cosmetics.* New York, USA , John Wiley & Sons, 2011.
3. A. Jovanović, V. Djordjević, P. Petrović, D. Pljevljakušić, G. Zdunić, K. Šavikin, B. Bugarski, The influence of different extraction conditions on polyphenol content, antioxidant and antimicrobial activities of wild thyme, *J. Appl. Res. Med. Aromat. Plants*, **25**, 100328, 2021. https://doi.org/10.1016/j.jarmap.2021.100328
4. A. Mustafa, C. Turner, Pressurized liquid extraction as a green approach in food and herbal plants extraction: A review *Anal. Chim. Acta*, **703**, 8-18, 2011.
5. L. G. Galván d'Alessandro, K. Kriaa, I. Niko, K. Dimitrov, Ultrasound assisted extraction of polyphenols from black chokeberry, *Sep. Pur. Tech.*, **93**, 42-47. https://doi.org/10.1016/j.seppur.2012.03.024
6. R. Re, N. Pellegrini, A. Proteggente, A. Pannala, M. Yang, C. Rice-Evans Antioxidant activity applying an improved ABTS radical cation decolorization assay, *Free Radic. Biol. Med.* **26**, 1231-1237, 1999. https://doi.org/10.1016/S0891-5849(98)00315-3
7. D. Horžić, A. Režek Jambrak, A. Belščak-Cvitanović, D. Komes, V. Lelas, Comparison of conventional and ultrasound assisted extraction techniques of yellow tea and bioactive composition of obtained extracts, *Food Bioproc. Tech.*, **5**, 2858-2870, 2012.
8. P. Petrović, K. Ivanović, K., A. Jovanović, A., M. Simović, V. Milutinović, M. Kozarski, M.Petković, A., Cvetković, A. Klaus, B. Bugarski, The impact of puffball autolysis on selected chemical and biological properties: puffball extracts as potential ingredients of skin-care products, *Arch. Biol. Sci.*, **71**, 721-733, 2019. https://doi.org/10.2298/ABS190725055P
9. Y. Deng, Y. Zhao, O. Padilla-Zakour, G. Yang Polyphenols, antioxidant and antimicrobial activities of leaf and bark extracts of *Solidago canadensis* L., *Ind.Crops Prod.*, **74**, 803-809, 2015.
10. D. Horžić, A. Režek Jambrak, A. Belščak-Cvitanović, D. Komes, V. Lelas V. Comparison of conventional and ultrasound assisted extraction techniques of yellow tea and bioactive composition of obtained extracts, *Food Bioproc. Tech.*, **5**, 2858-2870, 2012.
11. L. Bi, X. Tian, F. Dou, L. Hong, H. Tang, S. Wang, New antioxidant and antiglycation active triterpenoid saponins from the root bark of *Aralia taibaiensis*, *Fitoterapia*, **83**, 234-240, 2012.
12. M. C. Foti, R. Amorati, Non-phenolic radical-trapping antioxidants, *J. Pharm. Pharmacol.*, **61**, 1435-1448, 2010.
13. R. Hirano, W. Sasamoto, A. Matsumoto, H. Itakura, O. Igarashi, K. Kondo, Antioxidant ability of various flavonoids against DPPH radicals and LDL oxidation, *J. Nutr. Sci. Vitaminol.* **47**, 357-362, 2001. http://dx.doi.org/10.3177/jnsv.47.357

14. R. Apak, K. Güçlü, M. Özyürek, S. Esin Karademir, E. Erçağ, The cupric ion reducing antioxidant capacity and polyphenolic content of some herbal teas, *Int. J. Food Sci. Nutr.*, **57**, 292-304, 2006. https://doi.org/10.1080/09637480600798132
15. M. Özyürek, K. Güçlü, E. Tütem, K. Sözgen Başkan, E. Erçağ, S. Esin Çelik, S. Baki, L. Yildiz, S. Karamanc, R. Apak A comprehensive review of CUPRAC methodology, *Anal. Met.*, **11**, 2439-2453, 2011. https://doi.org/10.1039/C1AY05320E

ORAL PRESENTATIONS
USMENA SAOPŠTENJA

Determination of micronutrient accumulation in livestock fodder and soil in three Belgrade municipalities

Marija Matić*, Dragana Pavlović, Veljko Perović, Olga Kostić, Milica Marković, Miroslava Mitrović, Pavle Pavlović

Department of Ecology, Institute for Biological Research "Siniša Stanković", National Institute of the Republic of Serbia, University of Belgrade, Bulevar despota Stefana 142, 11000 Belgrade, Serbia

* *Corresponding_author: marija.pavlovic@ibiss.bg.ac.rs*

Abstract

Mineral nutrients (micronutrients) are essential for plant growth and develpment. In low concentrations they have a stimulating effect on plant functioning, but in high concentrations they can be toxic. These micronutrients are naturally present in the environment, but can also originate from industrial plants or from contaminated water used to irrigate agricultural fields. These elements are taken up by plants used for human consumption or grown to feed domestic animals (fodder). In order to evaluate and reduce the risk of growing potentially contaminated plants for livestock feed on soils in the immediate vicinity of coal mines and thermal power plants, the presence of Mn, Se and Zn in alfalfa (Medicago sativa L.) samples was determined. Alfalfa samples and associated soils were collected from the territory of municipalities of Lazarevac (village Sokolovo) and Obrenovac (village Krtinka), while the territory of the municipality of Surčin (village Jakovo) was chosen as the control site. The bioconcentration factor (BCF), as well as Spearman correlations were calculated, which can provide information about the potential efficiency of the removal of elements from the soil by the plant. The results of the content of the studied elements in fodder were within the usual concentrations for conventional production, except in the case of Se. The Se content in the studied Medicago sativa samples was in a range that can cause chronic or acute poisoning in livestock if consumed, so special attention is needed if these plants are used in the diet of livestock. However, alfalfa was found not to be a significant accumulator of Mn, Se and Zn, as the values of the bioconcentration factor were below 1. Examined element concentrations in soil were within MAC values for soils according to the regulations of the Republic of Serbia. These results urge caution in the cultivation of fodder at investigated sampling sites.

Keywords: *micronutrients; Medicago sativa; livestock nutrition; bioconcentration factor; Spearman correlations*

Introduction

Mineral nutrients (micronutrients) are essential for plant growth and development, and it is considered that there are 14 of them in total. There are also elements that have some beneficial effect on plants, although plants can survive without them, and are called beneficial elements. In low concentrations they have a stimulating effect on plants, but in high concentrations they can be toxic. Essential elements have a significant physiological and biochemical role in plants, being involved in the biosynthesis of chlorophyll and DNA, in the process of photosynthesis, in redox reactions in chloroplasts and mitochondria, in sugar metabolism and in nitrogen fixation, etc. [1].

All micronutrients are naturally present in the environment in higher or lower concentrations. However, a large proportion of them, as well as other pollutants in soil and water originate from industrial plants, as a result of the use of pesticides and mineral fertilizers or from contaminated water used to irrigate agricultural fields. These micronutrients are taken up actively or passively by plants that can be used for human consumption, or feed for domestic animals. Depending on their total

abundance in the soil, these concentrations can sometimes rise to levels that are toxic to plants, animals and, consequently, to humans who consume food produced on such soils, as they are incorporated into the food chain [2-4]. The uptake of micronutrients by plants depends on numerous parameters in the soil and the species-specific characteristics of the plant itself [5,6].

In order to determine the presence of essential micronutrients - Mn, Se and Zn in the food chain, to assess and reduce the risk of growing plants for animal feed on soils in the immediate vicinity of coal mines and thermal power plants, samples of alfalfa (*Medicago sativa* L.) and soils were collected on the territory of the municipalities of Lazarevac (village Krtinka) and Obrenovac (village Sokolovo). The area of Surčin municipality (village Jakovo) was chosen as the control site without direct industrial activity. In addition, the bioconcentration factor (BCF) and Spearman correlations were calculated, which can provide information about the potential efficiency of the removal of chemical elements from the soil by the plant.

Materials and methods

Species description

Medicago sativa is a perennial herb that is one of the most important fodder crops (Figure 1). It is important for improving the physical, chemical and microbiological properties of the soil, as its harvest leaves significant amounts of organic matter in the soil, which is further decomposed. Owing to its deep root system, it helps improve the nitrogen fertility of the soil and protect it from soil erosion. The depth of root system makes it very resistant, especially to droughts. It is one of the most important commercial plants in livestock nutrition [7].

Figure 1. *Medicago sativa* L. *(alfalfa)*

Sample collection and preparation

Sampling was conducted in three Belgrade municipalities – Surčin (village Jakovo), Lazarevac (village Sokolovo) and Obrenovac (village Krtinka). At each of the three villages, three sampling sites (gardens) were randomly selected for plant and associated soil sampling. All of the chosen gardens are located in the vicinity of the fly ash disposal site of the 'Nikola Tesla-A' thermal power plant. *Medicago sativa* was sampled in the form of hay in the amount of approximately 2 kg. Samples of plant material were first dried at room temperature for 10 days, then in drying chamber (Binder, Tuttlingen, Germany**)** to a constant weight. The associated soil was also sampled from three individual sampling points and then mixed into a composite sample at the depth of 0-20 cm following a harmonised sampling regime (approximately 2 kg per sample). The surface layer of soil was chosen for analysis because element deposition in soil mostly occurs in top soil [8]. Soil samples were dried to a constant mass and homogenized.

Micronutrients analysis

The concentrations of selected micronutrients in *Medicago sativa* material were measured after wet digestion following USEPA 3052 protocol. Concentrations were measured by the method of optical emission spectrometry for simultaneous multielemental analysis (ICP - OES, Spectro Genesis). Beech leaves (BCR - 100) were used as the reference material for validation of the analytical procedure and quality control of the laboratory protocol. The analysis was performed in six replicates (n=6). The detection limits (mg kg^{-1}) are as follows: Mn- 0.000157, Se- 0.0102 and Zn- 0.00348. The element content in the soil was determined in the same manner as for the plant material, using the USEPA method (3052) with the standard reference material (Loam soil - ERM - CC141) to validate the analytical procedure. Detection limits were identical to those of the plant material.

Statistical analysis and bioconcentration factor (BCF)

The data from this study was analysed using statistical analysis (ANOVA) and means were separated with a Bonferroni test at a level of significance of $p<0.05$, using the Statistica software package (StatSoft In., Tulsa, USA, 2007). Correlations between the levels of the tested elements in soil and associated fodder were obtained using the non-parametric Spearman rank-order correlation coefficient at a level of significance of $P<0.05$.

Parameter which indicates the potential efficiency of removal of chemical element from soil by plants - the bioconcentration factor (BCF) was also determined. This factor defines the ratio between the available amount of a chemical element in the soil and the amount in the plant material ($[Element]_{leaf}/[Element]_{soil}$] [9,10]. A value of BCF > 1 indicates the potential of plant for phytostabilization of certain soil element.

Results and discussion

The concentrations of micronutrients in plant material were compared with reference values for the leaves of most herbaceous plants [11], and the maximum allowable concentration of certain elements in fodder that do not adversely affect the diet of domestic animals [12,13], Table 1.

Table. 1 Limit values of micronutrients in plants and fodder (mg kg^{-1})

	Mn	Se	Zn
TL[a]	300-500	5-30	100-400
MAC	100-250[b]	2-5[c]	2000[b]

[a] Critical or toxic levels in leaf tissue for various species [11]; [b] maximum allowable concentration in fodder [12]; [c] Edmondson et al. [13]

The concentrations of micronutrients in fodder and associated soil at the investigated sampling sites are shown in Table 2.

Table 2. Difference in micronutrients content between sampling sites in fodder and associated soil

	Fodder				Soil			
Mn (mg kg^{-1})	av ± st dev	Surčin	Lazarevac	Obrenovac	av ± st dev	Surčin	Lazarevac	Obrenovac
Surčin	26.89±2.96	/	***	***	777.57±28.68	/	***	ns
Lazarevac	37.46±0.71	***	/	*	613.57±18.39	***	/	***
Obrenovac	33.30±2.31	***	*	/	792.26±17.75	ns	***	/
Se (mg kg^{-1})								
Surčin	2.48±0.86	/	ns	ns	7.99±1.38	/	ns	ns
Lazarevac	3.31±1.30	ns	/	ns	9.49±1.60	ns	/	ns
Obrenovac	2.39±0.66	ns	ns	/	8.86±1.47	ns	ns	/
Zn (mg kg^{-1})								
Surčin	39.16±3.37	/	***	ns	107.89±5.58	/	***	***
Lazarevac	55.63±4.11	***	/	***	89.98±7.58	***	/	ns
Obrenovac	37.69±2.25	ns	***	/	84.80±1.75	***	ns	/

ANOVA, n=5, *p<0,05, **p<0,01, ***p<0,001, ns-no statistical significance

Manganese is an essential micronutrient that plants need for photosynthesis, respiration, synthesis of chlorophyll, synthesis of ATP, synthesis of acyl lipids, flavonoids, lignin and proteins. It is also an essential component of numerous enzymes [14, 15]. Its uptake is metabolically controlled, but under conditions of elevated Mn concentrations, passive absorption is also possible [16]. Manganese has an irreplaceable function in plants, but despite this, the lack of this element is often accompanied by the absence of visible symptoms of damage. Normal Mn concentrations were measured in the studied *Medicago sativa* samples (26-37 mg kg^{-1}, [11], Table 1), with statistically significant differences in accumulation capacity among all sampling sites (Table 2). All obtained results were well below the MAC for animal fodder (Table 1). Maximum allowable concentrations, limit and background values for Mn in soil are not defined in European and national legislation [17–20]. The highest average values for Mn in soil were measured in Obrenovac (792 mg kg^{-1}). Statistically significant differences in Mn content (<0.001***) were found between the control site in Surčin and Obrenovac (Table 2). The higher Mn content at these sites is probably due to local sources of pollution (thermal power plant), since Mn can enter the soil not only through the decomposition of the parent rock, but also through various anthropogenic activities [16]. To understand the pathways of element uptake, distribution and accumulation, the relationships between the content of micronutrients in fodder and the associated soil at all sampling sites were analyzed using the Pearson correlation coefficient. The correlation analysis showed a statistically significant positive correlation at all sites (Table 3), indicating the accumulation of Mn from the soil, except for the control site in Jakovo, where the lowest Mn content (26.89 mg kg^{-1}) was measured in the fodder. The presence of both positive and negative correlations indicates a double origin of Mn in the studied samples of *M. sativa*.

Selenium is an important micronutrient, necessary for the most basic physiological functions as a component of the amino acid selenocysteine. However, it is a relatively rare element. The uptake of selenium by plants and the total amount in plant tissues is influenced by many factors, including its content in the soil, its form, the pH and redox potential of the soil, and the mineral structure of the soil and fertilizers. From the plant physiological point of view, selenium belongs to the group of useful or beneficial elements. Selenium concentrations in animal feed from 0.1 do 0.5 mg kg^{-1} dry weight are considered safe with respect to possible selenium toxicity. Chronic and acute symptoms of poisoning are described at concentrations of 2 do 5 mg kg^{-1} [21-23]. From the obtained results (Table 2), it appears that the Se concentrations in the fodder are in a range that can be considered potentially risky, i.e., they can lead to poisoning or death of farm animals during consumption [23]. Namely, in 2012 in Saskatoon, Saskatchewan, Canada, there was a mass mortality of lambs given Se in the form of sodium selenite intramuscularly, resulting in pancreatic hemorrhage, subacute to acute heart failure and myocardial necrosis three days after treatment, suggesting acute selenium

intoxication. These results urge caution in consumption of fodder at the studied sampling sites. From a statistical point of view, no significant differences in Se content were found between sampling sites, either in fodder nor in soil (Table 2). Most noncontaminated world soils contain 0.10 to 2 ppm of total Se [24]. In principle, soils that contain above 6 ppm of Se are considered selenium-rich. These soils are also known as seleniferous. The Se content in the studied soils varied between 8 and 9.5 mg kg^{-1}, indicating that these soils are enriched in Se, although the MAC regulations for harmful elements in agricultural soils do not specify values for this element [18]. In contrast, the National regulation of the Republic of Serbia [19] sets the upper limit for Se of 0.7 mg kg^{-1}, while concentrations of 100 mg kg^{-1} indicate significant contamination. Such inconsistencies in setting the MAC indicate the need to adopt new regulations, legislation, and harmonization of the MAC at the national level. The highest Se concentrations in fodder and soil were measured in Lazarevac. Correlation analysis revealed two significant negative correlations in Surčin and Obrenovac (Table 3), indicating that there is a different uptake of Se from soil and that this may be related to pollution from thermal power plants.

Zinc is an essential element that represents a building component of enzyme structure, is involved in the metabolism of carbohydrates and proteins, affects the permeability of membranes and the resistance of plants to pathogens. It also affects membrane permeability and stabilization of cellular components [16,25,26] and has a particular importance for chloroplasts, i.e., enzymes involved in the process of photosynthesis [27]. The normal Zn content in plants is in the range of 15-150 mg kg^{-1} [11], so it is evident from the results obtained (Table 2) that the fodder absorbed Zn in sufficient quantity for normal function. The accumulation of Zn depends on the amount available in the soil solution, from which the plant takes it up either as Zn^{2+} or in hydrated form, although it can also be absorbed in the form of complexes and organic chelates [11,28]. Statistically significant differences in Zn content (<0.001***) were found between the control site in Surčin and Lazarevac, while there were no differences between Surčin and Obrenovac (Table 2). All obtained results were well below the MAC for animal fodder (Table 1). Soil Zn content depends on the nature of the parent rock, organic matter content, soil texture, and pH [16,24] and did not exceed the MAC in soil and limit values proposed by European and national legislation (300 mg kg^{-1} ,[18]; 50 - 300 mg kg^{-1}, [17]). The highest Zn content in soil was measured in Surčin, the control sampling site (108 mg kg^{-1}), which was significantly different from the other two sampling sites (< 0.001***, Table 2). Correlation analysis revealed only one significant correlation in Obrenovac (Table 3), indicating that Zn is taken up from the soil at this site.

Table 3. Spearman's correlation coefficient for the tested micronutrients between fodder and associated soil

		Medicago sativa		
Sampling site		Mn_{soil}	Se_{soil}	Zn_{soil}
Surčin Jakovo	Mn	-.975**		
	Se		-.850*	
	Zn			-0.067
Lazarevac Sokolovo	Mn	0.992**		
	Se		0.211	
	Zn			-0.615
Obrenovac Krtinska	Mn	0.885*		
	Se		-0.891*	
	Zn			0.855*

Based on the obtained element concentrations in soil and plant material, the bioconcentration factor (BCF) was also determined. This parameter indicates the potential efficiency of removal of chemical element from soil by plant, so called phytostabilization. From the results obtained it was

found that *Medicago sativa* is not effective in immobilizing the examined micronutrients, as all obtained values for BCF were below 1 (Figure 2).

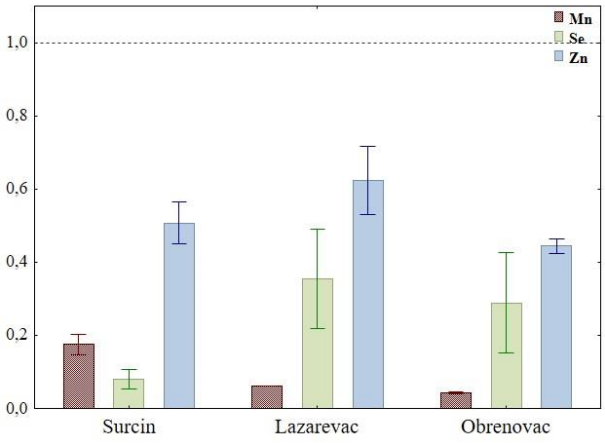

Figure 2. *Affinity of fodder to accumulate the tested micronutrients at the sampling sites based on the bioconcentration factor (BCF)*

Conclusion

The concentration of the examined micronutients measured in livestock fodder from the selected sampling sites was within the usual concentrations for conventional production, except in case of Se. According to the available literature data, the Se concentration in the studied samples of *Medicago sativa* was in a range that can cause chronic or acute poisoning of livestock when consumed, so special caution should be exercised when it is used as livestock feed. Nevertheless, the fodder was found not to be a significant accumulator of Mn, Se and Zn, as the bioconcentration factor values were less than 1, indicating that the fodder is not suitable for phytostabilization of these elements in the studied soils. It was found that the highest content of micronutrients in fodder was measured in Sokolovo (Lazarevac). On the other hand, no clear pattern was observed in the soils. The investigated micronutrient concentrations in soil were within the MAC values for soils according to the regulations of the Republic of Serbia and the limit values proposed by the Council Directive of the European Community. However, the results for Se in soil also show that the regulations and laws of the Republic of Serbia need to be revised, as there are clear contradictions between the maximum allowable concentrations, limit and remediation values.

Acknowledgements

This work was supported by the Ministry of Science, Technological Development and Innovation of the Republic of Serbia, grant no. 451-03-47/2023-01/200007.

References

1. H. Marschner, *Mineral Nutrition of Higher Plants*. Academic Press, Elsevier, 2012.
2. F. Madrid, M. Biasioli, F. Ajmone-Marsan, Availability and bioaccessibility of metals in fine particles of some urban soils, *Arch. Environ. Contam. Toxicol*., **55**, 21-32, 2008.
3. A. Bielicka-Giełdoń, E. Rylko, K. Zamojc, Distribution, Bioavailability and Fractionation of Metallic Elements in Allotment Garden Soils Using the BCR Sequential Extraction Procedure, *Pol. J. Environ. Stud*., **22(4)**, 1013-1021, 2013.
4. L. Pan, J. Ma, J. Hu, B. Su, G. Fang, Y. Wang, Z. Wang, L. Wang, B. Xiang, Assessments of levels, potential ecological risk, and human health risk of heavy metals in the soils from a typical county in Shanxi Province,

China, *Environ. Sci. Pollut. Res*., **23(19)**, 19330-19340, 2016.
5. H. A. Ghrefat, N. Yusuf, A. Jamarh, J. Nazzal, Fractionation and risk assessment of heavy metals in soil samples collected along Zerqa River, Jordan, *Environ. Earth Sci*., **66**, 199-208, 2012.
6. I. Gržetić, R. H. A. Ghariani, Potential health risk assessment for soil heavy metal contamination in the central zone of Belgrade (Serbia), *J. Serb. Chem. Soc*., **73(8-9)**, 923-934, 2008.
7. L. Latrach, M. Farissi, M. Mouradi, B. Makoudi, A. Bouizgaren, C. Ghoulam, Growth and nodulation of alfalfa-rhizobia symbiosis under salinity: electrolyte leakage, stomatal conductance, and chlorophyll fluorescence, *Turk. J. Agric. For*., **38(3)**, 320-326, 2014.
8. D. Pavlović, M. Pavlović, V. Perović, Z. Mataruga, D. Čakmak, M. Mitrović, P. Pavlović, Chemical fractionation, environmental and human health risk assessment of potentially toxic elements in soil of industrialised urban areas in Serbia, *Int. J. Environ. Res. Public Health*, **18(17)**, 9412, 2021.
9. A. Migeon, P. Richaud, F. Guinet, D. Blaudez, M. Chalot, Hydroponic screening of Poplar for trace element tolerance and accumulation, *Water Air Soil Pollut*., **204**, 89-101, 2009.
10. M. Chen, Y. L. Tang, J. Ao, D. Wang, Effects of strontium on photosynthetic characteristics of oilseed rape seedlings, *Russ. J. Plant Physiol*., **59(6)**, 772-780, 2012.
11. A. Kabata-Pendias, H. Pendias, *Trace elements in soils and plants*. CRC Press, Boca Raton, FL, 2001.
12. OGSFRJ (1990). Official Gazette of Social Federative Republic of Yugoslavia, no. 2/90 and no. 27/90.
13. A. J. Edmondson, B. B. Norman, I. D. Suther, Survey of state veterinarians and state veterinary diagnostic laboratories for selenium deficiency and toxicosis in animals, *J. Am. Vet. Med. Assoc*., **202**, 865-874, 1993.
14. R. Millaleo, M. Reyes-Díaz, M. Alberdi, A. G. Ivanov, M. Krol, N. P. A. Hüner, Excess manganese differentially inhibits photosystem I versus II in *Arabidopsis thaliana*, *J. Exp. Bot*., **64(1)**, 343-354, 2013.
15. J. Zhao, W. Wang, H. Zhou, R. Wang, P. Zhang, H. Wang, X. Pan, J. Xu, Manganese toxicity inhibited root growth by disrupting auxin biosynthesis and transport in *Arabidopsis*, *Front. Plant Sci*., **8**, 272, 2017.
16. A. Kabata-Pendias, A. B. Mukherjee, *Trace elements from soil to human*. Springer Berlin Heidelberg, New York, 2007.
17. Directive 86/278/EEC, Council Directive of 12 June 1986 on the protection of the environment, and in particular of the soil, when sewage sludge is used in agriculture, *Off. J. Eur. Communities*., **181**, 6-12, 1986.
18. OGRS (1994). Regulation about allowable quantities of hazardous and harmful substances in the soil and methods for their investigation. Official Gazette of the Republic of Serbia, 23, 1994.
19. OGRS (2010). Regulations on a systematic soil quality monitoring programme, indicators for assessing the risk of soil degradation, and methodology for the preparation of remediation programmes. Official Gazette of the Republic of Serbia, 88, 2010.
20. B. M. Gawlik, G. Bidoglio, Background values in European soils and sewage sludges PART III Results of a JRC-coordinated study on background values. European Commision, Joint Research Centre EUR 22265 EN, 2006.
21. U. C. Gupta, S. C. Gupta, Selenium in soils and crops, its deficiencies in livestock and humans: Implications for management, Commun. *Soil Sci. Plan*., **31**, 1791-1807, 2000.
22. P. Aitken, Selenium toxicity, *In Pract*., **23**, 286-289, 2001.
23. C. M. McKenzie, A. N. Al-Dissi, Case report. Accidental selenium toxicosis in lambs, *Can. Vet. J*., **58**, 1110-1112, 2017.
24. D. C. Adriano, *Trace elements in terrestrial environments*. New York, Springer, 2001.
25. S. R. Mousavi, M. Galavi, M. Rezaei, The interaction of zinc with other elements in plants: a review, *Int. J. Agric. Crop Sci*., **4**, 1881-1884, 2012.
26. E. M. Mattiello, H. A. Ruiz, J. C. L. Neves, C. Ventrella, Zinc deficiency affects physiological and anatomical characteristics in maize leaves, *J. Plant Physiol*., **183**, 138-143, 2015.
27. I. Cakmak, Possible roles of zinc in protecting plant cells from damage by reactive oxygen species. *New Phytol*., **146**, 185-205, 2000.
28. B. J. Storey, „Zinc," in *Handbook of plant nutrition*, A. V. Barker, D. J. Pilbeam, Eds. CRC Press, Taylor & Francis Group, LLC, Boca Raton, FL, 2007, 411-430.

Machine learning assisted screening of materials for Li-ion batteries

Razvoj materijala za litijum-jonske baterije korišćenjem mašinskog učenja

Katarina Batalović*, Mirjana Medić Ilić, Bojana Kuzmanović, Bojana Paskaš Mamula, Jana Radaković

[1] *CONVINCE-Center of excellence for hydrogen and renewable energy, VINCA Institute of nuclear sciences-national institute of the Republic of Serbia, Mike Petrovića Alasa 12-14, Belgrade, Serbia*

**kciric@vin.bg.ac.rs*

Abstract

The development of novel materials is seen as the key approach to improvements in the performance of Li-ion batteries. Recently, conversion-type electrodes have been demonstrated to improve battery capacity and energy density. Metal hydrides are considered promising anode materials, while some hydride materials are also considered solid ionic conductors. In this research, we rely on the machine learning approach to predict the properties of novel anode materials depending on hydride conversion reactions. We limit our search to Mg-containing intermetallic compounds and screen a vast database of optimized crystal structures obtained using density functional theory calculations. The composition and crystal structure of selected metals/intermetallics are input for a graph neural network-based machine learning model to predict hydride formation enthalpy and equilibrium electrode potential vs. Li^+/Li^0. Among 245 intermetallic compounds found to be satisfactory as anode materials, we particularly discuss La-Mg-X intermetallics. The work demonstrates the advantages of combining artificial intelligence tools and theoretical approaches with experimental results for property prediction and fast screening of vast combinatorial space.

Keywords: *Li-ion batteries; anodes; machine learning; metal hydride; Mg*

Izvod

Brojna istraživanja usmerena su na razvoj novih materijala kao ključnog pristupa u poboljšanju performansi litijum-jonskih baterija. Poslednjih godina posebno se ispituju konverzione elektrode koje omogućavaju veće kapacitete i gustine energija. Posebno, metalni hidridi se ispituju kao pogodni materijali za anode konverzionog tipa, dok se takođe neki hidridi ispituju i kao pogodni jonski provodnici. U ovom radu koristimo modele mašinskog učenja za predviđanje osobina novih anodnih materijala, oslanjajući se na reakcije konverzije hidrida. Pretraga novih intermetalnih jedinjenja ograničana je na one koji sadrže magnezijum, a kao izvor podataka korišćene su dostupne baze kristalnih struktura oprimizovanih proračunima zasnovanim na teoriji funkcionala gustine. Sastav i kristalna struktura odabranih metala/intermetalnih jedinjenja korišćeni su kao ulazni podaci za model mašinskog učenja zasnovan na graf neuronskim mrežama. Na taj način predviđene su entalpije formiranja hidrida i ravnotežni elektrodni potencijali u odnosu na Li^+/Li^0. Od 245 intermetalnih jedinjenja koja zadovoljavaju uslov za anodni materijal izdvojena su i diskutovana ternarna jedinjenja La-Mg-X. Ovaj rad pokazuje prednost kombinovanja alata veštačke inteligencije i teorijskih pristupa sa eksperimentalnim radom u cilju predviđanja osobina novih materijala i brze pretrage velikog prostora mogućih intermetalnih jedinjenja.

Ključne reči: *litijum-jonske baterije; anode; mašinsko učenje; metalni hidridi; magnezijum*

Introduction

The development of innovative electrode materials [1] and novel solid-state electrolytes [2] is seen as a route toward the improvement of Li-ion batteries (LIBs). The relatively low theoretical capacities and the problem of capacity fading in the active materials of classical intercalation reactions led to the consideration of novel anode electrode materials, including various conversion materials. Metal hydrides have been demonstrated to have a high theoretical capacity and energy density [2,3]. In addition, some metal hydrides are investigated as solid-state electrolytes [4].
The expansion of machine learning (ML) and artificial intelligence (AI) approaches in the last decade led to a new scientific paradigm in material discovery and optimization [5]. The data-centric approach in materials science and the development of accurate ML models enable the prediction of various material properties. In particular, hydride materials' thermodynamic characteristics, hydrogen storage properties [6,7,8], and solid compounds' ionic conductivity [9] are addressed.
Motivated by the importance of LIBs and opportunities offered by in-silico material design, we provide machine learning-guided exploration of potential conversion-type anode materials for LIBs.

Methodology

Data acquisition and machine learning approach

To consider hydride-forming intermetallic compounds which can be used as conversion-type electrodes in LIBs, we examined the Material Project (MP) database [10] containing a large number of crystal structures optimized using density functional theory (DFT). We limit our search to Mg-containing intermetallic compounds shown to be stable in DFT calculations. The latter is ensured by posing a constraint of intermetallic stability in DFT calculations (energy above convex Hull equals 0).
Hydride formation enthalpy and equilibrium potential of metal hydride conversion electrode for LIBs are obtained using MetalHydEnth[11], a graph neural network model. The model considers intermetallic compounds' chemical composition and crystal structure by transforming structural features into an index-type graph. A graph node corresponds to the vector of atomic numbers of constituent atoms. Edges of the graph are constructed for atom pairs within 5Å of spatial distance. In addition, the global states placeholder is initialized to store information and as a portal to enter state variables (e.g., temperature). All state attributes (atom, bond, global) are interconnected by definition and updated simultaneously through message-passing MEGNet blocks. A 16-dimensional element embedding layer, obtained from the Mp-2019.4.1 model [12] trained on the data set containing 133,420 data from the Materials Project [10], is included as the chemical intuition layer in the transfer learning approach.
The model predicts the heat of hydride formation based on the crystal structure and atomic composition, with a mean absolute error (MAE) value of 9.1kJ/molH_2 and MAE of 5.5kJ/molH_2 for Mg-containing intermetallics [8]. Hydride formation enthalpy (ΔH_{hyd}) is obtained as ΔH_{hyd}= - the heat of hydride formation. Enthalpy change in the reaction of hydride formation (expressed in kJ/molH_2) is obtained for any input struct file. Importantly, representing the enthalpy of hydride formation reaction in kJ/molH_2 allows comparison of various metal hydrides regardless of the stoichiometry of their hydride formation reaction.

Theoretical background

In metal hydride Li-ion batteries, a conversion reaction between LiH and metal hydride (MH_x) occurs at the anode [3]. The overall reaction and the corresponding change in the Gibbs free energy at T=25˚C are presented in equations (1) and (2).

$$MH_x + xLi^+ + xe^- \leftrightarrow M^0 + xLiH \quad (1)$$

$$\Delta_r G^\circ_{298} = x\Delta_f G^\circ_{298}(LiH) - \Delta_f G^\circ_{298}(MH_x) = -xEF \quad (2)$$

Changes in Gibbs free energy during metal hydride formation for all metal-hydrogen systems are reasonably approximated by the entropy change of 130 J/K mol H_2. Therefore the enthalpy change remains the variable that determines the behavior of various metal hydrides. Taking the experimental value for the difference in Gibbs free energy in the formation of LiH and enthalpy of hydride formation in intermetallic compound predicted by the machine learning model, we calculate the equilibrium potential versus Li^+/Li^0 following equation (3):

$$E^\circ_0 = \frac{\Delta_f G^\circ_{298}(LiH)}{F} - \frac{\Delta_f G^\circ_{298}(MH_x)}{xF} \quad (3)$$

Results and discussion

Mg-containing alloys are selected as promising candidates, given that MgH_2 conversion electrodes are already demonstrated and that availability and low cost of Mg make them promising for broad applications. The initial search on the Materials Project database gave over 19000 compounds containing Mg. Applying conditions regarding stability and composition listed in the methodology section, we obtain 437 Mg-containing intermetallics. For all of them, hydride formation enthalpy prediction is made using MetalHydEnth [11], and the equilibrium potential of conversion electrode versus Li^+/Li^0 (in the text also referred as potential or equilibrium potential) is calculated as explained in the chapter theoretical background. Figure 1 displays the predictions as the function of volume per atom in the intermetallic compound.

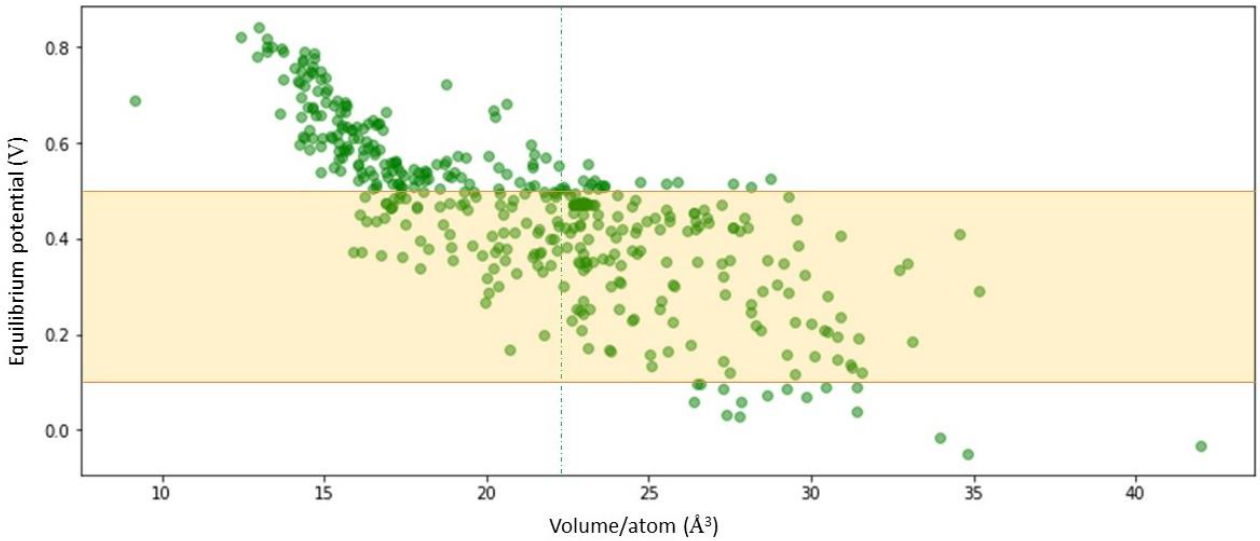

Figure 1. *Equilibrium potential of conversion-type metal hydride electrode vs. Li^+/Li^0 as a function of volume per atom in corresponding metal/intermetallic compound. The dashed vertical line shows the volume per atom in Mg metal, while the orange horizontal region marks desired 0.1-0.5V potential range.*

In the search for negative electrodes in Li-ion batteries, 0.1–0.5 V versus Li^+/Li^0 is taken as the safe potential range [3]. Of the 437 Mg-containing compounds, 245 have predicted potentials in this range, as marked in fig.1. We consider them further. Fig. 2 displays some properties of this subset.

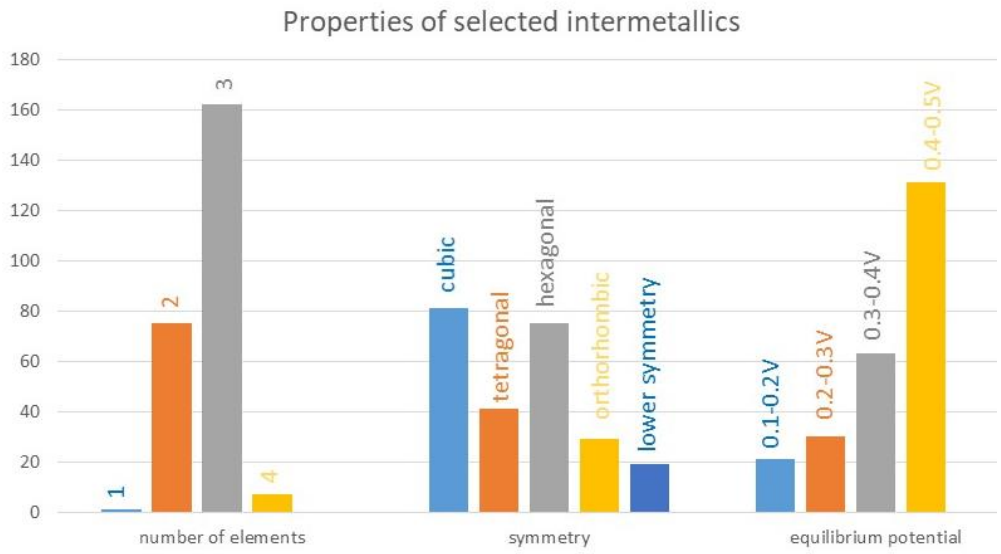

Figure 2. *Charts presenting selected properties (number of distinct elements, symmetry of the unit cell, and range of the predicted potentials) of 245 Mg-containing intermetallics selected as potential materials for conversion-type anodes in Li-ion batteries.*

As seen from the charts in fig.2, most selected intermetallics are ternary and binary. The predicted range of equilibrium potential is near the one for pure magnesium (0.56 V) (13) in many binary intermetallics of formula $Mg_{149}X$; these are omitted from the discussion, due to a slight variation in their enthalpy of hydride formation compared to MgH_2.

Table 1. Dominant elements among 245 intermetallics having 0.1-0.5 V equilibrium potential vs. Li^+/Li^0. Determined equilibrium potentials for binary intermetallics and potential range for ternary intermetallics are provided

Element	Binary compound	Potential (V)	No. ternary compounds	Potential range (V)
Ba	Ba_2Mg_{17} Ba_6Mg_{23}	0.43 0.28	11	0.19-0.35
Ca	/	/	11	0.12-0.41
Ce	$CeMg_3$	0.44	16	0.27-0.45
Gd	GdMg $GdMg_3$	0.42 0.49	11	0.41-0.47
La	LaMg $LaMg_3$	0.14 0.42	22	0.13-0.50
Sr	Sr_6Mg_{23}	0.36	10	0.12-0.35
Sc	MgSc $MgSc_2$	0.35 0.17	10	0.17-0.46
Nd	NdMg $NdMg_3$	0.29 0.46	27	0.21-0.49
Y	YMg YMg_3	0.12 0.43	19	0.14-0.42

A more detailed examination of ternary compounds is done. When alloyed with Mg, certain elements provide the most suitable intermetallics that are candidates for conversion electrodes. We identified Ba, Ca, Ce, La, Sr, Sc, and Nd as the most dominant elements in these compounds, which modulate Mg properties favorably for this application. These elements and the number of obtained ternary compounds containing them in addition to Mg are listed in Table 1.
In addition, we examine La-containing intermetallics, given that La compounds are well-established, stable hydride-forming materials. Fig.3 displays binary and ternary La-Mg containing intermetallics determined to have suitable potential vs. Li^+/Li^0 electrode, where each intermetallic is presented based on the crystal structure.

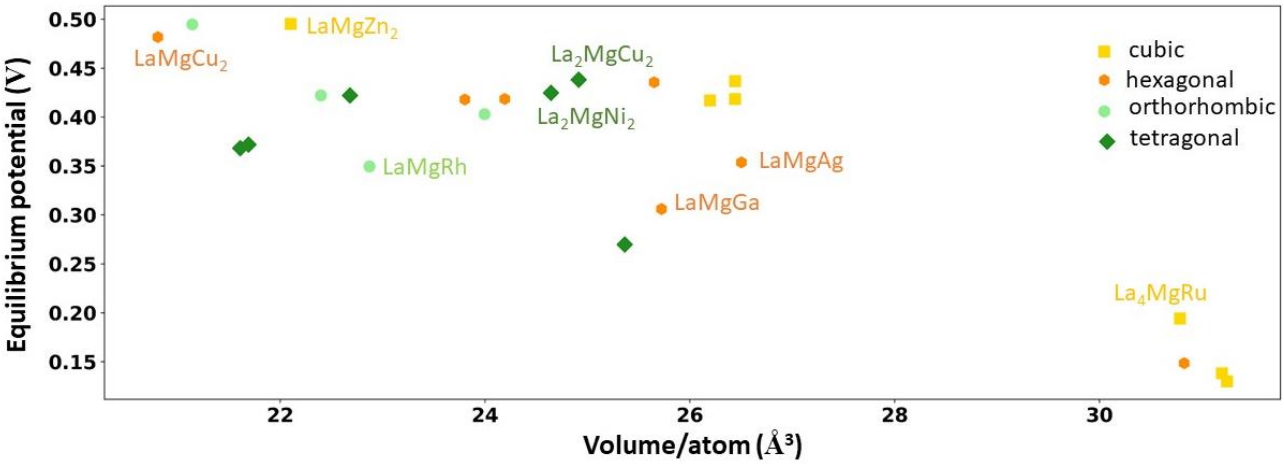

Figure 3. *La-Mg-containing intermetallics with predicted equilibrium potential in the 0.1-0.5V range; each point represents one of the 24 intermetallic compounds by crystal structure, while the formula is presented for the selected ones.*

We see that various intermetallics, formed with Mg and La, with or without the third element, are expected to provide suitable equilibrium potentials. In particular, Mg-La-Ir compounds and LaMg provide the smallest electrode potentials vs. Li^+/Li^0. La_4MgRu with a predicted potential of 0.19 V is a good choice, due to the known catalytic effect of noble metals in hydrogen sorption reactions. Intermetallics containing Cu, Zn, and Ni as a third element next to La and Mg are seen with higher potentials, near 0.5 V, in agreement with the known property of these metals to form less stable hydrides. Also important to note, while the potential is determined more by the chemical nature of the elements, intermetallics having various crystal structures have systematically different densities or volumes per atom, so all these aspects should be examined further to select those materials that will prove as the most stable in repeated charge/discharge cycles.

Conclusion

We present a screening study aimed at finding novel conversion-type anode materials for Li-ion batteries. We combine DFT and machine learning with domain knowledge to narrow the search for Mg-containing intermetallics. A total of 437 intermetallic compounds are identified in the Materials project database. Using structural data as input for the graph neural network-based machine learning model, we predict equilibrium potential vs. Li^+/Li^0 and found that 245 intermetallics satisfy the requirement of having his potential in the 0.1-0.5V range. We identify Ba, Ca, Ce, La, Sr, Sc, and Nd as suitable alloying elements for Mg, and point out some of the selected La-Mg-containing ternary intermetallics.

Acknowledgments

The funding for this research is provided by the Ministry of Science, Technological Development and Innovation of the Republic of Serbia, under Grant. No. 451-03-47/2023-01/200017.

References

1. Q. Cheng, D. Sun, X. Yu, Metal hydrides for lithium-ion battery application: A review, J Alloys Compds, 769, 167-185, 2018.
2. J.C. Bachman, M. Sokseiha Muy, A. Grimaud, et al. Inorganic Solid-State Electrolytes for Lithium Batteries: Mechanisms and Properties Governing Ion Conduction, Chem. Rev., 116, 140-162, 2016.
3. Y. Oumellal, A. Rougier, G. A. Nazri, J-M. Tarascon, L. Aymard, Metal hydrides for lithium-ion batteries, Nat. Mater., 7, 916-921, 2008.
4. L. M. de Kort, V. Gulino, P. E. de Jongh, P. Ngene, Ionic conductivity in complex metal hydride-based nanocomposite materials: The impact of nanostructuring and nanocomposite formation, J. Alloys Compds., 901, 163474, 2022.
5. B.L. DeCost, J.R. Hattrick-Simpers, Z. Trautt, A.G. Kusne, E. Campo, M.L. Green. Scientific AI in materials science: a path to a sustainable and scalable paradigm, Mach. Learn.: Sci. Technol. 1, 033001, 2020.
6. M. Witman, S. Ling, D. M. Grant, G. S. Walker, S. Agarwal, V. Stavila, M. D. Allendorf, Extracting an Empirical Intermetallic Hydride Design Principle from Limited Data via Interpretable Machine Learning, J. Phys. Chem. Lett., 11, 40–47, 2020.
7. S. Suwarno, G. Dicky, A. Suyuthi, M. Effendi, W. Witantyo, L. Noerochim, M. Ismail, Machine learning analysis of alloying element effects on hydrogen storage properties of AB2 metal hydrides, Int. J. Hydrogen Energy, 47, 11938 - 11947, 2022.
8. K. Batalović, J. Radaković, B. Paskaš Mamula, B. Kuzmanović, M. Medić Ilić, Predicting the heat of hydride formation by graph neural network - exploring the structure–property relation for metal hydrides, Adv.Theory Simul., 5, 2200293, 2022.
9. C. J. Hargreaves, M.W. Gaultois, et al. A database of experimentally measured lithium solid electrolyte conductivities evaluated with machine learning, *npj Comput. Mater.* , **9**, 9, 2023.
10. A. Jain, S.P. Ong, G. Hautier, W. Chen, W. Davidson Richards, S. Dacek, S. Cholia, D. Gunter, D. Skinner, G. Ceder, K. A. Persson, Commentary: The Materials Project: A materials genome approach to accelerating materials innovation, *APL Mater*., 1, 011002, 2013.
11. K. Batalović, J. Radaković, B. Kuzmanović, M. Medić Iiić, B. Paskaš Mamula, "MetalHydrideEnth". Mendeley Data, V1,. doi: 10.17632/4tpmdzxtf6.1[Online] 2022.
12. C. Chen, W. Ye, Y. Zuo, C. Zheng, S. Ping Ong, Graph Networks as a Universal Machine Learning Framework for Molecules and Crystals, *Chem. Mater.*, 31, 3564–3572, 2019.
13. F. Cano-Banda, R. Singh, A. Hernandez-Guerrero, A. Jain, T. Ichikawa, Enhanced performance of MgH_2 composite electrode using glass-ceramic electrolytes for all-solid-state Li-ion batteries, *J. Alloys Compds.*, 863, 158729, 2021.

Aktivna katodna zaštita od elektrohemijske korozije čelične konstrukcije pontona za pretovar naftnih derivata

Željko Krivačević, Dejan Grgić, Saša Stojanović, Aleksandar Pešić

Transnafta AD, Pančevo, Srbija

Izvod

Aktivna katodna zaštita nametnutom strujom noseće čelične konstrukcije pontona na reci za potrebe istovara/utovara derivata nafte i njen uticaj na produženje veka trajanja i sigurnosti rada pontona kao objekta izloženog stalnom uticaju elektrohemijske korozije.

Uvod

Za potrebe ugradnje aktivne katodne zaštite nametnutom strujom, izradjen je elaborat u skladu sa važećim standardima i propisima za zaštitu podzemnih i uronjenih objekata od elektrohemijske korozije (SRPS EN 12954 Katodna zaštita-opšti principi, EN 14505 Katodna zaštita kompleksnih struktura). Na osnovu elaborata ugradjena je oprema i izvršeni su radovi a nakon merenja nametnutog potencijala, puštena je u rad aktivna katodna zaštita nametnutom strujom, odnosno aktivna zaštita od elektrohemijske korozije čeličnih konstrukcija pontona (slika 1.) kao jedna od najpogodnijih metoda za aktivnu zaštitu od korozije čeličnih konstrukcija kako sa spoljašnje tako i sa unutrašnje strane.

Prepoznavanje glavnih elementarnih tačaka za potrebe ugradnje predvidjene opreme

Dovodno/odvodni čelični cevovodi do i od pontona, imaju svoj sistem katodne zaštite u koji delom spada i stanica katodne zaštite SKZ br.1 uradjena prema prethodnim projektima. Ovaj sistem je izveden i nalazi se u funkciji. Ovim novim elaboratom, smatramo ga projektom faze II, treba rešiti sistem katodne zaštite plovnih i ukopanih delova istovarnog mesta (pontona za pristajanje barži) i uskladiti ovaj sistem zaštite sa postojećim sistemom katodne zaštite samih ukopanih čeličnih cevovoda. Od navedenih struktura koje čine istovarnu strukturu jedan deo površina dolazi u dodir samo sa atmosferom, vlagom u vazduhu, oborinama i sl. Ove površine se štite pasivnom zaštitom, odnosno zaštitnim premazima (farbama) i ne čine deo površina štićenih katodnom zaštitom.
Katodnom zaštitom se štite površine struktura koje su u stalnom kontaktu sa tlom (ukopani delovi, nosači, vodjice) i površine u kontaktu sa vodom (ponton, vodjice, ledobran) od kojih su neke površine fiksne, a neke se menjaju sa oscilacijama vodostaja (budu poplavljene kod porasta nivoa vode). Za izgradnju sistema katodne zaštite ovakve strukture, koja se sastoji od više medjusobno pokretnih i nepokretnih delova (ponton, vodjice, ledobran) povezanih metalnim stazama treba prvo sprovesti tzv. „katodno povezivanje“ kako bi se obezbedila zaštita svih elemenata bez medjusobnih pojava struja interferencija katodne zaštite. Ovim povezivanjem treba obezbediti dobru električnu vezu, tj. dovodjenje na isti potencijal svih elemenata koje treba staviti pod katodnu zaštitu. Veze izmedju medjusobno nepokretnih delova, staza, ledobrana i sl. rade se kao čvrste – krute. Mogu se privarivati i trake. Kod medjusobno pokretnih elemenata (ponton u odnosu na vodjice, staze i sl.) povezivanje se radi sa savitljivim provodnicima, takvih dužina, koje omogućuju da se elementi mogu medjusobno pomicati do maksimalnih razdaljina uslovljenih oscilacijama vodostaja Dunava bez naprezanja odnosno kidanja. Anode, u ovoj fazi izgradnje katodne zaštite za zaštitu plovećih i uronjenih delova pristana treba rasporediti sa strane suprotne od obale. Stranu koja je okrenuta prema obali, svakako delom štiti stanica katodne zaštite br. 1 (SKZ 01) koja je izvedena kao prva faza u sklopu zaštite samog dovodnog/odvodnog čeličnog cevovoda koji nije električno odvojen od sklopa istovarnih struktura (pristana). Anodna ležišta (AL 01 i AL 02) ove stanice su u samom pojasu do reke, pa će kod izrade „katodnog“ spoja medju cevovodom i metalnom stazom do pristana odnosno pontona, svakako pokriti izložene strane štićenih struktura prema obali. Kao anode koje će se postaviti za zaštitu objekta u vodi koristiće se anode od titanijuma aktivirane oksidima retkih metala (MMO).

Anode će se rasporediti tako da se dobija što ravnomernija raspodela zaštitne struje na površinama štićenih struktura. Pri tome treba voditi računa da anode ne dodju na suvo i da ne budu izložene mehaničkim oštećenjima usled kretanja plovećih otpadaka, drvenih elemenata odnosno leda na Dunavu, prilikom pristajanja plovila (slika 2.) odnosno da ne ometaju plovila, korišćenje protivpožarnih elemenata (topova), funkcionisanje vodjica pri dizanju ili spuštanju pontona kod porasta odnosno smanjenja vodostaja i slično Za kontrolu polarisanosti štićenih površina ugradiće se stacionarna referentna merna elektroda na mestu koje se smatra karakterističnim. Kao referentna elektroda koristiće se zasićena bakar/bakarsulfatna ili cinkova merna sonda, s obzirom da se radi o slatkoj vodi. Pored ove stacionarne sonde treba ostaviti fiksno mesto za merenje potencijala pomoću prenosne sonde, s obzirom da se usled rečnih nanosa, ispiranja bakarsulfata u toku eksploatacije, stacionarna sonda može postati nepouzdana.

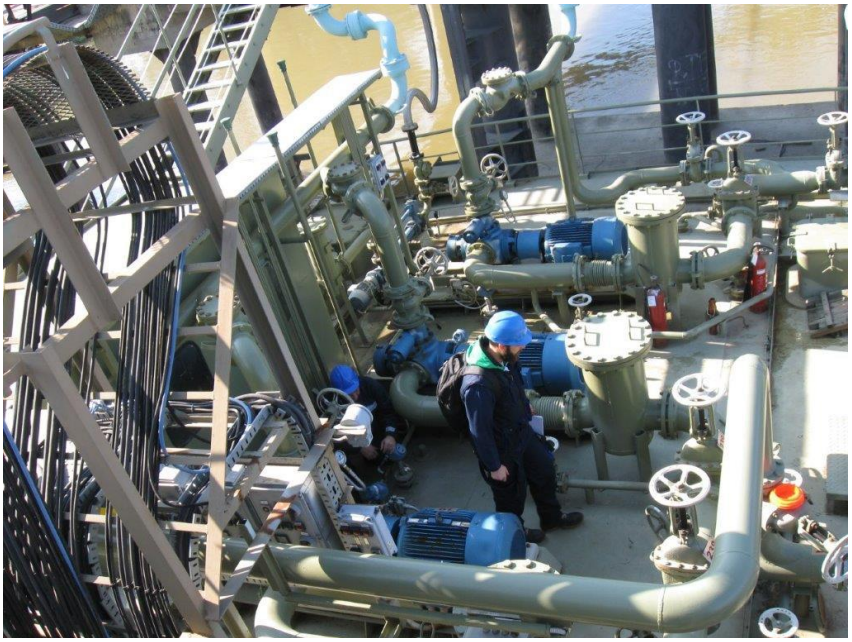

Slika 1. Ponton za utovar/istovar derivata nafte na reci

Objekti na istovarnom mestu na obali Dunava su: pristan, ponton za priključenje plovila na istovarna creva, vodjice pontona, ledobran (slika3.).

Slika 2. Pristajanje plovila-barže prilikom istovara derivata nafte

Slika 3. Pristan pontona

Izvodjenje pasivne zaštite delova čeličnih cevovoda za utovar/istovar na pontonu sa ispitivanjem instalacije na pritisak, iziskuje ogromne napore kako izvođača radova tako i zaposlenih na održavanju i upravljanju objektom (slika 4. i slika5.)

Slika 4. Montaža delova istovarnih ruku nakon pasivne zaštite i ispitivanja

Slika 5. Izvodjenje pasivne zaštite od korozije premazima i ispitivanje na pritisak istovarne ruke

Katodna zaštita pontona i ugradnja predvidjene opreme

Postojeće stanje struktura koje treba staviti pod katodnu zaštitu su objekti na istovarnom mestu na obali Dunava: pristan, ponton za priključenje plovila na istovarna creva, vodjice pontona, ledobran i svi ovi objekti imaju delove koji se stalno ili povremeno nalaze u kontaktu sa vlagom u tlu (koritom

Dunava) odnosno vodom koja protiče pored njih. Pri tome, s obzirom da vlaga predstavlja elektrolit dolazi do razvoja elektrolitičkih (tzv. korozionih) ćelija i do elektrolitičke korozije koju katodnom zaštitom treba eliminisati. Sistem katodne zaštite će se dimenzionirati tako, da obezbedjuje polarizaciju površina izloženih kontaktu sa elektrolitom (vodom, vlagom u tlu) kod svih vodostaja Dunava na tzv. zaštitni potencijal. Tako površine ubetonirane u korito reke (u kontaktu sa tlom i vlagom – elektrolitom, preko betona) i delovi struktura u vodi kod minimalnog vodostaja su površine stalno izložene delovanju elektrolitičke korozije, dok delovi koji u kontaktu sa vodom dolaze povremeno kod oscilacije vodostaja izmedju minimalnog i maksimalnog su u tom vremenskom periodu izloženi delovanju elektrolitičke korozije. Sistem će se dimenzionirati za maksimalni vodostaj tj. za zaštitu svih površina koje mogu doći u kontakt sa elektrolitom (vlagom u tlu odnosno vodom). Prema podacima iz ranijih projekata katodne zaštite „Tehnološka celina ponton-vodjice pontona-pristan-ledobran sa svim pripadajućim uronjenim i ukopanim metalnim masama“ površine izložene kontaktu sa tlom odnosno vodom pri maksimalnom vodostaju su (tabela 1.):

Tabela 1. Površine izložene kontaktu sa tlom odnosno vodom pri maksimalnom vodostaju

Struktura kontakt sa vodom	Kontakt sa tlom m^2	Pri maksimalnom vodostaju m^2
Ponton	100	
Pristan	496	866
Ledobran	1205	631
Vodjice	60	
Ukupno:	**1861 m^2**	**1497 m^2**

Potrebni radovi za pripremu struktura za katodnu zaštitu

Za ostvarivanje katodne zaštite na svim elementima u kontaktu sa tlom odnosno vodom, potrebno je, da se njihove površine u kontaktu sa tlom (vodom) (kroz pore betona ili oštećenja i pora u zaštitnim oblogama – farbama, premazima), zaštitnom strujom polarizuju na zaštitni potencijal prema tlu. Pojedine strukture nisu tehnološki ili na drugi način pouzdano električno povezani u jednu celinu koja bi omogućila polarizaciju na zaštitni potencijal pa iste treba na mestima gde postoje medjusobni fizički kontakti (naleganjem, pomeranjem po vodjicama i sl.) pouzdano povezati u jednu električnu celinu. Na taj način se izbegavaju interferencije u sistemu gde razlike u potencijalima pojedinih delova mogu dovesti do tzv. „lutajućih“ struja medju delovima štićenih struktura, koje mogu izazvati pojačanu koroziju na delovima gde napuštaju strukturu a u krajnjem slučaju vremenom i do varničenja, što, s obzirom da se radi na objektu gde se vrši manipulacija sa gorivima može imati nesagledive posledice. U konkretnom slučaju treba izvesti pouzdano povezivanje električnih spojeva izmedju svih elemenata sistema za istovar goriva na mestima gde su isti u fizičkom kontaktu provodnikom preseka najmanje 16 mm^2 koji može biti ili kabel ili použeni provodnik. Pričvršćivanje na pojedine elemente može biti preko papučica (ako za to postoje pogodni uslovi) ili direktnim (alumotermitnim) zavarivanjem. Koji će se način primeniti odlučiće se na licu mesta s obzirom da na raspolaganju ne postoji detaljna mašinska dokumentacija na osnovu koje bi se pojedine veze mogle unapred isprojektovati. Bitno je da ove veze pružaju pouzdane električne kontakte a da ne sprečavaju potrebno medjusobno pokretanje elemenata i da ih kretanje istih ne napreže mehanički.

Anode i anodna ležišta

U prvoj fazi izgradnje sistema izvedena su dva anodna ležišta (AL 01 i AL 02) koja su postavljena u samu obalu Dunava. Ova ležišta su izvedena kao plitka sa horizontalno položenim ferosilicijumskim anodama u koksnom punilu i u funkciji su sa stanicom katodne zaštite SKZ 01, za delimično napajanje sistema zaštite samog cevovoda (dovodno/odvodni čelični cevovodi). Ova stanica i anodna ležišta

predvidjene su pored zaštite kraja cevovoda i za pokrivanje zaštitnom strujom za stranu istovarne strukture okrenute prema obali. U drugoj (ovoj) fazi izgradnje sistema predvidja se postavljanje stanice katodne zaštite SKZ 02 koja treba da štiti stranu istovarne strukture sa strane Dunava. Ovde će se 6 anoda (A1, A2, A3, A4, A5 i A6) postaviti pojedinačno, tako da se obezbedi raspodela zaštitne struje što ravnomernije na površine okrenute Dunavu. Koristiće se pojedinačne anode MMO (titanijum sa aktiviranim površinama) koje će se direktno položiti u vodu. Anode se pričvršćuju na betonske nosače (korita), koja obezbedjuju da iste ostanu na dnu reke na lokaciji uz konstrukcije koje treba da štite. Pri tome treba voditi računa da se anode postavljaju na mesta koja će i kod najnižih vodostaja biti pod vodom. Mesta za postavljanje anoda (mikro lokacija) mora se izabrati tako da anoda ne ometa pristajanje barži i ne bude izložena plutajućim nanosima koje Dunav nosi (slika 6., 7., 8.). Nosači anoda moraju biti tako oblikovani da omogućavaju raspodelu struje u svim smerovima, sprečavajući da se s obzirom na blizinu dela štićene strukture (koju treba da štiti) ne dolazi do „kratkog spoja“ polarizacione struje. Same MMO anode će se montirati unutar korita izlivenih od betona. Ova korita obezbedjuju težinu, da anoda ostaje na dnu reke. Voda koja protiče Dunavom može slobodno doći u kontakt sa anodama, a eventualni nanos peska samo stvaraju bolji kontakt sa sredinom kroz koju će i struja potrebna za polarizaciju strukture prelaziti u vodu i teći ka štićenim strukturama. Ova korita služiće i kao štitnici od krupnih rečnih nanosa koji bi mogli oštetiti anode. Specifična otpornost betona korita od oko 500 om.m usmerava zaštitnu struju ka vodi (40 om.m) i sprečava da se velikim delom najkraćim putem zatvori kroz tlo na mestu strukture, smanjujući na taj način zaštitnu zonu iste. Dovodni (anodni kablovi) do anoda uvlače se na delu izmedju kablovskih nosača na strukturi (gde se polažu u sklopu ostalih kablova) i anoda na dnu reke u zaštitne cevi. Ove zaštitne cevi konstruisaće se u odnosu na deo štićene strukture na koju se pričvršćuju. Kako detaljnih crteža konstrukcije istovarnog mesta nema na raspolaganju, a mesta pričvršćenja zaštitnih cevi za anodne kablove na strukturu su različita, za svaku anodu će se konstruisati nosač za pričvršćenje zaštitne cevi za strukturu, uzimajući potrebne podatke i mere na licu mesta. Anode će se priključivati preko kontrolno spojnih kutija postavljenih na kablovskim nosačima na konstrukciji ispod staza (KS1 anode A1 i A2; KS2 anode A4 A5 i A6 i KS3 anoda A3).

Slika 6. 7. 8. Led na Dunavu kod pontona

Povezivanje sistema katodne zaštite

Kablovi za povezivanje sistema katodne zaštite (anodni, drenažni i merni sa kontrolne sonde) postaviće se na kablovske regale pored i ispod staza sa ostalim energetskim i signalnim kablovima. Priključna (drenažna) mesta na štićenoj strukturi, priključci anoda u koritima i za merenje potencijala: Svi priključci na štićene strukture u cilju merenja (kontrole potencijala) kao i za spajanje na stanicu za katodnu zaštitu (tačke drenaže) izvode se privarivanjem kablova alumotermitnim postupkom. Mesto zavara se mora izolovati, pa privareni kabel uvesti u mernu kutiju postavljenu na pogodnom mestu (KM2 i KM3) gde se vrši spajanje na kablove za povezivanje sistema. Po potrebi ovde se mogu postaviti i otpornici za usaglašavanje sistema ukoliko merenja pokazuju nedozvoljena odstupanja potencijala medju pojedinim delovima strukture. Drenažna mesta su locirana na pristanu i na pontonu. Na ovim mestima postaviće se kotrolno merne kutije KM 2 odnosno KM 3 u kojima se provodnici privareni na strukture spajaju sa drenažnim kablom. Svi kablovi u drenažnom sistemu kao i za povezivanje mernih sondi su zbog unifikacije izvedene kablovima tipa PP 00 4 x 2,5 mm^2 pri čemu se sve četiri žile u kablu na oba kraja spajaju paralelno. Za kontrolu zaštitnog potencijala ugradiće se stacionarne merne sonde na mestima gde se očekuju potencijali koji su karakteristični za celu strukturu. Sonde se preko kontrolno mernih kutija KM 2 i KM 3 povezuju u sistem i na taj način mogu se potencijali kontrolisati i podešavati na samoj stanici za katodnu zaštitu. Povezivanje anoda: Anode se do priključnih kutija (KS 1, KS 2 i KS 3) povezuju ulivenim kablom kojim su isporučene, a dalje se povezuju kablovima tipa PP 00 4x2,5 mm^2 do kontrolno spojne kutije KS 3. Veza izmedju kontrolno spojne kutije KS 3 i stanice katodne zaštite SKZ 02 izvešće se kablom PP 00 4x4 mm^2 položenim zajedno sa drugim kablovima na pristanu na nosače kablova na konstrukciji pristana. Stanica za katodnu zaštitu: Stanica za katodnu zaštitu postaviće se kao slobodno stojeća pored stanice SKZ 01 (koja je u pogonu) i napajaće se sa istog razvoda električne energije. Stanica se preko posebnog instalacionog osigurača povezuje monofazno na napajanje sa ulaznog dela razvoda sa faznog napona 220 V, tako da ostaje pod naponom i u slučaju da se ostala oprema napajana sa ovog razvoda, iz bilo kog razloga isključuje sa napajanja. Napajanje se izvodi kablom PP 00-Y-3x2,5 mm^2 koji se spaja na fazni, neutralni i zaštitni vod u razvodu sa kojeg se vrši napajanje i na taj način se na stanici katodne zaštite sprovodi isti sistem zaštite od napona dodira kao i na ostalim sistemima i delovima postrojenja na istovarnom mestu. Stanica sadrži transformator sa odvojenim namotajima za sniženje napona i odvajanje. Sekundar transformatora ima izvode na koje se preko prekidača (preklopke) za biranje napona priključuje ispravljački slog, koji obezbedjuje na izlazu stanice jednosmerni napon podesiv u koracima od 2 V u području od 0 do 50 V. S obzirom da se stanica priključuje na merenu struju nema potrebe za ugradnjom strujomera za merenje utroška električne energije. Za kontrolu izlaznih veličina iz stanice, ugradiće se voltmetar za jednosmernu struju mernog opsega od 0 do 60 V kao i ampermetar mernog područja od 0 do 30 A. Za kontrolu funkcije sistema katodne zaštite može se ugraditi i instrument za pokazivanje funkcioniranja (postojanja potencijala) zaštite. Oprema stanice za katodnu zaštitu ugradjena je u limeno kućište koje obezbedjuje zaštitu od prodiranja stranih tela odnosno vode IP 54 što odgovara mestu ugradnje kao slobodno stojeća na otvorenom. Svi izvodi odnosno uvodi u kućište stanice nalaze se sa donje strane kućišta i izvedeni su pomoću uvodnica odgovarajućeg prečnika prema kablovima (anodni, drenažni, merni, napojni).

Stavljanje u pogon sistema katodne zaštite

Nakon završenih radova na montaži svih elemenata u sistemu katodne zaštite sistem treba povezati i staviti u pogon. Radovi pre uključenja stanice katodne zaštite: Pre uključenja stanice za katodnu zaštitu treba prvo proveriti da li su svi kablovi povezani na predvidjeni način kako u stanici katodne zaštite tako i u svim kontrolno mernim kutijama. Proveriti sistem zaštite od opasnih napona dodira na stanici katodne zaštite (vrši ovlašćena organizacija). Izvršiti merenja prirodnog potencijala na mernim mestima (stabilno postavljenim referentnim elektrodama i mestu za pokretnu sondu na strukturi). Ovi podaci čine bazu prema kojima se vrednosti potencijala, a na taj način i postojanje

zaštite u toku eksploatacije sistema mogu uporedjivati. Sve izmerene podatke treba zabeležiti jer služe kao osnova za pogonsku dokumentaciju sistema katodne zaštite. Radovi i merenja posle uključenja stanice za katodnu zaštitu: uključiti stanicu za katodnu zaštitu i proveriti da li funkcioniše regulacija izlaznog napona - podesiti izlazne veličine na stanici za katodnu zaštitu prema merenom potencijalu na drenažnom mestu na vrednost oko - 0,95 do - 1,0 V prema standardnoj zasićenoj bakar/bakarsulfatnoj mernoj sondi (za sondu na bazi cinka +0,25 V) - prekontrolisati potencijale na svim mernim izvodima. Minimalni potencijal za zaštitu od elektrolitičke korozije u tlu odnosno vodi je - 0,85 V mereno prema zasićenoj bakar/bakarsulfatnoj mernoj sondi. Po potrebi podešavati izlazne veličine stanice da se na svim mernim mestima dostigne zaštitni potencijal. Po potrebi podesiti i raspodelu polarizacione struje medju anodama ugradnjom otpornika u spojne kutije za priključivanje anoda (KS1 do KS3) - Sve podešene podatke na stanici katodne zaštite (izlazni napon, struja, položaj preklopki i sl.) kao i izmerene podešene vrenosti treba zabeležiti u izveštaj koji ulazi u dokumentaciju sistema katodne zaštite.
S obzirom na konfiguraciju sistema, za zaštitu samog plovnog objekta (pontona) i svih pomoćnih struktura (pristan, vodjice, ledobran) veći deo struje daće SKZ 02 oko 60 %, za površine izložene sa strane prema vodi (Dunavu), dok će SKZ 01 dati oko 40 % potrebne struje za polarizaciju pristanišnog objekta na zaštitni potencijal sa strane prema obali.

Aktivna katodna zaštita nametnutom strujom

Katodna zaštita od elektrohemijske korozije zasniva se na katodnoj polarizaciji metala do potencijala (minus 850 mV) pri kom se usporava proces jonizacije i prekida proces korozije. Izvor struje polarizacije je spoljni izvor jednosmerne struje. Kriterijumi katodne zaštite definišu uslove pod kojima je moguće sistemom katodne zaštite izvesti zaštitu od elektrohemijske korozije spoljašnjih ili unutrašnjih površina metalnih konstrukcija koje su položene u elektrolit. Osnovni kriterijumi katodne zaštite su električne veličine, zaštitni potencijal Ez (V), odnosno minimalna katodna polarizacija i minimalna gustina zaštitne struje. U praksi najčešće primenjivan je kriterijum minimalnog zaštitnog potencijala - Ezmin. Stacionarni potencijal čelika u prirodnim sredinama se najčešće kreće u granicama od - 0,55 V do - 0,65 V u odnosu na referentnu Cu / CuSO4 elektrodu.
Da bi se ostvarila katodna zaštita, neophodno je izvršiti polarizaciju čeličnih konstrukcija najmanje za - 0,3 V ili vrednost zaštitnog potencijala u svakoj tački mora iznositi najmanje E = Ez min., odnosno E = - 0,85 V mereno između kontrolno mernog stuba i zasićene referentne Cu/CuSO4 elektrode (za anaerobne sredine u kojima bakterije redukuju sulfate do sulfida, minimalan zaštitni potencijal iznosi - 0,95 V).

Rezultati kontrolnog merenja uspostavljenog sistema katodne zaštite

Nakon polarizacije zaštićene strukture sistemom katodne zaštite izvršena je kontrola rada sistema katodne zaštite, postavljanja i povezivanja stanica za katodnu zaštitu, a izvršena merenja su u skladu sa standardom SRPS/EN 13509. Vršeno je merenje prirodnog potencijala, a nakon puštanja u rad i potencijali na svim postavljenim mernim elementima (sondama). Posle perioda polarizacije od oko 6 meseci, izvršena su kontrolna merenja.

Održavanje i kontrola sistema katodne zaštite

Za potrebu sistema katodne zaštite na pontonu ugradjena je oprema za katodnu zaštitu i oprema je puštena u rad. Pri redovnom održavanju opreme treba ispoštovati uputstvo za uključenje i podešavanje parametara na stanici katodne zaštite, i to sledeće:

- uključiti stanicu za katodnu zaštitu i proveriti da li funkcioniše regulacija izlaznog napona;

- podesiti izlazne veličine na stanici za katodnu zaštitu prema merenom potencijalu na drenažnom mestu na vrednost oko - 0,95 do - 1,0 V prema standardnoj zasićenoj bakar/bakarsulfatnoj mernoj sondi (za sondu na bazi cinka +0,25 V);
- prekontrolisati potencijale na svim mernim izvodima. Minimalni potencijal za zaštitu od elektrolitičke korozije u tlu odnosno vodi je - 0,85 V mereno prema zasićenoj bakar/bakarsulfatnoj mernoj sondi. Po potrebi podešavati izlazne veličine stanice da se na svim mernim mestima dostigne zaštitni potencijal. Po potrebi podesiti i raspodelu polarizacione struje medju anodama ugradnjom otpornika u spojne kutije za priključivanje anoda (AK1 do AK3);
- sve podešene podatke na stanici katodne zaštite (izlazni napon, struja, položaj preklopki i sl.), kao i izmerene podešene vrenosti treba zabeležiti u izveštaj koji ulazi u dokumentaciju sistema katodne zaštite;
- rad sistema katodne zaštite treba prekontrolisati merenjem svih izmerenih veličina pri podešavanju posle 30 dana rada sistema i po potrebi podesiti s obzirom da se usled polarizacije struktura podešeni potencijal može poremetiti. Nova podešenja uneti u dokumentaciju;
- nakon toga sistem treba kontrolisati i podešavati u prve godine četiri puta a posle najmanje dva puta godišnje i o tome sačiniti izveštaj koji čini dokumentaciju sistema katodne zaštite;
- u slučaju pokazivanja instrumenta u stanici katodne zaštite da zaštita nije u funkciji što znači da su strukture izložene koroziji (crvena polja, ukoliko postoji instrument za pokazivanja postojanja zaštitnog potencijala katodne zaštite, ampermetar na nuli, ili nema izlaznog napona na stanici katodne zaštite), pozvati kompetentnu organizaciju, ili lice da podesi sistem katodne zaštite, ili u slučaju kvara da kvar na istom otkloni.

Zaključak

1. Da je potrebno kao i kod svakog sistema, redovno održavanje čelične konstrukcije pontona (pasivna zaštita premazima).
2. Da je potrebno kao i kod svakog sistema, redovno održavanje sistema katodne zaštite prema upustvu isporučioca katodne zaštite i prema upustvu o održavanju i ispitivanjima sistema katodne zaštite koje je predložio izvodjač radova.
3. Da je potrebno redovno ispitivanje, pregled i merenje katodne zaštite;
4. Praksa je pokazala da je tokom veka eksploatacije pontona za pretovar derivata nafte više od 80 % oštećenja nastaje na donjoj konstrukciji bliže vodi. Zato je potrebno da katodna funkcioniše besprekorno kao i sistem redovnog održavanja.

Assessment of Emissions into the Atmosphere from Biogas Cogeneration Plant in Serbia

Procena Emisija u Atmosferu iz Biogasnog Kogenerativnog Postrojenja u Srbiji

Slobodan Cvetković[1*], Jovana Perendija[1], Aleksandra Radomirović[2]

[1]*Univerzitet u Beogradu, Institut za hemiju,tehnologiju i metalurgiju, Njegoševa 12, 11000 Beograd, Srbija*

[2]*Društvo "Chemical And Energy Engineering",11000 Beograd ,Srbija*

[1]*University of Belgrade, Institute of Chemistry, Technology and Metallurgy (ICTM), Njegoseva 12, 11000 Belgrade, Serbia*

[2]*Society "Chemical and Energy Engineering",11000 Belgrade, Serbia*

**Corresponding Author: slobodan.cvetkovic@ihtm.bg.ac.rs*

Abstrakt

Biogas je gasna smeša koja nastaje tretmanom otpadnih tokova u procesu anaerobne digestije. Proizvodnja električne energije iz kogeneracionih postrojenja koja koriste biogas je u porastu u Republici Srbiji. U ovom radu je izvršena kvantifikacija emisija (ugljen-dioksida, sumpor-dioksida, oksida azota, metana i čestica) u atmosferu iz tipičnog biogasnog postrojenja u Republici Srbiji, instalisanog kapaciteta od 1 MW. Dobijeni rezultati su pokazali da proizvodnja električne energije iz kogeneracije biogasa predstavlja dobro rešenje u cilju smanjenja emisije gasova sa efektom staklene bašte i racionalne upotrebe prirodnih resursa.
Ključne reči*:biogas; energija;kogeneracija;emisija*

Abstract

Biogas is the gas mixture generated by the treatment of waste streams in the process of anaerobic digestion. The production of electricity from cogeneration plants that use the biogas is increasing in the Republic of Serbia. In this paper, the quantification of emissions (carbon dioxide, sulphur dioxide, nitrogen oxides, methane and particles) into the atmosphere from a typical biogas plant in the Republic of Serbia with an installed capacity of 1 MW was carried out. The obtained results showed that the production of electricity from biogas cogeneration is a good solution in order to reducing the emission of greenhouse gases and rational use of natural resources.
Key Words*: Biogas; Energy; Cogeneration; Emission*

Uvod

Fosilna goriva su ograničena svojom dostupnošću u prirodi i zagađuju životnu sredinu prilikom sagorevanja. Sve veći uticaj ovih procesa na prirodno okruženje, intenzivirao je primenu obnovljivih resursa kako bi se obezbedila čistija i ekološki prihvatljivija goriva. Globalno zagrevanje i klimatske promene koje su rezultirale ekološkim i zdravstvenim problemima, kao i rastuće cene goriva i energije, pojačale su pritisak na nacionalne ekonomije da se postepeno okreću ka upotrebi obnovljivih izvora energije. Stoga, korišćenje obnovljivih izvora energije kontinuirano raste zbog njihovog manjeg ekološkog uticaja, kao i doprinosa dekarbonizaciji energetskog sektora [1].

Među dostupnim rešenjima za proizvodnju energije iz biomase, biogas predstavlja dobro rešenje za alternativnu proizvodnju energije, usled nižih kapitalnih i operativnih troškova. Takođe, korišćenje širokog spektra otpadne organske biomase (stajnjak, komunalni otpad, poljoprivredni ostaci, otpadne

vode iz prehrambene industrije, itd.), koja bi u suprotnom bila deponovana u životnu sredinu i doprinosila emisiji gasova staklene bašte (GHG), izbacilo je ovu tehnologiju u prvi plan. Proizvedeni biogas može se koristiti za različite svrhe kao što su grejanje i proizvodnja električne energije (kogeneracija), transport, ili ubrizgavanje u mrežu prirodnog gasa, nakon uklanjanja zagađivača [2]. Procenjuje se da se upotreba energije iz biogasa udvostručila za jednu deceniju sa 14.5 GV u 2012. na 29.5 GV u 2022. godini [3]. Postoji sve veće interesovanje za proizvodnju biogasa širom sveta usled ekoloških, kao i ekonomskih i socijalnih razloga. Proizvodnja energije iz biogasa doprinosi proizvodnji obnovljive i održive energije, pošto se biogas može koristiti kao fleksibilna i predvidljiva alternativa za fosilna goriva.

Republika Srbija je kao zemlja kandidat za članstvo u Evropskoj Uniji prihvatila obavezu većeg korišćenja obnovljivih izvora energije u svom energetskom miksu. Donošenjem podsticajnog zakonodavnog okvira 2010. godine za investicije u obnovljive izvore energije, počela je izgradnja biogasnih postrojenja. Proizvodnja energije iz ovih ekološko-energetskih sistema beleži značajan rast poslednjih godina (Slika 1).

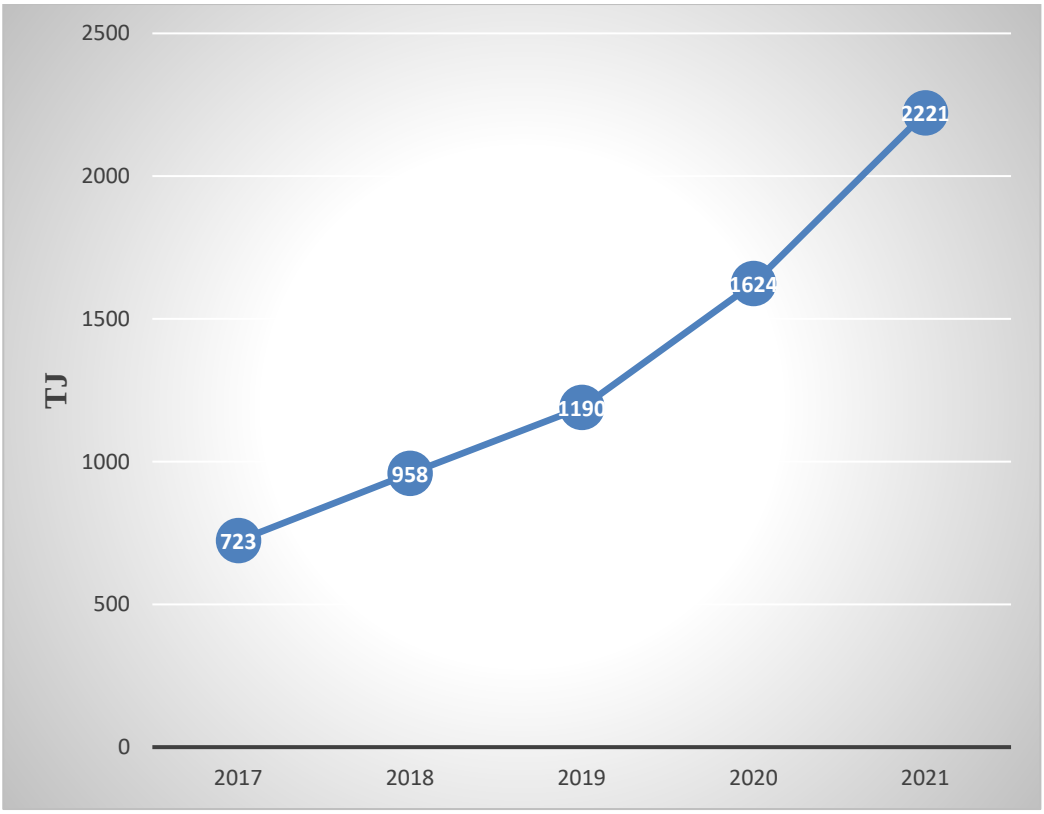

Slika 1. Primarna energija iz biogasa u Republici Srbiji u periodu od 2017.-2021.[4]

Najviše biogasnih postrojenja u Republici Srbiji locirano je na teritoriji AP Vojvodina (Slika 2), imajući u vidu da je to područje sa najvećom poljoprivrednom proizvodnjom, čiji se otpadni tokovi koriste za proizvodnju biogasa. Ukupna instalisana snaga biogasnih postrojenja u Republici Srbiji iznosi 34.28 MW[5].

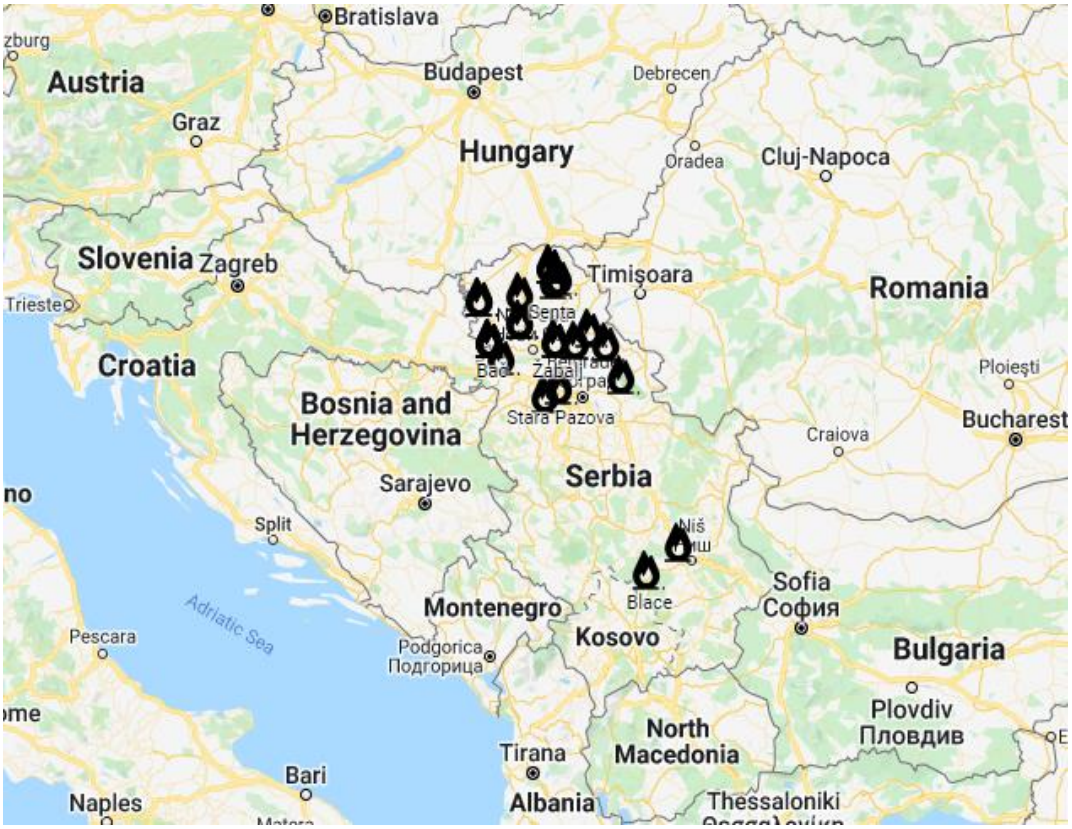

Slika 2. Lokaliteti biogasnih postrojenja u Srbiji [5]

Tokom procesa kogeneracije biogasa nastaje emisija gasova (ugljen dioksida, sumpor dioksida, azotnih oksida, metana) i čestica. Neke od ovih supstanci su gasovi sa efektom staklene bašte (ugljen dioksida i metan), dok sumpor dioksid, azotni oksidi i čestice imaju štetan uticaj na ljudsko zdravlje. Cilj ovog rada je da razmatrajući sistem najčešće instalisanih biogasnih elektrana u Srbiji, kvantifikuje ovu emisiju u atmosferu iz biogasnog postrojenja, kao i da uporedi sa referentnom vrednošću emisije gasova sa efektom stalene bašte za kogenerativna postrojenja koja koriste fosilna goriva.

Metodologija

Razmatrajući proizvođače električne energije iz biogasa, može se zaključiti da se najveći broj biogasnih postrojenja u Srbiji nalazi na velikim poljoprivrednim farmama i postrojenjima za tretman otpadnih voda. Kada govorimo o instalisanoj snazi ovih postrojenja ona se krece od 250 kW do 3.5 MW [5]. Najveći broj postrojenja ima instalisanu snagu od 999 kW (~1 MW) i ova instalisana snaga (PBG) biogasnog postrojenja je korišćena u ovom radu za razmatranje emisija u atmosferu tokom proizvodnje električne energije u kogenerativnom procesu iz biogasa.

Imajući u vidu činjenicu da broj radnih sati biogas postrojenja iznosi od 5,000 - 7,800 godišnje [6,7], usvojeno je u ovom istraživanju da broj radnih sati biogas postrojenja (N) iznosi 7,500 časova godišnje.

Godišnja proizvedena električna energije (WE) u procesu kogeneracije iz biogasa računata je kao:

$$WE = PBG * N \quad (1)$$

Za ovu proizvedenu količinu električne energije potrebno je obezbediti odgovarajuću zapreminu biogasa (VBG) koja je određena iz jednačine (2).

$$VBG = WE/(LHVBG*\mu) \quad (2)$$

gde je:
μ -Stepen energetske efikasnosti u proizvodnji električne energije, koji je u biogas kogenerativnim postrojenjima u opsegu od 0.25 - 0.6 [2,8-9], i u ovoj studiji usvojeno je da μ iznosi 0.4.
LHVBG je donja toplotna moć biogasa (60% metana u biogasu) - 6 kWh/m^3N [10].
Količina svakog emitovanog polutanta Q_{PI}, determinisana je korišćenjem jednačine (3).

$$Q_{PI} = VBG * LHVBG * E_{fi} \quad (3)$$

Emisioni faktori za svaki polutant dati su u Tabeli 1.

Tabela 1. Emisioni faktori polutanata iz kogenerativnog biogas postrojenja

Substanca	Emisioni faktor (E_{fi}) (g/GJ)	Reference
CO_2	77,170	[11]
SO_2	25	[11]
NOx	202	[11]
CH_4	323	[12]
PM	2.63	[12]

Rezultati i Diskusija

Korišćenjem jednačine (1) izračunata je godišnja proizvedena električna energija iz biogasnog postrojenja snage 1MW, koja je iznosila 7,500,000 kWh. Za ovu proizvodnju električne energije bilo je potrebno obezbediti 3,125,000 m^3_N biogasa, koji je određena iz jednačine (2). Imajući u vidu da prosečno domaćinstvo u Srbiji troši godišnje oko 5,000 kWh električne energije [13], proizvedena količina električne energije iz biogasnog postrojenja je dovoljna za snabdevanje električnom energijom 1,500 domaćinstava. Korišćenjem jednačine (3) i emisionih faktora iz Tabele 1. izračunate su vrednosti emisije za svaku zagađujuću supstancu i prikazane su u Tabeli 2.

Tabela 2.Emisije za svaku zagađujuću supstancu iz biogas kogeneracije

Substanca	**Ukupna emisija polutnata (kg)**
CO_2	5,208,975
SO_2	1,687.5
NOx	13,635
CH_4	21,802.5
PM	177.525

Poznajući vrednosti u Tabeli 2. za ugljen dioksid i metan, kao i preporuke Međunarodnog panela za klimatske promene za sledeće faktore: 1kg CO_2 = 1 kg CO_2 eq, 1 kg CH_4 = 25 kg CO_2 eq [6], moguće je izračunati ekvivalentnu emisiju gasova sa efektom staklene bašte (kg CO2 eq) kao:

$$TCO_2eq=TCO_2 +TCH_4 \quad (4)$$

gde su:

TCO_2eq -ukupna ekvivalenta emisija gasova sa efektom staklene bašte
TCO_2- ekvivalenta emisija GHG za ugljen-dioksid
TCH_4- ekvivalenta emisija GHG za metan

Sprovedena kalkulacija je pokazala da ekvivalentna emisija gasova sa efektom staklene bašte iznosi 5,754,037.5 kg CO2eq. Koristeći ovu vrednost i količinu proizvedene električne energije, moguće je odrediti specifičnu emisiju gasova sa efektom staklene bašte, kao 0.77 kg CO_2 eq/kWh električne energije. Dobijeni rezultat je daleko manji od specifične emisje gasova sa efektom staklene bašte za proizvodnju električne i toplotne energije u Republici Srbiji (1.085 kg CO_2 eq/kWh energije) [14].Takođe, izračunata specifična emisija gasova sa efektom staklene bašte je u dobrom slaganju sa onom koju su dobili Bachmaier i saradnici u svojim istraživanjima (573–910 g CO_2eq/kWh) [15], kao i (Cuéllar i Webber) (685 g CO_2eq/kWh) [16].

Zaključak

U ovom radu izvršena je kvantifikacija emisija (ugljen dioksida, sumpor dioksida, azotnih oksida metana i čvrstih čestica) u atmosferu iz tipičnog biogasnog postrojenja u Republici Srbiji instalisane snage od 1 MW. Rezultati dobijeni u ovom radu pokazuju da kogenerativna proizvodnja energije iz analiziranog biogasnog postrojenja dovodi do emisije 5,208.975 tona CO_2, 1.687 tona SO_2, 13.635 tona NO_X, 21.80 tona CH_4, kao i 0.177 tona PM čestica. Nadalje, sprovedena analiza pokazala je da ukupna ekvivalentna emisija gasova sa efektom staklene bašte za ovo biogasno postrojenje iznosi 5,754,037.5 kg CO2eq, dok specifična emisija iznosi 0.77 kg CO2eq/kWh električne energije. Dobijeni rezultati pokazuju da proizvodnja električene energije iz kogeneracije biogasa predstavlja dobru alternativu za proizvodnju električne energije iz fosilnih resursa.

Zahvalnica

Ovaj rad finansijski je podržalo Ministarstvo nauke, tehnološkog razvoja i inovacija Republike Srbije (Grant br. 451-03-68/2023-14/200026).

Reference

1. M.A. Qyyum, R. Dickson, S.F.A. Shah, H. Niaz, A. Khan, J. J. Liu, M. Lee, Availability, versatility, and viability of feedstocks for hydrogen production: product space perspective, *Renew. Sustain. Energy. Rev.*, **110843**, 2021.
2. A. Rafiee, K. R. Khalilpour, J. Prest, I. Skryabin, Biogas As An Energy Vector, *Biomass And Bioenergy*, 144, **105935**, 2021.
3. A.I. Adnan, M.Y. Ong, S. Nomanbhay, K.W. Chew, P. L. Show, Technologies For Biogas Upgrading To Biomethane: A Review, *Bioengineering*, **6**, 92, 2019.
4. Bilans Biogasa. Available: https://www.stat.gov.rs/media/358394/balance-of-biogas-in-2021-previous-data.pdf.
5. Registar Povlašćenih Proizvođača, Available: https://mre.gov.rs/sites/default/files/registri/RegistarPovlasPro12-8-2022.html#Sec_Biogas

6. J. Pucker, G. Jungmeier, S. Siegl, E.M. Potsch, Anaerobic digestion of agricultural and other substrates–implications for greenhouse gas emissions, *Animal*, **7**, 283–29, 2013.
7. C. Hennig, M. Gawor, Bioenergy production and use: Comparative analysis of the economic and environmental effects, *Energ. Convers. Manage*., **63**, 130–13, 2012.
8. A. Trendewicz, R.J. Braun, Techno-economic analysis of solid oxide fuel cell based combined heat and power systems for biogas utilization at waste water treatment facilities, *J. Power Source*, **233**, 380-393, 2013.
9. M. J. B. Kabeyi & O. A. Olanrewaju, Technologies for biogas to electricity conversion, *Energy Reports*, **8**, 774-786, 2022.
10. AEBIOM, 2009. A biogas road map for Europe. European Biomass Association Available: https://www.big-east.eu/downloads/brochure_biogasroadmap_web%5b1%5d.pdf.
11. V. Paolini, F. Petracchini, M. Segreto, L. Tomassetti, N. Naja, A. Cecinato, 2018. Environmental impact of biogas: a short review of current knowledge, *J. Environ. Sci. Health A*, **53 (10),** 899–906.
12. P.G. Kristensen, J. K. Jensen, M. Nielsen, J. B. Illerup, Emission Factors for Gas Fired CHP Units <25 MW, Danish Gas Technology Centre and National Environmental Research Institute of Denmark, 2004.
13. Potrošnja Električne Energije. Available: https://www.politika.rs/scc/clanak/455113/Domacinstva-u-Srbiji-trose-50-odsto-vise-struje-od-evropskih.
14. IRENA, Available:https://www.irena.org/irenadocuments/statistical_profiles/europe/serbia_europe_re_sp.pdf
15. J. Bachmaier, M. Effenberger, A. Gronauer, Greenhouse gas balance and resource demand of biogas plants in agriculture, *Eng. Life Sci.* **6**, 560–569, 2010.
16. A. D. Cuélar, M. E. Webber, Cow power: the energy and emissions benefits of converting manure to biogas, *Environ. Res. Lett.*, **3(3)**, 034002, 2008.

When the Oxygen Might Be Applyied for Corrosion Protection at Steel Surface

Zoran Karastojković[a], Ognjen Ristić[b], Mladen Mladenović[b]

[a]*Society for ethics and evaluation in culture and science, 11000 Belgrade, str. Strahinjića bana 27, Serbia*

[b]*Institute IMS, blvd. v. Mišića 43, 11000 Belgrade, Serbia*

ABSTRACT

Steel already has a huge application both in industry and common life, and it is well known that corrosion atack represents a great financial problem all over the world. It is established that corrosion could not be fully avoided, but only lowered. After metallurgical cycle of steel production is finished, the pretty small quantity of oxygen obligatory is retained at solidified melt, but either of such minor amount this oxygen has a detrimental effect on numerous properties of steel, including some mechanical properties (first of all on reducing the toughness) and lowering the corrosion resistance. From that point of view the oxygen either in the bulk or at surface could not be considered as an desired element, it means must be avoided anyway.

In practice of steel drill production is shown that the oxygen could be applyied as a meaning for lowering the corrosion process, sometimes may be consider as protection against corrosion. It seems that introduction of oxygen into steel surface as fully contradictory fact: from one point of view the oxygen must escape during metallurgical treating (melting&refining) of steel, and further at the finishing stage of producing the steel component (drill) the oxygen is introducing into the surface. Some tool makers of twist drills used the oxidizing process of steel drill surface for obtaining the layer which is more stable against corrosion than the bare metal.

Key words: iron oxides, twist drill, surface oxidizing, oxidizing after nitriding

Introduction

The oxygen is a pretty reactive element, it means that makes undesired compounds (oxides) with
many metals and elements, excluding however the noble metals.

The origin of iron oxide(s) into melted steel during metallurgical treatment (oxidation or reduction) is in mineralogical nature of used ore(s) and other materials, which further leads to melting [1]. The solubility of oxygen in molten metal generally is pretty great, so the total removing the oxygen from crystallized steel is rather impossible [1÷3]. The crucial phase in melting of any metal is a refining process, particularlly the deoxidation process, when most of oxygen (and other undesired elements or compounds, which are able to make a slag) should be removed from the melted metal. At the beginning of metallurgical production of steel, the blowing with oxygen was widely used, first for oxidation and after that for reduction of molten steel [4,5]. In the stage of the refining of the molten steel, great amount of oxides form a slag, which is removed before casting.

One of the improved methods for oxidation of molten steel represents the blowing of the air with increased amount of oxygen for removing the impurities. As great volume of blowed oxygen should be applied, some amounts of oxygen, however, will be absorbed and remained just in the final steel product. After oxidation is finished, the next process is a reduction of formed oxides.

Instead of using the blowing of enriched air with oxygen [1,4], this practice is almost

abounded, and nowadays is widespread accepted the blowing the argon or applying the vacuum, as a better solution, or other solutions. The amount of oxygen after such treating of steel is markably lowered, which has shown the positive effect in improving the steel properties. But, some amount of dissolved oxygen still remains in solidified steel, as a retained oxygen [2-4]. A long time ago is established that the presence of oxygen is considered as an undesired element, either in structural or tool steel(s).

The presence of oxygen is generally controlled through the amount of oxides, as a part of nonmetallic inclusion(s), rarely in solid solutions with ferrite or austenite. In producing&controling the qualitative steels are well established and wide accepted the scale for assessment oxide both of amount and shapes, so the many national standards were accepted such scales (or charts).

For any further discussion about the possible layers and structures of iron oxides their phase diagram should be know.

Oxide types and Fe – O_2 phase diagram

Iron with oxygen makes two principal oxides, while the third oxide principally is a mixture between those oxides, Fig. 1, Iron oxide with the lower content of oxygen is FeO (Wüstite).

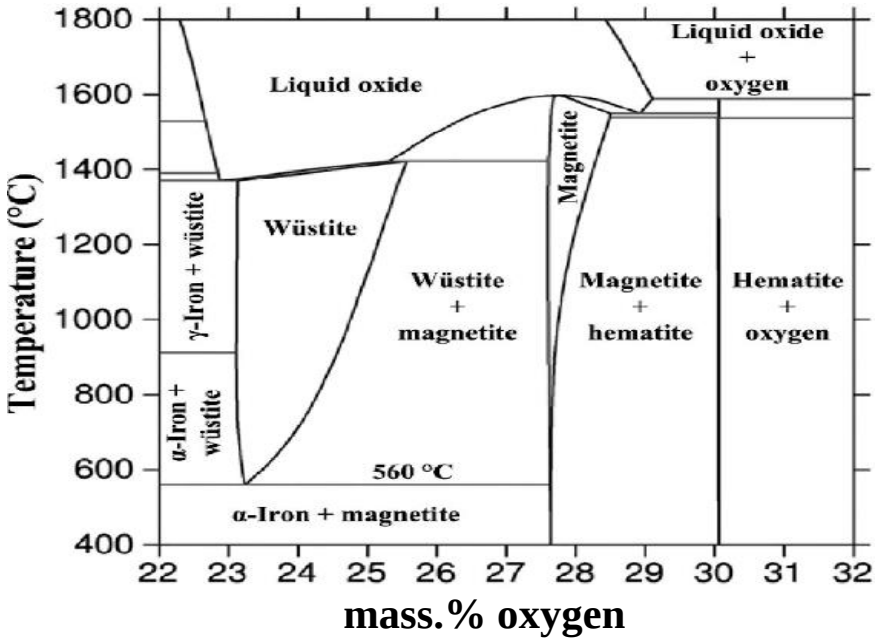

Fig. 1. Iron – oxygen phase diagram in contact of iron with air at normal atmospheric pressure

This diagram could not be considered as a valid for every steel, it is usable only for plain (low carbon) steels. The presence of alloying element(s) in steel markably may change the concentration borders/limits for oxygen dissolution. After long time contact of iron with air haematite (Fe_2O_3) may be formed, with the greatest amount of oxygen, while the magnetite (Fe_3O_4) is a mixture of previous two oxides, Fig. 1. The ironoxide (FeO) usually is expressed as alternating rows of iron and oxygen atoms, with approximately same radii Fig, 2a). But, it must be kept in mind that atomic radii of those elements are not similar, the oxygen atoms are larger, carefully see Fig. 2b).

The larger atomic radius and position of an element at the beginning of Periodic table does not mean a greater strength, frequently just contrary. This fact is of a crucial explanation why the steels with these iron oxides possess low toughness, lowered plasticity, and as many other oxides they are pretty brittle [4]. Also, if the larger quantity of oxides is present in the steel, than the strength and particularly the toughness will be markably lowered.

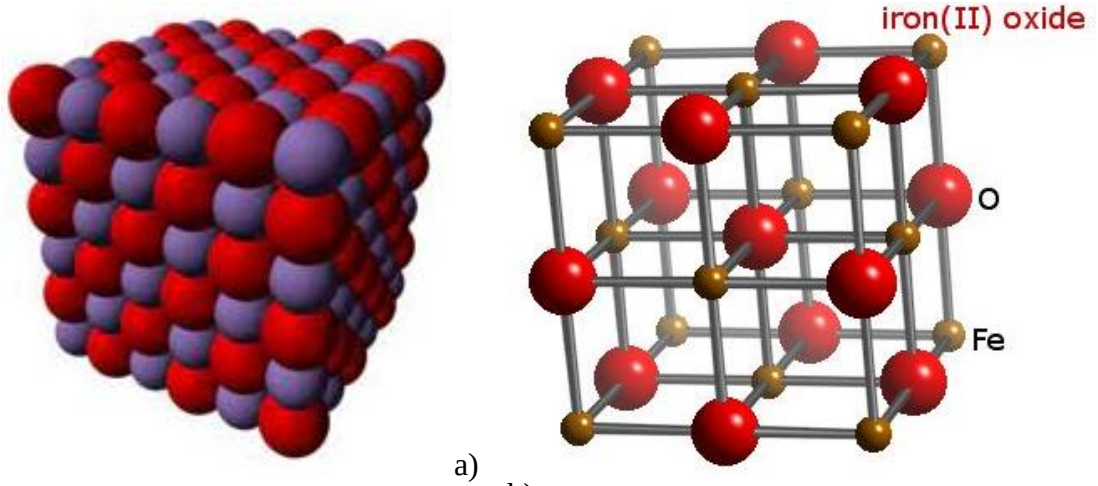

a) b)

Fig. 2. Ideal crystal lattice of iron(II) oxide, FeO

Warning: in some literature sources could be found that oxygen atoms are smaller than iron atoms!

The oxide Fe_3O_4 in crystal lattice commonly contains large amount of voids (unfilled atom places), and that is farther explanation for poor mechanical properties of such oxidized steel.

Black or grey iron oxide on twist drill surface

The presence of oxides onto steel surface might be considered only for the purpose of lowering further corrosion attack or progress, but at the same time the lowering of friction coefficient which could not be neglected, just contrary. Typical surface appearance of twist drill bits made from HSS are shown in Fig. 3a), and few examples for their application on figs. b)÷d)..

a)

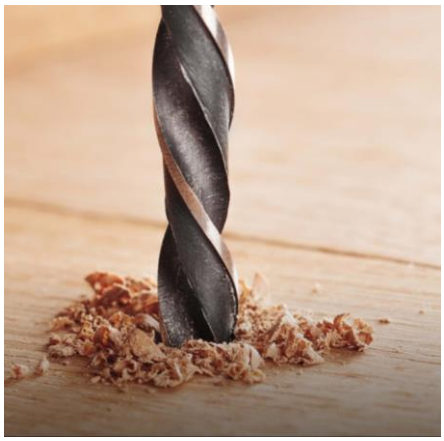

b)

c)

d)

Fig. 3. Versatility of colors&materials used for surface treating of twist drills a); drill bits with black oxide in cutting of: wood b), aluminium c) and steel d)

The bright surface usually is achieved after grinding of (previously quenched and tempered) twist drill, made from high-speed steel (HSS). Other hard layers from Fig. 3a) were not obtained on diffusion manner but by deposition, so called coating technology. Here shown layers usually are made for example from TiN or (Ti,Al)N, when the coating is done by using Physical Vapor Deposition (PVD) method. Such or similar methods for deposition of hard coatings are pretty expensive, because they need application of vacuum equipment (chamber, pumps, etc.) and many other high-tech devices (for evaporation, magnetic transport of ions, rotation of a specimen, etc.).

Figs. 3b)÷d) show that chip-flow is good. Formation of long chip primarly depends on the kind of the metal and chemical composition of used alloy to be drilled.

Oxidizing of twist drill at water solution, hot water steam and salt bath

The possibility of oxidizing of iron&steels in water, more precisely in hot water steam containing atmosphere in wide temperature range is based on next diagram, Fig. 4.

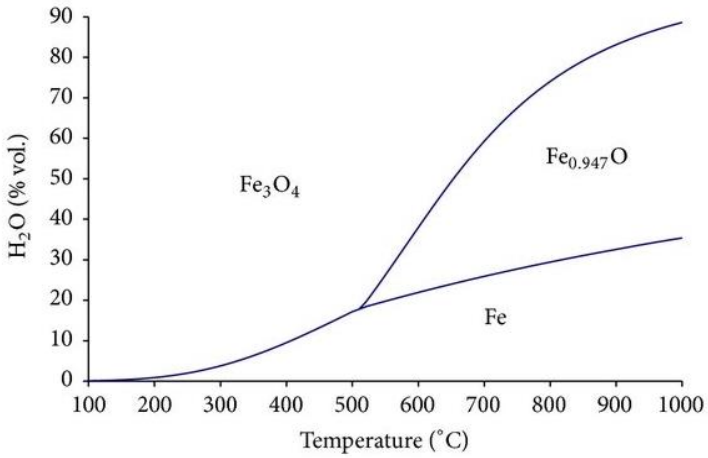

Fig. 4. Iron oxides in water steam surrounding atmosphere at wide temperature range

The oxide FeO is not a fully chemical compound, because in its crystal structure commonly may be present vacant places, so the exactly chemical formulae for example rather is $Fe_{0,947}O$, as given in Fig. 4.

The oxidizing is typical diffusive process, it means that should be provided at elevated temperatures [5-12]. After grinding is finished than is getting the bright surface, but oxidizing gives a black color, as shown in Fig. 3. Main demand in oxidizing treatment is to apply the temperature near or below the tempering temperature (usually up to 580 ^oC) of previously quenched HSS steel [2-7]. Gas nitriding or gas carbo-nitriding commonly are available processes. Phases at layer, after nitro-carburizing is applied, mainly are composed from ε-$Fe_{2-3}(N,C)$ and γ'- Fe_4N.

In treating of twist drill made from HSS, even with cobalt, rarely is used boiling water solution (200-250 g/l $NaNO_3$ and 600-650g/l NaOH) at ≈140 ^oC), but rather the hot/dry water steam. Oxidizing in hot water steam is provided in range up to 550-570 ^oC, for 30-60/90 min.

Other techniques for oxidation of tool surface were developed [5-14], one of them is oxidation in salt bath (30-35%KNO_3 and 65-70%$NaNO_3$) when these salts are melted at 160 ^oC, but process is provided at 480-510 ^oC, in duration of 30-60 min. It is worth to mention that such grey or black or grey layer becomes more resistant to oxidation than bright surface and treated drills on described way offer increasing tool life up to 40-70% over bright finish surface. Obtaining the black-gray oxide film (layer) 3-4 μm thick principally is simple and inexpensive method. Drill bits with such oxide show satisfied durability and easily could be resharpened in comparison to some PVD coatings. The coefficient of friction of such layer principally is less than untreated ("bare") surface, and effect of lubrication becomes better.

Oxidizing after nitriding or carbo-nitriding

Oxidizing is also a typical diffusive process. These processes are also known as post-oxidation treatment after nitriding or carbo-nitriding (cyanizing) is done [9-14]. The purpose is in farther improving the surface properties of nitrided or carbo-nitrided surface, and also achieving the prolongation of servicing life up to 2,5 times [5-8]. Greater temperatures of oxidizing, 640-700 °C, resulting in formation a thicker layer of Fe_2O_3, with greater brittleness in comparison to previous oxide. Versatility of steels (structural or tool) and irons might be carbonitrided and then post-oxidized, two examples (structural steel and nodular iron, type NL600) are given in Table 1.

Table 1. Changes of hardness and depth of layer after carbonitriding and postoxidation [11]

material	treatment	HV0,5	effective depth of layer, mm	total depth of layer, mm
42CrMo4	untreated	298	-	-
	nitrocarburized	705	0,2	0,32
	nitrocarburized+post-oxidized	710	0,25	0,47
NL 600	untreated	210	.	-
	nitrocarburized	520	0,16	0,20
	nitrocarburized+post-oxidized	515	0,19	0,25

The oxidizing also is possible to provide during plasma nitriding, at the same chamber.

The microstructure of one structural steel with nitrided diffusive layer, in depth of 360 μm, which is than oxidized (forming the depth of layer less than 4μm) is shown in Fig. 5.

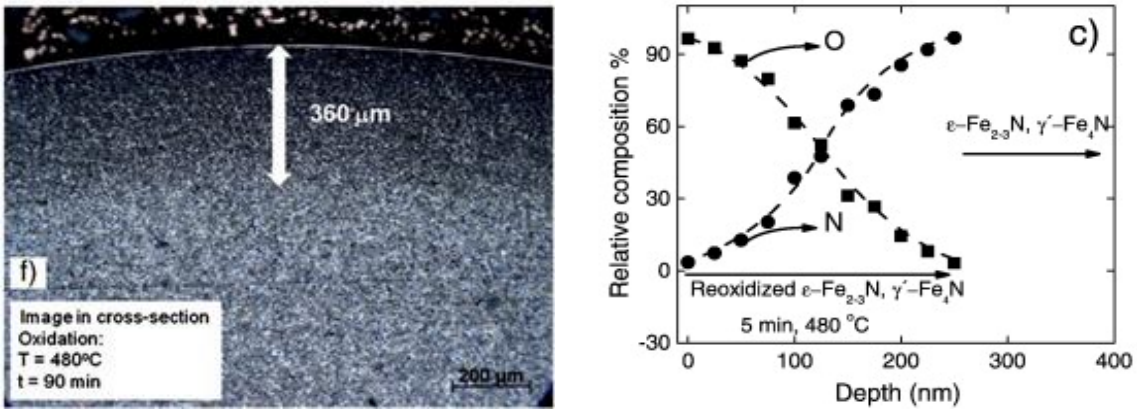

а) б)

Fig. 5. Microstructure of oxidiyed previously nitrided layer a) and distribution of oxygen and nitrogen at oxidized and previously nitrided layer b)

Reason for lowering the nitrogen concentration is explanable by diffusion of oxygen into the surface, see Fig. 5b). It is confirmed that after nitriding of steel the corrosion resistance of such steel is improved [11,14],

Depth of oxidized layer in function of temperature is shown in Fig- 6a), according to Arhenius equation, while the type of time dependance is rather parabolic, see Fig. 6b). Further oxidizing of previously nitrided or carbo-nitrided surface has the positive effect on improving the corrosion resistance and lowering the wear rate [6,11,14].

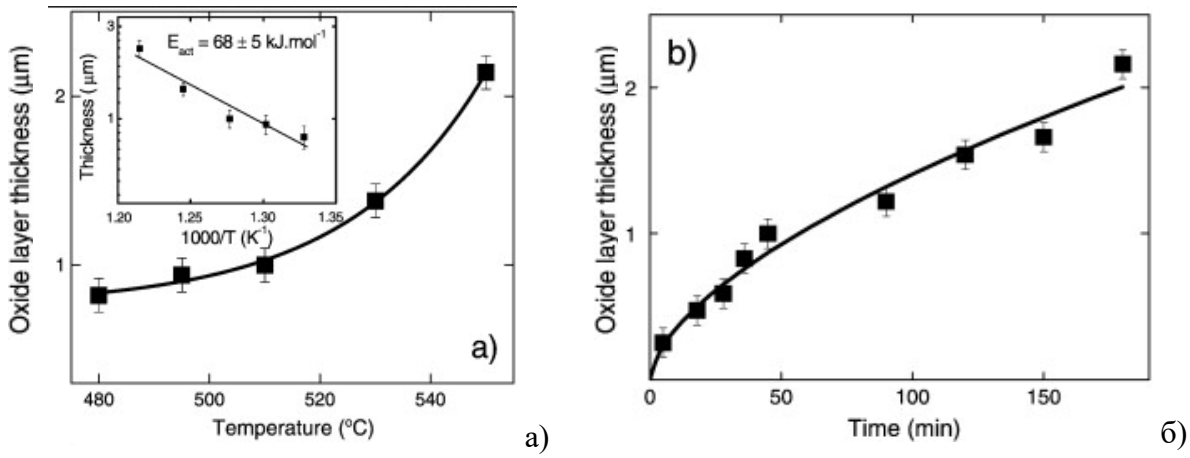

а) б)

Fig. 6. Dependance of oxide layer thickness from: a) temperature and b) time

Conclusion

In metallurgical production of steel is well established that the presence of oxygen is not welcome, because many mechaanical properties are degraded. Either the presence of oxygen leads to degradation of mechanical properties (decreasing the toughness, etc.), it is stated that after specific thermo-chemical treatment the influence of oxygen may be useful. Here is shown that introducing the oxygen into the steel surface in dept less than 4µm, which previously is nitrided or carbo-nitrided, offers some advantages. These advantages are in domain of increasing the hardness, however not at significant quantity, when the friction coefficient and wear are lowered, at the same time the corrosion resistance is improved.

The manners for providing of described oxidizing the drill steel surface (into black or grey-black color) are available on termo-chemical treatment methods, and such treatments does not represent a kind of technical difficulty, and also means that all of those processes are fast and cheap and usefull.

Acknowledgements

This research is supported by the Ministry of Education, Science and Technological Development of the Republic of Serbia (Contract No. 451-03-47/2023-01/ 200012).

References:

1. V.A. Kudrin: Metallurgija stalji, in Rusian, Moscow 1989, Metallurgija, p. 95-175.
2. H. Šuman: Metalografija, Belgrade 1965, in Serbian, Zavod za izdavanje udžbenika Srbije, p. 320-330.
3. Yu.A. Geller, A.G. Rakhstadt: Science of materials, English translation, Moscow 1987, Mir Publ, p. 321-327.
4. D. Seferijan: Metalurgija zavarivanja, in Serbian, Belgrade 1969, IP Građevinska knjiga, p. 117-126.
5. Yu.A. Bašnin, B.K. Ušakov, A.G. Sekej: Tehnologija termičeskoj obrabotki, in Russian, Moscow 1986, Metallurgija, p. 408-412.
6. E.A. Smoljnikov: Termičeskaja i himiko-termičeskaja obrabotka instrumentov v soljnah vannah, in Russian, Moscow 1989, Mašinostroenie, p. 204-221.
7. G. Keller, W. Weiss, W. Ranke, R. Schlögl: Bulk and surface phases of iron oxides in oxygen and water atmosphere at low pressure, Physical Chemistry Chemical Physics,3/2001/1114-1122.
8. L.N. Parikov, V.I. Isajčev: Diffuzija v metallah i splavov, in Russian, Kiev 1986, Naukova dumka, p. 73-77.
9. I. Artinger: Instrumentaljnije stalji i ih termičeskaja obrabotka, in Russian, Moscow 1982, Metallurgija, p. 115-165.

10. Z. Karastojković, R. Perić: Nerdjajući čelici, Belgrade 2021, in Serbian, Industrijsko društvo za koroziju-Belgrade and „Perić&Perić“ Požarevac, p. 165-186.
11. R. Sola, R. Giovanardi, at all: Development of post-oxidation treatments to improve wear and corrosion resistance, La Metallurgia Italiana, sept. 2008.
12. S. Meddeb, J-L. Courouau, at all: Effect of temperature and dissolved oxygen content on the dissolved iron concentration in liquid sodium at equilibrium, J. of nuclear materials, 566/2022.
13. Z. Karastojković: Prevlake otporne na habanje i abraziju, in Serbian, invited lecture, Inženjerska komora Srbije, Belgrade juni 2022.
14. H. Tanei, Y. Kondo: Phase transformation of oxide scale and its control, Nippon steel&Sumitomo metal technical report, No 111, march 2016.

POSTER PRESENTATIONS
POSTERSKA SAOPŠTENJA

The influence of the voltage on formation and morphology of hydroxyapatite/titanium composite coatings

Katarina Đ. Božić[1,2,*], Miroslav M. Pavlović[1,2], Đorđe V. Gjumišev[1], Đorđe N. Veljović[3], Marijana R. Pantović Pavlović[1,2]

[1] *Institute of Chemistry, Technology and Metallurgy, Department of Electrochemistry, University of Belgrade, Njegoševa 12, Belgrade, Serbia*

[2] *Centre of Excellence in Environmental Chemistry and Engineering - ICTM, University of Belgrade, Njegoševa 12, Belgrade, Serbia*

[3] *Faculty of Technology and Metallurgy, University of Belgrade, Karnegijeva 4, Belgrade, Serbia*

**katarina.bozic@ihtm.bg.ac.rs*

Abstract

This study focused on investigating the effects of voltage and deposition time on the formation and morphology of hydroxyapatite/titanium oxide coatings, which were obtained using an in-situ synthesis process. The coatings were prepared under various voltage conditions and deposition times to analyze their characteristics. To evaluate the morphology of the coatings, optical microscopy and field emission scanning electron microscopy (FE-SEM) techniques were employed. Additionally, Fourier transform infrared spectroscopy (FTIR) was utilized to confirm the presence of hydroxyapatite coatings on the substrate. The results revealed that an increase in voltage led to a more uniform coating. The voltage parameter had a significant impact on the morphology of the initial hydroxyapatite powder, causing the agglomerates to disperse and resulting in smaller particle sizes within the coating. Furthermore, the FTIR analysis provided solid evidence of the presence of hydroxyapatite within the obtained coatings. These findings emphasize the importance of voltage control and deposition time in the in-situ synthesis process for achieving desirable hydroxyapatite/titanium oxide coatings. Understanding the influence of these parameters on coating formation and morphology can contribute to the development of improved techniques for biomedical applications, such as enhanced osseointegration in orthopedic and dental implants.

Keywords: *anodization; in-situ synthesis; deposition time; titanium substrate*

The Stability of Wild Thyme Extract-Loaded Phospholipid-Cholesterol Liposomal Particles

Stabilnost lipozomalnih čestica sa inkapsuliranim ekstraktom majčine dušice

Aleksandra A. Jovanović[1,*], Muna Rajab Elferjane[2,3], Milena Milošević[4], Petar Batinić[5], Jovana Bošnjaković[6], Milica Rančić[7], Aleksandar Marinković[2]

[1] *University of Belgrade, Institute for the Application of Nuclear Energy INEP, Banatska 31b, 11080 Zemun Belgrade, Serbia*

[2] *University of Belgrade, Faculty of Technology and Metallurgy, Karnegijeva 4, 11000 Belgrade, Serbia*

[3] *University of Misurata, Faculty of Nursing and Health Sciences, Misurata, Libiya*

[4] *University of Belgrade, Institute of Chemistry, Technology and Metallurgy, National Institute of the Republic of Serbia, Njegoševa 12, 11000 Belgrade, Serbia*

[5]*Institute for Medicinal Plants Research "Dr Josif Pančić", Tadeuša Košćuška 1, 11000 Belgrade, Serbia*

[6]*Research and Development Institute Lola L.T.D., Kneza Višeslava 70A, 11030 Belgrade, Serbia*

[7]*Faculty of Forestry, University of Belgrade, Kneza Višeslava 1, 11030 Beograd, Serbia*

[*]*ajovanovic@inep.co.rs*

Abstract

Wild thyme contains biologically active compounds, particularly polyphenols (flavonoids and phenolic acids) that exert antitumor, antimicrobial, anti-inflammatory, antioxidant, immunomodulatory, analgesic, and spasmolytic activities. Nevertheless, the mentioned bioactive compounds have low stability, solubility, and bioavailability, thus their application is limited. Liposomal particles have been widely used for the encapsulation of bioactive components, due to their high structural integrity, stability during storage, and controlled release capability. In the present study, phospholipid-cholesterol liposomal particles, as the carrier for wild thyme extract, were developed. The stability of extract-loaded liposomes was monitored for 21 days by measuring vesicle size, polydispersity index (PDI), and zeta potential. The particle size and PDI of extract-loaded liposomes did not change drastically during 21 days of storage and amounted to ~450 nm and ~0.155, respectively. The zeta potential varied in the liposomes and started to decrease after 7 days of storage (from -21.0 mV to 20.3 mV, without a statistically significant difference), while the zeta potential value after 21 days was statistically significantly lower in comparison to the 1st day (19.3 mV). The beneficial effects of polyphenols on human health, as well as showed storage stability of the prepared liposomes highlight the use of the wild thyme extract-loaded phospholipid-cholesterol liposomal particles for potential application in food, pharmaceutical, and cosmetic industries.
Keywords: *liposomal particles; phospholipids; stability; wild thyme*

Izvod

Majčina dušica sadrži biološki aktivna jedinjenja, posebno polifenole (flavonoide i fenolne kiseline) koji imaju antitumorsko, antimikrobno, antiinflamatorno, antioksidativno, imunomodulatorno, analgetično i spazmolitično dejstvo. Ipak, pomenuta bioaktivna jedinjenja imaju nisku stabilnost, rastvorljivost i bioraspoloživost, te je njihova primena ograničena. Lipozomalne čestice se široko koriste za inkapsulaciju bioaktivnih komponenti, zbog njihovog visokog strukturnog integriteta, stabilnosti tokom čuvanja i sposobnosti kontrolisanog oslobađanja aktivnih komponenti. U ovoj

studiji su razvijene lipozomalne čestice sa fosfolipidima i holesterolom, kao nosači za ekstrakt majčine dušice. Stabilnost lipozoma sa inkapsuliranim ekstraktom je praćena 21 dan merenjem veličine čestica, indeksa polidisperzije (PDI) i zeta potencijala. Veličina čestica i PDI lipozoma sa inkapsuliranim ekstraktom nisu se drastično promenili tokom 21 dana čuvanja i vrednosti su iznosile ~450 nm i ~0,150. Zeta potencijal je varirao u lipozomima i počeo je da opada nakon 7 dana čuvanja (od -21,0 mV do 20,3 mV, bez statistički značajne razlike), dok je vrednost zeta potencijala nakon 21 dana bila statistički značajno niža u odnosu na 1. dan (19,3 mV). Blagotvorni efekti polifenola na zdravlje ljudi, kao i pokazana stabilnost pri čuvanju pripremljenih lipozoma, ističu upotrebu lipozomalnih čestica sa inkapsuliranim ekstraktom majčine dušice za potencijalnu primenu u prehrambenoj, farmaceutskoj i kozmetičkoj industriji.
Ključne reči: *lipozomalne čestice; fosfolipidi; stabilnost; majčina dušica*

Introduction

Wild thyme contains biologically active compounds, polyphenols (flavonoids and phenolic acids), essential oil, monoterpenes, polysaccharides, and proteins that exert antitumor, antimicrobial, anti-inflammatory, antioxidant, immunomodulatory, analgesic, and spasmolytic activities [1,2]. Nevertheless, the mentioned bioactive compounds have low stability, solubility, and bioavailability, thus their application is limited [3].

With the aim to overcome the mentioned disadvantages, various encapsulation techniques were established [3-5]. Liposomal particles have been widely used as the carrier for bioactive components, due to their high structural integrity, storage stability, and controlled release of target compounds [4,6]. Liposomal spheres are usually constituted by phospholipids or other kinds of lipids and can be used for the encapsulation of hydrophilic, lipophilic, and amphiphilic molecules [7,8]. Furthermore, liposomal preparation is simple and readily functionalized for active targeted delivery. Liposomes represent an ideal drug delivery carrier due to their superior biocompatibility since their bilayer is an analog of a biological membrane [6]. Depending on the formulation process, liposomal vesicles can have a quite small diameter, thus the water-dispersible preparations have a practically clear appearance [7]. Additionally, the addition of sterols, particularly cholesterol, during liposomal formulation can result in liposomes with satisfied physicochemical characteristics.

In the present study, phospholipid-cholesterol liposomal particles, as the carrier for wild thyme extract, were developed. The stability of extract-loaded liposomes was monitored for 21 days by measuring vesicle size, polydispersity index (PDI), and zeta potential.

Materials and Methods

Reagents and plant material

The following reagents were used: ethanol (Fisher Scientific, UK), Phospholipon 90 G, as unsaturated diacyl-phosphatidylcholine (Lipoid GmbH, Germany), and cholesterol (Sigma-Aldrich, Germany). Distilled water was purified through a Simplicity UV® water purification system (Merck Millipore, Merck KGaA, Germany).

Wild thyme herba was from the Institute for Medicinal Plants Research ”Dr Josif Pančić”, Pančevo, Serbia.

Preparation of the extract

Wild thyme extract was prepared using dried herba (1 g), 50% ethanol as the extraction medium (30 mL), and heat-assisted extraction at 80°C using the incubator shaker KS 4000i control (IKA, Germany) for 30 min [4]. The extraction was performed in Erlenmeyer flasks covered by aluminum foil to avoid light exposure and evaporation of the solvent. After the extraction, the sample was filtered through a cellulose filter (fine pore, 0.45 µm) and stored at 4°C until further experiments.

Preparation of liposomal particles with extract

Liposomal particles with wild thyme extract were obtained using the proliposome method and a mixture of phospholipids (Phospholipon) [9]. Phospholipids and 10 mol % of cholesterol (a total amount of 1 g) and ethanol wild thyme extract (4 mL) were stirred at 50°C to homogenize a mixture and evaporate ethanol. After cooling to 25°C, ultrapure water (20 mL) was added and the formulation was stirred at 800 rpm for 2 h. Subsequently, the liposomes were exposed to the ultrasound waves in an ultrasound bath (Sonorex, Bandelin, Germany) for 15 min, with the aim to reduce liposomal particle size.

Stability study

The measurements of vesicle size, PDI, zeta potential, conductivity, and mobility of liposomal particles with phospholipids, cholesterol, and wild thyme extract were performed using photon correlation spectroscopy in Zetasizer Nano Series, Nano ZS (Malvern Instruments Ltd., UK). The measurement was repeated on the 1st, 7th, 14th, and 21st days after the preparation of extract-loaded liposomes to monitor their stability at 4°C. Each sample was diluted 500 times and measured in triplicate at room temperature.

Statistical analysis

The statistical analysis was done by using analysis of variance (one-way ANOVA) and Duncan's *post hoc* test in STATISTICA 7.0. The differences were considered statistically significant at $p<0.05$.

Results and Discussion

Phospholipid-cholesterol liposomal particles with encapsulated wild thyme extract were developed and vesicle size, PDI, and zeta potential were measured during the 21-days storage study. The results are shown in the graphs of Figure 1.
Since the vesicle size of liposomes represents a relevant parameter for their stability, biodistribution, and release of the encapsulated components [10], the monitoring of this variable was done during 21 days of storage at 4ºC (Figure 1A).

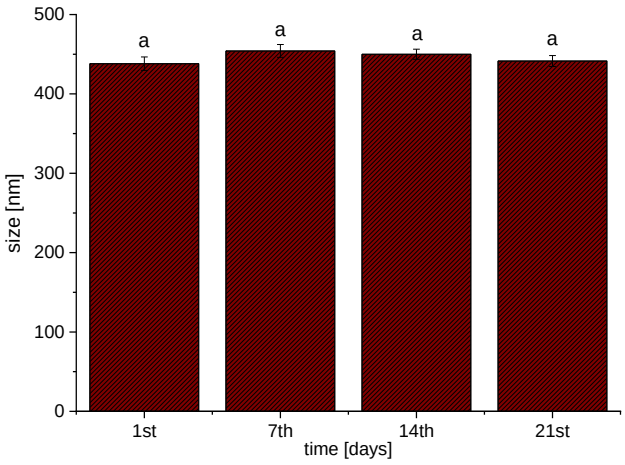

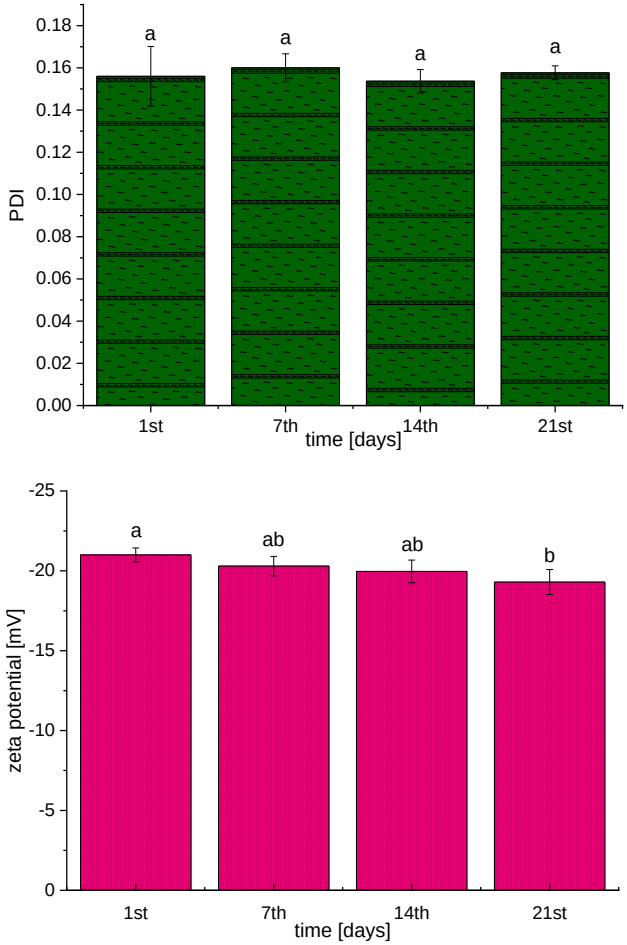

Figure 1. *(A) Vesicle size, (B) polydispersity index, and (C) zeta potential of wild thyme extract-loaded phospholipid-cholesterol liposomes, monitored during 21 days of storage at 4°C; the letters above bars showed statistically significant differences ($p<0.05$; $n=3$; analysis of variance, Duncan's post-hoc test).*

As can be seen from Figure 1A, the vesicle size of liposomal particles with wild thyme extract was 438.1±8.5 nm on the 1st day. The obtained values of particle size are in agreement with the literature data, where phospholipid liposomal particles with ergosterol and plant extract had a diameter of ~400 nm [11]. Namely, the type of lipids, the procedure for the liposomal preparation, the presence or absence of sterols, and the physicochemical characteristics of the entrapped compounds significantly influenced the vesicle size of the liposomes [4,9]. The measurements were repeated on the 7th, 14th, and 21st days and it can be concluded that there were no drastic changes in the liposome sizes (454.1±8.2 nm, 450.0±6.4 nm, and 441.4±6.9 nm, respectively). Due to a relatively high value of zeta potential (described below, Figure 1C), the absence of a significant change in vesicle size was expected.

Furthermore, PDI, as a measure of the vesicle size distribution in the liposomal suspension, was monitored as well, and the results are presented in Figure 1B. PDI value was 0.156±0.002 which indicates the existence of a uniform system. According to the literature data [12], higher liposomes (multilamellar vesicles, such as phospholipid-cholesterol liposomal particles with encapsulated wild thyme extract) possessed lower PDI values compared to smaller liposomes (small unilamellar vesicles, size ≤ 100 nm). The procedure used for liposomal formulation affects the uniformity of the liposomal population as well [4,9]. For example, Isailović et al. study [9] showed that liposomes produced using the proliposome technique (as in our case) had a PDI value of ~0.2, while the PDI of

the liposomal particles prepared using the thin film procedure was significantly higher, ~0.4. As can be seen in Figure 1B, PDI did not change during the 21-day storage study, as in the case of liposomal particle size (0.160±0.006, 0.154±0.002, and 0.158±0.003).
The zeta potential, as a measure of the stability of the liposomal system, was also measured during 21 days of storage at 4ºC (Figure 1C). The zeta potential was -21.0±0.4 mV indicating the presence of a stable system. Although phosphatidylcholines are neutral lipids in the water surrounding, the reorientation of the groups of the lipid heads results in the presence of a surface charge, which depends on the phase state and lipids/sterols types [12]. According to the literature [4], the negative value of zeta potential is related to the exposure of the phosphate group lying in an outer plane concerning the choline groups. The measured values of the zeta potential are in agreement with the Isailović et al. study [9], where the liposomal particles with polyphenol antioxidant formed using the proliposome method had a zeta potential of ~-25 mV. The zeta potential of wild thyme extract-loaded liposomes varied in the liposomal suspension and started to decrease after 7 and 14 days of storage (20.3±0.6 mV and 20.0±0.7 mV). However, there was no statistically significant difference between mentioned measured values. The zeta potential was statistically significantly lower after 21 days in comparison to the 1st day and amounted to 19.3±0.8 mV. Nevertheless, the mentioned zeta potential value was not statistically significantly lower compared to the values measured on the 7th and 14th days. Therefore, the results of zeta potential prove that liposomal particles with extract were stable during 21 days of storage at 4ºC. The stability was also confirmed by the absence of vesicle size and PDI value changes, i.e. there was no fusion or fission of the liposomal particles.

Conclusion

In the present paper, wild thyme extract-loaded phospholipid-cholesterol liposomal particles were prepared using the proliposome method, and their storage stability was monitored through the measuring of particle size, PDI, and zeta potential. The obtained liposomal particles were physically stable during 21 days of storage, i.e. there was no occurrence of agglomeration (changes in vesicle size) or significant changes in the size distribution and zeta potential of the liposomal suspension. The presented results qualify wild thyme extract-loaded phospholipid-cholesterol liposomal particles for application in food, functional foods, pharmaceutical or cosmetic products. Nevertheless, future experiments should deal with the biological potential of the developed liposomes and their widespread use in humans or industry.

Acknowledgements

The authors acknowledge their gratitude to the Ministry of Education, Science and Technological Development of Serbia, contract numbers 451-03-47/2023-01/200019, 451-03-47/2023-01/200135, 451-03-47/2023-01/200026, 451-03-47/2023-01/2003, 451-03-47/2023-01/200066, and 451-03-47/2023-01/200169.

References

1. S. Jarić, M. Mitrović, B. Karadžić, Plant resources used in Serbian medieval medicine. Ethnobotany and Ethnomedicine, *Genet. Resour. Crop Evol.*, **61**, 1359-1379, 2014. https://doi.org/10.1007/s10722-014-0118-1
2. A. Jovanović, V. Đorđević, G. Zdunić, D.Pljevljakušić, K. Šavikin, D. Gođevac, B. Bugarski, Optimization of the extraction process of polyphenols from *Thymus serpyllum* L, herb using maceration, heat- and ultrasound-assisted extraction, *Sep. Pur. Tech.*, **179**, 369-380, 2017. https://doi.org/10.1016/j.seppur.2017.01.055
3. Z. Fang, B. Bhandari, Encapsulation of polyphenols - a review, *Trends Food Sci. Technol.*, **21**, 510-523, 2010. https://doi.org/10.1016/j.tifs.2010.08.003

4. A. Jovanović, B. Balanč, V. Djordjević, A. Ota, M. Skrt, K. Šavikin, B. Bugarski, V. Nedović, N. Poklar Ulrih, Effect of gentisic acid on the structural-functional properties of liposomes incorporating β-sitosterol, *Colloids Surf. B.*, **183**, 110422, 2019. https://doi.org/10.1016/j.colsurfb.2019.110422
5. N. J. Zuidam, E. Shimoni, "Overview of microencapsulates for use in food products or processes and methods to make them", in *Encapsulation technologies for active food ingredients and food processing*, N. J. Zuidam, V. Nedović, Eds. New York, Springer, 2010, 3-29. https://doi.org/10.1007/978-1-4419-1008-0_2
6. K. Hadinoto, A. Sundaresan, W. S. Cheow, Lipid–polymer hybrid nanoparticles as a new generation therapeutic delivery platform: A review, *Eur. J. Pharm. Biopharm.*, **85**, 427-443, 2013.
7. Ribeiro H., Schuchmann H., Engel R., Walz E., Briviba K., "Encapsulation of carotenoids", in *Encapsulation technologies for active food ingredients and food processing*, N. J. Zuidam, V. Nedović, Eds. New York, Springer, 2010, 211-252.
8. M. Ricci, R. Oliva, P. Del Vecchio, M. Paolantoni, A. Morresi, P. Sassi, DMSO-induced perturbation of thermotropic properties of cholesterol-containing DPPC liposomes, *Biochim. Biophys. Acta*., **1858**, 3024-3031, 2016.
9. B. Isailović, I. Kostić, A. Zvonar, V. Đorđević, M.Gašperlin, V. Nedović, B. Bugarski, Resveratrol loaded liposomes produced by different techniques, *Innov. Food Sci. Emerg. Technol.*, **19**, 181-189, 2013. https://doi.org/10.1016/j.ifset.2013.03.006
10. M. Mozafari, C. Johanson, S. Hatziantoniou, C. Demetzos, Nanoliposomes and their applications in food nanotechnology, *J. Lipos. Res.*, ***18***, 309-327, 2008. https://doi.org/10.1080/08982100802465941.
11. A. Jovanović A., P. Petrović P., D. Ćujić, S. Stepanović, M. Gnjatović, A. Marinković, B. Bugarski, The stability of liposomes with ergosterol and *Thymus serpyllum* L. extract, *Proceedings of the VIII International Congress "Engineering, Environment and Materials in Process Industry"*, 20-23 March, Jahorina, Bosnia and Herzegovina, 2023.
12. A. Jovanović, B. Balanč, A. Ota, P. Ahlin Grabnar, V. Djordjević, K. Šavikin, B. Bugarski, V. Nedović, N. Poklar Ulrih, Comparative effects of cholesterol and β-sitosterol on the liposome membrane characteristics, Eur. J. Lipid Sci. Technol. **120**, 1-11, 2018. https://doi.org/10.1002/ejlt.201800039

Promoting effect of Zn in platinum catalyst for effective ethanol electrooxidation reaction

Promotivni efekat Zn u platinskom katalizatoru za efikasnu reakciju elektrooksidacije etanola

Sanja I. Stevanović[1,*], Dragana L. Milošević[1], Dušan V. Tripković[1], Vladan R. Ćosović[1], Vesna M. Maksimović[2] , Nebojša D. Nikolić[1]

[1] *University of Belgrade - Institute of Chemistry, Technology and Metallurgy, Njegoševa 12, 11000 Belgrade, Republic of Serbia*

[2] *University of Belgrade - Vinča Institute of Nuclear Sciences, Mike Petrovića Alasa 12-14, 11351 Vinča-Belgrade, Republic of Serbia,*

[*] *sanjas@ihtm.bg.ac.rs*

Abstract

Polymer electrolyte membrane fuel cells (PEMFCs) are pure electrochemical energy converters that are key components of energy sources for vehicles and for stationary and portable energy suppliers. Searching for a good catalyst for the ethanol oxidation reaction is one of the most significant issues in material science. To increase the economic potential of fuel cell technology, catalyst must be extremely active, stable, and inexpensive. Due to its high catalytic activity, structural and chemical stability, and widespread use in commercial fuel cells, platinum is still the material of choice for making cathodes. Although there is extensive continuing research to reduce the Pt concentration while keeping the high catalytic activity, its high cost remains a barrier to a wider adoption of fuel cell technology.Therefore, the potential for cost reduction lies in the optimization of the catalyst, i.e. obtaining the maximum catalytic efficiency with the lowest possible content of noble metals. The focus of this research will be on novel synthesis techniques for PtSnZn catalysts with better efficiency and durability for the ethanol oxidation reaction. This research demonstrates the potential of studying new PtSnZn catalytic materials as catalysts for the oxidation of ethanol. This study used the microwave assisted polyol technique to create PtZn and PtSnZn nanoparticles supported on high surface area carbon Vulcan XC-72R material. By using cyclic voltammetry, electro-oxidation of adsorbed CO, and the chronoamperometric method, the electrochemical behavior of synthesized catalysts was examined. X-ray diffractometry, transmission electron microscopy analysis and thermogravimetric analysis were applied to obtain the physicochemical properties of the catalyst. The advantages of microwave synthesis and carefully balanced metal alloying in the PtSnZn/C catalysts led to a high catalytic activity of the synthesized catalyst in the ethanol oxidation reaction compared to the Pt/C catalyst. *This work was financially supported by the Ministry of Education, Science and Technological Development of the Republic of Serbia (contract no. 451-03-68/2022-14/200026) and the Science Fund of the Republic of Serbia under grant no. 7739802.*

Keywords: *platinum catalysts; microwave polyol synthesis; ethanol oxidation;*

Izvod

Gorivne ćelije sa polimernim membranama (PEMFC) su čisti elektrohemijski izvori energije koji mogu biti ključne komponente izvora energije za vozila i za stacionarne i prenosive uređaje. Pronalaženje dobrog katalizatora za reakciju oksidacije etanola jedno je od najznačajnijih pitanja u nauci o materijalima. Da bi se povećao ekonomski potencijal tehnologije gorivnih ćelija, katalizator mora biti izuzetno aktivan, stabilan i jeftin. Zbog svoje visoke katalitičke aktivnosti, strukturne i hemijske stabilnosti i široke upotrebe u komercijalnim gorivnim ćelijama, platina je i dalje materijal

izbora za izradu katalizatora. Iako postoji opsežna kontinuirana istraživanja za smanjenje koncentracije Pt uz zadržavanje visoke katalitičke aktivnosti, visoka cena platine ostaje prepreka širem usvajanju tehnologije gorivih ćelija. Prema tome, potencijal za smanjenje troškova leži u optimizaciji katalizatora, tj. maksimalna katalitička efikasnost sa najmanjim mogućim sadržajem plemenitih metala. Fokus ovog istraživanja biće na novim tehnikama sinteze za PtSnZn katalizatore sa boljom efikasnošću i stabilnošću za reakciju oksidacije etanola. U istraživanju je korišćena poliol tehnika uz primenu mikrotalasne pećnice za kreiranje nanočestica PtZn i PtSnZn na ugljeničnom Vulcan XC-72R materijalu. Primenom ciklične voltametrije, elektrooksidacije adsorbovanog CO i hronoamperometrijske metode ispitano je elektrohemijsko ponašanje sintetizovanih katalizatora. Za dobijanje fizičko-hemijskih svojstava katalizatora primenjeni su rendgenska difraktometrija, transmisiona elektronska mikroskopska analiza i termogravimetrijska analiza. Prednosti mikrotalasne sinteze i pažljivo izbalansiranog legiranja metala u PtSnZn/C katalizatorima dovele su do visoke katalitičke aktivnosti sintetizovanog katalizatora u reakciji oksidacije etanola u poređenju sa Pt/C katalizatorom.

Ovaj rad je finansijski podržalo Ministarstvo prosvete, nauke i tehnološkog razvoja Republike Srbije (ugovor br. 451-03-68/2022-14/200026) i Fond za nauku Republike Srbije u okviru granta br. 7739802.

***Ključne reči**: platinski katalizatori; mikrotalasna sinteza;oksidacija etanola*

Effect of essential micronutrients on catalase enzyme activity in *Tilia sp.* leaves growing in urban areas

Dragana Pavlović*, Marija Matić, Veljko Perović, Natalija Radulović, Milica Marković, Miroslava Mitrović, Pavle Pavlović

Department of Ecology, Institute for Biological Research "Siniša Stanković", - National Institute of the Republic of Serbia, University of Belgrade, Bulevar despota Stefana 142, 11000 Belgrade, Serbia

Corresponding_author: dragana.pavlovic@ibiss.bg.ac.rs

Abstract

Changes in the urban environment can have serious effects on plants, including changes in the availability of certain essential micronutrients. Micronutrients are needed in very small amounts and are often required as cofactors for enzyme activity. In this study, the concentrations of selected essential micronutrients (B, Cu, Mn, and Zn) and the activity of the enzyme catalase in leaves of Tilia sp. were measured. The study was conducted in urban parks in Belgrade, Pancevo and Smederevo, exposed to various sources of pollution from traffic and industry. Control site was located in an area without a direct source of pollution. Results of this study revealed toxic B content in leaves of Tilia sp. from Belgrade, while deficiency of this element was measured in Pancevo. Deficit in Zn content was measured in almost all examined individuals, while Mn deficit was measured in Belgrade and at the Control site. The lowest values of catalase activity were measured in Tilia sp. at the Control site, which indicates that the Zn and Mn deficiencies cause slightly lower vitality of Tilia sp. at the Control site compared to the same trees at the other sites. On the other hand, the highest catalase activity measured in Belgrade could be the result of B toxicity. The results of the discriminant analysis (DA) showed that Belgrade site is clearly separated from the other three sites, with B and Mn contributing the most.

Keywords: *urban environment; essential micronutrients; catalase enzyme activity; Tilia sp.*

Introduction

The growth of human population and increasingly pronounced urbanization and industrialization during the last two centuries have led to extensive emission of pollutants that have dramatically changed the quality of the urban environment [1,2]. A particular problem in urban areas represent potentially toxic elements (PTEs), which accumulate in the surface layers of the soil and can easily enter the food chain from there. Significant sources of PTEs in urban areas are emissions from traffic, urban heating plants, and industrial facilities [3-5]. In recent years, increasing attention has been paid to research on the potential impact of accumulation, bioavailability, and monitoring of the content of PTEs in the urban environment [5-9]. Trees, as an integral part of the urban environment, are exposed to the harmful effects of pollutants, including PTEs [2,4]. Plants take up PTEs from the soil through their roots and from the air through their leaves. Their uptake, accumulation, and translocation depend on species characteristics, soil properties, and other ecological factors in the environment [5,6]. Elements such as B, Cu, Fe, Mn, Mo, Ni, and Zn are essential for plants and play an important physiological and biochemical role, being involved in the biosynthesis of chlorophyll and DNA, the process of photosynthesis, redox reactions in chloroplasts and mitochondria, carbohydrate metabolism. In order to develop and grow, plants need to maintain concentrations of essential elements within optimal values [10]. However, when concentrations exceed these values, essential elements can negatively affect the functioning of physiological processes in plants, which is why they are called potentially toxic elements. Through their influence on enzymatic activity, they cause structural and functional damage and also act as antimetabolites, forming stable complexes with

essential metabolites, altering membrane permeability, replacing important structural or electrochemically significant elements in cells. Their influence is also reflected in the disruption of the nutritional status of plants, as they enter into active competition with essential nutrients [11,12]. Essential element deficiency can lead to the appearance of visible leaf damage in the form of chlorosis and necrosis, reduced number of leaves, and reduced leaf area, which affects sunlight absorption and biomass production [13,14]. Essential elements are required by plants throughout their life cycle, and each of them has a specific physiological function that cannot be replaced by other elements. Numerous biochemical reactions in plants can be stressed by a deficiency or excess of essential elements. Most of these reactions lead to increased production of reactive oxygen species (ROS) and oxidative stress, which in turn leads to the activation of certain defense mechanisms in the plant. Defense mechanisms include enzymatic (superoxide dismutase, catalase) and non-enzymatic components (ascorbate and glutathione, carotenoids), which have the ability to detoxify ROS [10].

Considering the importance of trees for environmental quality in cities and the role that essential elements play in their functioning, the aim of this work was to determine the content of four essential microelements (B, Cu, Mn and Zn) in the leaves of *Tilia* sp. growing in urban parks in Belgrade, Pancevo, Smederevo and at the Control site. Another objective was to evaluate the adaptation potential of this species by measuring catalase enzyme activity.

Materials and methods

Sampling site description

The study was conducted in urban parks in Belgrade, Pancevo and Smederevo, which are exposed to various sources of pollution from traffic and industrial activities. The sampling site in Belgrade was the park "Hall Pioneer" in the city center, which is exposed to pollution from car exhaust. In Pancevo, sampling was conducted in the National Garden, the main city park in the southeastern part of the city. The main sources of pollution are the oil refinery, nitrogen fertilizer factory and petrochemical industry in Pancevo. The sampling site in Smederevo was the city park in the central zone of the city. The main source of pollution in Smederevo is a steel conglomerate located in the industrial area 7 km southeast of the city center. As a Control site we chose the Arboretum of the Faculty of Forestry, a protected natural area and a valuable archive of native and foreign tree species in Belgrade, located in an area without a direct source of pollution. The arboretum is located in the zone of mixed forest of *Quercus frainetto* and *Quercus cerris*.

Sample collection

Sampling was conducted from three to five randomly selected trees of approximately equal age at each site. Leaf samples were taken uniformly from each tree from different quarters of the canopy in all directions around the tree using stainless steel scissors which were then mixed to form a composite leaf sample, resulting in one composite leaf sample per sampling site. The leaf samples were stored in a paper envelope and then placed in a polyethylene bag prior to transport to the laboratory. In the laboratory, the samples were dried to a constant weight of 75°C for elemental analysis (Binder, Tuttlingen, Germany). Leaf samples for enzyme analysis were placed in liquid nitrogen immediately after sampling and stored at a temperature of -80°C until analysis.

Essential micronutrients analysis

Elemental concentrations in leaf samples were determined after wet digestion in a microwave oven (CEM, 39 MDS-2000) using method USEPA 3052. Certified reference materials was analysed to verify the accuracy of the analytical procedure: Plant material (beech leaves BCR-100) provided by the Institute for Reference Materials and Measurements (Geel, Belgium) and certified by the

European Commission - Joint Research Centre. The concentrations of B, Cu, Mn and Zn (mg kg^{-1}) in the studied samples were determined by optical emission spectrometry with inductively coupled plasma (ICP-OES, Spectro Genesis, Spectro-Analytical Instruments GmbH, Kleve, Germany). The detection limits (mg kg^{-1}) for the elements were as follows: B-0.001; Cu-0.006; Mn-0.003; and Zn-0.002. The average recoveries for the elements in the standard reference materials ranged from 95 to 110%.

Leaf extract preparation and enzyme activity analysis

For enzyme extraction, the frozen leaf tissue was homogenized in a mortar with pestle and liquid nitrogen and then extracted in ice-cold 0.1 M potassium phosphate extraction buffer (pH 6.5) containing 3% polyvinylpyrrolidine (PVP) and 5% phenylmethanesulfonyl fluoride (PMSF). After homogenization, the crude leaf extracts were centrifuged at 14,000 x g at 4°C for 20 min, and the supernatants obtained were aliquoted and used to measure protein content and enzyme activity. Protein content was determined according to Bradford [15], using bovine serum albumin (BSA) as a standard. Catalase activities were determined spectrophotometrically in duplicate at 20°C using a Shimadzu UV-160 spectrophotometer. Catalase activity was measured by adding 10 µl of the enzyme extract to 1 ml of a reaction mixture containing 50 mM K-phosphate buffer (pH 7) and 30% H_2O_2 and measuring the changes in absorbance at 240 nm for 3 min [16]. The results of catalase activity were expressed in units per mg of protein (U mg^{-1}).

Data analysis

Results were analyzed using one-way analysis of variance (ANOVA) by calculating the statistical significance of micronutrient (B, Cu, Mn and Zn) concentrations in relation to their locations. Discriminant analysis was performed to evaluate the differentiation among the studied sites based on the variations of B, Cu, Mn, Zn and catalase activity.

Results and discussion

The content of B in *Tilia* sp. leaves ranged from 11.89 mg kg^{-1} in Pancevo to 221.18 mg kg^{-1} in Belgrade (Table 1). Significant differences ($p<0.001$) in B content compared to the Control were found at all sites (Table 1). The Belgrade site is burdened with increased B content, which is more available to plants than at other sites. It is noticeable that the leaves of *Tilia* sp. growing in this park accumulate significantly more B than the leaves at other sites ($p<0.001$). Boron is an essential micronutrient required for plants at very low concentrations for normal growth and development, but its biochemical role is not well understood [17]. The specificity of B is reflected in the narrow range of concentrations between deficient and toxic, whereas normal concentrations in plant tissues are in a wide range of values (10-100 mg kg^{-1}, [11]). In this study, toxic B concentrations (>100 mg kg^{-1}, [11]) were determined in leaves of *Tilia* sp. in a park in Belgrade, while individuals from Pancevo were characterized by deficient B content (5-30 mg kg^{-1}, [11]). Boron deficiency affects a number of metabolic processes such as the ascorbate/glutathione cycle, membrane transport processes, photosynthesis, etc. [18], while B toxicity causes physiological and morphological defects such as reduced shoot and root growth, inhibition of photosynthesis, increased membrane permeability, peroxidation of lipids, and altered activities of antioxidant enzymes [19]. As a result of the physiological disturbances, toxic B levels cause oxidative stress and ROS are overproduced in plant cells [19,20].

Table 1. Comparison of B, Cu, Mn and Zn concentrations and catalase enzyme activities in leaves of *Tilia* sp. sampled from urban parks in Belgrade, Pancevo, Smederevo and Control site

	B [mg kg^{-1}]					Cu [mg kg^{-1}]				
	M±SD	**B**	**P**	**S**	**C**	**M±SD**	**B**	**P**	**S**	**C**
Belgrade	221.18±2.35	/	***	***	***	6.81±0.44	/	ns	***	ns
Pancevo	11.89±0.57	***	/	***	***	7.08±0.15	ns	/	***	ns
Smederevo	32.15±2.36	***	***	/	***	3.32±0.29	***	***	/	***
Control	86.80±2.44	***	***	***	/	6.85±0.12	ns	ns	***	/
	Mn [mg kg^{-1}]					**Zn [mg kg^{-1}]**				
	M±SD	**B**	**P**	**S**	**C**	**M±SD**	**B**	**P**	**S**	**C**
Belgrade	17.79±0.36	/	***	***	***	26.07±1.36	/	***	***	***
Pancevo	32.56±0.51	***	/	ns	***	18.67±1.15	***	/	***	***
Smederevo	32.97±0.40	***	ns	/	***	11.37±0.36	***	***	/	ns
Control	29.56±0.61	***	***	***	/	13.02±1.51	***	***	ns	/
	Catalase [U mg^{-1}]									
	M±SD	**B**	**P**	**S**	**C**					
Belgrade	812.08±65.60	/	ns	ns	***					
Pancevo	749.14±13.30	ns	/	ns	***					
Smederevo	731.47±29.20	ns	ns	/	***					
Control	524.84±5.32	***	***	***	/					

ANOVA, n=5, ***p<0.001, ns-not significant

The Cu content in the leaves of *Tilia* sp. ranged from 3.32 mg kg^{-1} in Smederevo to 7.08 mg kg^{-1} in Pancevo (Table 1). No significant differences (ns) in Cu content in the leaves in the sampled parks compared to the Control site were found. The exception is *Tilia* sp. from Smederevo, where a significant difference ($p<0.001$) was found compared to the Control (Table 1). Similar Cu content in leaves of *Tilia argentea* L. was found in the study of Greksa et al. [21], while Hrotkó et al. [22] found higher Cu content in *Tilia tomentosa*. Copper, like B, belongs to the group of essential micronutrients necessary for normal plant growth and development. As a structural component of regulatory proteins, Cu is involved in a number of processes necessary for the normal functioning of plants, such as photosynthesis, respiration, reduction and fixation of nitrogen, carbohydrate metabolism, response to oxidative stress, etc. [11,18]. For normal functioning of basic physiological processes in plants, 5-30 mg kg^{-1} Cu is required [11], and its average content in plant tissues is about 10 mg kg^{-1} [23], while the deficit occurs at concentrations <5 mg kg^{-1} [11]. The Cu content was below average values, but in a range that could be regarded as sufficient (Table 1), except for *Tilia* sp. from Smederevo, where a deficit of this element was measured. According to literature data, the activity of Cu enzymes decreases rapidly under Cu deficiency, and in most cases this decrease is associated with metabolic changes and inhibition of plant growth [18]. In addition, due to its low mobility in the plant, insufficient supply of Cu leads to morphological changes in the apical parts of leaves, which spread along the leaf margins as the growing season progresses [4,24,25].

The amount of accumulated Mn in *Tilia* sp. leaves ranged from 17.79 mg kg^{-1} in Belgrade to 32.97 mg kg^{-1} in Smederevo (Table 1). Significant differences ($p<0.001$) in Mn content compared to the Control were found at all sites (Table 1). The influence of sampling site on the differences in Mn content was also observed in the research of Tomašević et al. [26], who found that in the leaves of *Tilia cordata* sampled at different locations in Belgrade, the Mn content ranged from 9-103 mg kg^{-1}. Manganese is another essential micronutrient, which is primarily involved in the process of oxygen production by photosynthesis and plays a key role in the transport of electrons in this process [10]. In addition, Mn is an important component of several enzymes, and its most important function is to participate in various oxidation-reduction processes and build resistance to abiotic and biotic stress

factors [10]. The optimal Mn concentration in plants is in the range of 30-300 mg kg^{-1}, and the deficit occurs at concentrations of 10-30 mg kg^{-1} [11]. From the obtained results, it appears that the *Tilia* sp. trees from Belgrade and the Control site have a deficit of this element (Table 1). Oliveira et al. [27] found that Mn deficit induces oxidative stress and decreases the activity of antioxidant enzymes and total phenols, affecting the quantum efficiency of the photosystem II and pigment content.

Zinc content in *Tilia* sp. leaves ranged from 11.37 mg kg^{-1} in Smederevo to 26.07 mg kg^{-1} in Belgrade (Table 1). Significant differences ($p<0.001$) in Zn content compared to the Control site were found at all sites. The exception was *Tilia* sp. from Smederevo, where no significant differences (ns) were found compared to the Control (Table 1). Slightly higher Zn content was found by Greksa et al. [21] (20 mg kg^{-1}) in leaves of *Tilia argentea* L. in Novi Sad and Tomašević et al. [26] (19-32 mg kg^{-1}) in *Tilia cordata* leaves in Belgrade. After Fe, zinc is the second most important essential element, participating as an integral part of numerous enzymes in the metabolism of proteins, carbohydrates and phosphates, in the formation of ribosomes and in the regulation of auxin synthesis. It also affects membrane permeability and stabilization of cellular components [17,28], and it has a particular importance in chloroplasts, i.e., enzymes involved in the process of photosynthesis [29]. From the obtained results, it appears that there is a deficiency of this element at all sites (10-20 mg kg^{-1}, [11]), except for Belgrade, where its content is below the range considered sufficient for the normal functioning of plants (27-150 mg kg^{-1}, [11]). Since Zn ions are involved in the enzymatic defense of cells against free radical damage [30], Zn deficiency can lead to high ROS production and cell damage [29].

Catalase enzyme activity ranged from 524.84 U mg^{-1} at the Control site to 812.08 U mg^{-1} in Belgrade. Significant differences ($p<0.001$) in catalase activity compared to the Control site were found at all sites (Table 1). Lower catalase activity in the Control could be induced by deficiency of Mn and Zn. Zinc deficit was also measured at other sites, but only at Control site it was accompanied by Mn deficit. Manganese is known to play an important role in the antioxidant defense system of plants due to its functions as an enzyme activator, enzyme cofactor, and electron transporter [31]. Manganese deficiency causes changes in oxidative metabolism, leading to an imbalance between the production and elimination of reactive oxygen species (ROS) by modulating the activities of enzymes responsible for the reduction of these compounds in plant cells. In addition to the enzyme system, Mn is also required for the synthesis of the components of the non-enzymatic antioxidant defense system [27]. On the other hand, in Belgrade, despite the Mn deficit, the highest activity of catalase was measured, which may be related to the toxic B content in the leaves. Studies by Carville et al. [32] showed that excess B affects abiotic stress indicators such as proline, carotenoids, etc. Esim et al. [19] investigated the changes in antioxidant catalase enzyme activities in maize roots exposed to two different B concentrations and found that catalase activity was unaffected by both B treatments in the roots of 11-day plants compared to the Control. However, in 15-day plants, root catalase activity was significantly increased in both B treatments. The mechanisms of B tolerance and toxicity are not yet well understood. It has been suggested that antioxidants and antioxidant enzymes may reduce B toxicity in some plants. This antioxidant response is considered to be a crucial process in protecting plants from oxidative damage caused by a wide range of environmental factors [33].

Differentiation among examined sites

Discriminant analysis (DA) was applied to determine differences between sites based on total B, Cu, Mn, and Zn content and catalase enzyme activity in *Tilia* sp. leaves. All sites are clearly separated, with Belgrade standing out on relation to the other sites based on the first discriminant function (DC1), which explains 99.00% of the differences (Figure 1). The parameters that most influenced the separation were B and Mn (Figure 1). Belgrade and Pancevo sites are also separated from Smederevo and the Control site, and based on DC 2, which explains 1.00% of the differences, their separation is mainly influenced by Zn and catalase activity (Figure 1).

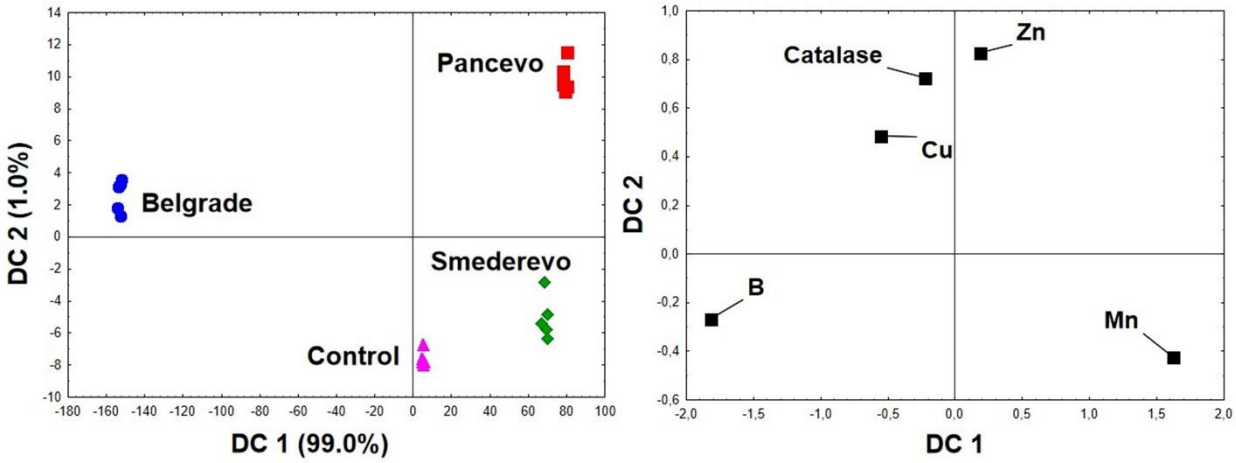

Figure 1. *Discriminant analysis (DA) for four sampling sites based on B, Cu, Mn, and Zn concentrations and catalase activity in leaves of Tilia sp.*

Conclusion

Based on the results presented in this research, it can be concluded that *Tilia* sp. potential for micronutrient accumulation is site specific. Toxic content of B was measured only in *Tilia* sp. leaves from Belgrade, while deficiency of this element was measured in Pancevo. Alongside B deficiency in Pancevo, the Zn deficit stood out in almost all studied individuals, while the Mn deficit was measured in Belgrade and the Control site, and the Cu deficit in Smederevo. In general, the lowest values of catalase activity were measured in the Tilia sp. trees at the Control site, indicating that the deficiency of Zn and Mn causes a slightly lower vitality of the Tilia sp. trees at the Control site compared to the individuals from other sites. The *Tilia* sp. trees in Belgrade showed the highest enzyme activity despite the Mn deficit and toxic B concentrations in the leaves, which could represent some kind of adaptation mechanism of the studied plants for existence under unfavorable site conditions.

Acknowledgements

The authors are grateful to the Ministry of Science, Technological Development and Innovation of the Republic of Serbia for financial support according to the contract with the registration number (451-03-47/2023-01/200007).

References

1. WHO (2017). Environment and health for European cities in the 21st century: making a difference, by L. Carmichael, F. Racioppi, T. Calvert, D. Sinnett. WHO Regional Office for Europe, Copenhagen, Denmark [Online]. Available: https://www.euro.who.int/__data/assets/pdf_file/0020/341615/bookletdef.pdf
2. M. Mitrović, T. Blanusa, M. Pavlović, D. Pavlović, O. Kostić, V. Perović, S. Jarić, P. Pavlović, Using fractionation profile of potentially toxic elements in soils to investigate their accumulation in *Tilia* sp. leaves in urban areas with different pollution levels, *Sustain.*, **13**, 9784, 2021.
3. L. Foti, F. Dubs, J. Gignoux, J. C. Lata, Z. T. Lerch, J. Mathieu, F. Nold, N. Nunan, X. Raynaud, L. Abbadie, S. Barot, Trace element concentrations along a gradient of urban pressure in forest and lawn soils of the Paris region (France), *Sci. Total Environ.*, **598**, 938-948, 2017.
4. M. Pavlović, T. Rakić, D. Pavlović, O. Kostić, S. Jarić, Z. Mataruga, P. Pavlović, M. Mitrović, Seasonal variations of trace element contents in leaves and bark of horse chestnut (*Aesculus hippocastanum* L.) in urban and industrial regions in Serbia, *Arch. Biol. Sci.*, **69(2)**, 201-214, 2017.
5. D. Pavlović, M. Pavlović, D. Čakmak, O. Kostić, S. Jarić, S. Sakan, D. Đorđević, M. Mitrović, I. Gržetić, P. Pavlović, Fractionation, mobility, and contamination assessment of potentially toxic metals in urban soils in

four industrial Serbian cities, *Arch. Environ. Contam. Toxicol*., **75**, 335-350, 2018.
6. A. Jayarathne, P. Egodawatta, G. A. Ayoko, A. Goonetilleke, Assessment of ecological and human health risks of metals in urban road dust based on geochemical fractionation and potential bioavailability, *Sci. Total Environ*., **635**, 1609-1619, 2018.
7. X. C. Duan, H. H. Yu, T. R. Ye, Y. Huang, J. Li, G. L. Yuan, S. Albanese, Geostatistical mapping and quantitative source apportionment of potentially toxic elements in top- and sub-soils: A case of suburban area in Beijing, China, *Ecol. Indic*., **112**, 106085, 2020.
8. D. Čakmak, V. Perović, M. Kresović, D. Pavlović, M. Pavlović, M. Mitrović, P. Pavlović, Sources and health risk assessment of potentially toxic elements in dust at children's playgrounds with artificial surfaces: A case study in Belgrade, *Arch. Environ. Contam. Toxicol*., **78**, 190-205, 2020.
9. D. Pavlović, M. Pavlović, V. Perović, Z. Mataruga, D. Čakmak, M. Mitrović, P. Pavlović, Chemical fractionation, environmental and human health risk assessment of potentially toxic elements in soil of industrialised urban areas in Serbia, *Int. J. Environ. Res. Public Health*, **18(17)**, 9412, 2021.
10. S. Č. Alagić, Strategije biljaka u borbi protiv fitotoksičnih koncentracija metala kao ključni preduslov uspešne fitoremedijacije: Ćelijski mehanizmi, deo I, *Zaštita materijala*, **55(3)**, 313-322, 2014.
11. A. Kabata-Pendias, H. Pendias, *Trace elements in soils and plants*. CRC Press, Boca Raton, FL, 2001.
12. O. Kostić, G. Gajić, S. Jarić, T. Vukov, M. Matić, M. Mitrović, P. Pavlović, An assessment of the phytoremediation potential of planted and spontaneously colonized woody plant species on chronosequence fly ash disposal sites in Serbia-Case study, *Plants*, **11**, 110, 2022.
13. D. M. Yeh, L. Lina, C. J. Wrightb, Effects of mineral nutrient defficiences on leaf development, visual symptoms and shoot±root ratio of Spathiphyllum, *Sci. Hortic*., **86**, 223-233, 2000.
14. A. Hussain, S. Ali, M. Rizwan, M. Zia-ur-Rehman, T. Yasmeen, M. T. Hayat, I. Hussain, Q. Ali, S. M. Hussain, "Morphological and physiological responses of plants to cadmium toxicity," in: *Cadmium Toxicity and Tolerance in Plants*, M. Hasanuzzaman, M. N. V. Prasad, M. Fujita, Eds. Academic Press, 2019, 47-72.
15. M. M. Bradford, A rapid and sensitive method for quantification of microgram of protein utilizing the priniciple of protein-dye binding, *Anal. Biochem*., **72**, 248-254, 1976.
16. H. Aebi, Catalase in vitro, *Meth. Enzymol*., **105**, 121-126, 1984.
17. A. Kabata-Pendias, A. B. Mukherjee, *Trace elements from soil to human*. Springer Berlin Heidelberg, New York, 2007.
18. H. Marschner, *Mineral Nutrition of Higher Plants*. Academic Press, Elsevier, 2012.
19. N. Esim, D. Tiryaki, O. Karadagoglu, O. Atici, Toxic effects of boron on growth and antioxidant system parameters of maize (*Zea mays* L.) roots, *Toxicol. Ind. Health*, **29(9)**, 800-805, 2012.
20. S. Mutlu, O. Atici, N. Esim, E. Mete, Essential oils of catmint (*Nepeta meyeri*) induce oxidative stress in early seedlings of various weed species. *Acta Physiol. Plant*., **33(3)**, 943-951, 2011.
21. A. Greksa, B. Ljevnaić-Mašić, J. Grabić, P. Benka, V. Radonić, B. Blagojević, M. Sekulić, Potential of urban trees for mitigating heavy metal pollution in the city of Novi Sad, Serbia. *Environ. Monit. Assess*., **191**, 636, 2019.
22. K. Hrotkó, M. Gyeviki, D. M. Sütöriné, L. Magyar, R. Mészáros, P. Honfi, L. Kardos, Foliar dust and heavy metal deposit on leaves of urban trees in Budapest (Hungary). *Environ.Geochem. Health*, **43**, 1927-1940, 2021.
23. D. E. Baker, J. P. Seneft, "Copper," in: *Heavy metals in soils*, B. J. Alloway, Ed. London, Blackie Academic and Professional, 1995, 179-205.
24. I. Yruela, Copper in plants, Braz. J. Plant Physiol., 17(1), 145-156, 2005.
25. D. E. Kopsell, D. A. Kopsell, "Copper," in: *Handbook of plant nutrition*, A. V. Barker, D J. Pilbeam, Eds. CRC Press, Taylor & Francis Group, LLC, Boca Raton, FL, 2007, 293-328.
26. M. Tomašević, M. Aničić, Lj. Jovanović, A. Perić-Grujić, M. Ristić, Deciduous tree leaves in trace elements biomonitoring: A contribution to methodology *Ecol. Indic*., **11**, 1689-1695, 2011.
27. K. S. Oliveira, R. de Mello Prado, M. V. Checchio, P. L. Gratao, Interaction of silicon and manganese in nutritional and physiological aspects of energy cane with high fiber content, *BMC Plant Biol*., **22**, 374, 2022.
28. E. M. Mattiello, H. A. Ruiz, J. C. L. Neves, C. Ventrella, Zinc deficiency affects physiological and anatomical characteristics in maize leaves, *J. Plant Physiol*., **183**, 138-143, 2015.
29. I. Cakmak, Possible roles of zinc in protecting plant cells from damage by reactive oxygen species. *New Phytol.*, **146**, 185-205, 2000.
30. I. Cakmak, H. Marschner, Effect of zinc nutritional status on activities of superoxide radical and hydrogen peroxide scavenging enzymes in bean leaves, *Plant Soil*, **155/156**, 127-130, 1993.

31. R. Millaleo, M. Reyes-Díaz, M. Alberdi, A. G. Ivanov, M. Krol, N. P. A. Hüner, Excess manganese differentially inhibits photosystem I versus II in *Arabidopsis thaliana*, *J. Exp. Bot*., **64(1)**, 343-354, 2013.
32. L. M. Cervilla, B. Blasco, J. J. Rios, M. A. Rosales, E. Sánchez-Rodríguez, M. M. Rubio-Wilhelmi, L. Romero, J. M. Ruiz, Parameters symptomatic for boron toxicity in leaves of tomato plants, *J. Bot*., 726206, 2012.
33. M. Ardıc, A. H. Sekmen, S. Tokur, F. Ozdemir, I. Turkan, Antioxidant responses of chickpea plants subjected to boron toxicity, *Plant Biol*., **11**, 328-338, 2009.

Synthesis of iridescent crystal vanadium-oxide ceramic glazes

Sinteza kristalnih vanadijum-oksidnih keramićkih glazura

Bojan Jokić[1,*], Milica Gvozdenović[2], Branimir Jugović[2]

[1] *Faculty of Applied Arts in Belgrade, University of Arts in Belgrade, Kralja Petra 4, Belgrade, Serbia*

[2] *Faculty of Technology and Metallurgy, University of Belgrade, Karnegijeva 4, Belgrade, Serbia*

[3] *Institute of Technical Sciences of SASA, Kneza Mihaila 35/IV, Belgrade, Serbia*

[*] *bojan.jokic@fpu.bg.ac.rs*

Abstract

The crystalline phase is the dominant phase in the ceramic body with a small amount of glassy phase. The preparation of ceramic glazes with characteristics similar to glass-ceramics can be performed by controlling the raw glaze composition and nucleating agent. The choice of appropriate nucleating agents that dominate bulk crystallization can be essential. Among multiple nucleating agents such as zirconia, titania, metallic molybdenum, and wolfram particles investigation of the influence of vanadium compound was not well studied on aluminum-silicate glass-ceramics. Metal such as vanadium forms oxides in an oxidation atmosphere at lower temperatures compared to metallic molybdenum and wolfram helping elucidate the effect of oxide on the crystallization behavior. Controlling the microstructure of glass-ceramic by processing parameters further control mechanical and optical properties. The addition of vanadium–pentoxide promotes the formation of entangled flower-like crystals on the porcelain ceramic body in combination with different commercial high-temperature glazes. Red and dark red colorations due to the presence of V^{5+} were obtained for aluminosilicate glass with a V_2O_5 content in the 5-10 mass % range. A pronounced spread of crystals beyond the glazed surface is observed on densely sintered stoneware and porcelain, which enables the formation of a decorative effect using simple application techniques.

Keywords: *crystal glaze; vanadium-pentoxide; porcelain; stoneware*

Izvod

Kristalna faza predstavlja dominantnu fazu porcelana i kamenine sa malim udelom staklaste faze. Priprema keramičkih glazura sa karakteristikama sličnim staklo-keramici može se vršiti kontrolisanjem sastava sirove glazure i sredstva za nukleaciju. Izbor odgovarajućih agenasa ima značajan uticaj na odvijanje procesa nukleacije. Za razliku od najčešće korišćenih nukleatora, kao što je cirkonijum, titanijum, metalni molibden i čestice volframa, ispitivanje uticaja jedinjenja vanadijuma nije dovoljno istraženo u formiranju aluminijum-silikatne staklo-keramike. Metal kao što je vanadijum formira okside u oksidacionoj atmosferi na nižim temperaturama u poređenju sa metalnim molibdenom i volframom, što omogućava proučavanje uticaja oksida na proces kristalizacije. Kontrolisanjem mikrostrukture staklo-keramike kontrolom procesnih parametara moguće je dobiti staklo-keramiku željenih mehaničkih i optičkih svojstava. Dodatak vanadijum-pentoksida promoviše formiranje umrežanih igličastih kristala nalik cvetu na porcelanskoj masi u kombinaciji sa različitim komercijalnim visokotemperaturnim glazurama. Crvena i tamnocrvena boja, uzrokovana prisustvom V^{5+} dobijena je u alumo-silikatnoj fazi pri koncentraciji V_2O_5 u opsegu od 5-10 masenih %. Na gusto sinterovanoj kamenini i porcelanu primećen je izraženi rast kristala izvan glazirane površine, što omogućava stvaranje dekorativnog efekta korišćenjem jednostavnih tehnika nanošenja.

Ključne reči: *kristalne glazure; vanadium-pentoksid; porcelan; kamenina*

Chemometric approach in detection the effect of environment and type of TiNi alloy on its corrosion degradation

Đenđi Vaštag[1,*], Špiro Ivošević[2]

[1]*University Novi Sad, Faculty of Sciences, Trg D. Obradovića 3, Novi Sad, Serbia*

[2]*University of Montenegro, Faculty of Maritime Studies Kotor, Dobrota 36, Kotor, Montenegro*

[*]*djendji.vastag@dh.uns.ac.rs*

Abstract

The aim of this study was to examine the possibility of applying methods of multivariate analysis in the processing of corrosion test results in real conditions. Namely, the monitoring of the corrosion process in real conditions often results in extensive data, characterized by complex interdependence, as well as by large degree of mutual deviation. All of the above makes it difficult to form a realistic and correct conclusion. Multivariate analysis, and the Principal component analysis especially (PCA), become increasingly popular in the processing of this type of data. The PCA as the main characteristic has the ability to recognize and eliminate redundant data, thus achieving a significant reduction in the number of analyzed data with minimal loss of essential information. Therefore, its application significantly facilitates the understanding of the connection of a large number of analyzed data of different origin. In this paper, the corrosion behavior of two TiNi alloys of the same composition, produced by different procedures was monitored. After 6 months of exposure to the corrosive effects of different coastal environments, TiNi alloy samples were analyzed by using the Energy Dispersive Spectrometer (EDS). The obtained EDS results were processed by using selected multivariate analysis methods in order to identify the most important corrosion factors, as well as their influence on the degradation of these alloys under given conditions.

Keywords:*Multivariate analysis; TiNi Alloy; corrosion; coastal environments*

Izvod

Cilj ovog rada je bio ispitivanje mogućnosti primene multivarijantnih metoda analize u obradi rezultata korozionih ispitivanja u realnim uslovima. Naime, monitoring korozionih procesa u realnim uslovima vrlo često kao rezultat daje obimne podatke, koji se odlikuju kompleksnim međuzavisnostima, kao i velikim stepenom međusobnog odstupanja. Sve navedeno u značajnoj meri otežava formiranje realnog i ispravnog zaključka. Multivarijantne metode analize, a u okviru njih, Analize glavnih komponenti (PCA) postaje sve popularnija pri obradi ovakvih podataka. Analiza glavnih komponenti kao glavnu karakteristiku ima mogućnost prepoznavanja i eliminisanja suvišnih podataka, čime se postiže značajna redukcija broja analiziranih podataka uz minimalan gubitak esencijalnih informacija. Stoga njenom primenom se znatno olakšava sagledavanje povezanosti velikog broja analiziranih podataka različitog porekla. U ovom radu praćeno je koroziono ponašanje dve TiNi legure, istog sastava, proizvedenih različitim postupcima. Uzorci TiNi legure nakon 6 meseci izloženosti korozionom efektu različitih primorskih okruženja analizirani su primenom Energetsko Disperzivnog Spektrometra (EDS). Dobijeni EDS rezultati su obrađeni primenom odabranih multivarijantnih metoda analize u cilju identifikacije najvažnijih faktora korozije, kao i njihovog uticaja na degradaciju ovih legura pri datim uslovima.

Ključne reči:*multivarijantna analiza;TiNi legura; korozija; primorsko okruženje*

Efficiency of methylene blue removal and hydrogen production using noble metals modified MoO_3 under UV and simulated solar radiation

Ivana Jagodić[1], Dina Tenji[2], Teodora Vidović[1], Jovana Cvetić[1], Nemanja Banić[1]*

[1]*University of Novi Sad, Faculty of Sciences, Department of Chemistry, Biochemistry and Environmental Protection, Trg D. Obradovića 3, 21000 Novi Sad, Serbia, nemanja.banic@dh.uns.ac.rs**

[2]*University of Novi Sad, Faculty of Sciences, Department of Biology and Ecology, Laboratory for Ecophysiology and Ecotoxicology - LECOTOX, Novi Sad, Serbia*

Abstract

The development of clean and renewable energy resources has attracted much attention due to the growing concern over energy and environmental challenges. The use of photochemical water splitting process to create hydrogen has been recognized as a possible alternative to fossil fuels because solar energy is clean, renewable, and environmentally friendly. Additionally, growing industry including excessive chemical production, use and discharge inevitably results in water pollution. For instance, organic dyes are utilized in many industrial applications (such as textiles, food products, cosmetics, and pharmaceuticals), with 10-15% of the dyes used in the coloring process ending up in wastewater. It has been observed that a vast number of physiological processes in aquatic biota, can be disturbed by dyes present in the wastewaters, posing a frequently detected environmental problem. Semiconductor-based photocatalytic processes offer potentially cost-effective, efficient, and environmentally friendly methods to generate renewable hydrogen and purify water. In this study, using the photochemical deposition method, four photocatalysts with a 5% noble metal : MoO_3 mass ratio were synthesized: Ag/MoO_3, Au/MoO_3, Pd/MoO_3, and Pt/MoO_3. Also, the photocatalytic efficiency of these nanopowders for hydrogen production and removal of methylene blue under UV and simulated solar radiation was investigated. The cytotoxicity of the samples was tested on two mammalian cell lines by MTT assay after 24 h exposure. Compared with unmodified MoO_3 (7.5 μmol/hg H_2), under UV radiation, synthesized nanopowders: Ag/MoO_3 (9.3 μmol/hg H_2), Au/MoO_3 (12.6 μmol/hg H_2), Pd/MoO_3 (8.6 μmol/hg H_2), and Pt/MoO_3 (11.8 μmol/hg H_2) exhibited greater rate in terms of hydrogen generation at a time interval of 300 min. Compared with an unmodified MoO_3 photocatalyst, the presence of 5 wt% Au increased the hydrogen production rate by 1.7 times. The kinetics of methylene blue removal using the aforementioned photocatalysts was monitored photometrically. Under simulated solar radiation, Au/MoO_3 catalyst proved to be the most efficient, where the photodegradation efficiency was 62.4% after 120 min. In the presence of UV radiation Pt/MoO_3 showed the highest photodegradation efficiency, where 39.1% methylene blue was degraded. The adsorption efficiency was the highest using Pd/MoO_3 (100.0%). The cytotoxicity assessment results show higher sensitivity of SH-SY5Y compared to the HepG2 cell line.

***Acknowledgements**: This study is supported by the Ministry of Education, Science and Technological Development of the Republic of Serbia (grant no. 451-03-68/2022-14/200125 and grant no. 451-03-47/2023-01/200125). The authors pay special gratitude to the Srbijagas company, which, by donating the gas chromatograph, enabled the realisation of this research.*

Reusable Fe_2O_3/TiO_2/PVC photocatalysts synthesis and application for the removal of methylene blue in the presence of simulated solar radiation

Ivana Jagodić[1], Dina Tenji[2], Teodora Vidović[1], Jovana Cvetić[1], Nemanja Banić[1]*

[1]*University of Novi Sad, Faculty of Sciences, Department of Chemistry, Biochemistry and Environmental Protection, Trg Dositeja Obradovića 3, 21000 Novi Sad, Serbia,*

*nemanja.banic@dh.uns.ac.rs**

[2]*University of Novi Sad, Faculty of Sciences, Department of Biology and Ecology, Laboratory for Ecophysiology and Ecotoxicology - LECOTOX, Novi Sad, Serbia*

Abstract

A large number of industries dye their products and consume large amounts of water in these processes. As a result, arises a significant amount of wastewater. Methylene blue is a common primary dye used in industrial processes and in higher concentrations leading to serious health problems, so removing it from wastewater is essential. Advanced oxidation processes that degrade pollutants into biodegradable products are promising strategies for efficiently treating wastewater. The most demanding challenge is developing a photocatalyst with characteristics such as high photocatalytic efficiency, recyclability, and full use of the potential of sunlight. Newly synthesized composites (Fe_2O_3/(TiO_2)/PVC) were used as catalysts in the process of removing methylene blue ($c_0=2.45\cdot10^{-2}$ mM) in the presence/absence of simulated solar radiation. Commercial TiO_2, PVC, and iron(III) oxide, which is synthesized by different methods, were used for the synthesis. Six Fe_2O_3/(TiO_2)/PVC composites were prepared, with the same mass ratio of Fe to TiO_2, which was 7.2% w/w, and the percentage of nanocatalyst in the final sample with PVC was 2.5%. The composites were used as tablets, with a diameter of 5 mm and a thickness of 2 mm. The highest percentage of methylene blue removal (70.6%) from the solution in the presence of simulated solar radiation was achieved using Fe_2O_3/TiO_2/PVC photocatalyst synthesized with commercial Fe_2O_3. The methylene blue removal kinetics were monitored by UV/Vis spectrophotometry. For the most efficient Fe_2O_3/TiO_2/PVC composite, the possibility of photo-cleaning and reusing was examined five times in a row.

***Acknowledgements**: This study is supported by the Ministry of Education, Science and Technological Development of the Republic of Serbia (grant no. 451-03-68/2022-14/200125).*

Impact of deposition conditions on the electrocatalytic performances of Sn-Pd catalysts in ethanol oxidation reaction

Uticaj uslova taloženja na elektrohemijske performanse Sn-Pd katalizatora u reakciji oksidacije etanola

Jelena D. Lović*, Nebojša D. Nikolić*

Department of Electrochemistry, Institute of Chemistry, Technology and Metallurgy, University of Belgrade, Njegoševa 12, 11000 Belgrade, Serbia

**jelena.lovic@ihtm.bg.ac.rs; *nnikolic@ihtm.bg.ac.rs*

Abstract

We are reporting the electrochemical behavior of bimetallic Sn-Pd catalysts in ethanol oxidation reaction (EOR). Sn-Pd catalysts were prepared by two step electrodeposition technique whereby by regulating deposition conditions various forms of Sn dendrites and different atomic ratios of Sn:Pd were achieved. The electrocatalytic activity of Sn-Pd catalysts were evaluated for EOR in alkaline solution using cyclic voltammetry (CV) and chronoamperometric (CA) measurements. The highest activity and anti-poisoning ability exhibited $Sn_{0.67}$-$Pd_{0.33}$ catalyst due to the better utilization of Pd. At $Sn_{0.67}$-$Pd_{0.33}$ catalyst Sn better contribute Pd to oxidize chemisorbed species by providing adsorbed OH^- species, thereby enabling well synergy of Sn with Pd.

Keywords: *electrodeposition; electrocatalysts; electrooxidation; dendrites.*

Izvod

U ovom radu se bavimo ispitivanjem elektrohemijskog ponašanja Sn-Pd katalizatora u reakciji oksidacije etanola (ROE). Sn-Pd katalizatori su dobijeni dvostepenim elektrohemijskim taloženjem, pri čemu se regulisanjem uslova taloženja dobijaju različite forme Sn dendrita i različiti atomski odnosi Sn:Pd. Elektrohemijska aktivnost Sn-Pd katalizatora je procenjena u ROE u alkalnoj sredini korišćenjem ciklične voltametrije (CV) i hronoamperometrijskim merenjima. Najveću aktivnost i toleranciju prema otrovima je pokazao $Sn_{0.67}$-$Pd_{0.33}$ katalizator zbog boljeg iskorišćenja Pd. Primećeno je da kod $Sn_{0.67}$-$Pd_{0.33}$ katalizatora Sn bolje doprinosi oksidaciji hemisorbovanih čestica na Pd obezbeđivanjem OH^- čestica, omogućujući tako dobru sinergiju Sn sa Pd.

Ključne reči: *elektrohemijsko taloženje;elektrokatalizatori; elektrooksidacija; dendriti.*

Introduction

Direct alcohol fuel cells (DAFCs) have obtained considerable attention because of their promising commercialization as the power source for portable electronic devices and fuel-cell vehicles [1,2]. The use of alcohols as fuel has several advantages in regard to hydrogen, such as easy storage and transportation [3,4]. Ethanol is an attractive fuel because it has relatively high theoretical energy density, low toxicity and can be produced easily from the fermentation of maize, sugar came, wheat and some other raw materials [4]. With the development of anion-exchange membrane more attention has been paid to electrocatalysis in alkaline medium because the kinetics of alcohol oxidation enhanced as compared with that in acidic medium [3,5]. The design of active and poisoning tolerant anodic catalyst is major subject in the development of direct ethanol fuel cell (DEFC). Pd is a prospective substitute for Pt because of its relatively abundant reserves. Moreover, Pd presents high electrocatalytic activity for ethanol oxidation in alkaline medium [6]. Thus Pd-based catalyst is an excellent candidate for the application in DEFCs. Designing a new type of catalyst with less consumption of Pd metal by combining Pd with one or more transition metals such as, Sn [7,8], Cu

[9], Ag [10,11], Ni [12, 13], and adjusting their morphologies and compositions can further improve their electrocatalytic activity for ethanol oxidation.

We reported the synthesis of Sn sub-layer covered with a smaller fraction of Pd by means of two step electrodeposition technique [14]. According to morphological and elemental analysis of Sn and Sn–Pd, various forms of dendrites were obtained depending on the regime of Sn electrodeposition, while Pd on Sn creates electrodeposited islands [14-16]. It was demonstrated that the electrocatalytic activity of Pd in Sn–Pd depended strongly on the structure and morphology of dendrites [14]. Since Sn has no catalytic activity in the potential range of EOR [14], the electrooxidation of ethanol on the Sn–Pd catalysts is mainly attributed to the electrocatalysis of Pd component. The role of Sn is to contribute Pd to oxidize chemisorbed species formed during the electrooxidation of ethanol by providing adsorbed OH- species [17, 18], thereby enhancing the catalytic performance of the bimetallic catalysts. It was shown based on XPS measurements that the presence of Sn affects the electronic state of Pd by reducing the adsorption strength of the reaction intermediates on Pd, which has a positive effect on Sn-Pd electrocatalytic activity during the EOR [14]. By vary the amount of Sn loading prepared in the potentiostatic regime and keeping constant Pd loading, a series of Sn-Pd electrocatalysts with various ratios of Sn and Pd were synthesized and among them, $Sn_{0.6}$-$Pd_{0.4}$ showed to be the most active and poisoning tolerant catalyst in EOR [19].

In this work, the Sn-Pd electrocatalysts with various forms of Sn dendrites and different atomic ratios of Sn:Pd were prepared via a facile template-free two step electrodeposition technique. The electrocatalytic activity of Sn-Pd catalysts toward EOR were investigated by the electrochemical measurements.

Experimental

All the experiments were performed in three-compartment electrochemical glass cells with Pt electrode as the counter electrodes and Ag/AgCl/3.5 M KCl as the reference electrodes and all potentials were referred to this electrode denoted as Ag/AgCl. The electrolytes were prepared with high purity water (Millipore, 18M cm resistivity) and the chemicals provided by Merck. The experiments were conducted at 298±0.5 K. BioLogic SP 200 potentiostat/galvanostat was employed. Cylindrical electrodes of Cu, with a surface area of 0.25 cm^2 were used as substrate for Sn electrodeposition. Cu working electrode was prepared as described previously [15]. Sn electrodeposition was performed on Cu electrode from deaerated electrolyte containing 20 g/L $SnCl_2 \times 2H_2O$ in 250 g/L NaOH at a cathodic potential of –1.8 V or at a current density of –3 mA cm^{-2} [15]. After the Sn deposition, electrode was rinsed and transferred to the electrochemical cell containing deaerated 1 M NH_4Cl and 0.01 M $PdCl_2$. The electrodeposition of Pd was performed galvanostatically at a current density of –5 mA cm^{-2} [12]. Electrode obtained by electrodeposition of Sn at –3 mA cm^{-2} with the same amount of electricity like Pd (600 mC) was denoted as Sn(–3mA cm^{-2})-Pd while electrode prepared by electrodeposition of Sn at –1.8 V keeping the same condition for Pd electrodeposition was designated as Sn(–1.8 V)-Pd. Next set of electrodes were prepared with constant amount of electricity for Sn obtained by electrodeposition at –1.8 V (600 mC), while the amount of electricity for Pd varies (300, 900, and 1200 mC) to correspond the atomic ratio of Sn:Pd = 0.67:0.33 or 0.4:0.6 or 0.33:0.67. Depending on the atomic ratio electrodes were marked as $Sn_{0.67}$-$Pd_{0.33}$, $Sn_{0.4}$-$Pd_{0.6}$ and $Sn_{0.33}$-$Pd_{0.67}$. After preparation the electrode was rinsed with water and transferred into a cell containing 1 M NaOH with 1 M ethanol. EOR was examined using CV by scanning the potential starting from –0.8 to 0.2 V at a rate of 50 mV s^{-1}. In chronoamperometric measurements, the potential was stepped from –0.8 to –0.4 V. The reaction currents obtained in electrochemical experiments were normalized to the mass amount of Pd metal in catalysts.

Results and discussion

Influence of a regime of the electrodeposition

The electrochemical behavior of Sn-Pd catalysts was directed to examination of Sn deposition regime keeping the constant atomic ratio of 50 at.% Sn–50 at.% Pd. It was reported that the electrocatalytic activity of Pd in Sn-Pd depend strongly on the morphology of Sn [14]. Depending on the regime of Sn electrodeposition different morphology of the dendrites can be obtained [14, 15]. Thus for the Sn electrodeposition at constant current density (j = – 3 mA cm^{-2}) two dimensional branchy dendrites with branches in a form of prisms were mainly created while when Sn was electrodeposited at constant potential (E = –1.8 V) the intertwined network of highly-branched fern-like dendrites was obtained. The selected current density for Sn deposition in galvanostatic regime is higher than the plateau of the limiting diffusion current density while the chosen electrodeposition potential is outside the plateau of the limiting diffusion current density[15, 16]. The synthetized electrocatalysts are denoted as Sn(–1.8V)-Pd and Sn(–3 mAcm^{-2})-Pd. Two well-defined peaks for ethanol oxidation are measured and presented in Fig. 1. The oxidation of newly chemisorbed species derived from the adsorption of ethanol can be detected by the peak in the forward scan while the reverse oxidation peak is mainly assigned to the removal of carbonaceous species that were incompletely oxidized in the forward scan [18]. According to Fig. 1 some lower activity of Sn(–3 mA cm^{-2})-Pd catalyst for Sn obtained at galvanostatic regime in regard to Sn(–1.8V)-Pd catalyst for Sn prepared at potentiostatic regime can be explained due to lower utilization of Pd on the Sn of certain morphology. It seems that intertwined network of highly-branched fern-like Sn dendrites provide better accessibility of Pd to EOR compared to dendrites with the branches of prismatic shape.

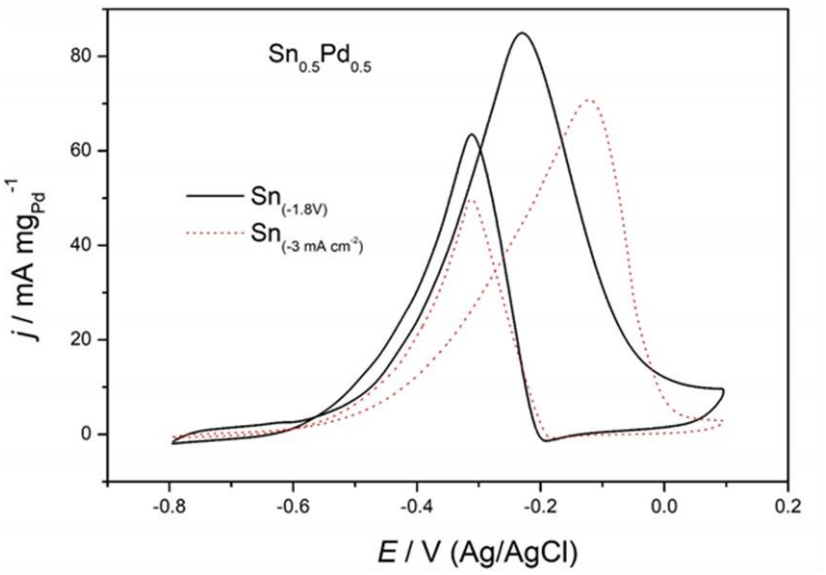

Figure 1.*CVs of Sn$_{(-1.8V)}$-Pd and Sn$_{(-3\ mA\ cm^{-2})}$-Pd catalysts in 1 M NaOH +1 M C_2H_5OH solution recorded at v = 50 mV s^{-1}.*

According to Fig. 1 Sn(–1.8V)-Pd catalyst has more negative initial potential (E_{in}) and more negative peak potential (E_p) value for approximately 0.1 V in regard to Sn(–3 mA cm^{-2})-Pd, indicating higher oxidation efficiency for EOR. It seems that Sn(–1.8V)-Pd catalyst more easily formed adsorbed OH^- species due to appropriate Sn morphology and improve the ability to remove adsorbed intermediate species on Pd thus increasing the activity of the electrocatalyst.

The activity and the stability of Sn(–1.8V)-Pd and Sn(–3 mA cm^{-2})-Pd catalysts were also investigated by chronoamperometry. The current densities of EOR at a potential of – 0.4 V were traced over 20 min. The current-time transients presented in Fig. 2 show that the initial activity of Sn(–1.8V)-Pd catalyst is much higher compared with Sn(–3 mA cm^{-2})-Pd. The decrease of initial activity of 3.8 times for Sn(–1.8V)-Pd catalyst and 5 times for Sn(–3 mA cm^{-2})-Pd was observed over 20 min at a constant potential. Better stability of Sn-Pd catalyst for Sn prepared at potentiostatic regime in regard of Sn-Pd catalyst for Sn obtained at galvanostatic regime was established and that is in accordance with the results presented in Fig 1.

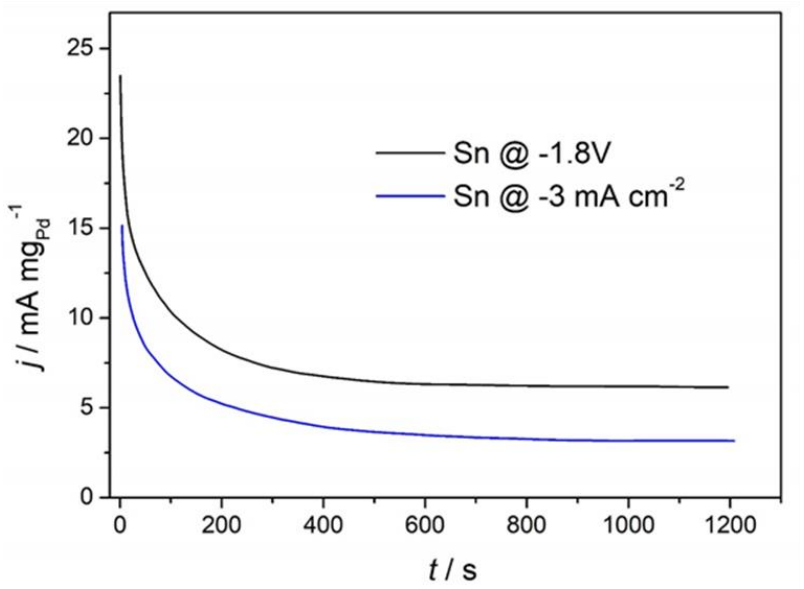

Figure 2.*Chronoamperograms of $Sn_{(-1.8V)}$-Pd and $Sn_{(-3\ mA\ cm^{-2})}$-Pd catalysts in 1 M NaOH +1 M C_2H_5OH solution recorded at E = −0.4 V.*

Effect of Pd deposited charge for constant current

Sn synthetized at –1.8 V creates networking of the dendrites and serve as substrate for deposition of Pd of various deposition charges under the same electrodeposition regime (–5 mA cm^{-2}). Namely it was necessary to ensure not only the loading of the Pd as the main catalyst, but sufficient reactive sites for the surface reaction of the catalysts and because of that fraction of Pd was vary. Figure 3 presents CVs recorded on Sn-Pd catalysts prepared for constant Sn deposited charge followed by Pd deposition at the constant current for various charges. According to Fig. 3 the most active one was found to be $Sn_{0.67}$-$Pd_{0.33}$, with the current densities of the forward peak being almost 2 times higher in regard to $Sn_{0.4}$-$Pd_{0.6}$ and $Sn_{0.33}$-$Pd_{0.67}$. In addition if the fraction of Pd in the Sn-Pd is too high, the catalytic performance of Pd will be obstructed, causing the decrease of the overall activity of Sn-Pd catalysts. Therefore better utilization of Pd with sufficient reactive sites for EOR was accomplished at $Sn_{0.67}$-$Pd_{0.33}$ catalyst. It seems that at $Sn_{0.67}$-$Pd_{0.33}$ catalyst Sn better contribute Pd to oxidize chemisorbed species coming from electrooxidation of ethanol by providing adsorbed OH^- species, thereby facilitating well synergy of Sn with Pd. Besides lower E_{in} and E_p was achieved on $Sn_{0.67}$-$Pd_{0.33}$ electrocatalyst pointing out that this catalyst is more prone for use in the EOR compared to other Sn-Pd presented in Fig. 3.

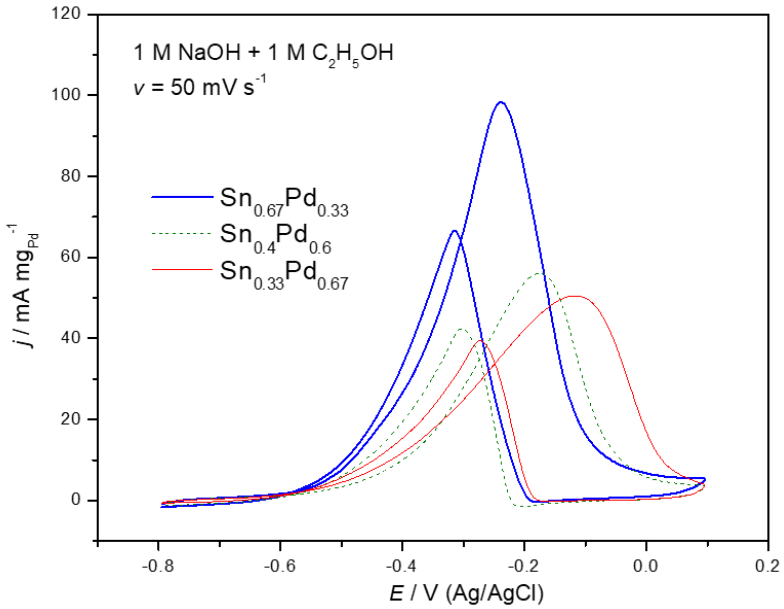

Figure 3.*CVs of $Sn_{0.33}$-$Pd_{0.67}$, $Sn_{0.4}$-$Pd_{0.6}$, and $Sn_{0.67}$-$Pd_{0.33}$ catalysts in 1 M NaOH +1 M C_2H_5OH solution recorded at v = 50 mV s^{-1}.*

Generally, the activity of electrocatalyst for EOR can be depicted by measuring the magnitude of the peak current density in the forward scan, while the ratio of the forward anodic peak current density (j_f) to the reverse anodic peak current density (j_b) is utilized to describe the tolerance of electrocatalyst to the accumulated intermediate carbonaceous species on the surface of electrode [20]. Thus a greater ratio of j_f/j_b implies higher completeness of ethanol oxidation during the forward scan as well as less carbonaceous residues accumulated on electrode surface. The obtained values of j_f/j_b are 1.10; 1.30; and 1.50 for $Sn_{0.33}$-$Pd_{0.67}$, $Sn_{0.4}$-$Pd_{0.6}$, and $Sn_{0.67}$-$Pd_{0.33}$, respectively, as illustrated in Fig. 4. Therefore Sn0.67-Pd0.33 exhibited the highest anti-poisoning ability.

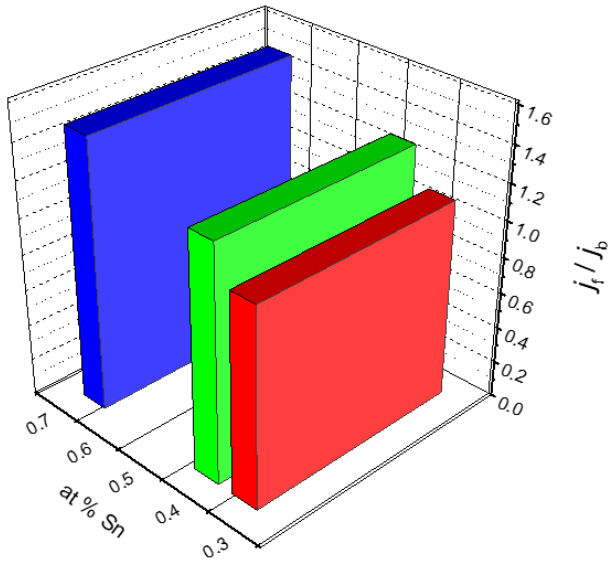

Figure 4.*Dependencies of j_f/j_b from the fraction of Sn in Sn-Pd catalysts (data derived from Fig. 3).*

Conclusion

In summary, we reported the activity of Sn-Pd electrocatalysts in ethanol oxidation reaction. Impact of deposition conditions on electrochemical performances was presented. It was demonstrated that different morphology of Sn contribute and determine Pd electrochemical behavior in EOR thus the higher activity was obtained on Sn-Pd catalyst that contain Pd on intertwined network of highly-branched fern-like Sn dendrites as sub-layer in comparison to Pd on the Sn dendrites with the branches of prismatic shape. The highest activity and anti-poisoning ability exhibited $Sn_{0.67}$-$Pd_{0.33}$ catalyst due to the better utilization of Pd. At $Sn_{0.67}$-$Pd_{0.33}$ catalyst Sn better contribute Pd to oxidize chemisorbed species by providing adsorbed OH^- species, thereby enabling well synergy of Sn with Pd.

Acknowledgements

This work was funded by Ministry of Science, Technological Development and Innovation of Republic of Serbia (RS) (Grant No. 451-03-47/2023-01/200026) and Science Fund of RS (Grant No. AdCatFC: 7739802).

References

1. J. Guo, S. Jiao, X. Ya, H. Zheng, R. Wang, J. Yu, H. Wang, Z. Zhang, W. Liu, C. He, X. Fu, Ultrathin Pd-Based Perforated Nanosheets for Fuel Cells Electrocatalysis, *Chemelectrochem*, **9**, 202200729, 2022.
2. A. Chen, C. Ostrom, Palladium-Based Nanomaterials: Synthesis and Electrochemical Applications, *Chem. Rev*., **115**, 11999–12044, 2015.
3. E.M. Halim, S. Chemchoub, A. El Attar, F.E. Salih, L. Oularbi, M. El Rhazi, Recent Advances in Anode Metallic Catalysts Supported on Conducting Polymer-Based Materials for Direct Alcohol Fuel Cells, *Front. Energy Res*., **10**, 843736, 2022.
4. E. Antolini, J.R.C. Salgado, E.R. Gonzalez,The stability of Pt–M (M = first row transition metal) alloy catalysts and its effect on the activity in low temperature fuel cells. A literature review and tests on a Pt–Co catalyst, *J. Power Sources*, **160**, 957–968, 2006.
5. E. Antolinia, E.R. Gonzalez, Alkaline direct alcohol fuel cells, *J. Power Sources*, **195**, 3431–3450, 2010.
6. Z. Zhang, L. Xin, K. Sun, W. Li, PdeNielectrocatalysts for efficient ethanol oxidation reaction in alkaline electrolyte, *Int. J. Hydrogen Energ*., **36**, 12686–12697, 2011.
7. N. Xaba, R.M. Modibedi, M.K. Mathe, L.E. Khotseng, Pd, PdSn, PdBi, and PdBiSn Nanostructured Thin Films for the Electro-Oxidation of Ethanol in Alkaline Media, *Electrocatalysis*, **10**, 332–341, 2019.
8. M. Ali Kamyabi, S.Jadali, T.Alizadeh, Ethanol Electrooxidation on Nickel Foam Arrayed with Templated PdSn; From Catalyst Fabrication to Electrooxidation Dominance Route, *ChemElectroChem*, **10**, 202200914, 2023.
9. P. Mukherjee, P.S. Roy, K. Mandal, D. Bhattacharjee, S. Dasgupta, S.K. Bhattacharya, Improved catalysis of room temperature synthesized Pd-Cu alloy nanoparticles for anodic oxidation of ethanol in alkaline media, *Electrochim. Acta*, **154**, 447–455, 2015.
10. J.D. Lović, N.R. Elezović, B.M. Jović, P. Zabinski, Lj. Gajić-Krstajić, V.D. Jović,Electrodeposited AgPd alloy coatings as efficient catalysts for the ethanol oxidation reaction, *Int. J. Hydrogen Energ*.,**43**, 18498–18508, 2018.
11. G. Zhang, Y. Wang, Y. Ma, Y. Zheng, H. Zhang, M. Tang, Y. Dai,U. V. Koc, K. R. Liu, Ultrathin samarium-doped palladium nanocrystals with exotic shapes for efficient electrocatalytic ethanol oxidation, *Catal. Today*, **409**, 63–70, 2023.
12. J.D. Lović, V.D. Jović, Electrodeposited Pd and PdNi coatings as electrodes for the electrochemical oxidation of ethanol in alkaline media. *J. Solid State Electrochem*., **21**, 2433–2441,2017.
13. A. Dutta, J.Datta, Energy efficient role of Ni/NiO in PdNi nanocatalyst used in alkaline DEFC, *J. Mater. Chem. A*, **2**, 3237–3250, 2014.
14. J.D. Lović, S. Eraković Pantović, L.Z. Rakočević, N.L. Ignjatović, S.B.Dimitrijević, N.D. Nikolić, A Novel Two-Step Electrochemical Deposition Method for Sn-Pd Electrocatalyst Synthesis for a Potential Application in Direct Ethanol Fuel Cell, *Processes*, **11**,120, 2023.

15. N.D. Nikolić, J.D. Lović, V.M. Maksimović, P.M. Živković, Morphology and Structure of Electrolytically Synthesized Tin Dendritic Nanostructures, *Metals*, **12**,1201, 2022.
16. N.D. Nikolić, J.D. Lović, V.M. Maksimović, The control of morphology and structure of galvanostatically produced tin dendrites by analysis of chronopotentiometry response, *J. Solid State Electrochem.*, 2023.
17. A. M. Makin Adam, A. Zhu, L.Ning, M. Deng, Q. Zhang, Q. Liu, Carbon supported PdSn nanocatalysts with enhanced performance for ethanol electrooxidation in alkaline medium, *Int. J. Hydrogen Energ*., **44**, 20368–20379, 2019.
18. W. Du, K.E. Mackenzie, D.F. Milano, N.A. Deskins, D. Su, X. Teng, Palladium–Tin Alloyed Catalysts for the Ethanol Oxidation Reaction in an Alkaline Medium, *ACS Catal*., **2**, 287–297, 2012.
19. J.D. Lović, N.D. Nikolić, P.M. Živković, S.B. Dimitrijević, M. Stevanović, in press.
20. L. Ning, X. Liu, M. Deng, Z. Huang, A. Zhu, Q. Zhang, Q. Liu, Palladium-based nanocatalysts anchored on CNT with high activity and durability for ethanol electro-oxidation, *Electrochim. Acta*, **297**, 206–214, 2019.

Phenomena of Nucleation and Growth of Tin Dendrites from the Alkaline Solution

Fenomeni nukleacije i rasta dendrita kalaja iz alkalnog rastvora

Nebojša D. Nikolić,* Jelena D. Lović, Dragana L. Milošević, Sanja I. Stevanović

Institute of Chemistry, Technology and Metallurgy,University of Belgrade, Njegoševa 12, 11000 Belgrade, Serbia

**nnikolic@ihtm.bg.ac.rs*

Abstract

The processes of nucleation and growth of tin dendrites from the alkaline hydroxide solution have been investigated. Nucleation of tin was examined by chronoamperometry at the cathodic potentials which belonged to various positions at the polarization curve. The morphology of potentiostatically electrodeposited tin dendrites with various amounts of the electricity was characterized by scanning electron microscopy (SEM) technique. Depending on the cathodic potential applied for Sn electrodeposition, the following forms of Sn dendrites were obtained: the needle-like, the spear-like and the fern-like dendrites of various degree of ramification. Combining Sharifker and Hills (SH) model for a determination of nucleation type and results of morphological analysis of Sn dendrites, it is concluded that nucleation of Sn from the alkaline hydroxide solution follows the progressive type of nucleation.

Keywords: *electrodeposition; tin;dendrite; nucleation growth.*

Izvod

Analizirani su procesi nukleacije i rasta dendrita kalaja iz alkalnog hidroksilnog rastvora. Nukleacija kalaja je bila ispitana hronoamperometrijom na katodnim potencijalima koji su pripadali različitim pozicijama na polarizacionoj krivoj. Morfologija potenciostatski elektrohemijski istaloženih dendrita kalaja sa različitim količinama elektriciteta je bila okarakterisana tehnikom skenirajuće elektronske mikroskopije (SEM). U zavisnosti od katodnog potencijala primenjenog za elektrohemijsko taloženje kalaja, formirani su sledeći oblici dendrita kalaja: igličasti, dendriti nalik koplju i dendriti nalik paprati različitog stepena razgranatosti. Kombinovanjem Šarifkerovog i Hilsovog (SH) modela za određivanje tipa nukleacije i rezultata morfološke analize dendrita kalaja, zaključeno je da nukleacija kalaja iz alkalnog hidroksilnog rastvora sledi progresivni tip nukleacije.

Ključne reči: *elektrohemijsko taloženje; kalaj; dendrit; nukleacija; rast.*

Acknowledgments

This work was funded by the Ministry of Science, Technological Development and Innovation of the Republic of Serbia (Grant No. 451-03-47/2023-01/200026) and the Science Fund of the Republic of Serbia (Grant No. AdCatFC:7739802).

Anti-corrosion investigation of curcumin as a green and sustainable corrosion inhibitor for copper

Regina Fuchs–Godec[1]*, Marija Riđošić[2], Miomir. G. Pavlović[2], Milorad. V. Tomić[2]

[1]*Faculty of Chemistry and Chemical Engineering, University of Maribor,Smetanova 17, Maribor, Slovenia*

[2]*Faculty of Technology Zvornik, University of Eastern Sarajevo, Karakaj bb, Republic of Srpska*

**regina.fuchs@um.si*

Abstract

Curcumin, present in commercially available organic turmeric (Curcuma longa), was tested as a potential corrosion inhibitor for copper in acid rain solution using standard techniques such as electrochemical impedance spectroscopy (EIS) and potentiodynamic polarization. Curcumin was added to octadecanoic acid at various concentrations to form a hydrophobic, self-assembling layer on the copper surface. The results of electrochemical measurements showed that there is an optimal concentration of curcumin added to the formed hydrophobic layer, namely 0.1 wt.%. An increase in the added curcumin concentration leads to a slow destabilisation of the formed protective layer.

Keywords: *Copper; Acid rain; Curcuma longa; EIS; Self-assembling layer*

Introduction

Corrosion in the modern world is the deterioration of metal structures and materials due to chemical or electrochemical reactions with the environment. This is a significant problem in many industries, including oil and gas, transportation, infrastructure, and manufacturing. Copper is a relatively corrosion-resistant metal, but it can still corrode under certain conditions. The most common type of corrosion affecting copper is known as "oxidation corrosion," which occurs when copper reacts with oxygen in the air. This forms copper oxide, a greenish layer that can be seen on the surface of the metal. Other factors that can cause copper to corrode include moisture, acidic or alkaline environments, and contact with certain chemicals. For example, copper can corrode in the presence of sulphur compounds, which can be found in some types of environmental pollution. Avoiding contact with harsh environments and chemicals can also help minimize the risk of corrosion. Applying a protective coating or paint can also help prevent corrosion [1].

The use of functional coatings for corrosion protection is becoming increasingly popular as industry seeks to improve the performance and longevity of its equipment and structures while reducing maintenance and repair costs. By providing additional functions beyond corrosion protection, these coatings can add value to the end user and help improve the overall sustainability of the materials and structures they protect. The use of green corrosion inhibitors is also becoming an alternative, even if they are not as effective as conventional inhibitors in all situations and represents an important step toward sustainable and environmentally friendly corrosion protection practices [2-4]. By incorporating green inhibitors into functional coatings, the industry can reduce its environmental impact while providing effective corrosion protection and additional functional properties.

The objective of the present study is to use commercial organic turmeric (Curcuma longa) as a potential green inhibitor. It is a hydrophobic (water repellent) compound that is sparingly soluble in water and more soluble in organic solvents such as ethanol, methanol, and acetone. The solubility of turmeric in these solvents may vary depending on factors such as temperature and the concentration of turmeric in the solvent.

Mixtures of ethanolic solution of octadecanoic acid and various concentrations of commercial Curcumin (CUR) (0.05, 0.1, 0.25, and 0.5 wt.%) were used to prepare functional self-assembled hydrophobic protection coatings.
Two different electrochemical methods were used for this purpose, i.e., classical potentiodynamic measurement and electrochemical impedance spectroscopy (EIS).

Experimental

The conventional three-electrode configuration was applied to conduct the potentiodynamic studies. All the potentials were measured against the saturated calomel electrode (SCE), and the counter electrode was made from Pt. The potentiodynamic current-potential curves were recorded by automatically changing the electrode potential from -0.4 to not more than 0.2 V with a scanning-rate of 1 mVs^{-1}. EIS measurements were carried out within the 100 kHz –1 mHz frequency range at a steady open circuit potential (OCP) disturbed by an amplitude of 10 mV. Nyquist and polarization plots were obtained from the results of these experiments 60 mins after the working electrode had been immersed in the solution, to allow stabilization of the stationary potential. The corrosive media was artificially prepared urban rain (the mixture of 0.2 g L^{-1} Na_2SO_4, 0.2 g L^{-1} $NaHCO_3$, and 0.2 g L^{-1} $NaNO_3$, the pH was adjusted with 10% H_2SO_4 to pH 5). All experiments were performed at 25 °C ± 1°C. Potentiodynamic measurements were made after 1 hour and after 2, 5, and 7 days of immersion in the selected corrosion media, whereas EIS measurements were made after 1, 10, and 15 hours and after 1, 2, 4, and 6 days of immersion.
The measurements were performed Gamry 600™ potentiostat/galvanostat controlled by electrochemical program, respectively. Data were collected and analysed using CorrView, CorrWare, Zplot and ZView software, developed by Scribner Associates, Inc.

Results and discussion

The potentiodynamic curves in the simulated acid rain solution (pH = 5) after 1 hour for bare copper and for a modified copper surface (with a self-assembling hydrophobic layer consisting of different concentrations of curcumin added to 0.05 M octadecanoic acid) after 1 hour and after 2, 5, and 7 days of testing are shown in Figure 1. From the current potential response, the hydrophobic coating, consisting only of octadecanoic acid, greatly reduces both the cathodic and anodic current densities.
It is surprising that the addition of curcumin at the lowest chosen values, i.e., 0.05 wt.% and 0.1 wt.%, has a stronger inhibitory effect than in the case of the addition of curcumin at the higher chosen concentrations of 0.25 wt.% and 0.5 wt.%.
The results of the EIS measurements also show the same response. Figure 2 shows the Nyquist diagrams at different immersion times of the modified copper surface. From the Nyquist plots, the high values of polarization resistance of all the coatings formed can be seen. Again, coatings with lower concentrations of curcumin in combination with octadecanoic acid resulted in coatings with better inhibition properties. Regarding the stability of this coating, the coating in the composition (0.05 M C18:0 + 0.1% CUR) stands out. It remains stable from the beginning of the measurement to the end, i.e., even after 6 days of immersion in a corrosion solution (acid rain). Regardless of the other selected concentrations of added curcumin, a decrease in polarization resistance is observed throughout the exposure to the corrosive medium. This phenomenon is again more pronounced at higher selected concentrations of added curcumin. Basically, it is most pronounced at the highest concentration shown of 0.5 wt.% CUR in the self-assembling hydrophobic layer. The electrochemical parameters obtained from the polarisation curves, and the inhibition efficiency, are shown in Table 1.

Corrosive media Acid rain pH = 5.0	i_{corr} (μA cm^{-2})	E_{corr} (V/SCE)	R (mmy^{-1})	% η_{icorr}
bare surface Cu	1.8310	0.0145	0.0106	
modified surface 0.05 M C18:0 + 0.05 w% CUR				
1h	0.00337	-0.219	1.96E-05	99.816
2 days	0.00042	-0.085	2.44E-06	99.977
5 days	0.0106	-0.063	6.16E-05	99.421
7 days	0.0116	-0.071	6.74E-05	99.366
modified surface 0.05 M C18:0 + 0.1 w% CUR				
1h	0.000507	-0.152	2.95E-06	99.972
2 days	0.000521	-0.089	3.03E-06	99.972
5 days	0.00118	-0.088	6.86E-06	99.936
7 days	0.0037	-0.085	2.15E-05	99.798
modified surface 0.05 M C18:0 + 0.25 w% CUR				
1h	0.00168	-0.163	9.76E-06	99.908
2 days	0.00423	-0.146	2.46E-05	99.769
5 days	0.0186	-0.122	1.08E-04	98.984
7 days	0.0235	-0.066	1.37E-04	98.717
modified surface 0.05 M C18:0 + 0.5 w% CUR				
1h	0.0033	-0.180	1.92E-05	99.819
2 days	0.00416	-0.171	2.42E-05	99.773
5 days	0.0108	-0.075	5.91E-05	99.444
7 days	0.0321	-0.087	1.87E-04	98.241

Table 1. *Kinetic parameters for corrosion of* Cu *for the bare surface after 1h, and for modified surfaces after 1h, and after 2, 5 and 7days duration test in the 'acid rain' solutions (pH = 5) at 25ºC. The modified surfaces were prepared by immersion of Cu in 0.05 M octadecanoic acid (C18:0) in ethanol with and without addition of curcumin.*

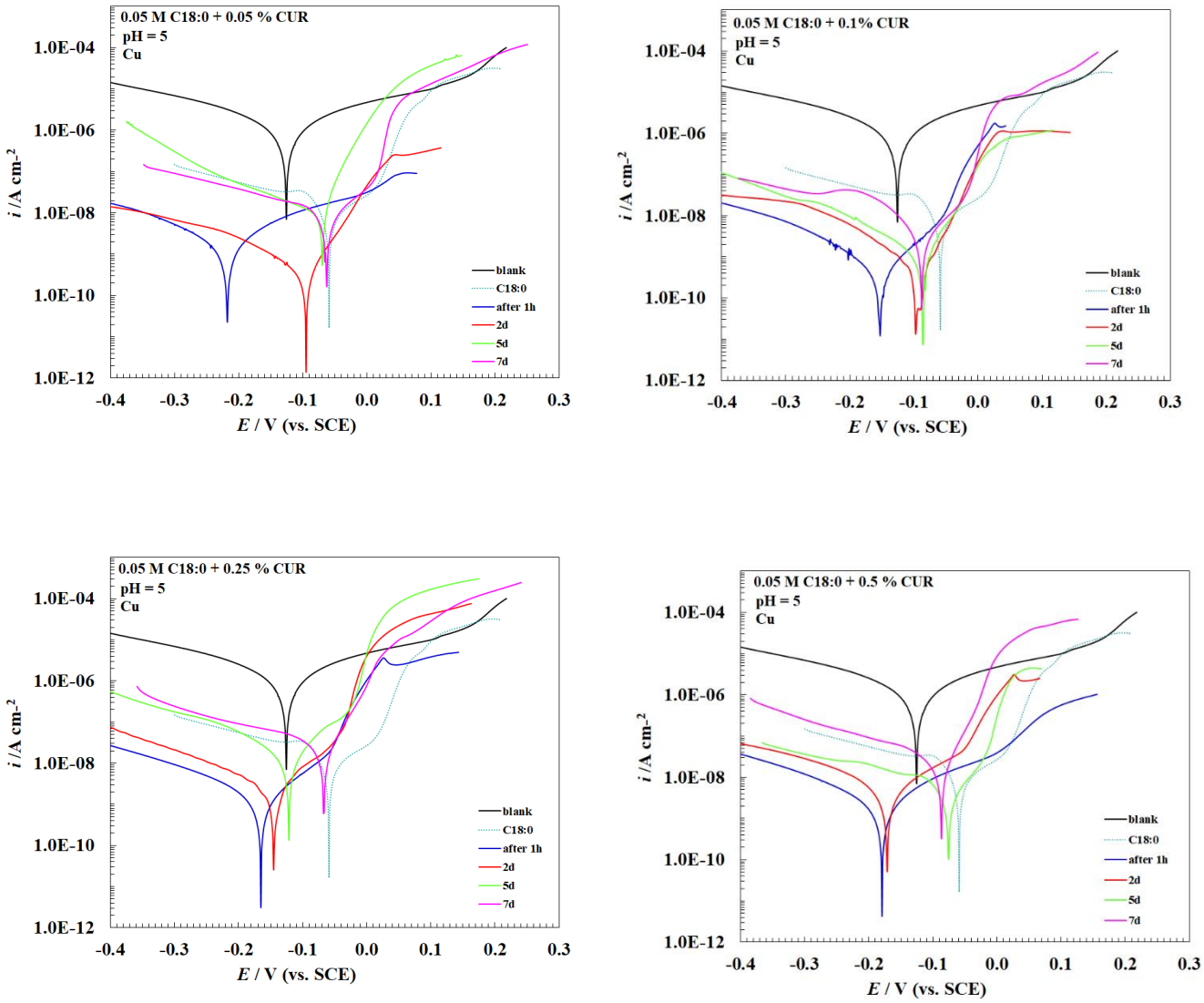

Figure 1: Potentiodynamic polarisation curves (1 mVs^{-1}) of Cu *for the bare surface after 1h, and for modified surfaces after 1h, and after 2, 5 and 7days duration test in the 'acid rain' solutions (pH = 5) at 25ºC . The modified surfaces were prepared by immersion of Cu in 0.05 M octadecanoic acid (C18:0) in ethanol with and without addition of curcumin.*

If the density of the hydrophobic layer increases with increasing concentration of the added curcumin, this has some influence on the increase in surface roughness. It is known that it is the micro-roughness that allows the gas to be trapped in these interstices, ultimately creating a barrier between the surface and the penetration of the electrolyte. What about the possibility of 'nanobubbles" forming on the electrolyte side?

If the layer is highly hydrophobic, it can create a lower energy surface for gas molecules to attach to, which can increase the attraction of gas bubbles to the hydrophobic layer. It is also known that when the surface tension of the liquid is high (which is also true to some extent for aqueous solutions), there can be a pressure difference at the gas-liquid interface that can lead to deformation of the interface and attraction of gas bubbles to hydrophobic surfaces. If conditions are such that the bubbles can remain on the organic layer, this can lead to damage of the hydrophobic layer, resulting in progressive degradation of the layer, even at the micro level.

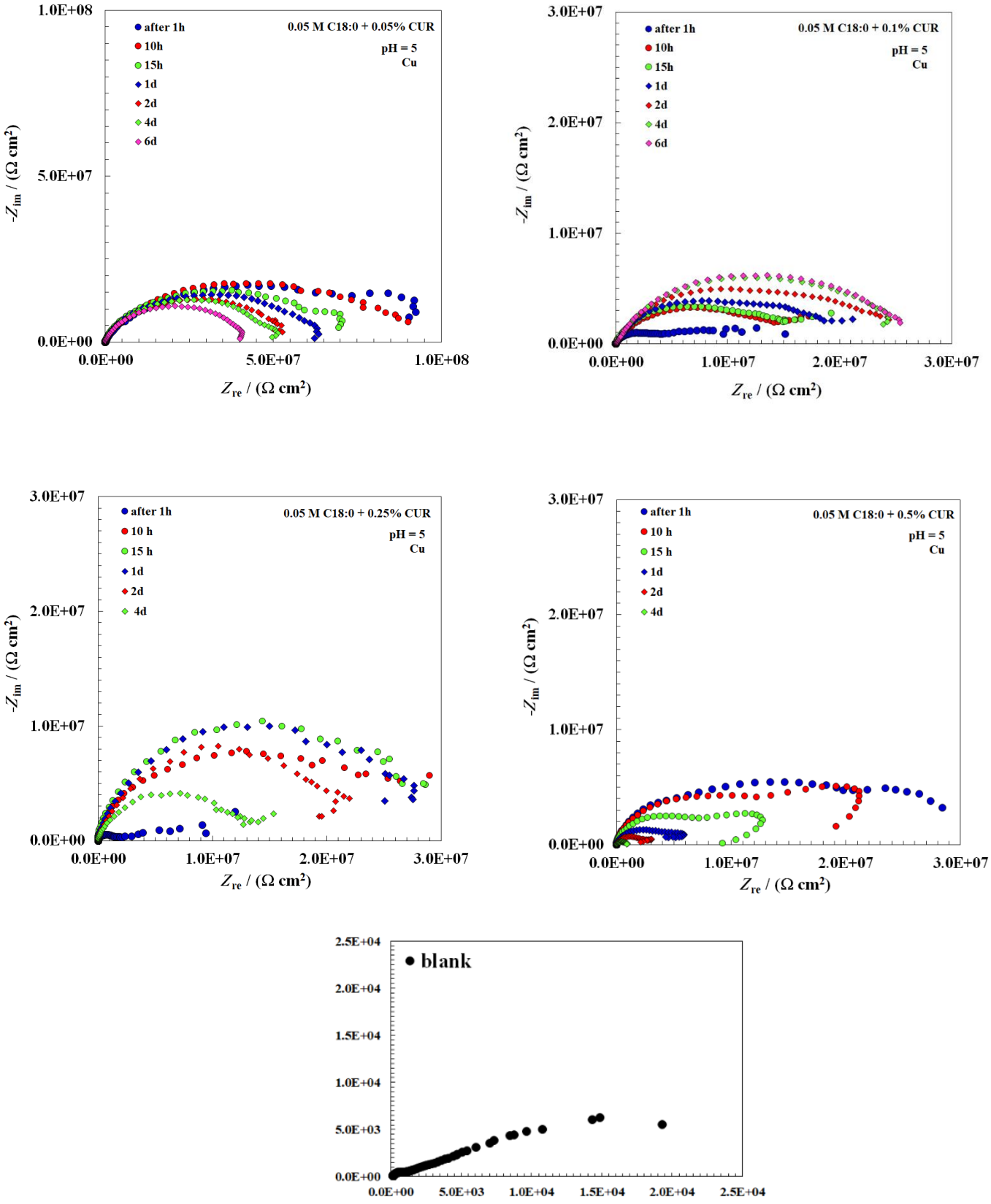

Figure 2. *EIS Nyquist plots of Cu for the bare after 1h and for modified surfaces after 1, 10 and 15h, and after 1, 2, 4 and 6 days duration test in the 'acid rain' solutions (pH =5) at 25ºC.*

Overall, the attraction of gas bubbles to a hydrophobic layer is a complex phenomenon that can be influenced by a variety of factors, including the surface tension of the liquid phase, the hydrophobicity of the layer, and the surface properties of the layer. Further investigation will provide the answers to the above conjecture.

Conclusion

The results of the electrochemical measurements showed that there is an optimal concentration of curcumin added to the formed hydrophobic layer, namely between 0.05 and 0.1 wt%. An increase in the added curcumin concentration leads to a slow destabilisation of the formed protective layer, although the obtained inhibition efficiencies are very high, up to 99% even after 6 days of immersion in the selected corrosion medium.

Acknowledgments

This work was financially supported by Slovenian Research Agency under research project “Physico-Chemical Processes on the Surface Layers and Application of Nanoparticles” (P2-0006).

References:

1. Z. Peng, K. Ogle, The Corrosion of Copper and Copper Alloys, *Encyclopedia of Interfacial Chemistry*, 478–489, 2018.
2. E.A. Florez-Frias, V. Barba, R. Lopez-Sesenes, L. L. Landeros-Martínez, J. P. Flores-De los Ríos, M. Casales, J.G. Gonzalez-Rodriguez, Use of a Metallic Complex Derived from Curcuma Longa as Green Corrosion Inhibitor for Carbon Steel in Sulfuric Acid, *International Journal of Corrosion*, 1–13, 2021.
3. G. Chávez-Díaza, M. G. Valladares-Cisnerosb, J. Uruchurtu-Chavarína, Evaluation of Curcuma Longa as Corrosion Green Inhibitor for 1018 Steel in Media Chloride, *The Electrochemical Society*, **101 (1),** 213-224, 2021.
4. P. Mahalakshmi, S. Rajendran, G. Nandhini, S.C. Joycee, N. Vijaya, T. Umasankareswari, N. Renuga Devi, Inhibition of corrosion of mild steel in sea water by an aqueous extract of turmeric powder, *Int. J. Corros. Scale Inhib.*, **9 (2),** 706–725 2020.

Corrosion resistance of hydrophobic FDTS self-assembly layer on silver-coated copper in acidic solution

Regina Fuchs–Godec*

Faculty of Chemistry and Chemical Engineering, University of Maribor,Smetanova 17, Maribor,

**regina.fuchs@um.si*

Abstract

In this study, the corrosion behaviour of copper coated with silver in combination with a self-assembled hydrophobic perfluorodecyltrichlorosilane (FDTS) layer is investigated in two selected corrosive media, namely simulated acid rain with pH values of 3 and 5, after 1 hour and after 5 and 7 days of immersion in the selected corrosion media. Two electrochemical methods were chosen for this study, namely the classical potentiodynamic method and the impedance spectroscopy method. In a simulated acid rain solution with a pH of 5, the corrosion current density does not change significantly even after prolonged exposure (7 days), and the inhibition effect is still 90% even after 7 days of exposure to the corrosive medium. In the more aggressive version of acid rain (pH=3), the inhibition effect ranges from 78-82% for up to 5 days of exposure, while after 7 days of exposure it drops to a value between 54-58%.

Keywords: *Copper; Silanes; Hydrophobic layers; EIS;*

Introduction

Copper can corrode in acidic media, and the rate of corrosion depends on several factors, such as the concentration and nature of the acid, temperature, the presence of oxidizing agents or inhibitors, and the surface condition of the copper.

Silanes are a class of chemical compounds containing silicon and hydrogen. They have been extensively studied for their use as corrosion inhibitors for various materials such as metals, concrete and other construction materials. Silanes could form a thin layer on the surface of the material to which they are applied, which can provide protection against corrosion.

They are particularly effective as corrosion inhibitors for metals because they can react with the metal surface to form a protective layer that prevents further corrosion. These layers are usually composed of silicate and hydrated oxide compounds that are stable and resistant to further chemical attack and have hydrophobic or superhydrophobic properties.

There are several methods for fabricating superhydrophobic surfaces, which can be classified as: i) fabrication of rough surfaces with low surface energy materials, and ii) fabrication of rough modified surfaces with low surface energy materials [1,2]. The most well-known methods for fabricating hydrophobic surfaces are the sol-gel method, electrospinning, layer-by-layer, and plasma application by spraying [3,4]. Although these methods are widely used, they have many disadvantages, such as: the sol-gel method requires several complex steps, the electrospinning method requires relatively specialized equipment while consuming a lot of energy, and usually only allows the production of a specific nanostructure (fibres). Special equipment is also required for the plasma spraying method, while the spinning method is also not environmentally friendly due to the use of environmentally harmful solvents. Another method commonly used to produce hydrophobic surfaces is the immersion method. In the literature, this process is described as a method that also involves several steps or requires a long residence time in solutions, or, even if it already meets the criteria of a simple and short method, results in coatings that do not have satisfactory properties, especially mechanical stability [5-6].

However, the key to creating a superhydrophobic surface is to create a micro/nanostructure on the surface. This can be done by various methods, e.g., etching, electrospinning or applying a thin layer of nanoparticles. In this study, hydrophobic coatings on copper were developed by a simple immersion method and with short immersion times in solutions. A simple reaction between copper and silver nitrate was used to prepare a nano-roughened copper surface. In the second step, the silver-coated copper is immersed in a 1 mM perfluorodecyltrichlorosilane (FDTS) solution.
The prepared hydrophobic surfaces showed very good resistance to the corrosive solution of a simulated acid rain acidified to pH = 5 and pH = 3. Two different electrochemical methods were used for this purpose, i.e., classical potentiodynamic measurement and electrochemical impedance spectroscopy (EIS). Measurements were performed after 1 hour and after 5 and 7 days of immersion in the selected corrosion media.

Experimental

The conventional three-electrode configuration was applied to conduct the potentiodynamic studies. All the potentials were measured against the saturated calomel electrode (SCE), and the counter electrode was made from Pt. The potentiodynamic current-potential curves were recorded by automatically changing the electrode potential from -0.3 to not more than 0.3 V with a scanning-rate of 1 mVs^{-1}. EIS measurements were carried out within the 100 kHz –1 mHz frequency range at a steady open circuit potential (OCP) disturbed by an amplitude of 10 mV. Nyquist and polarization plots were obtained from the results of these experiments 60 mins after the working electrode had been immersed in the solution, in order to allow stabilization of the stationary potential. The corrosive media was artificially prepared urban rain (the mixture of 0.2 g L^{-1} Na_2SO_4, 0.2 g L^{-1} $NaHCO_3$, and 0.2 g L^{-1} $NaNO_3$, the pH was adjusted with 10% H_2SO_4 to pH 3 and 5). All experiments were performed at 25 °C ± 1°C. Potentiodynamic curve measurements and EIS measurements were performed after 1h of immersion and after 5 and 7 days duration test. The measurements were performed Gamry 600™ potentiostat/galvanostat controlled by electrochemical program, respectively. Data were collected and analysed using CorrView, CorrWare, Zplot and ZView software, developed by Scribner Associates, Inc.

Results and discussion

Figures 1 and 2 show polarisation curves for bare and modified copper surfaces with hydrophobic properties in simulated solutions of acid rain with pH=3 and 5 after 1 hour after 5 and 7 days of immersion (Figures 1 and 2 show the dependence of log *i* - *E* and *i* - *E* (E vs. SCE). Based on the the Corrosion resistance of pure copper decreases sharply when the pH of the corrosion solution changes from 5 to 3 (Figs. 1 and 2). The corrosion current density values increased by almost two orders of magnitude with respect to the corrosion medium with a pH of 5, especially after a 7-day immersion period (Fig.1).
Compared to the bare copper surface, the modified copper surface showed a decrease in current density in the cathodic and anodic directions (Fig.1) in both selected corrosive media (acid rain pH = 3 and 5). This phenomenon is particularly pronounced in the anodic region, indicating the stability of the functionalized hydrophobic protective layer of the copper surface. Furthermore, in the case of the modified surface, a plateau in the range of about 400 mV is reached with a minimum current density. This is about 150 mV higher than for the bare copper surface. Only in the case of the modified surface with a self-assembled hydrophobic layer after 7 days immersion in a pH=3 solution is the above claim not valid (Fig.2).
In a simulated acid rain solution with pH=5, the corrosion current density does not change significantly even after prolonged exposure (7 days), and the inhibition effect is still 90% even after 7 days of exposure to the corrosive medium. In the more aggressive version of acid rain (pH=3), the

inhibition efficiency is between 78-82% for up to 5 days of exposure, while after 7 days of exposure it drops to a value between 54-58%.

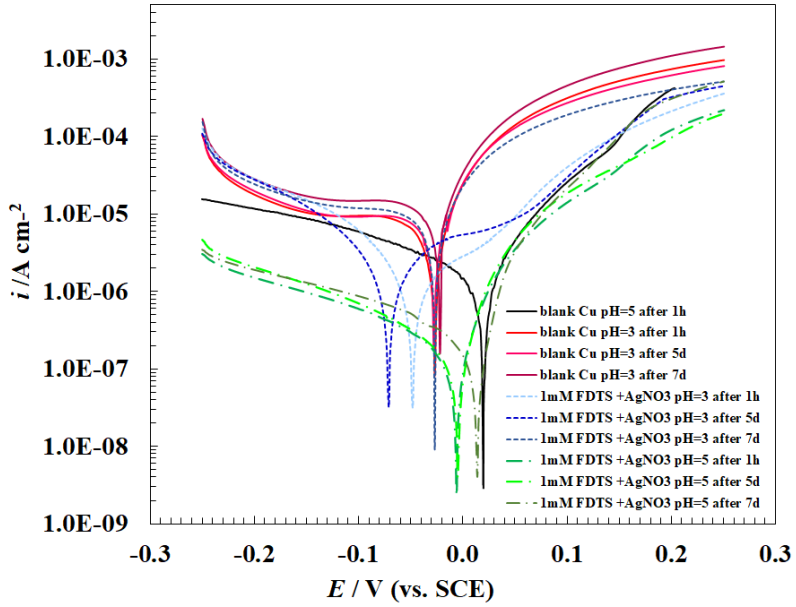

Figure 1. *Influence a self-assembled perfluorodecyltrichlorosilane (FDTS) layer on the cathodic and anodic behaviour of* Cu *in the 'acid rain' solutions (pH =3 and 5) at 25ºC, after 1h, after 5 and 7 days duration test. The modified surface was nano-roughened, silver-coated copper completed by a self-assembled perfluorodecyltrichlorosilane (FDTS) layer*

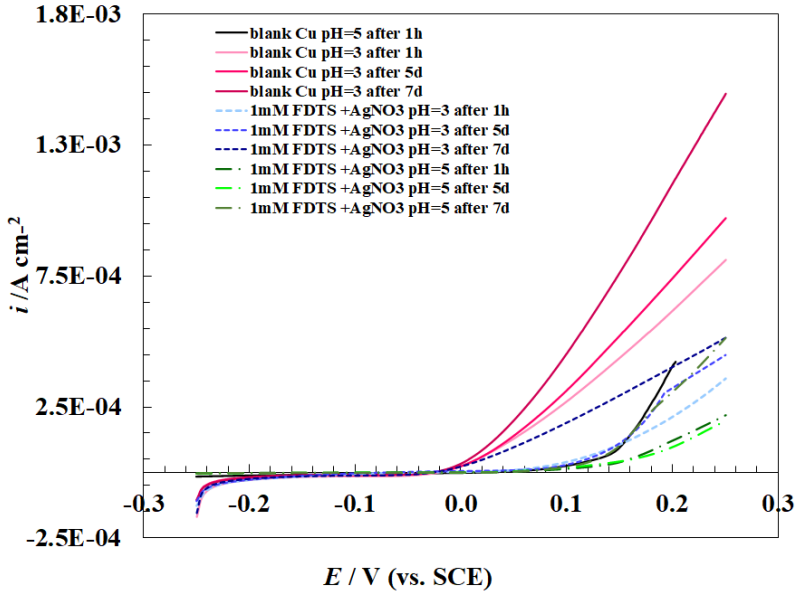

Figure 2. *Potentiodynamic polarisation curves (1 mVs^{-1}) of Cu for the bare and modified surfaces in the 'acid rain' solutions (pH =3 and 5) at 25ºC, after 1h, after 5 and 7days duration test. The modified surface was nano-roughened, silver-coated copper completed by a self-assembled perfluorodecyltrichlorosilane (FDTS) layer.*

The electrochemical parameters obtained from these polarization curves, corrosion potential (E_{corr}), corrosion current density (i_{corr}), the polarisation resistance (R_p), corrosion rate r, and the inhibition efficiency η, are shown in Table 1. The polarisation resistance was obtained from linear polarisation within the potential range of ±10 mV with respect to E_{corr}. Extrapolation of the Tafel line allowed us to calculate the corrosion current density icorr. All the parameters were determined simultaneously by CorrView software.

Table 1. Kinetic parameters for corrosion of Cu obtained from potentiodynamic polarisation curves for the bare and modified surfaces of the 'acid rain' solutions (pH =5, 3 and 1) at 25ºC, after 1h, after 5 and 7days duration test.

Corrosive media Acid rain pH = 5.0	i_{corr} (μA cm^{-2})	E_{corr} (V/SCE)	R_p (kΩ cm^2)	r (mm y^{-1})	% $\eta_{i_{corr}}$	% η_{R_p}
bare surface Cu	1.8310	0.0145	6.7	0.0106		
silver-coated copper + 1mM FDTS						
1h	0.160	-0.0062	64.95	0.00079	91.26	89.68
5 days	0.179	-0.0047	66.49	0.00087	90.22	89.92
7 days	0.189	0.0137	56.07	0.00095	89.68	88.05
Acid rain pH = 3.0						
bare surface Cu						
1h	6.855	-0.0269	2.107	0.0398		
5 days	7.295	-0.0279	1.660	0.0424		
7 days	20.80	-0.0219	1.253	0.1208		
silver-coated copper + 1mM FDTS						
1h	2.176	-0.0479	11.97	0.0126	82.39	82.40
5 days	2.627	-0.0709	9.918	0.0153	78.74	78.06
7 days	8.617	-0.0269	2.756	0.0513	58.57	54.53

Figure 3. *Hydrophobic effect on the copper coated with silver in combination with a self-assembled hydrophobic perfluorodecyltrichlorosilane (FDTS) layer.*

Figure 3 shows the hydrophobic surface of the copper surface after the formation of the self-assembled hydrophobic layer (copper coated with silver in combination with perfluorodecyltrichloro-silane (FDTS)).

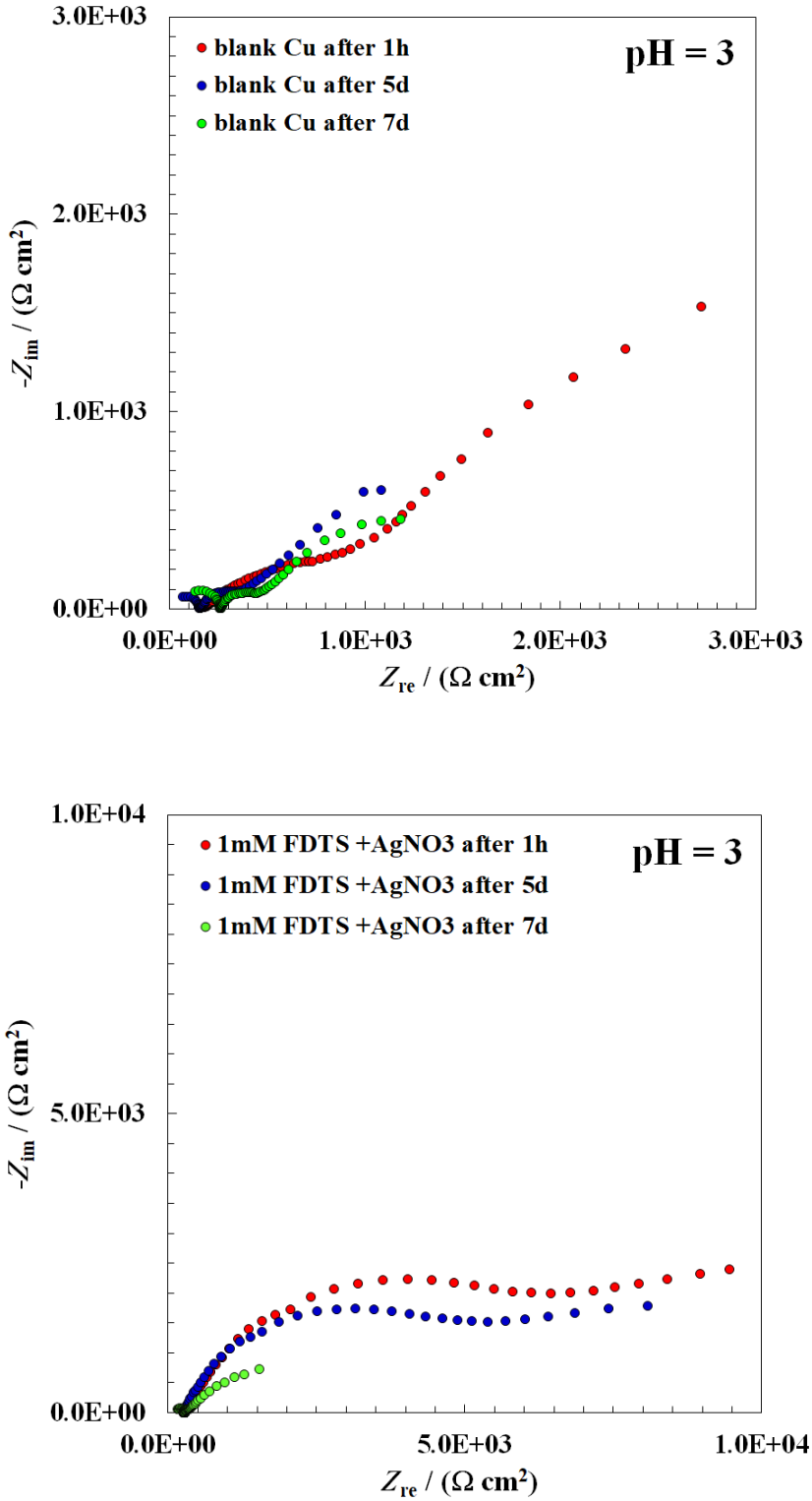

***Figure 4**. EIS Nyquist plots of* Cu *for the bare and modified surfaces in the 'acid rain' solutions (pH =3) at 25ºC, after 1h, after 5 and 7 days duration test.*

Figures 4 show the Nyquist diagrams of Cu for the bare and modified surfaces in the 'acid rain' solutions (pH =3) at 25ºC, after 1h after 5 and 7 days duration test. The results obtained by EIS in some way, confirm the interpretation mentioned above (polarization measurements).

Conclusion

- The creation of a micro/nanostructure based on the simple reaction between copper and silver nitrate has proven to be a good choice to achieve good adhesion properties of self-assembling hydrophobic layers of perfluorodecyltrichlorosilane (FDTS).
- In a simulated acid rain solution with a pH of 5, the corrosion current density of the self-assembling hydrophobic perfluorodecyltrichlorosilane layers does not change significantly even after prolonged exposure (7 days), and the inhibition effect is still 90% even after 7 days of exposure to the corrosive medium. For the more aggressive acid rain variant (pH=3), the inhibition effect ranges between 78-82% for up to 5 days of exposure, while after 7 days of exposure it drops to a value between 54-58%.

Acknowledgements

This work was financially supported by Slovenian Research Agency under research project "Physico-Chemical Processes on the Surface Layers and Application of Nanoparticles" (P2-0006).

References

1. P. Bi, H. Li, G. Zhao, M. Ran, L. Cao, H. Guo, Y. Xue, Robust super-hydrophobic coating prepared by electrochemical surface engineering for corrosion protection, *Coatings,* **452(9),** 2-28, 2019.
2. P. Dimitrakellis, E. Gogolides, Hydrophobic and superhydrophobic surfaces fabricated using atmospheric pressure cold plasma technology: A review., *Adv. Colloid Interface Sci.*, **254,** 1–21, 2018.
3. H.R. Talesh Bahrami, B. Ahmadi, H. Saffari, Optimal Condition for Fabricating Superhydrophobic Copper Surfaces with Controlled Oxidation and Modification Processes., *Mater. Lett.*, **189**, 62–65, 2017.
4. Y.Wan, M. Chen, W. Liu, X.X. Shen, Y. Min, Q. Xu, The research on preparation of superhydrophobic surfaces of pure copper by hydrothermal method and its corrosion resistance. *Electrochim. Acta*, **270,** 310–318, **2018**.
5. B. A. Butruk , P. A. Ziętek, T. Ciach, Simple method of fabrication of hydrophobic coatings for polyurethanes, *Cent. Eur. J. Chem*., 9(6), 1039-1045, 2011.
6. H. Cao, X. Guo, Y. Zhou, Y. Yan, W. Sun,Fabrication of Durable Hydrophobic/Superhydrophobic Wood Using an Alkyl Ketene Dimer by a Simple and Feasible Method, *ACS Omega*, **21(7)**, 17921–17928, 2022.

Production of Landfill Biogas and Examination of the Possibility of Its Utilization at the Možura Landfill in Bar

Proizvodnja deponijskog biogasa i ispitivanje mogućnosti njegovog iskorišćenja na deponiji Možura u Baru

D. Vuksanović[1*], J. Šćepanović[1], D. Radonjić[1], J. Ćeman[2], S. Arabelović[2]

[1]*University of Montenegro, Faculty of Metallurgy and Technology, Cetinjski put, 81000 Podgorica, Montenegro*

[2]*Možura d.o.o. Bar*

[*]*darkov@ucg.ac.me*

Abstract

The disposal of municipal waste at a sanitary landfill as a result of treatment and a greater degree of decomposition of waste within the landfill, due to anaerobic processes, additionally stimulated by the effect of moisture, generates significantly higher emissions of landfill gas. These emissions need to be removed from the body of the landfill in a controlled manner in order to primarily reduce the risk of explosion, eliminate unpleasant odors, reduce the risk to the environment, and then, through controlled combustion, reduce methane emissions into the atmosphere by reducing the impact on the greenhouse effect. The amount of generated landfill biogas can be obtained by measuring emissions or by applying different mathematical assessment models. The uncontrolled release of landfill biogas increases the emission of greenhouse gases that have a negative impact on the environment. Proper management of landfill biogas prevents air pollution and reduces greenhouse gas emissions. If landfill biogas is used for energy, an economic profit can be achieved. Proper management of landfill biogas includes: planned collection, control, treatment and its utilization.

The biogas production process allows organic materials to be converted into gas that can be used to produce electricity and heat.

The aim of the work is to analyze the amount of landfill biogas generated at the Možura landfill in Bar to see the possibilities of its use for the production of electricity.

Keywords: landfill biogas; renewable energy source; methane emission; combustion of landfill biogas; energy utilization of landfill biogas

Izvod

Odlaganjem komunalnog otpada na sanitarnu deponiju kao rezultat tretmana i većeg stepena razlaganja otpada unutar deponije, usljed anaerobnih procesa, dodatno podstaknutih dejstvom vlage, generišu se značajnije veće emisije deponijskog gasa. Ove emisije je potrebno kontrolisano odvesti iz tijela deponije kako bi se prvenstveno smanjio rizik od eksplozije, eliminisali neprijatni mirisi, smanjio rizik za okolinu, a potom putem kontrolisanog sagorijevanja redukovale i emisije metana u atmosferu smanjenjem uticaja na efekat staklene bašte. Količina nastalog deponijskog biogasa može se dobiti mjerenjem emisija ili primjenom različitih matematičkih modela procjene. Nekontrolisanim ispuštanjem deponijskog biogasa povećava se emisija gasova sa efektom staklene bašte koji negativno utiču na životnu sredinu. Pravilnim upravljanjem deponijskim biogasom sprečava se zagađivanje vazduha i smanjuje se emisija gasova sa efektom staklene bašte. Ukoliko se vrši energetsko iskorišćenje deponijskog biogasa može se postići i ekonomska dobit. Pravilno upravljanje deponijskim biogasom obuhvata: plansko sakupljanje, kontrolu, tretman i njegovo iskorišćenje.

Proces proizvodnje biogasa omogućava da se organski materijali pretvore u gas koji se može koristiti za proizvodnju električne i toplotne energije.

Cilj rada je da se kroz detaljnu analizu količina deponijskog biogasa koji nastaje na deponiji Možura u Baru sagledaju mogućnosti njegovog iskorišćenja za proizvodnju električne energije.
Ključne riječi: *deponijski biogas; obnovljivi izvor energije; emisija metana; sagorijevanje deponijskog biogasa; energetsko iskorišćenje deponijskog biogasa*

Uvod

Dosadašnji stepen i način eksploatacije resursa, kao i način njihove potrošnje u vrijeme sadašnje energetske i ekološke krize, postaju neodrživi. Ovaj zaključak proizilazi iz podataka o zagađenju vode i vazduha, o promjeni hemijskog sastava atmosfere, pojave ozonskih rupa, degradacije tla, nestanku biljnih i životinjskih vrsta, smanjenju površina pod šumama. Sa oko 6% svjetske populacije, zemlje Evropske unije koriste oko 14-15% svjetskih energetskih izvora. [1].
Tokom razgradnje otpada na sanitarnoj deponiji, u aerobnoj fazi razgradnje otpada u većoj mjeri nastaje ugljen-dioksid. dok u anaerbnoj fazi nastaje metan. Metan ima 21 put veći potencijal globalnog zagrijavanja od ugljendioksida, zbog čega se u prvoj fazi nastajanja deponijskog biogasa, instalira baklja pomoću koje se vrši spaljivanje deponijskog biogasa, pri čemu se metan prevodi u ugljen-dioksid, kao gas koji manje utiče na efekat staklene bašte.
Odloženi otpad stvara deponijski gas (LFG - Landfill gas). To je posljedica anaerobne degradacije organskih frakcija u deponovanom otpadu. U anaerobnim uslovima (bez kiseonika) na deponijama, organski otpad se razgrađuje od strane mikroorganizama, što dovodi do stvaranja LFG. LFG je gasovita smješa koja se uglavnom sastoji od metana i ugljen-dioksida, ali i od male količine vodonika i povremeno u tragovima vodonik-sulfida. Projekti prikupljanja tečnog gasa imaju za cilj sprečavanje emisije gasova (metana i drugih zagađivača) sa deponija. Osnovna ideja je da deponije budu pokrivene (npr. slojem zemlje) i da se gasovi sakupljaju kroz bunare i sisteme cjevovoda. Tako dobijeni metan može se spaliti ili koristiti za proizvodnju električne energije. Deponijski biogas ima pozitivna i negativna svojstva. Glavna negativna svojstva su neprijatan miris (uglavnom zbog sumpornih komponenti u gasu), doprinos problemu globalnog zagrijevanja i oštećenja vegetacije. Pozitivna svojstva su karakteristike sagorijevanja i energetski sadržaj. EU Direktiva o deponijama propisuje izdvajanje i sagorijevanje formiranog gasa [2].
Pošto se metan može sakupiti sa deponija, može se spaliti da bi se proizvela električna energija. Hvatanje metana prije nego što uđe u atmosferu takođe pomaže u smanjenju efekata klimatskih promjena. Sagorijevanje pomoću baklji se smatra minimumom. Daje se prednost sagorijevanju gasa u kotlu ili gasnom motoru. Izdvajanje i korišćenje deponijskog biogasa kombinuje rješavanje negativnih i korišćenje pozitivnih svojstava. Stoga se u ovom radu razmatra realizacija izdvajanja i korišćenja deponijskog biogasa za deponiju „Možura“.
Deponijski biogas može se spaljivati na baklji ili sagorijevati. Sagorijevanje biogasa je znatno energetski efikasnije rešenje, jer se nastala toplotna energija može direktno upotrebljavati. Direktna upotreba deponijskog biogasa je isplativa kada su objekti, koji bi koristili deponijski biogas kao gorivo, maksimalno udaljeni 8 km od deponije [3]. Toplotna energija se dalje može koristiti za potrebe domaćinstava, a električna energija se može prodavati Elektroprivredi Crne Gore po feed-in tarifi. Za tretman deponijskog biogasa mogu se koristiti različite tehnologije [4]. Prednost iskorišcenja LFG u energetske svrhe je zaštita vazduha od zagađenja, smanjenje emisije gasova sa efektom staklene bašte, a takođe postiže se i ekonomska dobit. Indirektna upotreba deponijskog biogasa je proizvodnja električne energije na generatorima. Proizvodnjom električne energije od CH4 može se preračunati ekvivalent emisije CO2 koji se dalje može prodavati kao karbonski kredit. 100 MW proizvedene energije na deponijski biogas, sprečilo bi efekat staklene baste za oko 988 t ekvivalenata emisije CO2 [5].
Neki autori [6] u svojim istraživanjima obrađivali su postrojenja za prečišćavanje komunalnih otpadnih voda koja imaju dovoljno organskog opterećenja i mogu se koristiti kao pouzdani generator biogasa. Predviđanje potencijala biogasifikacije je od suštinskog značaja za održavanje redovnosti

snabdijevanja biogasom i maksimalnog korišćenja za oporavak energije. Učinjeno je mnogo pokušaja da se predvidi biogas korišćenjem računarskih i logičkih modela. Iako zbog neizvjesnih karakteristika otpadnih voda tokom cijele godine, matematička formulacija biogasa je bila otežana.
U radu [7] vršena su ispitivanja proizvodnje biogasa anaerobnom digestijom otpada od hrane i relevantne implikacije na kvalitet vazduha. Biogas proizveden anaerobnom digestijom može da diverzifikuje snabdijevanje energijom i poboljša energetsko snabdijevanje. Povećanje proizvodnje bioenergije iz održive biomase može pružiti mnoge ekonomske i ekološke koristi.
Autori rada [8] bavili su se ispitivanjima mogućnosti eksploatacije deponijskog i biogasa kao obnovljivog izvora energije u Srbiji. U radu je dat kratak pregled alternativnih izvora energije sa aspekta održivog razvoja, energetske efikasnosti i zaštite okoline i uloga tehnologije eksploatacije deponijskog i biogasa kao energenta.
Sve prisutnije obaveze kada su u pitanju standardi u proizvodnji i potrošnji energije, kao i sve strožije granične vrijednosti emisija u životnu sredinu, koje zahtijevaju uvođenje novih proizvodnih tehnologija daju prednost primjeni biogasa kao energetskog izvora u sveobuhvatnom pristupu u rešavanju pitanja zaštite životne sredine.

Rezultati ispitivanja

Odlaganje otpada na sanitarnoj deponiji „Možura“

Ukupni projektovani kapacitet deponije je 1.056.036,21 m^3.
Navedeni kapacitet na deponiji se sastoji iz četiri faze rada deponije:

I faza 394.606,70 m^3;
II faza 293.601,01 m^3;
III faza 223.142,66 m^3;
IV faza 144.685,85 m^3.

Popunjenost kapaciteta deponije zaključno sa novembrom 2021. godine, nakon gotovo 10 godina rada, iznosi cca 660.000 m^3, što predstavlja 62% ukupnog predviđenog kapaciteta deponije, koji iznosi 1.056.036,21 m^3.

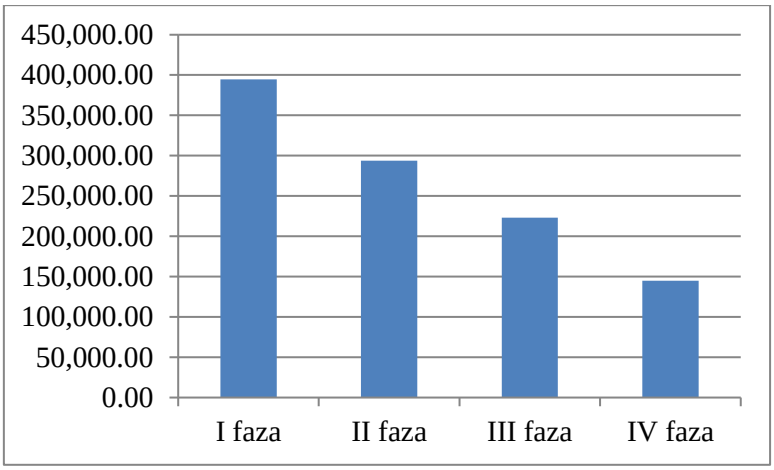

Slika 1. Prikaz kapaciteta i rada deponije kroz četiri faze izražen u m^3

Za očekivati je da će ukupni kapaciteti biti popunjeni za 4 do 5 godina, ukoliko dinamika deponovanog otpada bude na nivou prethodnih godina. Procjena proizvodnje za period od 10, 20 i 30 godina (bez reciklaže) data je u tabeli 1. Što se reciklaže tiče, kao što pokazuju podaci u tabeli 2, može se uočiti smanjenje količine deponovanog otpada.

Tabela 1. Prvobitna procjena proizvodnje za period od 10, 20 i 30 godina (bez reciklaže)

Vremenski period	Količina komunalnog otpada (bez Reciklažnog centra)
10 godina (2010-2019)	301.456 t
20 godina (2010-2029)	668.929 t
30 godina (2010-2039)	1.116.877 t

Tabela 2. Prvobitna procjena proizvodnje za period od 10, 20 i 30 godina (sa reciklažom)

Vremenski period	Količina komunalnog otpada (sa Reciklažnim centrom)
10 godina (2010-2019)	244.055,5 t
20 godina (2010-2029)	530.683,6 t
30 godina (2010-2039)	880.082,3 t

Sakupljanje i tretman biogasa

Za kontrolisanu degazaciju izgrađene sanitarne kade prema tehnološkom rješenju, usvojen je pasivni način odvođenja biogasa iz sanitarne kade putem tzv. biotrnova. Sistem za horizontalno sakupljanje biogasa i za spaljivanje biogasa je projektovan i instaliran.

Bunari za sakupljanje biogasa (biotrnovi) su postavljeni unutar tijela deponije u odgovarajućem rasporedu koji prati konturu deponije i koji je prilagođen načinu deponovanja otpada u pojedinim segmentima.

Prema preporukama dostupne literature i svjetskih standarda iz ove oblasti, vertikalne degazacione cijevi za gas se postavljaju 30-80 m odvojeno jedna od druge. Za regionalnu sanitarnu deponiju „Možura“ u Baru, predviđeno je da radijus uticaja biotrnova bude 30 m. Za sanitarnu deponiju „Možura“ Bar usvojeni broj biotrnova za evakuaciju deponijskog gasa deponije je 26 (dvadeset i šest).

Deponijski gas koji je sakupljen putem biotrnova se transportuje glavnim vodom izrađenim od HDPE do stanice za prikupljanje i pripremu gasa za spaljivanje. Na vodu, neposredno prije ulaska u stanicu za sakupljanje gasa se nalazi ventil koji služi da reguliše dotok gasa u stanicu. Ventilima je moguće podešavati protoke i pritiske. Kućica ima otvor za prirodno provjetravanje. U stanici se vrši odvajanje kondenzata i nečistoća iz deponijskog gasa i dalje se cijevnom instalacijom izrađenom od čeličnih cijevi odvodi do baklje (gorionika) za spaljivanje gasa. Na slici 2 prikazani su biotrnovi koji se koriste za prikupljanje deponijskog biogasa.

Slika 2. *Biotrnovi koji služe da prikupljanje deponijskog gasa*

Za kontrolisano spaljivanje deponijskog gasa instalirana je baklja sa zatvorenom komorom, visoke efikasnosti spaljivanja. Gorionik mora je opremljen sa nadzorom plamena preko UV fotoćelije i induktorskim sistemom za potpaljivanje. Uključivanje pilota odigrava se pomoću duple elektrode pri visokom naponu. U slučaju da nedostaje pilot plamen (što se može uočiti preko UV fotoćelije) zatvara se tok gasa i izvodi niz operacija paljenja. Samo nakon potvrđenog prisustva pilota ponovo se aktivira osnovni tok. Pilot linija opremljena je pneumatskim ventilom on/off i odgovarajućim blokatorom plamena.
Uzevši u obzir sve navedene faktore i količinu otpada koja se sada godišnje donosi na deponiju kao i onu pretpostavljenu u narednim godinama, kako je već navedeno u tabeli 1, ukupna teorijska količina deponijskog gasa koji će se stvoriti na čitavoj deponiji, računajući i preklapanje efekata kreće se maksimalno oko 495 m³/h kaptiranog deponijskog gasa u 2028.godini. Maksimalna teorijska količina proizvednog gasa sa deponije 2028. godine je 990 m³/h.
Tipični sastav i karakteristike deponijskog biogasa dat je u tabeli 3.

Tabela 3. Tipični sastav i karakteristike deponijskog biogasa

Komponente	**Sadržaj u suvom gasu (zapr.%)**
Metan	45 - 60
Ugljendioksid	40 - 60
Azot	2 - 5
Kiseonik 0,1- 1	
Sulfidi, disulfidi, merkaptani	0 - 1
Amonijak	0,1 - 1
Vodonik	0 - 0,2
Ugljenmonoksid	0 - 0,2
Sastojci u tragovima	0,01 - 0,6
Karakteristike	Vrijednost
Temperatura (°C)	38 - 50
Gustina (kg/Nm^3)	1,02 - 1,06
Vlažnost	zasićenje
Toplotna moć (kJ/Nm^3)	14900 - 20500

Obzirom da je deponijski biogas opasan po čovjekovu okolinu zbog visokog sadržaja ugljendioksida i metana, a kako je metan eksplozivan u granicama od 5-15% smješe sa vazduhom te zbog toga predstavlja izvor opasnosti, zbog čega je na lokaciji deponije izgrađeno postrojenje za ekstrakciju i sagorijevanje deponijskog biogasa, čije karakteristike su date u tabeli 4.

Tabela 4. Glavni tehnički podaci postrojenja za ekstrakciju i sagorijevanje biogasa

Model	HT 300 X2 F600 CO
Broj duvaljki	2
Broj baklji	1
Ukupni protok sisaljki	600 Nm^3/h
Ukupni protok sagorijevanja	600 Nm^3/h
Pritisak sisaljki	- 120 mbar
Pritisak uduvavanja	+ 180 mbar
Diferancijalni pritisak	300 mbar
Snaga duvaljki	7,5 kW
Instalisana snaga	7,5 kW

Snaga napajanja	380 V
Temperatura sagorijevanja	900 °C - 1200 °C
Snaga sagorijevanja	600 – 3000 kW
Raspon sagorijevanja	120-600 m^3/h CH4 50%
Minimum CH_4 postotak	25%
Trajanje zadržavanja plamena	>0,3 s
Omjer preklapanja	1:5

Toranj za spaljivanje biogasa je sastavni dio Ekstrakcione centrale (EC). Predviđeno je da se u gorioniku sa zatvorenom komorom, na kontrolisan način, sa visokom efikasnosnošću obavlja spaljivanje ekstrahovanog biogasa.
Gorionik mora biti opremljen uvijek raspoloživom pilot linijom, sa nadzorom preko UV fotoćelije. Uključivanje pilota odigrava se pomoću duple elektrode pri visokom naponu. U gorioniku je predviđen sistem za utvrđivanje temperature sagorijevanja, u slučaju da temperatura sagorijevanja nadmaši standardnu temperaturu (850 °C) za bar 10% (950 °C) mora se aktivirati automatski sistem za odvod prema pomoćnom tornju.
Termičko zračenje gorionika nije štetno za ljude i objekte na udaljenosti od 4 m od ose samog gorionika. Električna instalacija čitave ekstrakcione centrale konfigurisana je tako da ne bude zapaljiva. Vazduh neophodan za sagorijevanje dovodi se prirodnim putem bez prisilnog ubacivanja istog. Gorionik je u cjelosti napravljen od inox čelika.

Metode određivanja količina deponijskog biogasa

Koncentracija CH_4 u deponijskom biogasu prije spaljivanja u baklji utvrđena je korišćenjem LandGEM emisionog modela Američke agencije za životnu sredinu (EPA). Godišnja količina proizvedenog metana može se odrediti prema sljedećoj jednačini:

$$Q_{CH_4} = \sum_{i=1}^{n} \sum_{j=0.1}^{1} kL_0 \frac{M_i}{10} e^{-kt_{ij}}$$

Q_{CH4} – godišnja količina metana (m^3/god)
i – inkrement (1 godina)
n – početna godina za prihvatanje otpada
j – inkrement (0,1 godina)
k – brzina stvaranja metana (god^{-1})
L_o – potencijalni kapacitet stvaranja metana (m^3/t)
M_i – težina otpada deponovana u i-toj godini (t)
t_{ij} – starost j-te sekcije otpada mase Mi deponovane u i-toj godini

Parametri navedenog modela dati su u tabeli 5, a u tabeli 7 prikazane su količine proizvedenog biogasa od 2012. do 2021. godine.

Tabela 5. Parametri modela

Parametri modela	
Početak deponovanja	2012. godina
Zatvaranje deponije	2040. godina
Praćenje biogasa poslije zatvaranja deponije	2070. godina
k=0,004	god^{-1}
Lo=100 m^3/t	
Sadržaj metana	49 vol %

Sadržaj CO_2	50 vol %

Rezultati i diskusija

Sanitarna deponija „Možura“ počela je sa radom 2012. godine i bila je projektovana samo za odlaganje komunalnog otpada iz opština Bar i Ulcinj. Međutim, zbog nedostatka sanitarnih deponija u primorskom regionu, ova deponija se koristi i za odlaganje otpada iz opština Budva, Kotor i Tivat. Iz tih razloga su količine deponovanog otpada značajno veće na godišnjem nivou od projektovanih, posebno u ljetnjem periodu.
Količine komunalnog otpada koje su deponovane na deponiju „Možura“ u periodu 2012-2021. godine, iz više primorskih gradova, prikazane su u tabeli 6.

Tabela 6. Količine deponovanog otpada u tonama na sanitarnoj deponiji „Možura“ za period 2012-2021.

Godina	Bar	Ulcinj	Budva	Tivat	Kotor
2012	9.757,71	4.447,00	5.960,68	543,54	477,32
2013	21.364,81	9.328,04	20.676,03	2.366,84	7.172,02
2014	22.658,66	9.595,92	20.684,99	0,20	9.978,96
2015	22.946,07	10.296,75	21.483,67	214,34	11.082,07
2016	23.477,34	10.804,44	22.280,83	254,30	10.567,12
2017	23.254,30	12.233,72	22.785,45	4.796,26	10.485,02
2018	23.656,88	12.636,50	23.795,91	7.203,68	11.917,15
2019	25.417,74	14.202,92	24.765,14	8.112,84	10.392,42
2020	19.142,54	9.432,46	14.586,92	3.901,18	12.590,58
2021	23.717,94	13.496,38	21.263,28	5.611,10	12.261,08
Ukupno	**215.393,99**	**106.474,13**	**198.282,90**	**33.004,08**	**96.923,74**

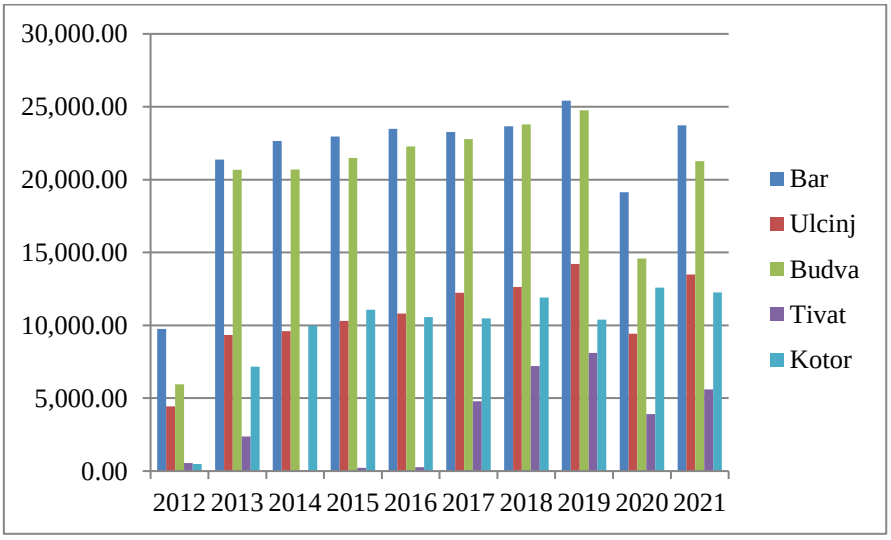

Na osnovu podataka iz tabele 6, ukupna količina otpada koja je odložena na deponiji „Možura“, za period 2012.-2021. godina, pet opština primorskog regiona iznosi 650.078,94 t. Najveća količina otpada je dovezena iz opštine Bar. Obzirom na to da opština Bar, u odnosu na druge opštine koje odlažu otpad na Možuri, ima najveći broj stanovnika, moglo se i očekivati da će proizvesti najveću količinu otpada.
Rezultati proizvedenih količina biogasa na deponiji „Možura“ za period 2012.-2021. godina prikazani su u tabeli 7.

Tabela 7. Prikaz količina proizvedenog biogasa na deponiji „Možura“ za period 2012.-2021. godina

Godina	Ukupan biogas		Metan		Ugljen-dioksid	
	m^3/god	m^3/h	m^3/god	m^3/h	m^3/god	m^3/h
2012	220.748	25,20	108.200	12,35	112.582	12,85
2013	437.259	49,92	214.300	24,46	223.002	25,46
2014	649.778	74,18	318.400	36,35	331.387	37,83
2015	858.559	98,01	420.700	48,03	437.865	49,98
2016	1.063.836	121,44	521.300	59,51	542.556	61,94
2017	1.265.842	144,50	620.300	70,81	645.580	73,70
2018	1.464.803	167,21	717.800	81,94	747.050	85,28
2019	1.660.934	189,60	813.900	92,91	847.076	96,70
2020	1.854.450	211,70	908.700	103,73	945.770	107,96
2021	2.045.550	233,51	1.002.000	114,38	1.043.231	119,09
Ukupno	**11.521.759**	**1.315,27**	**5.645.600**	**644,47**	**5.876.099**	**670,79**

Iz tabele 7 se vidi da se količine proizvedenog biogasa konstantno povećavaju iz godine u godinu, što dovodi do konstantnog povećanja metana i ugljen-dioksida. Kada se uporede vrijednosti iz 2012. godine i iz 2021. godine, vidi se da su proizvedene količine biogasa u 2021. godini skoro 10 puta veće u odnosu na 2012. godinu.
Na osnovu prikazanih vrijednosti u tabeli 7, na slici 3 grafički su prikazane količine proizvedenog biogasa za period 2012.-2021. godina.

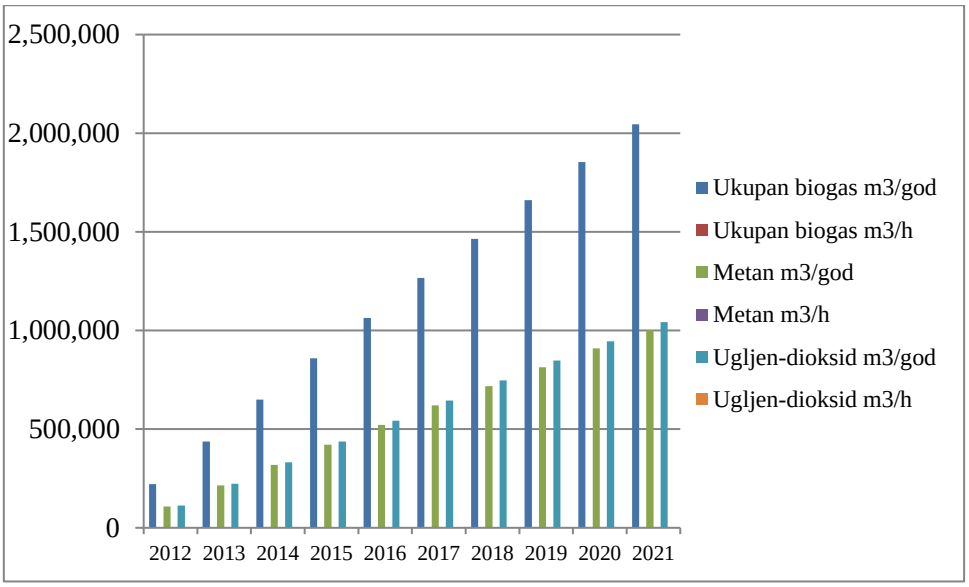

Sastav deponijskog biogasa praktično varira svakog minuta u toku cijele godine, ali se u prosjeku kreće u rasponu od 45-55% zapreminske koncentracije metana.Na osnovu svih mjerenja, kao i uvidom u dnevnik analizatora deponijskog biogasa na ekološkoj baklji, ova procjena je ispravna.
U tabeli 8 data je okvirna procijenjena efikasnost gasnog motora na deponijski biogas u zavisnosti od sastava biogasa, odnosno sadržaja metana.

Tabela 8. Efikasnost gasnih motora u zavisnosti od kvaliteta deponijskog biogasa

Promenljiva	**Jedinica**	**Očekivani min. sadržaj metana**		**Očekivani max. sadržaj metana**	
Sadržaj metana	%	45		55	
Ukupna energija (na osnovu niže vrijednosti sagorijevanja metana)	kWh/m^3	4,5		5,5	
Efikasnost motora na gas	%	33	36	33	36
Iskorišćenje struje	kWh/m^3	1,44	1,61	1,75	1,97

Efikasnost motora zavisi od kvaliteta biogasa, količine (između 60% i 100% zapremine motora na gas), uslova sagorijevanja i opreme za hlađenje. Klipni motori na gas za primjenu deponijskog biogasa se kreću od stehiometrijskog sagorijevanja (prirodno odsisavanje) do motora za slabije sagorijevanje (slabo sagorijevanje, turbo punjenje). Očekivano iskorišćenje struje iz motora na gas je u rasponu od 1,44 do 1,97 kWh/m^3. U kombinaciji sa prosječnim sadržajem metana od 50% očekuje se da iskorišćenje električne energije bude oko 1,75 kWh/m^3.
Samo dio metana koji se generiše na deponiji prikuplja se sistemom kaptacije i aspiracije. Ostatak se emituje u atmosferu ili se rastvara u ocjednim vodama. U tabeli 9 prikazan je izgubljen energetski potencijal koji je emitovan u atmosferu u periodu 2016.-2021. godina.

Tabela 9. Bilans deponijskog biogasa na lokaciji deponije „Možura“

Godina	**Kaptirano deponijskog gasa, Nm^3**	**Spaljeno deponijskog gasa, Nm^3**	**Izgubljena električna energija, kWh**
2016	288.000	288.000	544.320
2017	1.938.629	1.938.629	3.664.009
2018	1.869.528	1.869.528	3.533.408
2019	2.030.332	2.030.332	3.837.328
2020	2.827.851	2.827.851	5.344.638
2021	3.234.221	3.234.221	6.791.864
Ukupno	**12.188.561**	**12.188.561**	**23.715.567**

Sagorijevanje $1Nm^3$ deponijskog biogasa sa 50% metana (CH_4) daje 2,10 kWh električne energije, uz gubitke od 10%. Obračun je urađen u skladu sa srednjim očekivanim vrijednostima od 50% metana CH_4 u deponijskom biogasu, iako je taj sadržaj bio nešto niži prve dvije godine (prve dvije godine nisu imale više od 30% sadržaja metana u prosjeku, tako da nijesu mogle biti iskorišćene za proizvodnju električne energije).
Prema prethodnom, sagorijevanjem na eko baklji za 5 godina izgubljeno je oko 23.715.567 kWh. Na osnovu ovih podataka, za srednju vrijednost cijene električne energije od 5,5 centi/kWh i očekivane gubitke, od prodaje električne energije očekivani prihod bi bio u idealnom slučaju oko 1,25 miliona eura za isti period.

Zaključci

Na osnovu svih navedenih podataka koji se odnose na proizvodnju deponijskog biogasa i ispitivanje mogućnosti njegovog iskorišćenja na deponiji Možura u Baru, može se zaključiti sledeće:

1. Na lokaciji sanitarne deponije Možura proizvodi se deponijski biogas od 2012. godine, čija količina je konstantno rasla iz godine u godinu, pa kada se uporede količine deponijskog

biogasa iz 2012. godine sa količinama iz 2021. godine, vidi se da su proizvedene količine biogasa u 2021. godini skoro 10 puta veće u odnosu na 2012. godinu.

2. Mjerenja sastava deponijskog biogasa pokazuju da isti varira svakog minuta u toku cijele godine, ali da se u prosjeku zapreminska koncentracija metana kreće od 45-55%.
3. Kada se govori o iskorišćenju deponijskog biogasa za proizvodnju električne energije, može se zaključiti da se iksorišćenje struje iz motora na gas kreće u rapsonu od 1,44 – 1,97 kWh/m^3. Ako se uzme da je prosječni sadržaj metana 50%, onda se dobija da je iskorišćenje električne energije oko 1,75 kWh/m^3.
4. Prikazani bilans deponijskog gasa na lokaciji sanitarne deponije Možura za period od 2016.-2021. godine pokazuje ukupno izgubljenu električnu energiju na nivou od oko 23.715.567 kWh.
5. Generalno posmatrano, ako se uzme da je srednja vrijednost cijene električne energije 5,5 centi/kWh, uz očekivane gubitke, dobija se podatak da bi od prodaje električne energije očekivani prihod u idealnom slučaju bio oko 1,25 miliona eura za navedeni period.
6. Svi podaci i parametri koji se odnose na proizvodnju deponijskog biogasa na sanitarnoj deponiji Možura pokazuju neophodnost izgradnje odgovarajućeg kogeneratoskog postrojenja za proizvodnju električne energije.

Literatura

1. Pucar M, Nenković-Riznić M., Mogućnost primene solarne, geotermalne i energije iz komunalnog čvrstog otpada u Srbiji. Zlatibor: Energetika 2008, str. 114-120.
2. Directive 1999/31/EC on the landfill of waste. Off J Eur Union L. 1999;182:1-19.
3. Stevanovic-Carapina S. C. H., S. J. Stepanov, S. D. Savic, M. A. Mihajlov, Emisija toksicnih komponenti kao faktor izbora najbolje opcije za upravljanje otpadom primenom koncepta ocenjivanja životnog ciklusa, Hem. Ind. 65 (2) (2011) pp. 205-209.
4. Dudek D. J., K. P. Klimek, K. G. Kolodziejak, N. J. Niemczewska, J. Zaleska-Bartosz, Landfill gas energy technologies, Institut nafty i gazu, Kraków 2010.
5. Budisulistiorini B. S. H., Electricity generation from landfill gas, Jurnal Presipitasi (3) 2 September 2007, ISSN 1907-187X.
6. G. Anaokar, A. Khambete, R. Christian, Predicting Biogasification Potential of Urban Wastewater Using Multiparameter Aggregated Index of Influent, Engineering Environmental Progress & Sustainable Energy, 2019.
7. J. Kuo, Jason Dow, Biogas production from anaerobic digestion of food waste and relevant air quality implications, Engineering, Environmental Science Journal of the Air & Waste Management Association, 2017
8. D. Ugrinov, S. Komatina-Petrović, A. Stojanov, Mogućnosti eksploatacije deponijskog i biogasa kao obnovljivog izvora energije u Srbiji, Zaštita materijala 53 (2012) broj 4

Investigation of the Influence of Inorganic and Organic Inhibitors on the Corrosion Kinetics of AISI 304 Steel (1.4301) in Acidic and Neutral Solutions

Ispitivanje uticaja neorganskih i organskih inhibitora na kinetiku korozije čelika AISI 304 (1.4301) u kiselim i neutralnim rastvorima

J. Šćepanović*, B. Zindović, D. Radonjić, D. Vuksanović

University of Montenegro, Faculty of Metallurgy and Technology, Cetinjski put, 81000 Podgorica, Montenegro

**jelenapj@ucg.ac.me*

Abstract

Austenitic stainless steel is one of the materials most often used for construction and various branches of industry: chemical industry, metallurgy, etc., due to its good weldability, high temperature resistance and corrosion resistance. Corrosion resistance exists due to the rapid formation of a passive film caused by a layer of oxides of iron and chromium with hydroxide and water that instantly forms on steel and is studied by surface analysis. The corrosion resistance of austenitic stainless steels depends on their chemical composition and microstructure. Inhibitors are used to slow down or reduce the rate of corrosion. If some substance, which does not have a harmful effect on the environment, added in small quantities reduces or slows down the rate of corrosion and is also economical to use, it is considered an effective inhibitor.

The tests were performed at room temperature, using one inorganic and one organic inhibitor in two solutions, using the methods: potentiodynamic polarization and linear polarization.

Key words: *austenitic chrome-nickel steel; corrosion; inhibitor;, potentiodynamic polarization; linear polarization*

Izvod

Austenitni nerđajući čelik je jedan od materijala koji se najčešće koristi za primjenu u građevinarstvu i u raznim granama industrije: hemijska industrija, metalurgija itd., zbog dobre zavarljivosti, otpornosti na visoke temperature i otpornosti na koroziju. Otpornost na koroziju postoji zbog brzog formiranja pasivnog filma uzrokovanog slojem oksida željeza i hroma sa hidroksidom i vodom koji se trenutno formira na čeliku i proučavan je metodom površinske analize. Otpornost na koroziju austenitnih nerđajućih čelika zavisi od njihovog hemijskog sastava i mikrostrukture. Za usporavanje ili smanjenje brzine korozije primjenjuju se inhibitori. Ukoliko neka supstanca, koja nema štetnog uticaja na okruženje, dodata u malim količinama smanjuje ili usporava brzinu korozije i uz to je ekonomična za upotrebu smatra se efikasnim inhibitorom.

Ispitivanja su vršena na sobnoj temperaturi, upotrebom jednog neorganskog i jednog organskog inhibitora u dva rastvora, pomoću metoda: potenciodinamička polarizacija i linearna polarizacija.

Ključne riječi: *austenitni hrom-niklov čelik; korozija; inhibitor;, potenciodinamička polarizacija; linearna polarizacija*

Uvod

Zahvaljujući relativno niskoj cijeni, lakoj dostupnosti, dobroj čvrstoći i tvrdoći, kao i lakoj obradi, čelik zadovoljava sve uslove za industrijsku primjenu.

Korozija je jedan od problema današnjice koji je veoma zastupljen. Stalan izazov za inženjere svih struka predstavlja pitanje produženja vijeka trajanja opreme, tj. povećanje efikasnosti iste. Međutim gubici koji nastaju usled pojave korozije nijesu samo zamjena dijelova zahvaćenih korozijom, već

imaju za posledicu mnogo veće indirektne troškove (zastoji, onečišćenje proizvoda, trajno zagađenje okoline itd.) [1].
Čelik nije postojan u mnogim korozionim sredinama, pa se moraju primijeniti zaštitne mjere koje će omogućiti duži vijek trajanja čeličnih instalacija. Inhibitori u veoma malim koncentracijama smanjuju brzinu korozije na tehnološki prihvatljive vrijednosti, pa je njihova primjena sve veća, a pored toga su najčešće lako dostupni i jeftini. Inhibitori mogu biti organski i neorganski i mogu pružati različitu vrstu zaštite u zavisnosti od uslova sredine u kojima djeluju [2]. Nerđajući čelik je danas jedan od najčešće korišćenih materijala u svim granama industrije zahvaljujući svojim dobrim svojstvima. To je legirani materijal koji se sastoji od najmanje 10,5 % hroma i najviše 1,2 % ugljenika. Austenitni čelici primjenjuju se u vrlo različitim područjima, od nosivih konstrukcija i primjene u arhitekturi, preko kuhinjskih uređaja, do medicinske opreme. Široko područje primjene imaju ne samo zbog dobre korozione postojanosti, već i zbog dobre formabilnosti, zavarljivosti, izdržljivosti i dr. Neki austenitni čelici koji imaju visoki udio legiranih elemenata mogu izdržati visoke temperature i primjenjuju se do 1000°C. Najpoznatiji (osnovni) austenitni nerđajući čelik je AISI 304 ili 18/8. To je legura na bazi željeza koja sadrži nominalno 18% Cr i 8,5% Ni, uključujući manje količine C, N, Mn i Si [3].
Koroziona otpornost hrom-nikl čelika zasniva se na sadržaju određene količine hroma koji omogućava laku pasivizaciju metalne površine putem nastajanja adsorpcionih ili faznih oksidnih filmova trovalentnog hroma, odnosno preko dovođenja atoma gvožđa u pasivno stanje. Nerđajući hrom-nikl čelik, i pored svoje rezistentnosti, može da korodira pod određenim uslovima i na određeni način. Najčešći tipovi korozije kod nerđajućeg čelika, u rastvorima elektrolita su korozija u obliku pitinga, međukristalna korozija, kontaktna korozija i naponska korozija [4]. U zavisnosti od sredine dodaju se različiti inhibitori korozije kako bi se smanjila brzina kojom je sloj čelika oštećen. U kiselim sredinama inhibitori korozije poput organskih jedinjenja koja sadrze azot, sumpor i kiseonik i njihovi derivati su najefikasniji, jer se stvara sloj organskog filma na metalnoj površini. U neutralnim sredinama se najčešće koriste nitriti, hromati i permanganati. Izbor inhibitora zavisi od nekoliko faktora, pri čemu su tu uključeni i cijena, dostupnost i efekti na životnu sredinu [4].
Kroz radove su korišćena brojna organska jedinjenja, međutim primjena organskih inhibitora za inhibiciju korozije u obliku jame nerđajućih čelika je ograničena. Butan-1-ol (BTU) je primarni alkohol koji se prirodno javlja kao sporedni proizvod fermentacija šećera i drugih ugljenih hidrata. Butan-1-ol se najviše koristi kao industrijski intermedijar, posebno za proizvodnju butila [4].
Šifove baze, različitih struktura, su pronašle primjenu kao inhibitori korozije ovih čelika [5], [6] pri čemu su sintetisane hemijske strukture koje su korišćene u radu prvi put ispitivane.
Anodni inhibitori korozije su najčešće nitrati i nitriti kao oksidaciona sredstva, onda neorganski joni: hromatni, permanganatni, molibdatni, fosfatni, joni metala sa većim oksidacionim brojem: Cu^{+2}, Fe^{+3}, a u nekim situacijama vodonik-peroksid i kiseonik. Iako su redoks potencijali nitrata i nitrita bliskih vrijednosti, nitriti se pokazuju kao više efikasni inhibitori čelika. Objašnjenje za ovo je veća prenapetost pri redukciji nitrata u odnosu na nitrite, prvenstveno u neutralnim rastvorima. Sposobnost inhibitora da pasiviraju metal i utiču na proces korozije zavisi od veličine gustine struje izmjene. Ako je gustina struje izmjene veća, prenapetost elektrodnih reakcija je mala i obrnuto. [7]
Kalijum-permanganat je jedan od inhibitora koji se obično koristi kao „zeleni" inhibitor korozije [8]. Iz ekonomskih razloga je vrlo važno da inhibitori djeluju već u niskim koncentracijama. Obično se traži da ηi bude 80-90 %, što odgovara faktoru usporenja između 5 i 50, tj. inhibitor toliko puta usporava proces korozije. Efikasnost inhibitora korozije zavisi od mnogih faktora među kojima treba pomenuti: vrstu metala, metalne površine, sastav i koncentraciju korozione sredine, njenu pH-vrijednost i temperature, kao i vrstu i koncentraciju inhibitora. Većina inhibitora su specifični prilikom djelovanja na određeni metal. Inhibitor koji je efikasan za određenu vrstu metala može da ne djeluje na drugu vrstu metala ili čak može imati i negativan uticaj [9].
Korozijom čelika su se bavili razni istraživači. Tako je u radu [10] korozija čelika AISI 304 ispitivana u hloridnoj kiselini uz dodatak inhibitora kao što su derivati triazola, bilo da je korišćen sam ili u

kombinaciji sa heksametilen-tetraaminom (urotropinom), pri čemu su korišćene metode gubitka mase, potenciometrijske i polarizacione metode.
Uticaj koncentracije adenina na koroziju AISI 304 čelika proučavana je u rastvoru hloridne kiseline. Na osnovu Tafelove ekstrapolacije uočeno je da je adenin djelovao kao inhibitor mješovitog tipa, a takođe je efikasnost inhibicije povećana sa porastom koncentracije adenina. Utvrđeno je da se adsorpcija adenina događa na površini čelika prema Langmirovoj izotermi. I efekat inhibicije korozije raste sa porastom temperature za istu koncentraciju adenina. U 1,1M rastvoru hlorida, bez prisustva inhibitora Ecorr iznosi -396mV, a jcorr 0,046 mA/cm^2. Dodatkom 0,5 mM inhibitora Ecorr iznosi -382mV, a jcorr 0,024, efikasnost inhibitora je 48% [13].
Ovaj čelik su ispitivali naučnici u 0,1 M hloridnoj kiselini uz prisustvo kalijum hromata i natrijum-molibdata kao inhibitora. Hromat i molibdat utiču na nukleaciju jame deaktiviranjem mjesta na kojima se javljaju i smanjenjem njihove veličine. Niža gustina pasivne struje koju pokazuju čelici u prisustvu inhibitora u poređenju sa čistim HCl ukazuje na to da je pasivnost stabilnija u prisustvu inhibitora. Metoda koja je korišćena je potenciodinamička polarizacija [16].

Eksperimentalni dio

Eksperimentalni dio rada je urađen u laboratorijama Metalurško-tehnološkog fakulteta u Podgorici i Institutu za crnu metalurgiju, Nikšić.
Čelik ispitivan u ovom radu dobijen je u laboratoriji Instituta za crnu metalurgiju u Nikšiću.
Pripremljena šarža je topljena u indukcionoj peći, kapaciteta 120 kg. Proces topljenja sa naknadnim legiranjem trajao je oko 150 minuta. Nakon provjere hemijskog sastava na kvantometru, izvršeno je livenje u prethodno pripremljene kalupe. Dobijeni hemijski sastav čelika dat je u tabeli 1.

Tabela 1. Hemijski sastav dobijenog čelika AISI 304

Hemijski sastav (%)									
C	**Si**	**Mn**	**P**	**S**	**Cr**	**Ni**	**Al**	**Cu**	**Mo**
0,05	1,67	0,83	0,015	0,005	17,03	11,53	0,06	0,11	0,12

Za koroziona ispitivanja pripremljeni su uzorci prečnika 15 mm i debljine 5 mm, koji su korišćeni kao radna elektroda.
Za koroziona ispitivanja pripremljeni su radni rastvori i inhibitori određenih koncentracija. Ispitivanje korozionog ponašanja čelika AISI 304 urađeno je u rastvorima hloridne i nitratne kiseline, koncentracije 0,1 mol/dm^3 i u neutralnom rastvoru natrijum-hlorida. U istim rastvorima je ispitivano i dejstvo inhibitora. Za svaki eksperiment je korišćen svježe napravljen rastvor. Rastvori su pripremljeni na sledeći način:

1. 0,1 M HCl, dobijena razblaživanjem koncentrovane 35% HCl, gustine 1,175 g/cm^3, molarne mase 36,5 g/mol u destilovanoj vodi.
2. 0,1 M HNO_3 , dobijena razblaživanjem koncentrovane 65% HNO_3, gustine 1,4 g/cm^3, molarne mase 63 g/mol u destilovanoj vodi.

Koncentracija inhibitora koja je korišćena jeste 10^{-4} mol/dm^3. I svi su dobijeni rastvaranjem odvagane količine čvrstih supstanci p.a čistoće u destilovanoj vodi. Šifove baze nijesu rastvorne u destilovanoj vodi, pa su njihovi rastvori pravljeni u 96%-nom etanolu.
Inhibitori korišćeni u ovom radu su: $KMnO_4$ i Šifova baza, MK3: (2E)-N'-[(1E)-1-(2-hidroksifenil)etiliden]-2-[1-(2-hidroksifenil)etiliden] hidrazin-1-tiokarbohidrazid.
Dobijeni čelik je prvo elektrohemijskim metodama ispitivanja (potenciodinamika i linearna polarizacija) bio izloženi u rastvorima bez prisustva inhibitora, a kasnije je rađeno ispitivanje u prisustvu izabranih inhibitora.

Metode ispitivanja

Elektrohemijske metode

Elektrohemijske metode se zasnivaju na primjeni jednosmjerne struje ili naizmjenične struje (ili potencijala) na korozioni sistem i mjerenju odziva sistema. Pri elektrohemijskim ispitivanjima procesa korozije primjenom jednosmjerne struje (DC) koriste se polarizacione metode pri kojima se kontroliše ili struja (galvanostatska polarizacija) ili potencijal (potenciostatska polarizacija). Za određivanje brzine korozije u slučaju primjene jednosmjerne struje koristi se metoda ekstrapolacije Tafelovih pravih i metoda mjerenja polarizacionog otpora. Sve elektrohemijske metode su indirektne metode za određivanje brzine korozije metala. Elektrohemijska mjerenja izvode se u troelektrodnoj elektrohemijskoj ćeliji koja sadrži radnu, pomoćnu i referentnu elektrodu. Radnu elektrodu predstavlja ispitivani metal, pomoćnu platinska žica ili pločica, a u odnosu na referentnu elektrodu definiše se potencijal radne elektrode [17].

Potenciostatska polarizacija

Iz Faradejevog zakona proizilazi da je brzina elektrohemijske reakcije proporcionalna gustini struje koja protiče na granici faza elektroda-elektrolit. Stoga, mjerenjem gustine struje u funkciji potencijala mogu se dobiti informacije o kinetici elektrohemijskog procesa. Funkcionalna zavisnost između gustine struje i potencijala predstavlja se polarizacionim krivima. Eksperimentalno određivanje polarizacionih krivih kod potenciostatske polarizacije zasniva se na saopštavanju određene, konstantne vrijednosti potencijala radnoj elektrodi i mjerenju neto struje između radne i pomoćne elektrode [18].

Aparatura korišćena za koroziona ispitivanja

Elektrohemijska mjerenja vršena su pomoću stacionarne radne elektrode, od uzorka čelika u troelektrodnoj termički kontrolisanoj ćeliji (slika 1). Za sva mjerenja kao pomoćna elektroda korišćene su dvije visoko zasićene grafitne elektrode postavljene jedna nasuprot druge te nasuprot radnoj elektrodi da bi se postiglo simetrično električno polje. Kao referentna elektroda korišćena je zasićena kalomel elektroda koja je u kontaktu s radnom elektrodom bila preko Luggin kapilare, pa se na nju odnose sve vrijednosti potencijala prikazane u ovom radu. Prije svakog mjerenja čelična elektroda je očišćena šmirgl papirom (granulacije P600). Potom je čelična elektroda postavljena u rastvor, zajedno sa pomoćnom i referentnom i mjerena je linearna polarizacija i potenciodinamika. Princeton Applied Research, tip: Potentiostat/Galvanostat Model 273 služi za prenos podataka sa računara, preko diferencijalnog elektrometra na ćeliju. Dobijeni podaci se zatim vraćaju iz ćelije na računar. Ćelija je staklena posuda, u kojoj su smještene pomoćne elektrode, standardna kalomel elektroda i radna elektroda sa uzorkom (slika 2). Površina radne elektrode, u kojoj se nalazi uzorak iznosi 1 cm^2, pa vrijednosti jačine struje predstavljaju gustinu struje korozije. Ispitivanja su urađena na sobnoj temperaturi, bez uvođenja azota, vodonika ili kiseonika u rastvore, tako da dobijeni rezultati odgovaraju realnim sistemima.

Slika 1. *Ćelija sa troelektrodnim sistemom*

Slika 2. *Detaljniji prikaz elektrohemijske ćelije*

Rezultati i diskusija

Metoda linearne polarizacije

Za sve ispitane materijale proveden je postupak linearne polarizacije odnosno polarizacija ±20 mV u odnosu na korozioni potencijal E_{corr} uz zadatu promjenu brzine potencijala od 0,1 mV/s [21]. Rezultati korozionih ispitivanja metodom linearne polarizacije za uzorak čelika AISI 304 u tabelama 2 i 3 i na slikama 3 i 4.

Tabela 2. Čelik AISI 304, rastvor 0,1 M HCl

Inhibitor	e(j=0) [mV]	Rp [kΩ]	j_{corr} [μA/cm^2]
Bez inhibitora	-220,3	6,67	3,254
$KMnO_4$	-188,6	12,40	1,751
MK3	-99,90	20,40	1,064

Tabela 3. Čelik AISI 304, rastvor 0,1 M HNO_3

Inhibitor	e(j=0) [mV]	Rp [kΩ]	j_{corr} [μA/cm^2]
Bez inhibitora	-324	6,119	8,878
$KMnO_4$	-67,35	16,48	1,317
MK3	50,04	48,08	0,4516

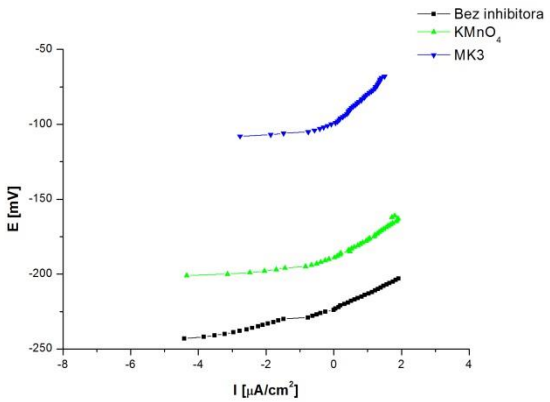

Slika 3. *Čelik AISI 304, rastvor 0,1 M HCl linearna polarizacija*

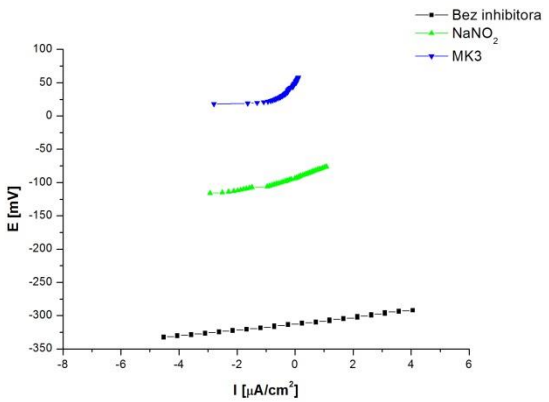

Slika 4. *Čelik AISI 304, rastvor 0,1 M HNO_3 linearna polarizacija*

Neorganski inhibitor u 0,1 M rastvoru HCl pokazuje dobre rezultate, a MK3 jedinjenje, čija se aktivnost prvi put ispituje pokazuje bolje dejstvo (slika 3). Bez prisustva inhibitora gustina struje korozije je bila j_{corr}= 3,254 μA/cm^2, a prisustvo neorganskog inhibitora $KMnO_4$ smanjuje tu vrijednost na j_{corr}=1,751 μA/cm^2, dok je u prisustvu Šifove baze MK3 j_{corr}=1,064 μA/cm^2. Na sličan način se ovaj čelik ponaša i kada je potencijal korozije u pitanju. Naime, iz tabele 2 i slike 3 se može vidjeti da bez prisustva inhibitora potencijal korozije e(j=0) iznosi -220,3 mV, dok se u prisustvu neorganskog inhibitora $KMnO_4$ pomjera prema pozitivnijim vrijednostima i iznosi -188,6 mV. U prisustvu Šifove baze MK3 kao inhibitora korozije, potencijal korozije se još više pomjera prema pozitivnijoj vrijednosti u odnosu na neorganski inhibitor i iznosi -99,90 mV. Na osnovu ovoga može se konstatovati da korišćenjem neorganskog inhibitora korozioni potencijal se pomjera prema pozitivnijim vrijednostima, a MK3 jedinjenje, čija se upotreba kao inhibitora prvi put ispituje pokazuje bolje dejstvo.

Kod ove metode, ispitivanje čelika AISI 304 u rastvoru 0,1 M HNO_3, bez prisustva inhibitora gustina struje iznosi j_{corr}=8,878 μA/cm^2, dodatkom neorganskog inhibitora $KMnO_4$ se smanjuje na j_{corr}=1,317 μA/cm^2, pri čemu je najveća razlika u prisustvu MK3 gdje vrijednost korozione gustine struje iznosi j_{corr}=0,4516 μA/cm^2.

Potenciodinamička polarizacija

Rezultati korozionih ispitivanja metodom potenciodinamičke polarizacije za čelik AISI 304 prikazani su u tabelama 4 i 5 i na slikama 5 i 6.

Tabela 4. Čelik AISI 304, rastvor 0,1 M HCl

Inhibitor	OCP [mV]	e(j=0) [mV]	b_a [mV/dec]	b_k [mV/dec]	j_{corr} [μA/cm^2]
Bez inhibitora	-174	-166,1	1002	371,6	8,426
$KMnO_4$	-119	-148,1	169,1	166,0	1,770
MK3	-96	-179,4	136,6	79,99	0,7476

Tabela 5. Čelik AISI 304, rastvor 0,1 M HNO_3

Inhibitor	OCP [mV]	e(j=0) [mV]	b_a [mV/dec]	b_k [mV/dec]	j_{corr} [μA/cm^2]
Bez inhibitora	-342	- 324	412	186	8,878
$KMnO_4$	-20	- 72,60	320,7	150,5	1,683
MK3	-81	- 26,78	263,0	124,7	0,3904

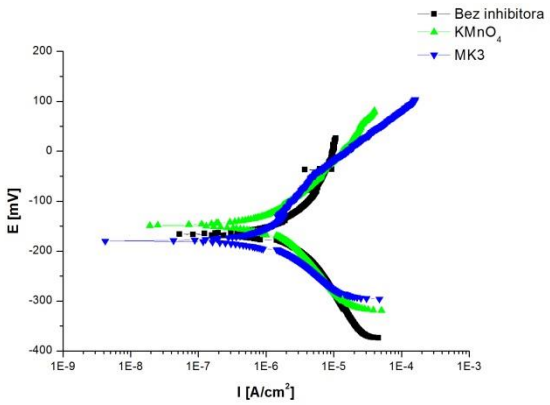

Slika 5. *Čelik AISI 304, rastvor HCl potenciodinamička polarizacija*

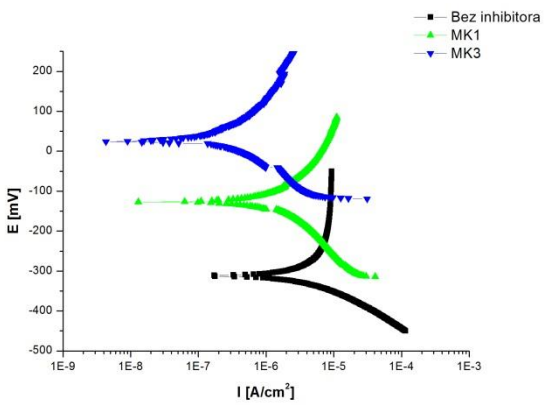

Slika 6. *Čelik AISI 304, rastvor HNO_3 potenciodinamička polarizacija*

Rezultati iz tabele 4 grafički su prikazani na slici 5. Iz tabele 4 se vidi da se korozioni potencijal u prisustvu inhibitora $KMnO_4$ pomjera prema pozitivnijim vrijednostima, dok se u prisustvu Šifove baze MK3, neznatno pomjera prema negativnijim vrijednostima. Vrijednost gustine struje u 0,1 M rastvoru HCl bez prisustva inhibitora iznosi j_{corr}= 8,426 μA. Dodatkom inhibitora struja korozije opada, i kreće se od j_{corr}=1,770 μA/cm^2 korišćenjem inhibitora $KMnO_4$**,** pa do Šifove baze MK3 gdje je j_{corr}=0,7476 μA/cm^2.
Rezultati ispitivanja čelika AISI304 u 0,1 M rastvoru HNO_3 prikazani su u tabeli 5 i grafički prikazani na slici 6. Dobijeni rezultati pokazuju da se potencijal korozije značajno pomjera prema pozitivnijim vrijednostima u prisustvu neorganskog i organskog inhibitora, pri čemu organski inhibitor (Šifova baza) značajnije pomjera potencijal korozije prema pozitivnijoj vrijednosti, koji iznosi -26,78 mV. Što se struje korozije tiče ona dodatkom inhibitora opada i kreće se od j_{corr}=1,683 μA/cm^2 korišćenjem inhibitora $KMnO_4$**,** dok je korišćenjem Šifove baze MK3, j_{corr}=0,3904 μA/cm^2.

Efikasnost zaštite

Efikasnost zaštite na osnovu podataka iz prethodnih tabela izračunava se po jednačini:

$$\eta = \frac{j_{corr} - (j_{corr})_{inh}}{j_{corr}}$$

gdje je j_{corr} gustina struje korozije u neinhibiranom, a $(j_{corr})_{inh}$ u inhibiranom rastvoru.

Linearna polarizacija

Pomoću gore navedene jednačine i podataka iz tabela 2 i 3 za uzorak čelika AISI 304, izračunata je efikasnost zaštite u procentima i rezultati su prikazani u tabelama 6 i 7.

Tabela 6. Efikasnost zaštite za uzorak čelika AISI 304, rastvor 0,1 M HCl

Inhibitor	**j_{corr} [μA/cm^2]**	**η [%]**
Bez inhibitora	3,254	-
$KMnO_4$	1,751	46,2
MK3	1,064	67,3

Tabela 7. Efikasnost zaštite za uzorak čelika AISI 304, rastvor 0,1 M HNO_3

Inhibitor	**j_{corr} [μA/cm^2]**	**η [%]**
Bez inhibitora	8,878	-
$KMnO_4$	1,317	85,2
MK3	0,4516	94,9

Pored mnogih primjena Šifovih baza jedna od interesantnijih je njihova upotreba kao efektivni inhibitori korozije, koja se bazira na njihovoj sposobnosti da spontano formiraju monosloj na površini koji štiti. Mnoga organska jedinjenja su proučavana u cilju dobijanja pogodnog rješenja za zaštitu od korozije. Neki komercijalni inhibitori sadrže aldehide ili amine u svojoj strukturi, ali zbog C=N veze Šifove baze mnogo efikasnije funkcionišu u većini slučajeva. Glavna interakcija između inhibitora i metalne površine je hemisorpcija. Molekul inhibitora treba da ima centre sposobne za formiranje veze sa metalnom površinom prenosom elektrona. U takvim slučajevima metal djeluje kao elektrofil i inhibitor djeluje kao Luisova baza. Nukleofilni centri, kao što su kiseonik i atomi azota zaštitnog jedinjenja imaju slobodne elektronske parove koji su lako dostupni za dijeljenje. Zajedno sa atomima benzenovog prstena stvaraju višestruku apsorpciju mjesta za inhibitor čime se omogućava stabilno formiranje monosloja. [9]

Ovim dobijenim rezultatima se potvrdilo ovo što je gore navedeno, jer Šifova baza MK3 pokazuje efikasnost u većini eksperimenata u radu pri čemu za uzorak AISI 304 iznosi 67,3 % u HCl, a 94,9 % u HNO_3.
Inhibitori korozije su jedinjenja koja se adsorbuju na površini metala pomoću Kulonovih, Van der Valsovih ili valentnih sila. Moguća je adsorbcija na površini metala pri istovremenom djelovanju više vrsta sila. Izbor inhibitora u velikoj mjeri zavisi od rastvora u kojima se primjenjuju. Praktična ispitivanja su pokazala da jedan inhibitor u istoj kiselini rijetko štiti različite materijale. Tako npr. tiourea je jedan od boljih inhibitora za željezo u sulfatnoj i fosfatnoj kiselini, dok je za aluminijum u fosfatnoj kiselini ova supstanca potpuno nepodesna, što su pokazala praktična ispitivanja, iako se u literaturi navodi kao jedna od mogućnosti. Ovaj primjer pokazuje da literaturne podatke treba kritički posmatrati i prije uvođenja u pogon ispitati. [28]
Nitratna kiselina kao medijum se pokazala kao veoma pogodna kod uzorka čelika AISI 304, što se može pripisati hemijskom sastavu samog uzorka.
Na slici 7 dat je uporedni histogram efikasnosti zaštite za uzorak čelika AISI 304 u svim ispitivanim rastvorima i za oba korišćena inhibitora.

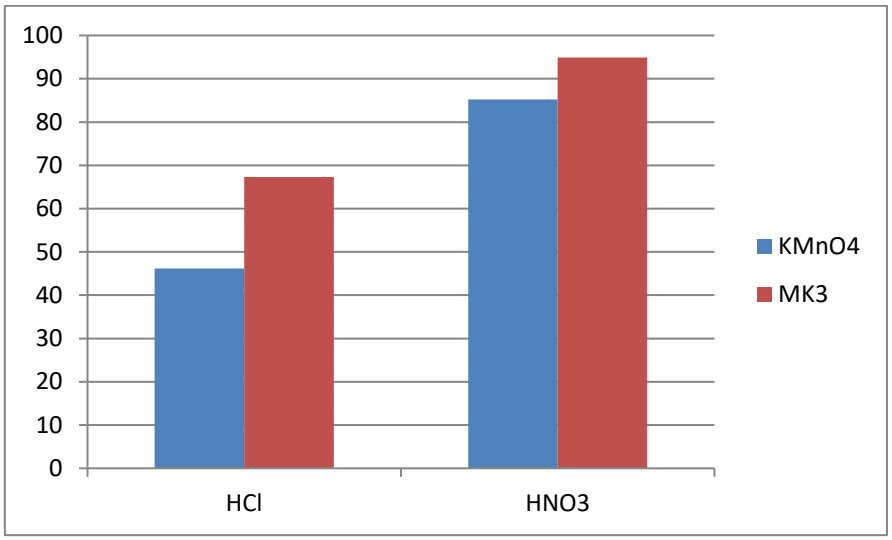

Slika 7. *Histogram efikasnost zaštite za uzorak čelika AISI 304*

Potenciodinamička metoda

Pomoću gore navedene jednačine za efikasnost i podataka iz tabela 4 i 5 za uzorak čelika AISI 304, izračunata je efikasnost zaštite u procentima i rezultati su prikazani u tabelama 8 i 9.

Tabela 8. Efikasnost zaštite čelika AISI 304, rastvor 0,1 M HCl

Inhibitor	**j_{corr} [µA/cm^2]**	**Ƞ [%]**
Bez inhibitora	8,426	-
$KMnO_4$	1,770	78,9
MK3	0,7476	91,1

Tabela 9. Efikasnost zaštite čelika AISI 304, rastvor 0,1 M HNO_3

Inhibitor	**j_{corr} [µA/cm^2]**	**Ƞ [%]**
Bez inhibitora	8,878	-
$KMnO_4$	1,683	81,1
MK3	0,3904	95,6

Uzorak čelika AISI 304 pokazuje dobre rezultate u oba ispitivana rastvora. U rastvoru hloridne kiseline efikasnosti zaštite u procentima su jako dobre (tabela 8).

Uzorak čelika AISI 304 pokazuje dobre rezultate u oba ispitivana rastvora. U rastvoru hloridne kiseline efikasnosti zaštite u procentima su jako dobre (tabela 8).
Koncentracija inhibitora kao i sastav korozione sredine utiču na efikasnost zaštitnog dejstva anodnog inhibitora. Prisustvo halogenidnih jona, u prvom redu hlorida, kao i povećanje aktivnosti vodoničnih jona otežavaju prevođenje metala u pasivno stanje. Sa povećanjem agresivnosti sredine povećava se gustina struje pasiviranja, pa je koncentracija anodnog inhibitora, neophodna za pasiviranje metala veća, a u nekim slučajevima nije moguće prevesti metal u pasivno stanje [6].
Iako hromati obično pokazuju dobre performanse i laki su za upotrebu, podvrgnuti su ozbiljnoj kontroli zbog njihove toksičnosti i kancerogene prirode.
Uzorak čelika AISI 304 u rastvoru nitratne kiseline pokazuje dobre rezultate i za neorganski i za organski inhibitor (tabela 9).
Na slici 8 dat je histogram efikasnosti zaštite uzorka čelika AISI 304 u oba ispitivana rastvora i u prisustvu oba inhibitora, za metodu potenciodinamike.

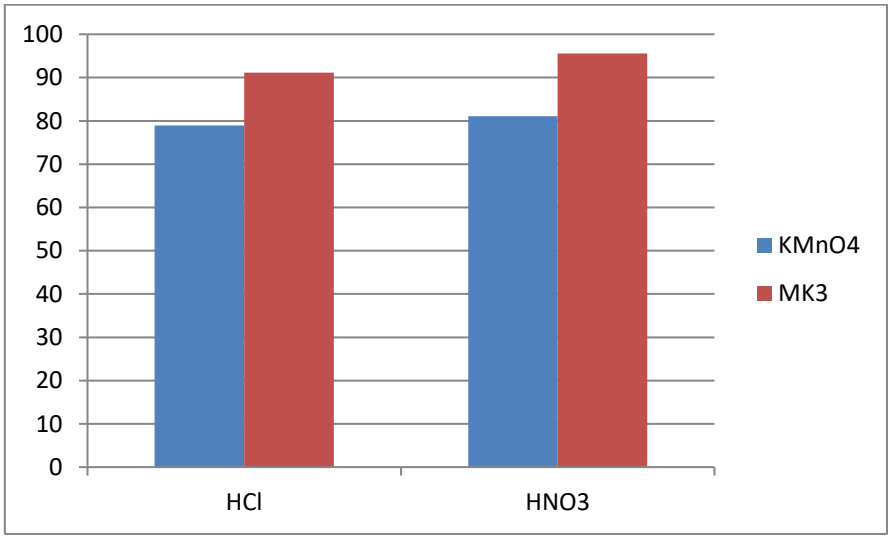

Slika 8. *Histogram efikasnost zaštite uzorak čelika AISI 304*

Ispitivani inhibitori su pokazali efikasnost u rastvoru 0,1 M HCl i u rastvoru 0,1 M HNO_3 kod linearne i kod potenciodinamičke polarizacije.

Zaključci

Na osnovu svih sprovedenih istraživanja u eksperimentalnom radu mogu se izvesti sledeći zaključci:

1. Za metodu linearne polarizacije najveću efikasnost zaštite čelika AISI 304 pokazuje Šifova baza MK3 u 0,1 M rastvoru HNO_3 čija vrijednost je 94,9%, čime su potvrđena prethodna istraživanja da je Šifova baza MK3 pogodan inhibitor u ovom rastvoru, dok u prisustvu hloridnih jona ima ograničen uticaj i nižu efikasnost inhibicije.
2. Uzorak čelika AISI 304 u rastvoru nitratne kiseline pokazao je efikasnost u prisustvu oba inhibitora, tako da se može zaključiti da je kod metode linearne polarizacije nitratna kiselina pogodniji medijum za ispitivanje.
3. Što se tiče metode potenciodinamičke polarizacije najveću efikasnost za uzorak čelika AISI 304 pokazuje inhibitor Šifova baza MK3 i efikasnost iznosi 95,6 % u nitratnoj kiselini.
4. Generalno posmatrano, isto kao i kod linearne polarizacije i kod potenciodinamičke metode nitratna kiselina je pogodniji medijum. Ovim se i potvrdilo da nerđajući čelici u prisustvu

halogenidnih jona, prije svega hloridnih prije podliježu koroziji i potrebna je veća koncentracija inhibitora za pasiviranje metala.

5. Šifova baza pokazuje veoma dobre rezultate u svim rastvorima, razlog tome je njihova hemijska struktura (C=N veza) i mogućnost obrazovanja zaštitnog monosloja na površini čelika. Promjene u funkcionalnosti grupe na terminalnom aromatičnom prstenu dovode do promjena efikasnosti inhibicije odgovarajućih Šifovih baznih jedinjenja. S obzirom da sintetisane Šifove baze nijesu ranije korišćene kao inhibitori, ovim eksperimentalnim radom se pokazuje da mogu imati i tu primjenu, pa se ostavlja prostor za dalji rad i ispitivanje na uzorcima različitih materijala i hemijskog sastava.

Literatura

1. Stupnišek - Lisac, Ema: *Korozija i zaštita konstrukcijskih materijala*. Zagreb, Fakultet kemijskog inženjerstva i tehnologije, 2007.
2. Uhlig, Herbert H.; Revie,R. W.: *Corrosion and Corrosion Control*. University of Michigan, New York, 1985.
3. Mario Barišić: *Svojstva nehrđajućih čelika, završni rad*, Veleučilište u Karlovcu, Strojarski odjel, Karlovac, 2015.
4. Avesta Sheffield, *Corrosion Handbook for Stainless Steels*, Avesta Sheffield AB, Švedska, 1994.
5. Roland T. LOTO: *Inhibition Effect of Butan-1-Ol on the Pitting Corrosion of Austenitic Stainless Steel (Type 304)*, Gazi University Journal of Science, 29 (1): 19-25 (2016)
6. Časlav M. Lačnjevac , Srba Nešić, *Katodna zaštita opreme termoenergetskih postrojenja od korozije*, stručni rad, 2007.
7. Michael Crouse, Albert E.Miller, M.G. Pujar, Kunigahalli L. Vasanth, *Evaluation of Potassium Permanganate ($KMnO_4$) as a Green Corrosion Inhibitor/Sealant for Anodized Al 2024 and Al 6061 at different pH values*, CORROSION 2002, Denver, Colorado, April 2002.
8. Roberge, P.R..; *Handbook of corrosion engineering*, New York, McGraw-Hill, Inc., 1999.
9. M. Talebian, K. Raeissi, M. Atapour, B. M. Fernandez-Perez, A. Betancor-Abreu, I. Llorente, S. Fajardo, Z. Salarvand, S. Meghdadi, M.Amirnasr, R. M. Souto: *Pitting corrosion inhibition of 304 stainless steel in NaCl solution by three newly synthesized carboxylic Schiff bases*, Corrosion Science 160, 108130 (2019)
10. Mouayed Y. Kadhum, Synthesis, *Identification and Study of Some New Schiff Bases as Inhibitors for Brass Corrosion and Bacterial Growth*, Journal of Basrah Researches (Sciences) , Volume 37.Number 2, 15 April (2011)
11. Ya. G. Avdeev, D. S. Kuznetsov, M. V. Tyurina, A. Yu. Luchkin, M. A. Chekulaev: *Protection of chromium-nickel steel in hydrochloric acid solution by a substituted triazole*, Int. J. Corros. Scale Inhib. no. 1, 1-4, (2015)
12. Thiago F. Soares, Roberta R. Moreira, Adalgisa R. De Andrade, Josimar Ribeiro: *Corrosion Behavior of AISI 304 and AISI 430 Stainless Steels in Presence of Benzimidazole Inhibitor*, International Journal of Engineering Innovation & Research, Volume 4, Issue 2, ISSN: 2277-5668 (2015)
13. Mieczyslaw Scendo, Joanna Trela: *Adenine as an Effective Corrosion Inhibitor for Stainless Steel in Chloride Solution*, Int. J.Electrochem.Sci. 8, 9201-9221, (2013)
14. Bore V. Jegdić, Biljana M. Bobić: *Ispitivanje piting korozije nerđajućeg čelika AISI 304 u rastvorima hlorida*, Zavarivanje i zavarene konstrukcije, 2015.
15. Killang Pratama, Zulfiadi Zulhan: *Study of Inhibiton Mechanism of Sodium Nitrite and Sodium Tungstate Inhibitors to Improve Corrosion Resistance of Sensitized AISI 304 in Chloride Containing Solution by EIS Method*, 2014.
16. G.O. Ilevbare, G.T. Burstein: *The inhibition of pitting corrosion of stainless steels by chromate and molybdate ions*, Corrosion Science 45 (2003) 1545–1569
17. Dolinar Andreja: *Zaštita od korozije u ljevaonici, završni rad, Veleučilište u Karlovcu*, Karlovac, 2021.
18. A. Lasia, *Electrochemical Impedance Spectroscopy and its Applications*, Springer, New York, 2014
19. Petra Kostanjevečki: *Razvoj nove, netoksične tehnike modifikacije površine čelika s ciljem poboljšanja korozijske stabilnosti u morskom okolišu*, Sveučilište u Zagrebu, Fakultet kemijskog inženjerstva i tehnologije, Zagreb, 2016.

20. Bojana Knežević, *Kinetika i termodinamika procesa korozije čelika u rastvoru NaCl u prisustvu pčelinjih proizvoda kao ekološki prihvatljivih inhibitora*, magistarski rad, Metalurško-tehnološki fakultet, Univerzitet Crne Gore, Podgorica, 2017.
21. Krešimir Mandić, *Utjecaj klorida na korozijsku postojanost nehrđajucih čelika u vodi*, diplomski rad, Sveučilište u Zagrebu, Fakultet strojarstva i brodogradnje, Zagreb, 2018.
22. Susanto, L.B., *Study of $NaNO_2$ Inhibitor Work to Protect Sensitized AISI 304 stainless steelfrom IGSCC Attack in Acidic Chloride Solution*, Thesis of ITB, 1998
23. Borislav Malinović, Tijana Djuričić, Duško Zorić, *Corrosion behaviour of stainless steel EN 1.4301 in acid media in presence of PBTCA inhibitor*, Zaštita Materijala 61 (2) 133 - 139 (2020)
24. Kvrgić Dario, *Usporedba korozijskog ponašanja AISI 304, AISI 316L i duplex čelika u otopini klorida*, završni rad, Sveučilište u Splitu, Kemijsko-tehnološki fakultet, Split, 2018
25. Tatjana Gazivoda Kraljević, *Određivanje struktura organskih spojeva, nastavni tekst*, Sveučilište u Zagrebu, Fakultet kemijskog inženjerstva i tehnologije, Zavod za organsku kemiju. 2018
26. Fernando B. Mainier, Pedro Ivo F. S. Pegoraro, Marcus Vinicius Santoro, *Propargyl alcohol as a corrosion inhibitor for AISI 304L stainless steel in hydrochloric acid*, International Journal of Advanced Engineering Research and Science (IJAERS) [Vol-5, Issue-10, Oct- 2018.]
27. Parinya Boonsa and Aphichart Rodchanarowan, *Virtual corrosion testing on stainless steel AISI 304 welded pipe with Hydroxyethyl Cellulose in 3.5% NaCl solution and turbulent flow*, Mater. Res. Express 7 (2020) 066519
28. Zoran Janković, Bosiljka Ljubičić, Saša Mićin, *Uloga i mehanizam dejstva inhibitora u rastvorima za nagrizanje čelika*, Zastita materijala 56 (4), 522-526 (2015)
29. Maan Hayyan, Shatha A. Sameh, Adeeb Hayyan , Inas M. AlNashef, *Utilizing of Sodium Nitrite as Inhibitor for Protection of Carbon Steel in Salt Solution*, Int. J. Electrochem. Sci., 7 (2012) 6941 – 6950

Influence of Temperature on Hard-Chrome Coatings Properties

Danijel Milošević[1], Stana Stanišić[2*], Regina Fuchs – Godec[3], Marija Mitrović[1], Snježana Vučićević[1], Zorica Ristić[2], Milorad Tomić[1]

[1]*University of East Sarajevo, Faculty of Technology, Karakaj 34A, 75400 Zvornik, Republic of Srpska*

[2]*Orao Company, Šabačkih đaka bb, 76300 Bijeljina, Republic of Srpska*

[3]*University of Maribor, Faculty of Chemistry and Chemical Engineering, Smetanova ulica 17, 2000 Maribor, Slovenia*

**stana.stanisic@orao.aero*

Abstract

Hard – chrome coatings were deposited in industry and laboratory conditions, and the obtained coatings properties were examined and compared. The influence of temperature on current efficiency, coatings thickness, roughness and morphology was examined. Also, the adhesion and hardness of the coatings were determined. Hard – chrome coatings were electrochemically deposited on steel plates, which chemical composition was determined by XRF method (X-MET 8000 device). Coatings were deposited on prepared steel plates from three plating baths. The first bath was commonly used industrial bath for chrome deposition in Orao company, composited of 250 g/dm^3 CrO_3 + 2.5 g/dm^3 H_2SO_4. The laboratory glass cell (volume 0.5 dm^3) was used for other two plating solutions. The second plating solution was same as one used in industrial conditions (250 g/dm^3 CrO_3 + 2.5 g/dm^3 H_2SO_4), and third plating solution was composed of 500 g/dm^3 CrO_3 + 5 g/dm^3 H_2SO_4. The deposition time and current density was same for all the coatings, 30 minutes and 50 A/dm^2, respectively. Three different temperature of plating solution was used and examined: 45, 50 and 55^{0}C. Coatings roughness was determined by Mitutoyo device, coatings thickness was determined by PosiTector device, the hardness was determined by Vickers method, and adhesion was examined by bending. Coatings morphology was examined by optical microscope. Obtained results pointed that with increase in temperature, the current efficiency and coatings thickness decreases. The optimal temperature for electrochemical deposition of hard – chrome coating was 45 ^{0}C.

Keywords: *chrome coatings, electrochemical deposition, hardness, current efficiency, roughness*

Endemic and protected taxa in subclasses Asteridae and Liliidae in Nature Park Trebević

Dragana Ašćerić[*1], Jelena Vulinović[1], Slađana Petronić[2]

[1]*Faculty of Technology Zvornik, University of East Sarajevo, Zvornik,, Bosnia and Herzegovina*

[2]*Faculty of Agriculture, University of East Sarajevo, 71123 East Sarajevo, Bosnia and Herzegovina*

[*]*asceric13@gmail.com*

Abstract

In this paper, data about endemic and protected taxa within subclasses Asteridae and Liliidae on Trebević Mountain are presented. The area itself is one of the protected areas in the Republic of Srpska, and since last year it has had the status of a Nature park by the decision of the Government of the Republic of Srpska, including the Miljacka river canyon ("Official Gazette of the Republic of Srpska", number 20/14). Within the specified taxonomic categories, the existence of 99 species with the status of endemic or protected species by multiple criteria was established. The existence of rich flora and vegetation in this region is a fact that will encourage future research.

Keywords: *endemic species; protected taxa; Trebević Mountain; Nature Park; Asteridae; Liliidae.*

Introduction

Trebević is a mountain in the southeast part of the Republic of Srpska, located southeast of the main city of Bosnia and Herzegovina, Sarajevo. The area itself is surrounded by mountains: from the southeast side there are Bjelašnica and Treskavica, and in the south and southeast Trebević is connected with mountain Jahorina. On the east and northeast sides is a river Paljanska Miljacka, on its way to Sarajevo [1]. In a biogeographical sense, the area belongs to the Eurosiberian-boreoamerican region and the Illyrian province [2]. Several mountain ridges are of medium height, with sharp edges and slightly rounded valleys; slopes on the southwest are steeper, brittle, and exposed in comparison to the northeast side which is more sheltered and shadier. These morphological differences are enough to create slightly different climatic conditions that caused the development of special flora and vegetation. The first records and research date back to 19. century (Blau (1877) [3], Formanek (1888) [4], Fiala (1889, 1891) [5, 6], Adamović (1889) [7]), where the focus was on exploring the flora of Bosnia and Herzegovina which, during that time, was part of Austro-Hungarian monarchy. In the 20. century, there were several published works about forestry vegetation by Gligić (1953) [8], Pintarić (1957, 1959) [9, 10], and Stefanović (1964, 1983, 1995) [11, 12, 13]. One of the most creditable explorers of the flora in Sarajevo and its surroundings was Karlo Malý (1899, 1904, 1910-1928, 1931, 1932, 1935) [14-19], whose work resulted in the collection of plant material that was deposited in the Herbarium of the National Museum in Sarajevo. It should be mentioned that Beck-Mannagetta (1901, 1903-1923, 1927, 1950) [20-23] also had a great contribution. Some newer research was done by Abadžić (1974, 1984) [24, 25], Protić (1902, 1908) [26, 27], Šoljan, Muratović, Jukić, Merdan, Ravlić (2006) [28], Lakušić (1967, 1991) [29, 30], Redžić (1997, 2009) [31-33] as a way to indicate the remarkable importance of biodiversity in Miljacka canyon.

Nature Park Trebević spreads through several municipalities: East Old City, Pale, and East New Sarajevo, all of which are part of East Sarajevo City. The protected area includes a bigger portion of Trebević Mountain, all the way through Paljanska and Mokranjska Miljacka river canyons and their delta in Miljacka River. A total of 5 036,37 ha has two-level protection regimes: gorge valleys of Paljanska and Mokranjska Miljacka rivers have 15% surface the second-degree of a protected area, and the rest falls to third-degree protection regime [34].

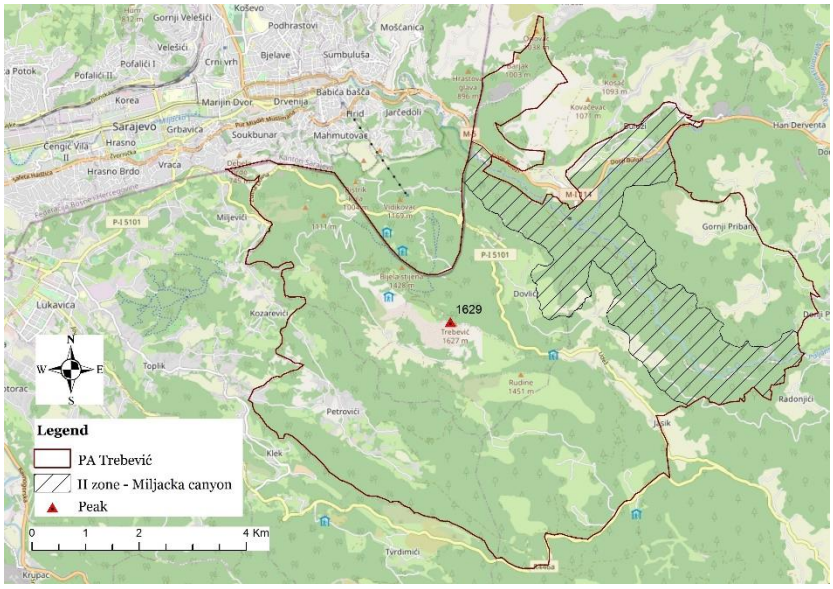

Figure 1. *A protected area of Trebević Mt.*

Research on the flora and vegetation aimed to highlight endemic and protected plant species according to national and international laws. At the same time, it has a goal to emphasize the importance of declaring the area of Trebević Mountain a nature park.

Materials and methods

The area of Trebević Mountain has a rich endemic fond represented by numerous species scattered around in the crevices of limestone rocks and on sluices, their abundance decreased towards dry rocky areas, mountain and subalpine meadows. Many of these species have relict character and are mainly sub-endemics spread over larger geographical areas (Dinaric, Balkan, Balkan-Apennine, Balkan-Alpine). In this paper, the taxa of endemic vascular plants are represented no matter their vulnerability status or protection level, and data about the status are given according to Lubarda et al. (2014) [35]. Bosnia and Herzegovina don't have a Red Book of Flora, but there is a Red List of Bosnia and Herzegovina as well as a Red List of the Republic of Srpska without vulnerability categories. The Red List of Bosnia and Herzegovina has formed thanks to the efforts of Dr Čedomir Šilić, who was given the task of creating a list of plants based on literature data on flora and vegetation collected during 19. and 20. century [36, 37]. This author used the old (classic) IUCNs in the mentioned paper (International Union for Conservation of Nature) threat categories: Ex – disappeared; Ex? - probably disappeared; E – endangered (in danger of disappearing); V – vulnerable (sensitive) species; R – rare species; I – insufficiently known species in terms of vulnerability; K – insufficiently known biology; nt – not endangered [37].

Strictly protected and protected wild species are determined by the Decree on Strictly Protected and Protected Wild Species ("Official Gazette of RS" No. 65/20). For them, except for species that are protected by other regulations, the use, destruction, and undertaking of all activities that may endanger those species and their habitats, as well as taking measures and activities to manage their populations, are prohibited. The care of species, i.e., the implementation of protection and management measures, is carried out within their competencies by the owners of those species, which can be managers of protected areas, users of forests and forest land, and users of hunting grounds and fishing areas. The Decree on Strictly Protected and Protected Wild Species was adopted by the Government of the Republic of Srpska at the proposal of the Ministry of Spatial Planning, Construction and Ecology, while expert activities on its preparation were led by the Republic Institute for the Protection of Cultural, Historical and Natural Heritage in cooperation with local experts. Strictly protected wild species and protected wild species, in accordance with the provisions of Article 46 of the Law on Nature Protection, together with protected areas and protected minerals and fossils constitute

protected natural assets and represent the most important mechanisms of nature protection in the Republic of Srpska [38].
Convention on International Trade in Endangered Species of Wild Fauna and Flora (CITES) Bosnia and Herzegovina ratified in 2008. The purpose of this Convention is to protect wild flora and fauna and their natural habitats, especially those whose protection requires the cooperation of several countries. The Convention has three appendices: I, II, and III. Appendix II contains the endangered species that are not immediately threatened with extinction but that must be monitored in international traffic to avoid excessive use, which would endanger their survival in nature [39].
The IUCN Red List of Threatened Species (also known as the IUCN Red List or Red Data List), founded in 1964, is the world's most comprehensive inventory of the global conservation status of biological species. It has updated categories: EX – disappeared in the wild; CR – critically endangered; EN – endangered; VU – sensitive; NT – near threatened; LC – Least Concern; DD - there is a lack of data on the basis of which the vulnerability evaluation would be carried out; NO – the species was not evaluated [40].
Identification of the collected plants is made according to Flora Europaea [41], nomenclature follows the Med-Checklist [42], Flora Europaea [41], as well as some new data sources like Euro+Med Plantbase [43]. Classification of the presented taxa was done by the book "Sistematika i filogenija viših biljaka" by authors Tatić and Blečić [44].

Results

This paper presents the results that include the list of endemic and protected taxa in two subclasses: Asteridae and Liliidae. Asteridae belongs to the class Magnoliopsida and in the Trebević Mountain is represented by 8 families of endemic and protected taxa (Asteraceae, Boraginaceae, Campanulaceae, Gentianaceae, Lamiaceae, Orobanchaceae, Rubiaceae and Scrophulariaceae) where most species fall to family Asteraceae (37), and the total number of species is 64. Subclass Liliidae is in class Liliopsida with 6 families (Alliaceae, Amaryllidaceae, Asparagiaceae, Iridaceae, Liliaceae, and Orchidaceae); family Orchidaceae is the most common one (27) while the total number of taxa is almost twice as small as the previous subclass (35).

Table 1. List of endemic and protected taxa in subclasses Asteridae and Liliidae on Trebević Mt: E – endemic, RLBIH – The Red List of Bosnia and Herzegovina, RLRS – The Red List of the Republic of Srpska, SPSRS – Strictly protected species of the Republic of Srpska, CITES – Convention on International Trade in Endangered Species of Wild Fauna and Flora, IUCN – International Union for Conservation of Nature.

SPECIES	E	RLBIH	RLRS	SPSRS	CITES	IUCN
ASTERIDAE						
Asteraceae						
Achillea lingulata Waldst. & Kit.		**V**	+			
Arnica montana L.		**V**		+		**LC**
Carduus ramosissimus Pancic	+	**K**	+			
Centaurea glaberrima subsp. *divergens* (Vis.) Hayek	+	**R**				
Centaurea kotschyana Heuff.		**V**	+			
Cirsium candelabrum Griseb.	+					
Crepis alpestris (Jacq.) Tausch		**V**	+			
Crepis aurea (L.) Cass.		**R**	+			

Crepis froelichiana subsp. *dinarica* (Beck) Gutermann	+	**R**				
Crepis paludosa (L.) Moench			+			
Crepis viscidula Froel.			+			
Erigeron atticus Vill.		**K**	+			
Echinops sphaerocephalus L.			+			
Hieracium bifidum subsp. *caesiotropum* K. Malý & Zahn	+					
Hieracium bjeluschae subsp. *barathron* K. Malý & Zahn	+					
Hieracium brevifolium subsp. *malyi-caroli* (Gus. Schneid.) Zahn	+					
Hieracium chalcidicum subsp. *divaricatum* (Fr.) Greuter	+					
Hieracium laevigatum subsp. *brevifoliiforme* Zahn	+					
Hieracium macrodon Nägeli & Peter subsp. *macrodon*	+					
Hieracium melanothyrsum K. Malý & Zahn	+					
Hieracium pallescentifrons K. Malý & Zahn	+					
Hieracium praecurrens subsp. *subumbelliramum* K. Malý & Zahn	+					
Hieraciumprenanthoides subsp. *auriflorens* Zahn	+					
Hieracium pseudobifidum subsp. *platyodontozoum* (K. Malý & Zahn) Zahn	+					
Hieracium pseudobifidum subsp. *trebevicianum* (K. Malý) Zahn	+	**R**	+			
Hieracium tommasinianum subsp. *setosissimum* (Nägeli & Peter) Gottschl.	+					
Hieracium waldsteinii subsp. *lanifolium* (Nägeli & Peter) Freyn	+		+			
Hieracium waldsteinii subsp. *plumulosum* (A. Kern.) Freyn	+		+			
Hieracium waldsteinii subsp. *suborieni* Zahn	+		+			
Hieracium waldsteinii subsp. *thapsiforme* (Asch. & Kanitz) Freyn	+		+			
Hieracium waldsteinii subsp. *trichobrachion* Zahn	+					
Hieracium waldsteinii Tausch subsp. *waldsteinii*	+	**R**	+			
Lactuca pancicii (Vis.) N. Kilian & Greuter	+	**V**		+		**LC**
Petasites kablikianus Bercht.		**R**				
Senecio hercynicus subsp. *dalmaticus* (Griseb.) Greuter	+					
Tephroseris crassifolia (Schult.) Griseb. & Schenk		**R**				
Telekia speciosa (Schreb.) Baumg.		**V**	+			
Boraginaceae						
Onosma stellulata Waldst. & Kit.	+	**R**	+			

Campanulaceae						
Asyneuma canescens (Waldst. & Kit.) Griseb. & Schenk			+			
Campanula scheuchzeri Vill.			+			
Edraianthus graminifolius (L.) A. DC.	+		+			
Gentianaceae						
Gentianella ciliata (L.) Borkh.		**R**				
Gentianella crispata (Vis.) Holub	+	**R**				
Gentiana lutea subsp. *symphyandra* (Murb.) Hayek		**V**				**LC**
Lamiaceae						
Ajuga pyramidalis L.		**R**	+			
Clinopodium alpinum (L.) Kuntze subsp. *alpinum*			+			
Clinopodium thymifolium (Scop.) Kuntze	+		+			
Melissa officinalis L.			+			**LC**
*Satureja subspicata*Bartl. ex Vis. subsp. *subspicata*	+	**V**				
Stachys anisochila Vis. & Pancic	+	**R**	+			
Stachys recta subsp. subcrenata (Vis.) Briq.			+			
Thymus longicaulis C. Presl			+			
Thymus praecox subsp. *jankae* (Čelak.) Jalas	+					
Orobanchaceae						
Euphrasia dinarica (Beck) Murb.	+	**R**	+			
Euphrasia liburnica Wettst.		**R**	+			
Melampyrum hoermannianum K. Malý	+	**V**	+			
Orobanche pancicii Beck	+	**V**	+			
Pedicularis brachyodonta Schloss. & Vuk.		**V**				
Pedicularis hoermannianum K. Malý	+	**V**	+			
Rhinanthus wagneri Degen			+			
Rubiaceae						
Asperula taurina L.			+			
Scrophulariaceae						
Scrophularia bosniaca Beck	+	**R**	+			
Scrophularia heterophylla subsp. *laciniata* (Waldst. & Kit.) Maire & Petitm.		**R**	+			
Verbascum chaixii Vill.			+			
LILIIDAE						
Alliaceae						
Allium lusitanicum Lam.				+		
Amaryllidaceae						

Galanthus nivalis L.		**V**			+	**NT**
Asparagaceae						
Maianthemum bifolium (L.) F. W. Schmidt		**V**				
Iridaceae						
Iris reichenbachii Heuff.	+	**R**		+		
Liliaceae						
Convallaria majalis L.		**V**	+			**LC**
Erythronium dens-canis L.		**V**				
Lilium bosniacum (Beck) Fritsch	+	**V**		+		
Lilium martagon L.		**V**				
Orchidaceae						
Anacamptis morio (L.) R. M. Bateman, Pridgeon & M. W. Chase					+	**NT**
Anacamptis morio subsp. *picta* (Loisel.) Jacquet & Scappat					+	
Anacamptis pyramidalis (L.) Rich.		**V**			+	**LC**
Cephalanthera damasonium (Mill.) Druce		**R**		+	+	**LC**
Cephalanthera longifolia (L.) R. M. Fritsch		**R**		+	+	**LC**
Cephalanthera rubra (L.) Rich.		**R**		+	+	
Dactylorhiza cordigera subsp. *bosniaca* (Beck) Soó	+			+	+	
Dactylorhiza maculata (L.) Soó subsp. *maculata*		**V**	+		+	**LC**
Dactylorhiza saccifera (Brongn.) Soó					+	
Dactylorhiza sambucina (L.) Soó			+		+	
Epipactis atrorubens (Hoffm.) Besser				+	+	**LC**
Gymnadenia conopsea (L.) R. Br.					+	
Gymnadenia nigra (L.) Rchb. F.			+	+	+	**LC**
Gymnadenia rhellicani (Tappner & E. Klein) Tappner & E. Klein					+	**LC**
Himantoglossum calcaratum (Beck) Schltr.	+			+	+	
Limodorum abortivum (L.) Sw.		**E**		+	+	**LC**
Neottia cordata (L.) Rich.				+	+	
Neottia nidus-avis (L.) Rich.					+	
Neotinea tridentata (Scop.) R. M. Bateman, Pridgeon & M. W. Chase			+		+	**LC**
Neotinea ustulata (L.) R. M. Bateman, Pridgeon & M. W. Chase			+		+	**LC**
Orchis mascula subsp. *speciosa* (Mutel) Hegi			+		+	**LC**
Orchis purpurea Huds.		**V**		+	+	**LC**
Orchis simia Lam.		**V**		+	+	**LC**
Ophrys apifera Huds.				+	+	**LC**

Platanthera bifolia (L.) Rich.		**R**		+	+	**LC**
Spiranthes autumnalis (Balb.) Rich.	+				+	
Spiranthes spiralis (L.) Chevall.		**E**		+	+	**LC**

Discussion

Within the class Asteridae there are 64 represented species, 37 are endemic (35%), 30 are on the Red List of Bosnia and Hercegovina (28%), 37 are on the Red List of the Republic of Srpska (35%), and there are 2 of them that are strictly protected as well (2%). Regarding the subclass Liliidae, among the 35 taxa, there are 5 endemic species (7%), 17 on the Red List of Bosnia and Hercegovina (23%), 7 on the Red List of the Republic of Srpska (9%), 17 on the list of strictly protected species (23%) and 28 of them on CITES list (38%).

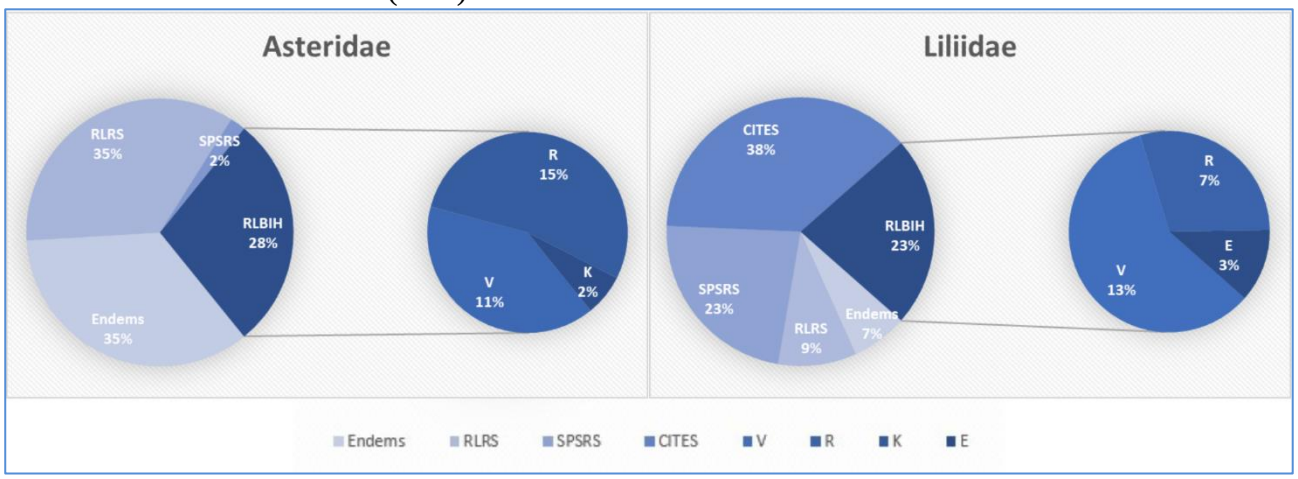

Figure 2. *Percentage share of endemic and protected taxa in subclasses Asteridae and Liliidae: Endems, RLRS – The Red List of the Republic of Srpska, SPSRS – Strictly protected species of the Republic of Srpska, CITES – Convention on International Trade in Endangered Species of Wild Fauna and Flora, RLBIH – The Red List of Bosnia and Herzegovina (V – vulnerable, R – rare, K – insufficiently known, E – endangered).*

Given the fact that there are many species among the endemic and protected categories, it is no surprise that the area of Trebević Mountain was declared a Nature Park. When we compare the data from some of the papers about endemic and protected taxa in the Balkan region, we can conclude that the explored area is of great importance for Bosnia and Herzegovina. One of the sites that are explored in a similar manner is the area of the city Banja Luka, where the threatened, rare and endemic taxa are listed in the same categories [45]. Comparing the data, it was determined that 25 endemic and protected species from the subclasses Asteridae and Liliidae are found in both locations. In the family Asteraceae, there are two common taxa: *Telekia speciosa* and *Hieracium waldsteinii*, same as the family Scrophulariaceae (*Scrophularia bosniaca* and *Scrophularia heterophylla* subsp. *laciniata*). Families with one common species are Gentianaceae (*Gentianella ciliata*) and Boraginaceae (*Onosma stellulata*). That makes a total number of 6 common taxa in the class Asteridae. By analyzing the subclass Liliidae it can be concluded that the remaining 19 common species are unevenly distributed between families Asparagiaceae (*Maianthemum bifolium*) and Amaryllidaceae (*Galanthus nivalis*) that have only one common species. Next, we have the family Lilliacea with three species (*Convallaria majalis*, *Lilium martagon*, and *Erythronium dens-canis*). Finally, family that has the most common taxa is Orchidaceae (14), including: *Ophrys apifera*, *Orchis simia*, *Orchis purpurea*, *Dactylorhiza sambucina*, *Dactylorhiza maculata*, *Anacamptis pyramidalis*, *Gymnadenia conopsea*, *Platanthera bifolia*, *Cephalanthera rubra*, *Cephalanthera damasonium*, *Cephalanthera longifolia*, *Limodorum abortivum*, *Spiranthes spiralis*, and *Neottia nidus-avis* [45].

Conclusion

Trebević is a mountain located in the Republic of Srpska, surrounded by mountains and rivers. The area itself has diverse flora and is rich when it comes to endemic and protected plant taxa. Although this paper mainly concentrates on the subclasses Asteridae and Liliidae, it is clear that the percentage of endemic and protected taxa is very high, and that this region has great potential when it comes to future research. The data concerning the high number of species within the Asteraceae family is not a surprise, and in contrast, we found an unexpected number of representatives from the Orchidaceae family, which may be significant. The subject of future research and data categorization could concern the adequate classification of endemic flora, as well as the work of preparing the Red Book of Bosnia and Herzegovina and the Red Book of the Republic of Srpska.

References

1. I. Trbojević, T. Trbojević, *Fauna Trebevića sa posebnim osvrtom na ugrožene vrste i predloženim smjernicama za aktivno upravljanje izdvojenih vrsta u GIS bazi podataka,* Republički zavod za zaštitu kulturno-istorijskog i prirodnog nasljeđa Republike Srpske, 2022.
2. D. Porej, S. Matić, Protected Area Management Effectiveness in Bosnia and Herzegovina, *Final report of the RAPPAM analysis*, 2017.
3. O. Blau, *Reisen in Bosnien und der Hertzegowina*. Paderborn, Deutschland, Salzwasser Verlag GmbH, 1877.
4. E. Formánek, Beitrag zur Flora von Bosnien und der Hercegovina, *Plant Systematics and Evolution,* **39(1)**, 55-60, 1888.
5. F. Fiala, O nekim endemičnim biljkama u okupiranim zemljama, G*lasnik Zemaljskog muzeja u Bosni i Hercegovini*, **1(1)**, 116–118, 1889.
6. F. Fiala, Floristički prilozi, *Glasnik Zemaljskog muzeja u Bosni i Hercegovini*, **3(3)**, 280-282, 1891.
7. A. Adamović, Naknadno k flori južne Bosne i Hercegovine od dr viteza G. Becka. Na osnovu rezultata dvadesetdnevnog putovanja u ljetu 1888, *Glasnik Zemaljskog muzeja u Bosni i Hercegovini*, **1(1)**, 44-50, 1889.
8. V. Gligić, Planinska botanička bašta na Trebeviću, *Radovi Šumarskog fakulteta Univerziteta u Sarajevu*, **2(2-3)**, 233-244, 1953.
9. K. Pintarić, et al, Virgin forests and forest reserves in Central and East European Countries, *Proceedings of the invited lecturers' reports presented at the COST E4 Management Committee and Working Groups*, Ljubljana, Slovenia, 1999, **4**, 1-15.
10. K. Pintarić, Perspektive šuma hrasta kitnjaka u Bosni, *Šumarski list*, **9(10)**, 399-406, 1998.
11. V. Stefanović, *Šumska vegetacija šireg područja Trebevića,* Naučno društvo SR Bosne i Hercegovine, Radovi XX, Knjiga 7, Sarajevo, 1964.
12. V. Stefanović, et al, Ekološko-vegetacijska rejonizacija Bosne i Hercegovine, *Radovi Šumarskog fakulteta Univerziteta u Sarajevu*, **17(1)**, 1-83, 1983.
13. V. Stefanović, *Prilog poznavanju nesamonikle dendroflore Sarajeva i okoline*, Naučno društvo NR BiH, Odjeljenje privredno-tehničkih nauka, **1(51)**, 1995.
14. K. Maly, Floristički prilozi, *Glasnik Zemaljskog muzeja u Bosni i Hercegovini*, 127-150, 1899.
15. K. Maly, *Beiträge zur Kenntnis der Flora Bosniens und der Herzegowina*, Verhand. Zool.-Bot. Gesellschaff LIV.Band, Druck von Adolf Holzhausen, K. und K. Hof. Und Universitäts-Buchdruckerer, 165-309, 1904.
16. K. Maly, Prilozi za floru Bosne i Hercegovine II-X, *Glasnik Zemaljskog muzeja u Bosni i Hercegovini*, Zemaljska štamparija, Sarajevo, 1910-1928.
17. K. Maly, Ein Beitrag zur Kenntnis einiger Pedicularis-Sippen Illyriens. *Glasn. Bot. zav. bašt. Univ. Beograd,* **2(1—2)**, 94—103, 1931.
18. K. Maly, Über neue und verkannte Pflanzensippen Illyriens, *Glasnik Zemaljskog muzeja u Bosni i Hercegovini*, **44**, 47-53, 1932.
19. K. Maly, Mitteilungen über die Flora Bosnien-Hercegovina, *Glasnik Zemaljskog muzeja u Bosni i Hercegovini*, **47**, 101-111, 1935.

20. G. Beck-Mannagetta, Die Vegetationsverhältnisse der illyrischen Länder, *Die Vegetation der Erde*, **4**, 1-534, 1901.
21. G. Beck-Mannagetta, *Flora Bosne, Hercegovine i Novopazarskog Sandžaka*, Sarajevo, Zemaljska štamparija, 1903-1923.
22. G. Beck-Mannagetta, Flora Bosnae, Hercegovinae et regionis Novi Pazar, III. Choripetalae (finis), *Srpska kraljevska akademija, Posebna izdanja 63, Prirodnjački i matematički spisi*, **15**, 1–487, 1927.
23. G. Beck-Mannagetta , K. Maly, Flora Bosnae et Hercegovinae, IV. Sympetalae (Gamopetalae), *Biološki institut u Sarajevu, Posebna izdanja*, **1**, 5–73, 1950.
24. S. Abadžić, Ekologija i varijabilnost unutar populacije vrste *Scabiosa leucophylla* Borb. na Orlovom krilu kod Sarajeva, *IV Kongres biologa Jugoslavije–Rezimei referata*, 63–64, 1974.
25. S. Abadžić, Ekološko-morfološka diferencijacija među populacijama vrste *Edraianthus jugoslavicus* Lakušić na vertikalnom profilu kanjona Miljacke-Trebević-Jahorina, *Glasnik Zemaljskog muzeja u Bosni i Hercegovini*, **23**, 229-253, 1984.
26. Đ. Protić, Treći prilog k poznavanju flore Bosne i Hercegovine, *Glasnik Zemaljskog muzeja u Bosni i Hercegovini*, **14(1)**, 17–68, 1902.
27. Đ. Protić, Prilozi k poznavanju flore Bosne i Hercegovine, *Glasnik Zemaljskog muzeja u Bosni i Hercegovini*, XX, **3**, 275-288, 1908.
28. D. Šoljan, E. Muratović, Lj. Jukić , A. Merdan , V. Ravlić, Caryophyllaceae, Fabaceae, Lamiaceae, Ranunculaceae i Scrophulariaceae u flori kanjona rijeke Miljacke od Bentbaše do Kozije ćuprije, *Hrvatska misao*, ***6***, 7-23, 2006.
29. R. Lakušić, Specifičnost vegetacije Dinarskih planina, *Bilten biološkog društva SR BiH,* **5**, 1-75, 1967.
30. R. Lakušić, S. Redžić, Flora i vegetacija vaskularnih biljaka u refugijalno-reliktnim ekosistemima kanjona rijeke Drine i njenih pritoka, *Bilten Društva ekologa BiH*, **6,** 25-73, 1991.
31. S. Redžić, Endemni centar u srcu metropole I, *Fondeko svijet 2*, 35-38, 1997a.
32. S. Redžić, Endemni centar u srcu metropole II, *Fondeko svijet 3*, 35-37, 1997b.
33. S. Redžić, S. Barudanović, Some models of sustainable use of medical plants in Dinaric Alpes (SE Europe), *Planta Medica,* **75(09),** 71–80, 2009.
34. Republički zavod za zaštitu kulturno-istorijskog i prirodnog nasleđa [Online]. Available: https://nasljedje.org/novo-zasticeno-podrucje-park-prirode-trebevic/
35. B. Lubarda, V. Stupar, Đ. Milanović, V. Stevanović, Chorological characterization and distribution of the Balkan endemic vascular flora in Bosnia and Herzegovina, *Botanica Serbica*, **38(1)**, 167–184, 2014.
36. Č. Šilić, *Endemične biljke III izdanje*, IP "Svjetlost" Zavod za udžbenike i nastavna sredstva Sarajevo, Zavod za udžbenike i nastavna sredstva, Beograd, 1990.
37. Č. Šilić, Spisak biljnih vrsta (Pteridophyta i Spermatophyta) za Crvenu knjigu Bosne i Hercegovine. *Glasnik Zemaljskog muzeja BiH,* **31,** 323-367, 1996.
38. Službeni glasnik Republike Srpske 65/20
39. CITES. (2022) Convention on International Trade in Endangered Species of Wild Fauna and Flora [Online]. Available: https://cites.org/eng
40. IUCN. (2022) The IUCN Red List of Threatened Species [Online]. Available: https://www.iucnredlist.org/
41. T. G. Tutin, V. H. Heywood, N. A. Burges, D. M. Moore, D. H. Valentine, S. M. Walters, D. A. Webb, *Flora Europaea*, Berkeley, California Botanical Society, 1964-1980.
42. W. Greuter, T. Raus, Med-Checklist Notulae, 12, *Willdenowia*, **15(2),** 413–432, 1986.
43. Euro+Med PlantBase (2022) [Online]. Available: https://europlusmed.org/
44. B. Tatić, V. Blečić, V. Vidović, S. Čuković, D. Varajić, *Sistematika i filogenija viših biljaka*, Zavod za udžbenike i nastavna sredstva. 1988.
45. V. Stupar, Đ. Milanović, J. Brujić, S. Buzadžija, J. Travar, Ugroženi, rijetki i endemični biljni taksoni područja grada Banja Luka, *Skup 4: Zbornik radova II Simpozijum biologa Republike Srpske i I Simpozijum ekologa Republike Srpske*, 165-179, 2011.

Formic acid electrooxidation on Ni-supported platinum thin film catalyst

Oksidacija mravlje kiseline na platinskim katalizatorima na Ni nosaču

Dragana L. Milošević[1,*], Sanja I. Stevanović[1], Nebojša D. Nikolić[1], Dušan V. Tripković[1]

[1] *University of Belgrade - Institute of Chemistry, Technology and Metallurgy, Njegoševa 12, 11000 Belgrade, Republic of Serbia*

[*] *dragana.milosevic@ihtm.bg.ac.rs*

Abstract

Pollution caused by the usage of fossil fuels is a consequence of industrialization, urbanization, and technological development, having a huge impact on the environment and human health. Thus, one of the biggest challenges that currently confront not only the scientific community but also humanity is reducing the use of fossil fuels, as well as the production and consumption of energy using renewable energy sources. In the last decades, small organic molecules such as methanol, ethanol and formic acid have attracted attention due to their properties that make them convenient for use in fuel cells. Among other precious metals, Pt is the most investigated as a promising catalyst for the anodic electrooxidation reaction of small organic molecules. However, high price, scarceness and susceptibility to poisoning are some of the limiting factors for the commercial use of pure Pt. There are two ways to mitigate those problems: lower the content of a noble metal present or make the catalyst more active for the particular reaction. To address the first problem nanocatalyst, produced by the deposition of platinum onto high surface area supports were introduced. A far greater challenge is to modify the catalyst to make it not just more active, but more stable as well, for a particular reaction. It is now well known that bimetallic catalysts fulfill these requirements quite well, and currently, they are widely used in many catalytic and electrocatalytic processes. In this study, a thin Pt film was electrochemically deposited on nickel support (Pt/Ni) and afterward subjected to the controlled thermal treatment in an attempt to reduce the proneness of Pt to poisoning species (CO) and therefore improve its catalytic performance at low potentials in the formic oxidation reaction. All produced catalysts were electrochemically characterized using cyclic voltammetry and oxidation of CO monolayer, while the influence of thermal annealing on the morphology was monitored using an atomic force microscope (AFM). Finally, catalyst performance was tested in a formic acid electrooxidation reaction. The obtained results clearly show that the exceptional activity for formic acid electrooxidation, measured on annealed Pt/Ni is a direct consequence of the nature of the substrate which manifests itself after controlled heat treatment through surface reconstruction and bifunctional effect.

Keywords: *Pt thin films; Ni support; thermal treatment; electrooxidation; formic acid*

Acknowledgments: *This work was financially supported by the Ministry of Science, Technological Development and Innovation of the Republic of Serbia (contract No 451-03-47/2023- 01/200026) and by the Science Fund of the Republic of Serbia under grant No 7739802*

Izvod

Zagađenje izazvano upotrebom fosilnih goriva posledica je industrijalizacije, urbanizacije i tehnološkog razvoja i ima ogroman uticaj na životnu sredinu i zdravlje ljudi. Dakle, jedan od najvećih izazova sa kojima se trenutno suočava ne samo naučna zajednica već i čovečanstvo jeste smanjenje upotrebe fosilnih goriva, kao i proizvodnja energije korišćenjem obnovljivih izvora energije. Poslednjih decenija mali organski molekuli poput metanola, etanola i mravlje kiseline privukli su pažnju zbog svojih svojstava koja ih čine pogodnim za upotrebu u gorivnim ćelijama. Među ostalim plemenitim metalima, Pt je najviše istraživana kao potencijalni katalizator za reakciju anodne elektrooksidacije malih organskih molekula. Međutim, visoka cena, iscrpljivi resursi i podložnost formiranja ometajućih nusprodukata tokom reakcije oksidacije (CO) su neki od ograničavajućih faktora za komercijalnu upotrebu čiste platine kao katalizatora. Postoje dva načina da se ti problemi ublaže, poput smanjenja sadržaja prisutnog plemenitog metala ili poboljšanja aktivnosti katalizatora za određenu reakciju. Da bi se rešio prvi problem, napravljeni su nanokatalizatori, proizvedeni taloženjem platine na nosače velike površine. Daleko veći izazov je modifikovati katalizator kako bi bio ne samo aktivniji, već i stabilniji za određenu reakciju. Dobro je poznato da bimetalni katalizatori dosta dobro ispunjavaju ove zahteve, a trenutno se široko koriste u mnogim katalitičkim i elektrokatalitičkim procesima. U ovoj studiji, tanak film platine je elektrohemijski nanesen na podlogu od nikla (Pt/Ni) i nakon toga podvrgnut kontrolisanom termičkom tretmanu u pokušaju da se ublaži trovanje platine sa CO i stoga poboljšaju njegove katalitičke performanse na nižim potencijalima u reakciji oksidacije mravlje kiseline. Svi proizvedeni katalizatori su elektrohemijski okarakterisani primenom ciklične voltametrije i oksidacije CO monosloja, dok je uticaj termičkog tretmana na morfologiju praćen pomoću atomskog mikroskopa (AFM). Performanse katalizatora su testirane u reakciji elektrooksidacije mravlje kiseline. Dobijeni rezultati jasno pokazuju da je izuzetna aktivnost za elektrooksidaciju mravlje kiseline, izmerena na termički tretiranom Pt/Ni, direktna posledica prirode nosača koja se manifestuje posle kontrolisanog termičkog tretmana kroz rekonstrukciju površine i bifunkcionalni efekat dobijen prisustvom nikla na povrsini.

Ključne reči: *Pt tanki filmovi; Ni nosač; termička obrada; elektrooksidacija; mravlja kiselina*

Zahvalnica: *Ovaj rad je finansijski podržan od strane Министарства науке, технолошког развоја и иновација Republike Srbije (broj ugovora 451-03-47/2023- 01/200026) i Fonda za nauku Republike Srbije (broj Projekta 7739802)*

Methanol electrooxidation on carbon-supported binary and ternary platinum catalysts

Elektrooksidacija metanola na binarnim i ternarnim platinskim katalizatorima na ugljeničnom nosaču

Dragana L. Milošević[1,*], Dušan V. Tripković[1], Vladan R. Ćosović[1], Vesna M. Maksimović[2], Nebojša D. Nikolić[1], Sanja I. Stevanović[1]

[1] *University of Belgrade - Institute of Chemistry, Technology and Metallurgy, Njegoševa 12, 11000 Belgrade, Republic of Serbia*

[2] *University of Belgrade - Vinča Institute of Nuclear Sciences, Mike Petrovića Alasa 12-14, 11351 Vinča-Belgrade, Republic of Serbia,*

[*] *dragana.milosevic@ihtm.bg.ac.rs*

Abstract

One of the most popular alternative sources of energy are direct methanol fuel cells (DMFCs) with platinum-based catalysts due to their non-toxicity, reduced emissions of hazardous pollutants and high energy density. However, significant challenges of the scientific community related to Pt catalysts are the high cost, depletable resources and formation of poisoning species i.e. CO, during the methanol oxidation reaction. To reduce the amount of expensive Pt and susceptibility of Pt to poisoning species and simultaneously improve its catalytic performance, recent studies are focusing on the synthesis of Pt alloys in which a certain amount of platinum is replaced with less expensive metals such as Ru, Sn, Ni, Cu, Rh and Co. The usage of carbon (Vulcan XC-72R) for catalyst support enables high dispersion of metal, high surface area and good electrical conductivity improving overall performances of DMFCs. In this work, PtZn/C and PtSnZn/C catalysts were synthesized by the microwave-assisted polyol method. The structure and morphology of the catalysts were characterized by transmission electron microscopy (TEM), thermogravimetric (TG) and X-ray diffraction (XRD) analysis. The activity and stability of synthesized catalysts for methanol oxidation in 0.5 M sulfuric acid were investigated. It was demonstrated that the activity of the platinum catalysts was improved thanks to the synergistic effects caused by the addition of different metals, such are bifunctional and electronic effects.

Keywords: *Fuel Cell; Platinum Catalysts; Methanol electrooxidation*

Acknowledgments: *This work was financially supported by the Ministry of Science, Technological Development and Innovation of the Republic of Serbia (contract No 451-03-47/2023- 01/200026) and by the Science Fund of the Republic of Serbia under grant No 7739802*

Izvod

Jedan od najpopularnijih alternativnih izvora energije su gorivne ćelije sa metanolom (DMFC) koje sadrze platinske katalizatore, zbog njihove netoksičnosti, smanjene emisije zagađujućih materija i velike gustine energije. Međutim, značajni izazovi sa kojima se susreće naučna zajednica, a koji se odnose na platinske katalizatore su visoka cena, iscrpljivi resursi i formiranje ometajućih nusprodukata tokom reakcije oksidacije metanola, kao što je CO. Da bi se smanjila količina Pt u katalizatoru i osetljivost Pt na ometajuće nusprodukte, a ujedno i poboljšale katalitičke performanse katalizatora, ulažu se veliki napori da se sintetišu legure na bazi Pt u kojima je određena količina platine zamenjena jeftinijim metalima kao što su Ru, Sn, Ni, Cu, Rh i Co. Upotreba ugljeničnog materijala (Vulcan XC-72R) kao nosača metala u katalizatoru omogućava bolju disperziju metala, veću površinu i dobru električnu provodljivost. U ovom radu, PtZn/C i PtSnZn/C katalizatori su

sintetisani poliol postupkom pomoću mikrotalasne pećnice. Struktura i morfologija katalizatora su okarakterisane transmisionom elektronskom mikroskopijom (TEM), termogravimetrijskom (TG) i rendgensko difrakcionom (XRD) analizom. Aktivnost i stabilnost sintetisanih katalizatora u 0,5 M sumpornoj kiselini je ispitivana za oksidaciju metanola. Pokazalo se da je aktivnost platinastih katalizatora poboljšana zahvaljujući sinergetskom efektu izazvanom dodavanjem različitih metala, poput bifunkcionalnog i elektronskog efekta.
Ključne reči: *Gorivna ćelija; Platinski katalizatori; Elektrooksidacija metanola*

Zahvalnica: *Ovaj rad je finansijski podržan od strane Министарства науке, технолошког развоја и иновација Republike Srbije (broj ugovora 451-03-47/2023- 01/200026) i Fonda za nauku Republike Srbije (broj Projekta 7739802)*

Zn/Au alloys formation by Zn electrodeposition from a deep eutectic system

Formiranje Zn/Au legura elektrohemijskim taloženjem Zn iz dubokog eutektikuma

Vesna S. Cvetković[1*], Nebojša D. Nikolić[1], Nataša M. Petrović[1], Tanja S. Barudžija[2], Silvana B. Dimitrijević[3], Jovan N. Jovićević[1]

[1]Department of Electrochemistry, Institute of Chemistry Technology and Metallurgy, University of Belgrade, Njegoševa 12, 11000 Belgrade, Serbia; [2]Institute for Nuclear Sciences Vinča, University of Belgrade, P.O.Box 522, 11001 Belgrade, Serbia; [3]Mining and Metallurgy Institute, Zeleni bulevar 35, Bor, Serbia

[*]Correspondence:v.cvetkovic@ihtm.bg.ac.rs

Abstract

The electrochemical deposition of Zn onto Au from a choline chloride/ethylene glycol deep eutectic system containing different $ZnCl_2$ concentrations has been investigated. The voltammetric results demonstrated that Zn electrodeposition commences in the zinc underpotential deposition (UPD) and proceeds through to the zinc overpotential deposition (OPD) region. The results of X-ray diffraction analysis revealed that the deposit prepared at a relatively low Zn overpotential of – 0.050 V vs. Zn was composed of cubic AuZn alloy. The morphology of the deposit has been characterized by means of a scanning electron microscope and displays a relatively compact and dendrite-free Zn/Au alloy deposit formed.

Keywords: *zinc electrodeposition; deep eutectic solvent; zinc/gold alloys; morphology*

Izvod

U radu je ispitivano elektrohemijsko taloženje Zn na Au iz dubokog eutektikuma koji se sastojao od holin hlorida/etilen glikola i sadržavao je različite koncentracije $ZnCl_2$. Na osnovu voltametrijskih rezultata ustanovljeno je da elektrohemijsko taloženje Zn započinje u oblasti potpotencijala Zn i nastavlja se u oblasti natpotencijala. Rezultati rengenske difrakcione tehnike su pokazali da se talog dobijen elektrohemijskim taloženjem Zn u oblasti natpotencijala Zn, na potencijalu od – 0.050 V vs. Zn sastoji od kubne AuZn legure. Skenirajuća elektronska mikroskopija je pokazala da je dobijeni AuZn talog relativno kompaktan i bez dendrita.

Ključne reči: *elektrohemijsko taloženje cinka; duboki eutektikum; cink/zlato legure; morfologija*

Introduction

The electrodeposition of metals from ionic liquids, particularly those employing deep eutectic solvents, (DESs), has gained significant attention recently [1,2]. Deep eutectic electrolytes have been suggested as alternatives to classical room temperature ionic liquids and nowadays are used on an industrial scale for the electrodeposition processes to produce protective metal coatings [2]. As it is well known, zinc is an important industrial metal, particularly in anticorrosion protection [3]. However, the electrodeposition of zinc coatings for anticorrosion protection from the aqueous electrolytes is accompanied by massive hydrogen evolution. Zinc deep eutectic solvents (DESs) have become an alternative choice of electrolytes for hydrogen-free industrial plating of zinc coatings. Several studies on the electrodeposition of Zn, Co, Ni, Pd, Ag, Cu, Sn, or Ru, from DESs have been reported. It has been shown that DES not only combines the advantages of the system's wide electrochemical window in low-temperature operation but can also provide metals and alloys that are

otherwise electrodeposited usually from high-temperature molten salts [4]. Several groups have studied the electrodeposition of Zn from deep eutectic systems mainly composed of choline chloride (ChCl):ethylene glycol (EG) or ChCl:Urea containing $ZnCl_2$ [1,4–6]. Abbot et al. studied the electrodeposition of Zn from ChCl:EG and ChCl:Urea DESs onto a platinum disc working electrode [1]. Whitehead et al. investigated the Zn electrodeposition process by cyclic voltammetry and potential step techniques from ChCl:EG containing $ZnCl_2$ using static and rotating glassy carbon (GC) disc cathodes at 30°C [7]. The voltammetric behavior of the Zn in ChCl:EG with 0.3 M $ZnCl_2$ by employing glassy carbon, stainless steel, Au, Pt, Cu, and Zn working electrodes was investigated by Vieira et al. [6]. In the literature, a number of studies reported the usage of additives, in order to improve deposit morphology and physical characteristics [1,5].

In this work, we have investigated zinc electrodeposition onto polycrystalline gold electrode from choline chloride (ChCl):ethylene glycol 1:2 (ChCl:EG) electrolyte at 60°C. The main task was to achieve a dendrite-free Zn coating onto polycrystalline gold electrodes without using additives. Cyclic voltammetry and chronoamperometry have been used to attain a better understanding of the nature of the electrode reaction involved in Zn electrodeposition.

Experimental

The electrolyte was prepared by mixing choline chloride (≥98%, $HOC_2H_4N(CH_3)_3Cl$) and ethylene glycol (99.8%, ethane-1,2-diol) at a 1:2 molar ratio. The mixture was then placed onto a hot plate for 2.5 hours at 40ºC, and slowly mixed under an argon atmosphere until a colorless liquid phase was formed. The electrolytes containing $ZnCl_2$ (0.01 M, 0.1 M and 0.5 M) were prepared similarly by adding zinc chloride (99.999% $ZnCl_2$), to the based electrolyte. The electrolyte was stirred again until all of the zinc salt had been completely dissolved. A three electrode electrochemical cell configuration was employed, in which gold (Au, 99.999%, wires or plates) was used as a working electrode, reference electrode was made from a Zn rod (Zn, ø =3mm, 99.99%) and the counter electrode was a zinc plate (active surface area in the electrolyte 7.5 cm^2, Zn 99.99%). The details of the electrochemical cell set up and procedure of the electrodes preparation have already been reported elsewhere [8,9]. All experiments were performed at 60 °C. The electrochemical measurements: cyclic voltammetry (CV, using various scan rates in the range of 2–20 mV/s), chronoamperometry, potentiodynamic and open-circuit potential chronopotentiometry, were controlled by an potentiostat/galvanostat Interface 1010 E (Gamry Instruments, Warminster, PA, US). Zn electrodeposition was performed by applying constant potentials to the Au cathode in the electrolytes containing Zn^{2+}ions. The structure analysis of the deposit was revealed by X-ray diffraction (XRD), employing a SmartLab® X-ray diffractometer (Rigaku Co., Tokyo, Japan). The morphology and composition of Zn deposits were explored using a scanning electron microscope (JOEL JSM-IT300LV), equipped with an energy-dispersive X-ray spectroscopy (EDS) Oxford Instruments X-MAX^N and AZtec version 3.1 software.

Results and Discussion

Figure 1. shows the CVs recorded on a polycrystalline Au electrode immersed in ChCl:EG with different $ZnCl_2$ concentrations at 60 ºC. One reduction (C_1) current wave with peak potentials at ≈ 0.170 V vs. Zn was observed in the Zn underpotential region (UPD) region, Fig. 1a) and b). In Zn overpotential region (OPD), at potentials negative to ≈ – 0.050 V vs. Zn, classical nucleation loops indicating the deposition of the Zn bulk metal were recorded. These nucleation and electro-crystallization loops have been often reported for Zn deposited on a foreign substrate from ionic liquid electrolyte media [5]. When the concentration of Zn^{2+} ions was increased in the electrolyte, the beginning of the current loops was shifted to less negative electrode potentials. In the 0.01 M $ZnCl_2$ electrolyte, the start of the nucleation loop was observed at potential of ≈ – 0.150 V, (Fig. 1a), in 0.1 M $ZnCl_2$ at ≈ – 0.100 V vs. Zn, (Fig. 1b). The cyclic voltammetry of zinc deposition/dissolution on

gold electrodes shows multiple stripping peaks in the anodic potential range which could be attributed to the dissolution of bulk zinc (A_3) and the dissolution of Zn/Au alloys at more positive potentials (A_2 and A_1). Diffusion controlled Zn bulk deposition in the voltammograms becomes obvious only at the cathodic end potentials applied above – 0.200 V vs. Zn.

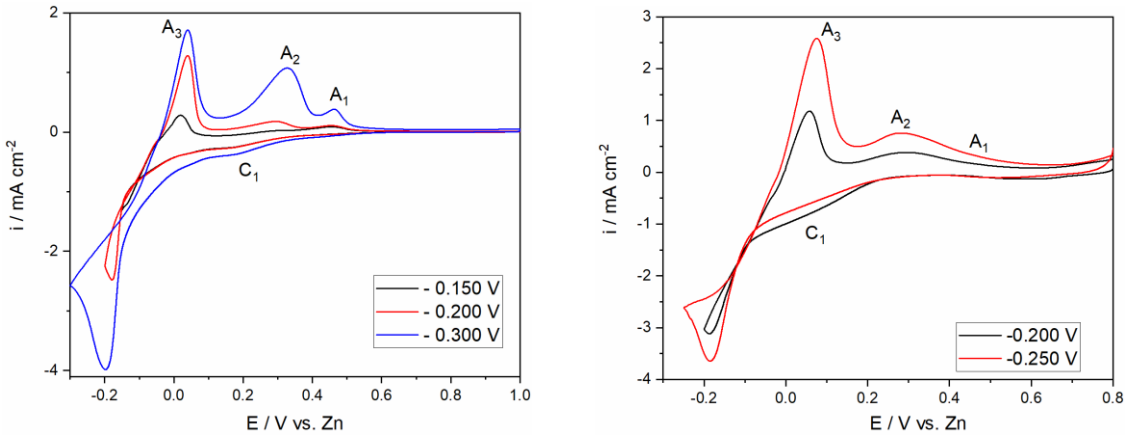

a) b)

Figure 1. *Cyclic voltammograms of Au cathodes in choline chloride:ethylene glycol (1:2 molar ratio) electrolyte containing different concentrations of $ZnCl_2$: a) 0.01 M $ZnCl_2$; b) 0.1 M $ZnCl_2$. The CVs started from initial potential E_i towards different cathodic end potential E_c with a scan rate of 5 mV/s.*

To get further inside into Zn electrodeposition the system was investigated by the open-circuit potentiometry. The open-circuit measurements were recorded after Zn deposition in the electrolytes containing different concentration of Zn(II). Open circuit measurements registered the start of dissolution of a solid phase at around 0.000 V vs. Zn in both systems, followed by a plateau I, Fig. 2a) and b). According to the open-circuit measurements in Fig. 2a) the plateau II at the potential of ≈ 0.300 V and the plateaux II and III at ≈ 0.280 and 0.400 V, Fig. 2b) were recorded. This dissolution current plateau after Zn deposition at E_{dep} = − 0.100V on Au cathode for only 3 min, suggests dissolution of zinc from deposited metal zinc and Zn/Au alloys formed during Zn deposition.

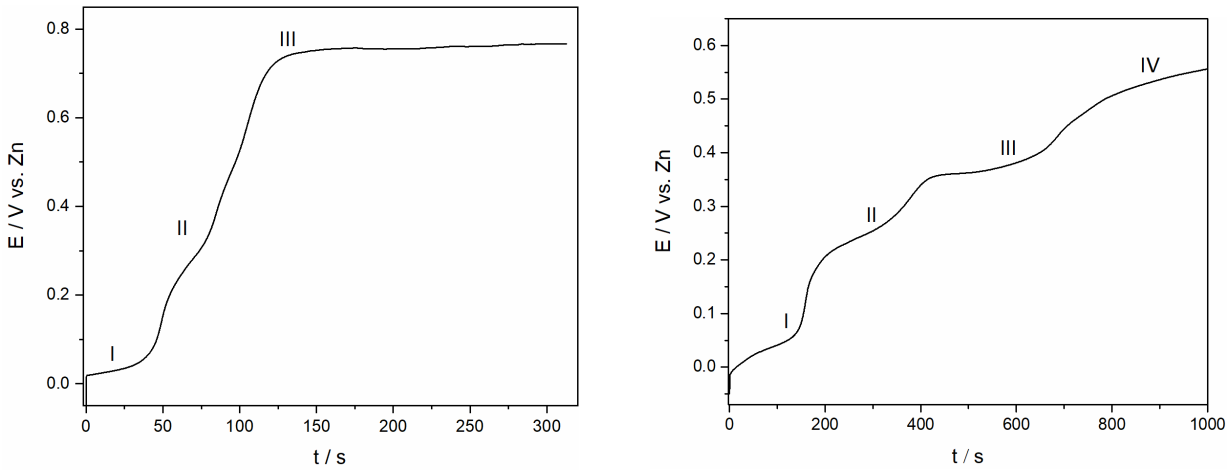

a) b)

Figure 2. *Open-circuit potential transient curves obtained after short polarization (t = 3 min), at – 0.100 V vs. Zn in choline chloride:ethylene glycol (1:2 molar ratio) electrolyte containing different concentrations of $ZnCl_2$: a) 0.01M $ZnCl_2$; b) 0.1 M $ZnCl_2$.*

Figure 3. shows surface morphology obtained by electrodeposition from 0.1 M Zn(II) at an overpotential of – 0.050 V vs. Zn (Fig. 3a)), and XRD analysis of the same sample in Fig. 3b). It is apparent that the Zn deposition under these electrodeposition conditions resulted in the formation of the compact, hard adherent and dendrite-free electrodeposit.

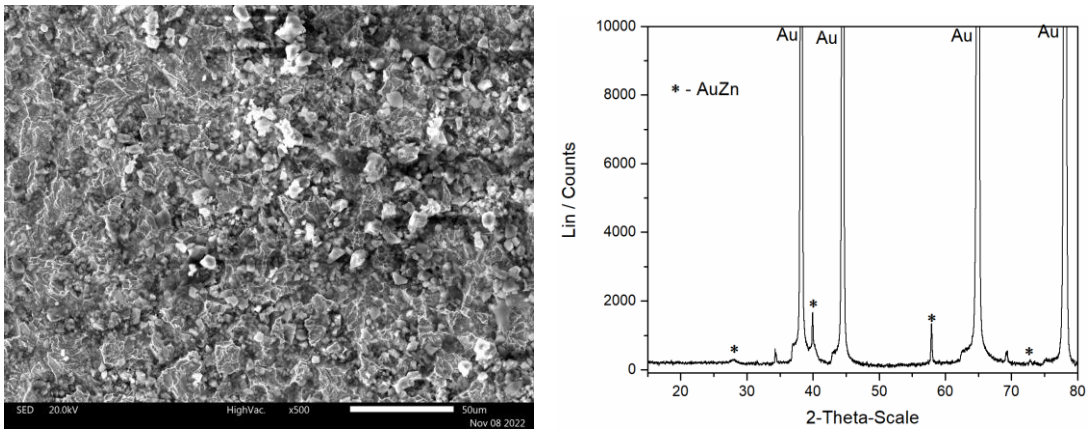

a) b)

Figure 3*. a) The SEM micrograph of deposit obtained by electrodeposition from 0.1 M Zn(II) in: an overpotential region (– 0.050 V vs. Zn) and b) X-ray diffraction analysis of the deposit obtained by Zn electrodeposition in potentiostatic mode (deposition potential – 0.050 V vs. Zn) from choline chloride:ethylene glycol (1:2 molar ratio), deposition time 30 min.*

X-ray diffraction analysis of the samples formed by Zn potentiostatic deposition from 0.1 M $ZnCl_2$ electrolyte onto the Au polycrystalline substrate at – 0.050 V vs. Zn revealed that AuZn phase was formed. The XRD results were in agreement with those reported in the literature which name the cubic $AuZn_3$ and AuZn phases, as well as the hexagonal $Au_{1.2}Zn_{8.8}$ phase, as the main alloys of gold and zinc [10]. However, recently it was suggested that the transition in AuZn phase at low temperature can be trigonal or rhombohedral with a very small distortion [11].

Conclusions

The electrochemical deposition of Zn from an ionic liquid based on a eutectic solvent of choline chloride and ethylene glycol (1:2) containing Zn(II) as a source of metal components was studied on the Au electrode. Cyclic voltammetry results indicated that electrodeposition of Zn commences in zinc underpotential deposition (UPD) and proceeds through to the zinc overpotential deposition (OPD) region. Applying relatively low Zn electrodeposition overpotential of – 0.050 V vs. Zn, resulted in a dendrite-free deposit consisting of cubic AuZn intermetallic.

Acknowledgements: This research has been financially supported by the Ministry of Science, Technological Development and Innovation of Republic of Serbia (Contract No: 451-03-47/2023-01/200026).

References

1. A. P. Abbott, J. C. Barron, G. Frisch, K. S. Ryder, A. F. Silva, The effect of additives on zinc electrodeposition from deep eutectic solvents, *Electrochim. Acta.*, **56,** 5272–5279, 2011. https://doi.org/10.1016/j.electacta.2011.02.095.
2. K. K. Maniam, S. Paul, Progress in electrodeposition of zinc and zinc nickel alloys using ionic liquids, *Appl. Sci.*, **10,** 1–20, 2020. https://doi.org/10.3390/APP10155321.
3. Y.-S. Wang, H.-W. Yeh, Y.-H. Tang, C.-L. Kao, P.-Y. Chen, Voltammetric Study and Electrodeposition of Zinc in Hydrophobic Room-Temperature Ionic Liquid 1-Butyl-1-methylpyrrolidinium

Bis((trifluoromethyl)sulfonyl)imide ([BMP][TFSI]): A Comparison between Chloride and TFSI Salts of Zinc, *J. Electrochem. Soc*., **164**, D39–D47, 2017. https://doi.org/10.1149/2.0451702jes.
4. H. Qian, X. Fu, Y. Chi, R. Zhang, C. Zhan, H. Sun, X. Zhou, J. Sun, Study on electrodeposition and corrosion resistance of Cu-Sn alloy prepared in ChCl-EG deep eutectic solvent, *J. Solid State Electrochem.*, **26,** 469–479, 2022. https://doi.org/10.1007/s10008-021-05086-7.
5. H. K. Ismail, Electrodeposition of a mirror zinc coating from a choline chloride-ethylene glycol-based deep eutectic solvent modified with methyl nicotinate, *J. Electroanal. Chem.*, **876,** 114737, 2020. https://doi.org/10.1016/j.jelechem.2020.114737.
6. L. Vieira, R. Schennach, B. Gollas, The effect of the electrode material on the electrodeposition of zinc from deep eutectic solvents, *Electrochim. Acta.*, **197**, 344–352, 2016. https://doi.org/10.1016/j.electacta.2015.11.030.
7. M. Pölzer, A. H. Whitehead, B. Gollas, A Study of Zinc Electrodeposition from Zinc Chloride: Choline Chloride: Ethylene Glycol, *ECS Trans.*, **25,** 43-55, 2010. DOI 10.1149/1.3378972.
8. N. Jovićević, V. S. Cvetković, Ž. J. Kamberović, J. N. Jovićević, Al-Zn alloy formation by aluminium underpotential deposition from $AlCl_3$+NaCl melts on zinc substrate, *Int. J. Electrochem. Sci.*, **7**, 10380–10393, 2012.
9. V. S. Cvetković, N. Jovićević, J. S. Stevanović, M. G. Pavlović, N. M. Vukićević, Z. Stevanović, J. N. Jovićević, Magnesium-Gold alloy formation by underpotential deposition of magnesium onto gold from nitrate melts, *Metals*, **7,** 95, 2017. https://doi.org/10.3390/met7030095.
10. F. M. Schuett, M. K. Heubach, J. Mayer, M. U. Ceblin, L. A. Kibler, T. Jacob, Electrodeposition of Zinc onto Au(111) and Au(100) from the Ionic Liquid [MPPip][TFSI], *Angew. Chemie - Int. Ed.*, **60**, 20461–20468, 2021. https://doi.org/10.1002/anie.202107195.
11. B. Winn, S. M. Shapiro, J. C. Lashley, C. Opeil, W. Ratcliff, Structural phase transition in AuZn alloys, *J. Phys. Conf. Ser.*, **251**, 012027 2010. http://dx.doi.org/10.1088/1742-6596/251/1/012027

Quasi Linear Spread of Air Pollution and the Environment Caused by a Periodic Source

Kvazi linearno širenje zagađenja vazduha i okoline uzrokovano periodičnimg izvorom

Jovan P. Šetrajčić[1*], Stevo K. Jaćimovski[2], Siniša M. Vučenović[3]

[1]*Academy of Sciences and Arts of the Republic of Srpska, Bana dr T. Lazarevića 1, Banja Luka, Republic of Srpska – B&H;*

[2]*University of Criminalistics and Police Studies, Cara Dušana 196, Zemun – Belgrad, Serbia;*

[3]*Univerzity of Banja Luka, Faculty of Siences and Mathematics, Banja Luka, Republic of Srpska – B&H.*

[*]*jovan.setrajcic@gmail.com*

Abstract

With the sudden technical, economic and technological development, the problem of pollution - especially air, especially in large industrial centers - has also emerged acutely. The paper analyzes the distribution of particulate air pollution that originates from a certain place and is in the form of a periodic point source. This pollution is considered along one dimension with the calculation of diffusion and absorption processes, in correlation with air flow. The partial differential equation that describes all the mentioned events is solved numerically for the adopted realistic characteristic parameters.

Keywords: *periodic point source; particulate air pollution; diffusion and absorption processes; spatial distribution*

Izvod

Naglim tehničkim, ekonomskim i tehnološkim razvojem, akutno se pojavio i problem zagađenja – posebno vazduha, posebno u velikim industrijskim centrima. U radu je analizirana distribucija čestičnog zagađenja vazduha koji potiče sa određenog mesta i oblika je periodičnog tačkastog izvora. Ovo zagađenje se razmatra duž jedne dimenzije uz obračun difuzionih i apsorpcionih procesa, u korelaciji sa protokom vazduha. Parcijalna diferencijalna jednačina koja opisuje sva pomenuta događanja, numerički se rešava za usvojene realne karakteristične parametre.

Ključne reči: *periodični tačkasti izvor; čestično zagađenje vazduha; difuzioni i apsorpcioni procesi; prostorna distribucija*

Uvod

Zagađenje vazduha – aero-zagađenje definiše se kao stanje atmosfere u kojoj su prisutne supstancije u koncentracijama iznad definisanih normalnih vrednosti,koje štete životnoj sredini i ljudima. Ovozagađenje je posledica prirodnih pojava i ljudskih aktivnosti i zato se može klasifikovati [1] kao zagađenje od *prirodnih izvora* i zagađenje od *antropogenih izvora*.

Prirodni izvori zagađenja vazduha su uvek bili prisutni u biosferi i njih čine:*deflacija* – prenos zemlje i peska (uobičajeno u pustinjskim i šumsko-stepskim zonama), *dimšumskih i stepskih požara* (sadrži CO, čađ, smole, katran i sl.), *vulkani* – tokom jakih erupcija emituju ogromne količine prašine, gasova, SO_2, CO_2, itd., *mineralna i termalna vrela* – mogu da emituju CO_2, H_2S, metan, itd., *kosmička prašina*, posebno ako se utvrdi da je radioaktivna, *velike okeanske površine* mogu biti izvori CO_2, CO, H_2S, hlorida itd., *elementarne katastrofe* mogu da prate značajne emisije zagađujućih materija u vazduh, te *oluje* i *zemljotresi*.

Antropogeni izvori zagađenja mogu se klasifikovati na *stacionarne* i na *mobilne*.Pri tome, mobilni izvori obuhvataju motorna vozila sa motorima sa unutrašnjim sagorevanjem. Izvori zagađenja iz zatvorenog prostora obuhvataju emisije sagorevanja i zagrevanja, emisije iz različitih materijala ili supstancija (isparavanje organskih jedinjenja, različitih sintetičkih hemikalija, duvanskog dima, itd.).

Po osnovu količine (broja) izvora i njihove prostorne distribucije,i zagađivači mogu biti jednostruki, tačkasti (statički ili mobilni), grupni (statički ili mobilni) i linearni.

Na bazi vrste emisije, izvori zagađenja se klasifikuju na emitere čestica i emitere gasova.

Najveća važnost poznavanja i predviđanja prostiranja aero-zagađenja je njen loš uticaj na ljudsko zdravlje. Veza između zdravstvenog stanja stanovništva i stanja životne sredine nije direktna, jer postoje razni drugi faktori koji utiču na zdravlje stanovništva. Međutim, faktor okoline je važan, pored baštine i individualnih karakteristika životnog stila, i radi dostupnosti i efikasnosti zdravstvene usluge. Smatra se da kvalitet vazduha u urbanim sredinama ima veći uticaj na zdravlje stanovništva u odnosu na druge faktore životne sredine i da zagađivači spoljnog vazduha predstavljaju jedan od najvažnijih uzroka zdravstvenih problema uopšte. Brojna epidemiološka ispitivanja nedvosmisleno su dokazala da je zagađenje vazduha u obliku čestica koje se mogu udisati povezano sa povećanjem morbiditeta i smrtnosti od respiratornih i kardiovaskularnih bolesti. Povećanje neke bolesti (kardiovaskularne i hipertenzije, bolesti disajnih organa, maligne bolesti, zarazne i parazitske bolesti) može biti rezultat savremenog načina života, ali i posledica zagađenja vazduha. APHEA projekat „Zagađenje vazduha i zdravlje: evropski pristup“ jedna je od epidemioloških studija u kojoj se prate kratkotrajni efekti aero-zagađenja prema nekim zdravstvenim parametrima. Posebna pažnja posvećena je dnevnoj promenljivosti funkcije pluća, učestalosti nege u bolnici i smrtnosti. U Parizu je rizik od smrtnosti zbog respiratornih bolesti porastao na 17%, sa 100 μg/m^3 prirasta lebdećih čestica. Lebdeće čestice, crni dim i sumpor dioksid (SO_2) povezani su sa hitnom hospitalizacijom respiratornih pacijenata. Studija u Španiji utvrdila je da su oksidi, posebno azot dioksid (NO_2) i ozon, povezani sa smrtnošću od kardiovaskularnih bolesti, naročito tokom leta. Takođe je utvrđen kancerogeni uticaj mnogih toksičnih jedinjenja.

Do sada je identifikovano nekoliko stotina različitih zagađivačkih materija (najznačajniji i najčešći su prikazani u tabeli 1), a trebalo bi uočiti moguće stvaranje novih, pod uticajem sunčeve svetlosti i električnog pražnjenja. Kvalitet vazduha određuje se koncentracijom zagađivačkih jedinjenja (zagađivača) u vazduhu ili njihovim taloženjem na površinu u toku određenog vremena. Koncentracija zagađivača je masa, zapremina ili količina materije koja se nalazi u određenoj zapremini ili masi vazduha.

Tabela 1. *Zagađivačka jedinjenja i izvori zagađenja*

Zagađivačko jedinjenje	Glavni izvor zagađenja
Sumpur diokside SO_2	Sagorevanje uglja, nafte, teška metalurgija i prateće
Vodonik sulfid H_2S	Hemijski procesi, rafinerije
Ugljen monokside CO	Sagorevanje
Azot oksidi NO_x	Sagorevanje
C_n H_{n+2}	Isparavanje tečnih goriva i izduvni gasovi
Čađ	Sagorevanje
Suspenziječestica	Tehnološki procesi, kamenolomi, proizvodnja cementa
Isparenja organskih jedinjenja	Hemijski procesi, proizvodnja nafte, distribucija benzina

Pored koncentracije zagađujućih jedinjenja iz izvora zagađivača, kvalitet vazduha na jednom području takođe je određen meteorološkim elementima i uslovima: stanje vazdušnog pritiska, smer i brzina vetra, vrtložne struje, vlažnost vazduha, prisustvo magle, količina kiša, temperatura vazduha i inverzija temperature. Najveća koncentracija zagađujućih jedinjenja se širi vodoravno u pravcu vetra. U periodima „tišine“ – nepostojanja kretanja vazduha, sva zagađujuća jedinjenja ostaju u naseljenom području. U nižim nivoima atmosfere vazduh je topliji i pomera se prema gornjim, hladnijim, slojevima koji omogućavaju normalnu disperziju. Međutim, u uslovima brzog hlađenja dolazi do inverzije zemljine temperature. Prizemni vazduh je hladniji od zraka u višim slojevima, pa disperzija nije moguća. Nizak vazdušni pritisak, odsustvo vetra, visoka vlažnost vazduha, izmaglica i temperaturska inverzija smanjuju raspodelu zagađujućih jedinjenja u visini i daljini, drže ih u nivou tla i koncentrišu se blizu izvora zagađenja. Moguće je da se smog formira zajedno sa jedinjenjima koja su izuzetno toksična i opasna za ljudsko zdravlje. Nivo zagađujućih jedinjenja određuje se merenjem [1,2].

Zagađenje vazduha se može preneti na velike udaljenosti u poređenju sa mestom izvora. Udaljenost zavisi od brzine distribucije (difuzije) zagađenih vazdušnih masa i brzine taloženja (taloženja) zagađujućih jedinjenja. Zbog svega toga, potrebno je definisati prognozu prostiranja aerozagađenja u datim uslovima. Ovo se postiže modelovanjem i to smo upravo učinili ovog puta i rezultate prikazujemo u ovom radu.

Za procenu prostiranja zagađenja vazduha neophodno potrebno je poznavati: kvalitet (fizička i fizičko-hemijska svojstva) zagađujućih jedinjenja i količinu (iznos/učešće), od čega zavisi dejstvo svakog zagađivača pojedinačno.

Model prostiranja aero-zagađenja

Procesi prostiranja čestica u atmosferi od velikog su interesa za mnoga područja ljudske aktivnosti. Sazrevanje svesti o važnosti ovih procesa omogućilo je stalnost merenja u službi praćenja i prikupljanja podataka. Na osnovu rezultata merenja nastali su empirijski modeli zagađenja vazduha. Kasnije, uloženi su značajni napori u razvoju metoda za analizu difuzije čestica u okolnoj atmosferi. Kao rezultat ovih napora, rezultati ovakvih istraživanja primenjuju se za prognozu posledica kada se dogodi vanredna situacija zbog različitih nezgoda i nesreća saučešćemprostiranja opasnih jedinjenja. Uprkos velikim naporima koji su uloženi u ova istraživanja, ne postoje opšte prihvaćeni modeli za analizu raspodele zagađenja u vazduhu. To je objektivno uslovljeno raznolikošću i složenošću ovih procesa. Zbog toga postoji veliki broj modela različitog tipa. Glavno svojstvo prema kojem se modeli klasifikuju je njihov empirijski ili zasnovani teorijski karakter [3].

Klasični empirijski model je Paskuil-Gifordovmodel [4], dok se Berlandsov model može dati kao primer teorijskog modela turbulentne difuzije [2,3]. Unutar empirijskih modela, fizika procesa u atmosferi se gotovo u potpunosti ne uzima u obzir ili je vrlo grubo uključena.Danas najbolje rezultate, uslovno rečeno, daju polu-empirijski modeli. Ovde je empirijski model dopunjen dobro razvijenim matematičko-numeričkim aparatima koji obuhvataju analizu veoma komplikovanih situacija i omogućavaju sintezu rezultata različitih eksperimenata, na primer meteoroloških i difuzijskih uslova istovremeno.

Modeli su, međutim i čak veoma različiti prema primenjenim matematičkim aparatima. Empirijski modeli koriste eksplicitne forme, dobijene nakon brojnih merenja, koje se mogu jednostavno uređivati na mikroračunalima. Polu-empirijske metode koriste postupke numeričkog rešavanja parcijalnih diferencijalnih jednačina kojima se opisuju posmatrani uslovi prosturanja. Teorijski modeli koriste najrazličitije postupke kao što su dimenzionalna analiza, analitička rešenja parcijalnih diferencijalnih jednačina, metode simulacija poput Monte Carlo i sl. Trebalo bi napomenuti da, kada se govori o pronalaženju analitičkih rešenja, uglavnom se analiziraju stacionarni procesi, dok se za numerički pristup analiziraju i nestacionarni procesi.

Trenutni modeli se mogu klasifikovati prema prostornim i vremenskim dimenzijama njihove primene na: *lokalne*, *regionalne* i *globalne*. Lokalne metode analiziraju zagađenje vazduha na području do deset kilometara u periodu od nekoliko minuta do nekoliko sati. Regionalni modeli analiziraju prostiranje aero-zagađenja od nekoliko desetina do nekoliko stotina kilometara, dok vremenska udaljenost traje od nekoliko sati do nekoliko dana. Globalni modeli obuhvataju problem širenja zagađenja vazduha na tom području od nekoliko stotina do nekoliko hiljada kilometara, dok vremenska dimenzija može da traje nekoliko nedelja [5].

U smislu matematičke obrade i tretiranja pomenutih procesa, modeli se mogu razvrstati na tri vrste: Gausove, Ojlerove i Lagrangeove. Jednadžbe u ovim modelima su dobijene različitim aproksimativnim pristupom rešavanju jednaćinai turbulentne difuzije. Najjednostavniji model za izračunavanje koncentracije čestica/nečistoća pri tlu je statistički Gaussov model. U osnovi ovog modela nalazi se pretpostavka da čestice koje izbacuju neprekidni tačkasti izvori stvaraju oblak dima u kojem se distribucija čestica pokorava normalnoj Gaussovoj raspodeli (slika 1).

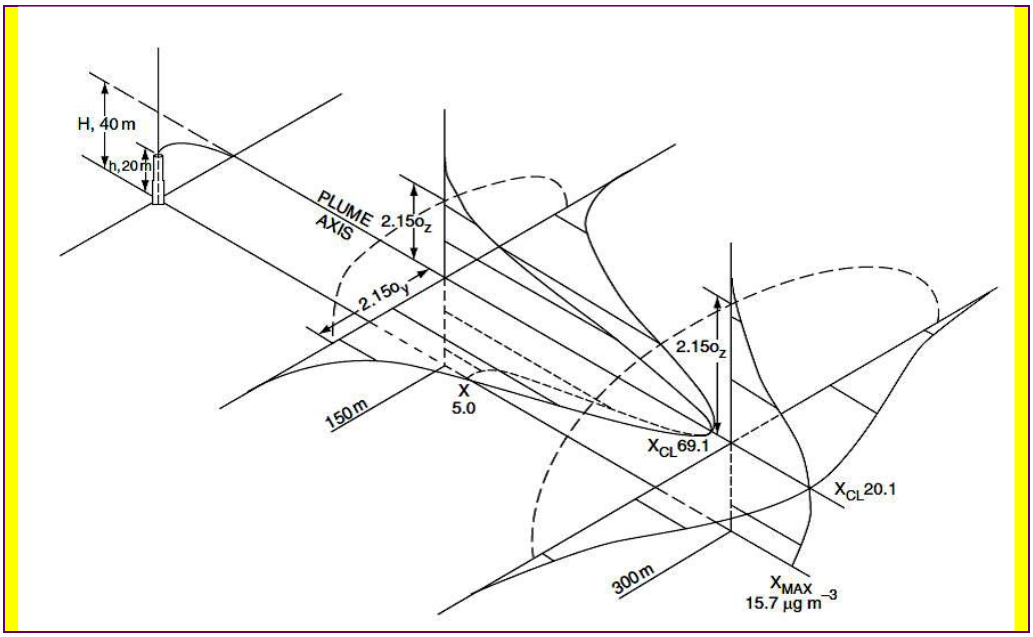

Slika 1. *Gausov model čestične emisije od tačkastog izvora* [2,6]

U ovom modelu informacije o brzini vetra uzimaju se kao parametar sa najbliže meteorološke stanice i pretpostavlja se da se brzina održava tokom vremena potrebnog za prenošenje čestica nečistoće na rastojanje 20 – 30 km. Nedostaci ovog modela su:

- Pretpostavlja da je vertikalno i horizontalno rasejanje čestica međusobno nezavisno;
- Komponente brzine vetra se ne uzimaju u obzir – pretpostavlja linearna putanja čestica;
- Oblik disperzije koja opisuje rasipanje oblaka čestica zavisi od udaljenosti od izvora;
- U početnom trenutku uzima se da je koncentracija čestica u izvoru beskonačno visoka;
- Pomoću ovog modela nije moguće izračunati koncentracije čestica za malu brzinu vetra (manju od 1 m/s).

Oilerov model zasnovan je na rešavanju polu-empirijske jednačine turbulentne difuzije [5]:

$$\frac{\partial q}{\partial t} = -\vec{V}\cdot\nabla q + \frac{\partial}{\partial x}\left(k_x \frac{\partial q}{\partial x}\right) + \frac{\partial}{\partial y}\left(k_y \frac{\partial q}{\partial y}\right) + \frac{\partial}{\partial z}\left(k_z \frac{\partial q}{\partial z}\right), \tag{1}$$

gde $\vec{V}\cdot\nabla q$ definiše odgovarajuću komponentu jednačine, k_x, k_y i k_z su koeficijenti turbulentne difuzije, a q je srednja vrednost koncentracije nečistoća.

Oilerov model prostiranja nečistoća uzima u obzir osnovne karakteristike ovog procesa: prenos čestica duž pravca konvekcije/protoka. Turbulentna difuzija, konvekcija, prostorno-vremenska nehomogenost parametara raspršivanja, interakcije čestica sa površinom zemlje itd.

Ovaj model omogućava izračunavanje koncentracije čestica na području udaljenom 50 km od tačke i drugih izvora koji kontinuirano zrače nečistoće, pod proizvoljno meteorološkim uslovima, iznad površine tla proizvoljnog reljefa. Takođe, on daje podatke o koncentraciji nečistoća u slučaju vetra malih brzinama, čak i u slučaju stabilnog vremena. Model mora dati rezultate za prostornu distribuciju koncentracije nečistoća, u skladu sa empirijskim modelima. Koeficijenti turbulencije zavise od brzine vetra, stanja atmosfere, površinskog reljefa i prelaska udaljenosti nečistoća iz posmatrane tačke – položaja izvora zagađenja:

$$k_z = U_z \frac{\kappa^2 h_{SBL}}{\ln(z_r / z_0)} \left(\frac{x}{x_1} \right)^b ; \quad k_y = k_z P^{-1}, \tag{2}$$

gde U_z predstavlja brzinu vetra, brzina vetra izmerena na nadmorskoj visini z_r iznad nivoa tla, z_0 je odlika površinskog reljefa, κ je Karmanova konstanta, h_{SLB} je visina blizu osnovnog nivoa atmosferskog sloja, x je udaljenost koju je prešla čestica nečistoće od izvora do posmatrane tačke, x_1 je standardno rastojanje jednako 1000 m, b je eksponent funkcije snage, dok je P koeficijent anizotropije turbulencije.

U svom opštem obliku zadatak matematičke prognoze zagađenja vazduha može se definisati kao rešavanje odgovarajuće jednačine turbulentne difuzije za adekvatne početne i granične uslove. Jednačina (2) opisuje prostornu raspodelu srednjih koncentracija kao i njihovu promenu u vremenu i u tom smislu može se tretirati kao jednačina prognoze.

Analitički pristup rešavanju jednačinai atmosferske difuzije veoma je složen problem, moguć jedinoako se iskoristi niz aproksimacija. Teškoće u rešavanju analitički navedenih jednačina javljaju se čak i za jednostavne slučajeve.Međutim, u slučajukada se pretpostavi da se brzina vetra logaritamski menja sa nadmorskom visinom i uz eliminaciju linearne i/ili energetske zavisnosti koeficijenata, na taj način olakšava posao pronalaženja analitičkog rešenja.

Istraživanje atmosferske difuzije iznad površine sa složenim reljefom pretpostavlja promenu mnogih meteoroloških elemenata, što svaki pojedinačno, usložnjavai praktično onemogućava analitičnost rešenja. Stoga, numerički pristupi se nameću kao jedino moguće rešenje za integraljenje jednačina turbulentne difuzije. Bez obzira na kapacitete i mogućnosti računarskih resursa, za uspešno pronalaženje raspodele zagađenja vazduha potrebno je veoma razumno odabrati parametre jednačine. [7]

Rešenje kvazi 1d problema

Ovaj deo je posvećen analizi prostiranja aero-zagađenja u blizini tačkastog izvora. Analiziraće se prostorna raspodela tačkastog zagađivača, kada se događaju procesi difuzije, apsorpcije i protoka vazduha. Ograničićemo se na linearan – 1D problem, jer nam je cilj da procenimo prostorno-vremensku raspodelu koncentracije od izvora aero-zagađenjaprema datoj dinamici zagađenja. Iako se radi o izvesnoj idealizaciji odabirom 1D problema, to se nadoknađuje razmatranjem praktično svih mogućih fizičkih mehanizama koji deluju tokom prenosa zagađujućih čwstica [8]. Takođe, modeli smo funkciju izvora u analitičkoj formi koja zaista deluje tokom rada jednog industrijskog postrojenja. Jednačina turbulentne difuzije za posmatrani slučaj [9] je oblika:

$$\frac{\partial q}{\partial t} + u \frac{\partial q}{\partial x} - b^2 \frac{\partial^2 q}{\partial x^2} + cq = A\varphi(t)\delta(x), \tag{3}$$

gde je u brzina vetra u pravcu i smeru x-ose, b je koeficijent difuzije nečistoća, $A\varphi(t)$ predstavlja funkciju količine emitovanih čestica nečistoća u jedinici vremena, c je koeficijent koji karakteriše

apsorpciju čestica nečistoća (može se dobiti nakon hemijske analize atmosferskih procesa koji dovode do transformacije nečistoća i njihove apsorpcije).

Da bi proces, opisan jednačinom (3), postao realniji, pretpostavićemo da je $\varphi(t)$ periodična funkcija $\phi(t)$ definisana sledećim oblikom [7]:

$$\phi(t)=\begin{cases}0, & t\in(0,t_1); \quad t_1<0;\\ 1, & t\in(t_1,t_2); \quad t_2<2T;\\ 0, & t\in(t_2,2T); \quad t_2>t_1.\end{cases} \tag{4}$$

Stoga tačkasti izvor emituju toksična jedinjenja u intervalu $t_2 - t_1$. Granični i početni uslovi, u tom slučaju mogu da se izraze u formi: $q(\pm\infty,t) = 0$ i $q(x,\pm\infty) = 0$. Treba napomenuti i da postulirane jednačine opisuju srednje vrijednosti koncentracija. U jednačini (3) uzimaju se sledeće vrednosti parametara: $u_1 = 1$ m/s; $u_2 = 4$ m/s; $4b^2 = 1.39\cdot10^{-2}$ m^2/s; $c = 2\cdot10^{-3}$; $A = 10^{12}$. Prihvaćena vrednost za koeficijent difuzije odnosi se na CO_2. Numeričkim pristupom uz pomoć matematičkog paketa *Mathematica*, nađeno je traženo rešenje i grafički je prikazano graficima na slici 2.

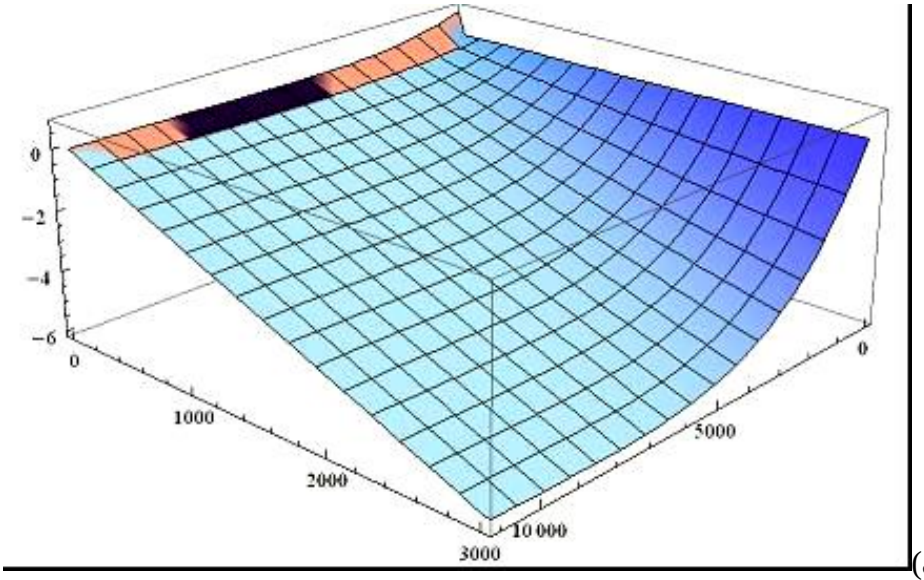

(a)

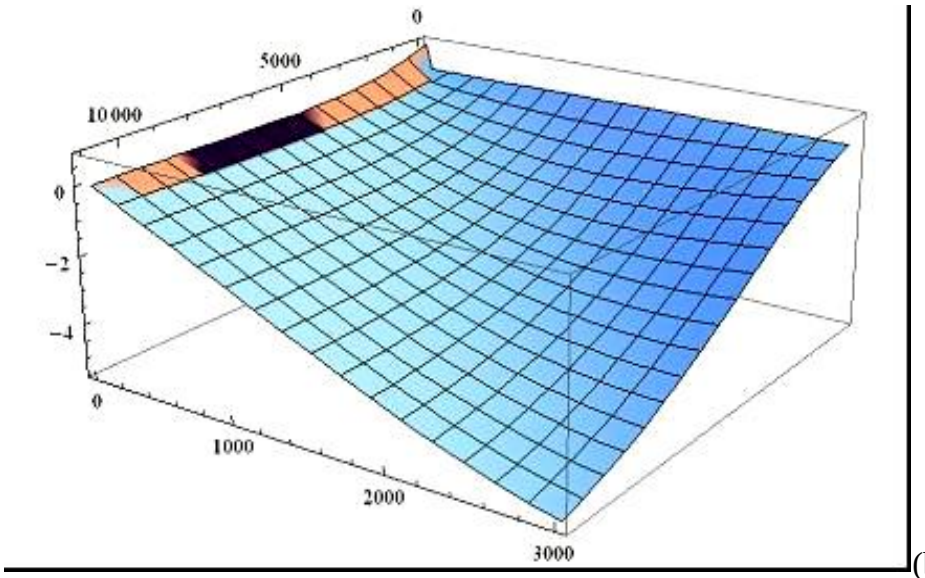

(b)

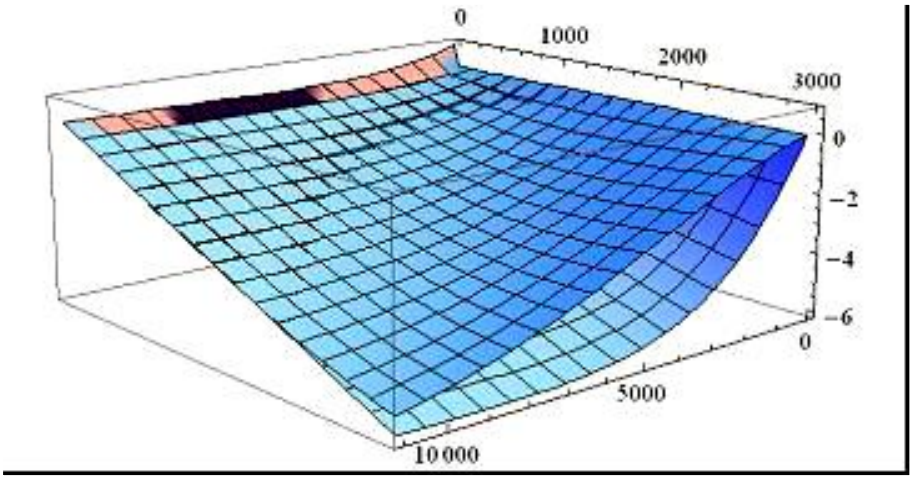

(c)

Slika 2. *Prostorna i vremenska distribucija koncentracija nečistoća*

Na slici 2a data je prostorno-vremenska raspodela za slučaj kada je brzina vetra 1 m/s, dok je na slici 2b data ista distribucija za slučaj kada ona iznosi 4 m/s. Na slici 2c prethodna dva slučaja su data zajedno radi lakšeg poređenja. Može se videti da koncentracija opada sa vremenom, sporija sa većim vrednostima brzine vetra. Takođe, koncentracija opada sa rastojanjem od izvora (u našem primeru 5 mg/m^3 za rastojanje od 3 km).

Zaključak

Problem zagađenja vazduha je usko povezan sa razvojem industrije i saobraćaja. U svim zemljama se uvodi kontrola stanja životne sredine, najviše atmosfere. Efikasnost kontrole stanja atmosfere određuju dve komponente: direktno – merenjem kvaliteta vazduha pomoću posebnih instrumenata koji se objedinjuje u jedinstven sistem – bazu praćenja atmosfere, i indirektno – teorijskim modelovanjem aero-zagađenja koji omogućava određivanje koncentracije toksičnih jedinjenja u oblastima koje nisu obuhvaćene direktnim merenjima, ali i prognozu distribucije nastalog zagađenja i u slučaju incitentne situacije. Na taj način modeliranje se uvodi u sklopu celokupnog praćenja zagađenja atmosfere.

Teorijsko modeliranje postaje sve efikasniji instrument za istraživanje atmosferskog stanja pod uticajem poboljšanja matematičkih metoda za analizu procesa prenosa i rasejanja gasovitih, tečnih i čvrstih komponenti zagađenja vazduha. Određivanje nivoa aero-zagađenosti primenom odgovarajućeg modela raspodele zagađenja omogućava simulaciju širenja toksičnih jedinjenja za različite pretpostavljene intenzitete emisije u topološkim, urbanim i meteorološkim uslovima.

Uz pomoć teorijskog pristupa i formiranjem odgovarajućeg materatičko-fizičkog modela može se dobiti realna slika disperzije čestica zagađivača u okolnu atmosferu, koja može poslužiti kao osnova za procenu potencijalne opasnosti. Na jednostavnijem – 1D modelu periodičnog (industrijskog) tačkastog zagađivača, demonstrirali smo prostorno-vremensku raspodelu koncentracije zagađivača u pravcu vetra (za dve različite vrednosti brzina) od izvora, pa do tačke udaljene 3 km od tog izvora. Pokazali smo da koncentracija zagađenja opada sa protekom vremena od tenutka prestanka emitovanja zagađenja, te da je to opadanje sporijepri većim vrednostima brzine vetra. Takođe, koncentracija zagađenjaskoro linearno opada sa udaljavanjem od izvora.

Zahvalnica

Rezultati izneti u ovom radu deo su istraživanja koja su finansijski podržana od strane Ministarstva za naučnOtehnološki razvoj, visoko obrazovanje i informaciono društvo Vlade Republike Srpske (19.032/961-36/19 и 19.032/961-42/19).

Referencije

1. A. Tiwary, J. Colls J., *Air Pollution*, New York, Routledge, 2010, str. 54-90.
2. S.K. Jaćimovski, S. Miladinović, V. Ilijazi,V.M. Zorić, I.J. Šetrajčić, S. Armaković, J.P. Šetrajčić, Linear Expansion of Air Pollution, *Proceedings 2nd UrbanEco*, Zrenjanin, 2012, 62-67.
3. M.E. Berlyander, *Contemporary Problems of Atmospheric Diffusion of Atmospheric Pollution*, Leningrad, Gidrometeoizdat, 1975, pp. 11-18.
4. F. Pasquill, F.B. Smith, *Atmosperic Diffusion*, New York, J.Wiley&Sons, 1983, pp. 20-80.
5. S.N. Stepanenko, V.G. Voloshin, S.V. Tipcov, Turbulent Diffusion Equation Solution for the Stationary Point Source, *UGZ* **3**, 13-25, 2008.
6. M. Lazaridis, *First principles of Meteorology and Air Pollutant*, New York, Springr, 2011, pp. 201-232.
7. M.E. Berlyander, *Forecast and Control of Atmospheric Pollution*, Leningrad, Gidrometeoizdat, 1985, pp. 8-79.
8. B.S. Tošić, S.D. Stojanović, M.J. Škrinjar, D.V. Kapor, The one dimensional problem of air-pollutant distribution, *Faculty of Sciences – Universityof Novi Sad, Review of Research* 12, 79-88, 1982.
9. G.I. Marchuk, *Mathematical Modeling in the Environmental Problem*, Moskwa, Nauka, 1982, pp. 175-187.

The influence of the brookite/anatase TiO_2 nanoparticles on structural and electrochemical properties of conducting polyaniline form

Uticaj nanočestica brukit/anatas TiO_2 na strukturna i elektrohemijska svojstva provodne forme polianilina

Bojana Kuzmanović[1,*], Nenad Ivanović[1], Nataša Tomić[2], Bojana Paskaš Mamula[1], Katarina Batalović[1], Mirjana Medić Ilić[1], MilicaVujković[3]

[1]*Vinča Institute of Nuclear Sciences – National Institute of the Republic of Serbia, University of Belgrade, P.O. Box 522, 11001, Belgrade, Serbia*

[2] *Institute of Physics, University of Belgrade, Pregrevica 118, 11080 Belgrade, Serbia*

[3]*Faculty of Physical Chemistry, University of Belgrade, Studentski Trg 12-16, 11000 Belgrade, Serbia*

[*]*kuzmob@vinca.rs*

Abstract

The emeraldine salt polyaniline/TiO_2 composite (PANI_ES@TiO_2_BA) was prepared by in situ chemical oxidation of aniline in the presence of the TiO_2 brookite(74%)/anatase(26%) nanoparticles. Raman spectroscopy and Cyclic Voltammetry were used to examine the properties of the obtained composites and their charge storage performances. A significant decrease of the composite charging/discharging capacity indicates that the incorporation of 33 wt% of the brookite/anatase TiO_2 nanoparticles into the PANI_ES matrix deteriorates the charge storage possibilities of the composite in comparison with the pure PANI_ES at a common scan rate of 20 mVs^{-1}.
Keywords: *polyaniline; TiO_2; composite; Raman spectroscopy; Cyclic Voltammetry; Charge storage.*

Izvod

Kompozit polianilina u formi emeraldin soli/TiO_2 (PANI_ES@TiO_2_BA) je sintetisan in situ hemijskom oksidativnom polimerizacijom anilina u prisustvu nanočestica TiO_2 brukit(74%)/anatas(26%). Za ispitivanje svojstava dobijenog kompozita i njegovih performansi za skladištenje naelektrisanja korišćena je metoda Ramanske spektroskopije i ciklična voltametrija. Značajno smanjenje kapaciteta punjenja/pražnjenja kompozita ukazuje na to da ugradnja 33 težinskih procenata (wt%) nanočestica brukit/anatas TiO_2 u PANI_ES matricu smanjuje sposobnost skladištenja naelektrisanja u kompozitu u poređenju sa čistim PANI_ES, pri brzini polarizacije od 20 mVs^{-1}.
Ključne reči: *polianilin; TiO_2; kompozit; Ramanska spektroskopija; ciklična voltametrija; skladištenje naelektrisanja.*

Introduction

Both organic and inorganic core-shell hybrid materials have been extensively studied in the literature [1]. The complementary characteristics of these materials and their synergistic attract much attention advocating them as promising candidates for potential applications in electronic and optical devices, photocatalysis, batteries, and protective coatings [2]. Among the most comprehensively studied combinations for hybrid nanocomposites production are those of conducting polyaniline (PANI) and numerous inorganic oxides (γ-Fe2O3, TiO_2, CeO_2, graphene oxide, ZnO, SiO_2) encapsulated inside the PANI shell [3-6]. A small amount of oxide nanoparticles (NP) incorporated into the PANI matrix can significantly modify its structural, morphological, electrical, and optical properties [7].

Most of the existing studies of PANI@TiO_2 composites have been focused on their applications in photocatalysts and gas sensors [8-10], but much less of them are focused on their possible use as electrode materials for supercapacitors [11].
In studies of the PANI@TiO_2 nanocomposites, the largest attention has been paid to the anatase TiO_2 crystal form [12,13], while the use of rutile and rutile/anatase TiO_2 crystal form nanocomposites is much less investigated [7,14]. Due to the difficulties encountered in the synthesis process, there is even less interest in the pure brookite TiO_2 crystal form nanocomposites.
In this work, brookite(74%)/anatase(26%) TiO_2 (TiO_2_BA) (NP) were synthesized using sol-gel hydrothermal method, while PANI was obtained in the form of emeraldine salt (ES) (PANI_ES) by typical chemical oxidation polymerization of aniline monomer under highly acidic conditions. The PANI_ES@TiO_2_BA dielectric material was developed by in situ chemical oxidative polymerization in order to investigate its charge storage capacity and to relate it to the influence of the anatase/brookite TiO_2 (NP) on properties of the conductive PANI_ES matrix.

Experimental details and characterisation

Synthesis of polyaniline

The PANI_ES form was synthesized by typical chemical polymerization of aniline in the presence of hydrochloric acid and ammonium persulfate as an oxidant, according to the procedure described in our previous paper [5]. 0.18 mL of aniline monomer was injected into 7 mL of 2 M HCl solution. Then, 0.45 g of $(NH_4)_2SO_4$, previously dissolved in 2 mL of deionized water, was added dropwise to the solution, with constant stirring on a magnetic stirrer. After washing with 2 M HCl, deionized water, and ethanol, the obtained precipitate was dried at 60 ◦C in an oven for 36 h.

Sol-gel hydrothermally synthesis of TiO_2_BA

The polymorphic brookite/anatase TiO_2 (NP) were synthesized by the sol-gel hydrothermal method, with $TiCl_4$ used as a precursor. An appropriate amount of $TiCl_4$ was dissolved in 50 mL of distilled water, with constant stirring in an ice bath. In order to form the hydrogel, the NaOH solution was gradually added until pH ~ 9. After 5 hours of aging, the V = 80 mL of hydrogel was transferred to an autoclave and treated at T = 200 ˚C for 24 hours. Using the XRD method, the brookite/anatase phases relation in the obtained nanopowder sample [15], was determined to be 74%/26%.

PANI@TiO_2_BA synthesis procedure

The PANI@TiO_2_BA composites were synthesized using the same procedure as for PANI_ES synthesis but in the presence of TiO_2_BA. Two times distilled aniline monomer was added to an aqueous solution of 2M HCl containing 33 wt% of TiO_2 (NP) of the brookite/anatase TiO_2 crystal structure synthesized in the previously described manner. In order to prevent aggregation, the solution was treated with ultrasound, after which $(NH_4)_2SO_4$ dissolved in deionized water was added with constant stirring. The resulting sample was washed with 2M HCl aqueous solution and deionized water and then dried in an oven.

Raman stady of PANI_ES@AB interaction

The Raman spectra of the PANI_ES and PANI_ES@TiO_2_BA samples were recorded using a DXR Raman microscope (Thermo Scientific) equipped with a research optical microscope and a CCD detector, and the results are presented in Fig.1. The PANI_ES Raman spectrum is typical for this protonated PANI form, and its peaks were assigned using literature data [16-18]. The TiO_2_BA Raman spectra were measured under the same conditions as those of PANI_ES and shown in the inset of Fig. 1. The PANI_ES@TiO_2_BA composite Raman spectrum shows all characteristic PANI vibration modes with a modified intensity of certain bands mainly (but not exclusively) in the range

of wave numbers characteristic for the incorporating oxide vibrations. Shifts of the PANI_ES Raman bands were not observed in the composite, which can be attributed to the stability of principal structural features of both individual components of the composite after its formation.

The assignment of the PANI_ES Raman bands in the 2000 cm^{-1} to 200 cm^{-1} range is given in Table 1. In the Raman spectrum of the mixed brookite/anatase TiO_2 phase, the bands that correspond to the brookite phase are: ~ 286 cm^{-1} (B_{1g}), ~ 412 cm^{-1} (A_{1g}), ~ 505 cm^{-1} (B_{3g}), ~ 544 cm^{-1} (A_{1g}) and ~ 640 cm^{-1} (A_{1g}). The Raman modes of the anatase phase were observed at positions ~ 399 cm^{-1} (B_{1g}), ~ 518 cm^{-1} (A_{1g}+B_{1g}), and ~ 639 cm^{-1} (E_g) [19].

Analyzing the Raman spectrum of the composite, one can observe the influence of the TiO_2_BA oxide (NP) on the PANI_ES band of medium intensity recorded at ~1490 cm^{-1}, which is related to the C=N stretching vibrations of the quinonoid structures. The oxide influence is also evident on mode at ~1509 cm^{-1}, which is attributed to the N-H deformation vibrations of the semi-quinonoid ring. In addition, the splitting of the band recorded at 1336 cm^{-1}, which is associated with $C{\sim}N^{+\bullet}$ vibrations in the delocalized polaronic structure [20] into ~1344 cm^{-1} and ~1326 cm^{-1} lines is significantly more pronounced in the composite than in pure PANI_ES, and the ratio of their intensities increases in the composite. It is indicative that all affected modes mentioned above originate from various vibrations that include PANI_ES N-atoms, so the cause for their modification should be searched in various interactions of N-atom, probably with both O and Ti atoms forming the TiO_2 surface [21]. The assumption that oxide Ti-atoms form a coordination compound with PANI_ES N-atoms is also possible [22].

Changes in the vibrational mode's intensity due to the PANI_ES - TiO_2_BA interaction are also pronounced in the wave number range in which the oxide modes appear. The intensity of the band at 718 cm^{-1}, which is associated to the deformation of the amine structure of the bipolaronic form of PANI_ES, decreases in the presence of oxide (partially overlapping brookite A_{1g} mode and the anatase E_g mode). This indicates the possible existence of the PANI - TiO_2 interaction involving the amine hydrogen, i.e., the NH-O-Ti interaction. Changes in the PANI_ES bands recorded at 585 cm^{-1} and 520 cm^{-1} are due to the interaction with A_{1g} and B_{3g} vibrational modes of the brookite phase, as well as with the A_{1g}+B_{1g} and B_{1g} anatase phase modes. The decrease of intensity of the PANI_ES band at 421 cm^{-1}, and increase of intensity of the ~ 298 cm^{-1} band can be attributed to the interaction of the brookite phase B_{1g} vibrational mode with these PANI_ES modes.

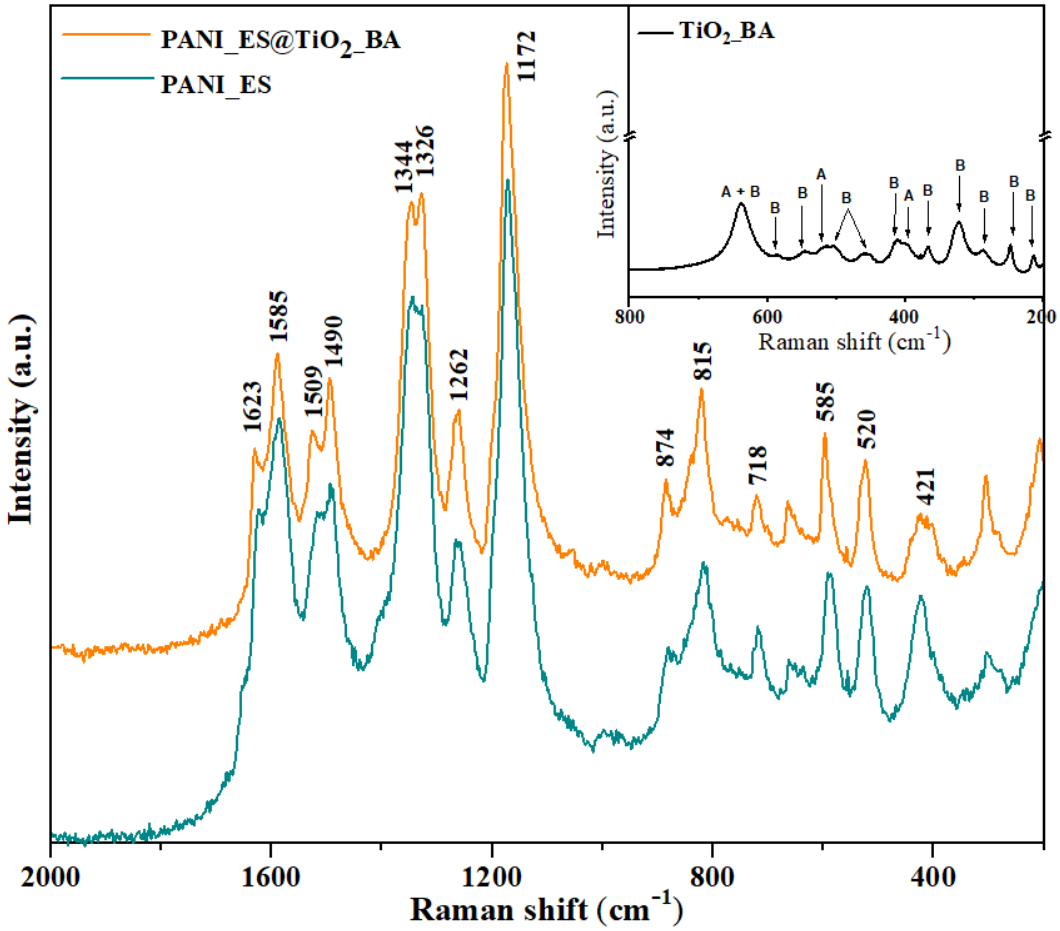

Figure 1. *Normalized Raman spectra of PANI_ES and PANI_ES@TiO_2_BA in the normalized scale. The spectrum of pure TiO_2_BA oxide phase is given in the inset. The symbols A and B indicate bands corresponding to anatase, i.e., the brookite phase.*

Table 1. The assignments of the PANI_ES Raman bands in the 2000 cm^{-1} - 200 cm^{-1} range. (ν)-stretching, (b)-bending, (w)-wagging, (τ)-torsion, (i-p) in plane, (o-p) out-of plane, (d) deformation, (r-d) deformation of ring, B: benzenoid, Q: quinonoid, SQ: semi-quinonoid rings.

Exp. frequencies (cm^{-1})	Assignments
1623	$\nu(C\text{-}C)_B$
1585	$\nu(C{=}C)_Q$; $\nu(C{\sim}C)_{SQ}$
1509	$\delta(N\text{-}H)$(i-p)
1490	$\nu(C{=}N)_Q$
1344, 1326	$\nu(C\text{-}N^{+\bullet})_{SQ}$
1262	ν(C-N)
1172	$b(CH)(i\text{-}p)_{SQ}$
874	$w(C\text{-}H)(r\text{-}d)_B(i\text{-}p)$
815	$b(C\text{-}H)_Q(o\text{-}p)$, $(r\text{-}d)_{SQ}$
718	$(r\text{-}d)_B(o\text{-}p)$
585	(o-p)(C-H)+(r-d)
520	τ(C-N-C)(o-p)
421	(CH)(o-p)

Electrohemical behavior

The influence of the brookite/anatase TiO_2 (NP) on the charge storage behavior of PANI_ES was studied by cyclic voltammetry method. The measurements were performed at Gamry PCI4/300 Potentiostat/Galvanostat in the typical three-electrode configuration. To examine the influence of the PANI_ES electrochemical over-oxidation, both samples were measured in an extended potential range of -0.2–1 V vs. SCE (Saturated Calomel Electrode) during ten consecutive cycles. The resulting cyclic voltammograms (CVs) are shown in Figure 2.

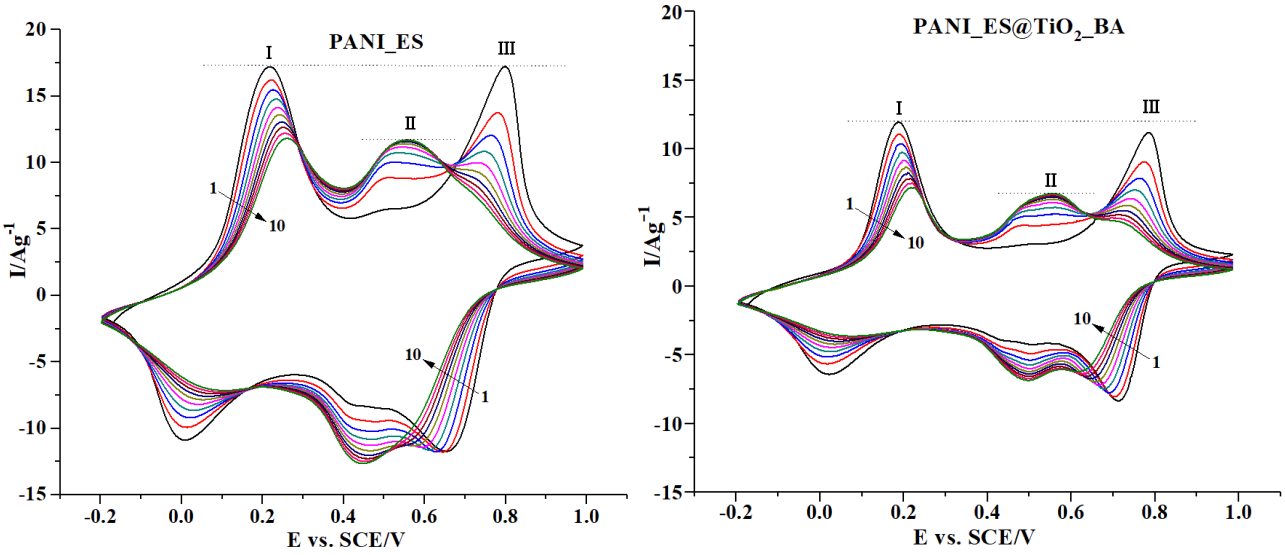

Figure 2. *Cyclic voltamograms of PANI_ES, and PANI_ES@TiO_2_BA samples measured in HCl in potential range from -0.2 (the 1st) to 1 V (the 10th) cycle vs. SCE, at scan rate of 20 mVs^{-1}.*

The first cycle anodic peak, which originates from oxidation of leucoemeraldine base (LB) into emeraldine salt (ES) is observed at 0.22 V, while the cathodic peak, which originates from reduction of (LB) to (ES), is observed at 0.001 V. The anodic peak of the second main redox pair originating from the oxidation of ES to pernigraniline salt (PNS) is positioned at 0.8 V, while the cathodic peak originating from reduction of PNS to ES is observed at 0.65 V. A low-intensity redox couple is positioned between these two main redox pairs of peaks, with the anodic peak at 0.55 V and the cathodic peak at 0.45 V. This pair of peaks is generally attributed to the formation of benzoquinone degradation products, leading to formation of the cross-linked PANI [23]. One can see that current of this middle peaks increase during the consecutive cycling of PANI within the extended water stability window, while the currents of redox peaks I and III decrease. This is in accord with previous observation that the formation of electrochemically inactive intermediates in preoxidized PANI leads to decrease of the current response during successive cycling [24].

The current responses of the anodic peaks in the first cycle is similar for processes I and III indicating similarity of the PANI_ES sample redox processes kinetics. After incorporation of the TiO_2_BA (NP) into the PANI_ES matrix, the reduced current response was reduced. The anodic peak III is smaller than anodic peak I indicating that the (PNS) formation takes place more slowly in the composite than in pure PANI_ES. This behavior can be explained by the fact that the interaction of the TiO_2_BA oxide with the PANI_ES chain hinders its deprotonation, which leads to a lower proportion of the (PNS) formed in the first anodic scan. Consequently, a slightly slower disappearance of the third peak was observed after the tenth cycle.

The charging/discharging capacitance of PANI is usually monitored in a narrower potential range (-0.2 to 0.6 V vs. SCE), in which the electrochemical preoxidation of PANI does not occur. In this regime, the calculated ratio of charging/discharging capacities was found to be 296/294 Fg^{-1} for pure PANI_ES and 165/160 Fg^{-1} for PANI_ES@TiO_2_BA. The significant decrease of the composite

capacity clearly shows that incorporation of 33 wt% of the TiO_2_BA (NP) into the PANI_ES matrix prevents the storage of significant amount of charge in the composite at a common scan rate of 20 mVs^{-1}.

Conclusion

The 33wt% of brookite(74%) and anatase(26%) TiO_2_BA nanoparticles (NP) mixture was incorporated into the PANI_ES matrix during in situ chemical oxidative polymerization. The Raman spectra analysis of the obtained samples suggests that formation of the PANI_ES@TiO_2_BA composite (NP) is accompanied by various interactions involving the N-atom from PANI_ES, and most likely the O-atoms from the TiO_2_BA (NP) surfaces of the both involved TiO_2 phases. However, some kind of Ti-N interaction is also possible. The charging/discharging capacitance features of pure PANI_ES and the composite were studied in 1M HCl using cyclic voltammetry at a common scan rate of 20 mV s^{-1}. In the -0.2 to 1 V SCE range, besides the two principle peaks pairs that correspond to the leucoemealdin base to emeraldine salt (0.22/0.001 V) and emeraldine salt to pernigraniline salt (0.8/0.65 V) oxidation/reduction, an additional pair of peaks (0.55/0.45 V) attributed to benzoquinone degradation products and subsequent PANI cross-linking appears. The relations between these peaks' current intensities in pure PANI_ES and the PANI_ES@TiO_2_BA composite and their changes during the consecutive cycling imply that interactions between the PANI_ES and TiO_2_BA (NP) in the PANI_ES@TiO_2_BA composite hinders the PANI_ES deprotonation and prevents about the half of the charge that could be stored in pure PANI_ES (in the -0.2 to 0.6 V SCE range) to be stored in the composite.

Acknowledgements

The funding for this research is provided by the Ministry of Science, Technological Development and Innovation of the Republic of Serbia, under Grant. No. 451-03-47/2023-01/200017.

References

1. S. H. Mir, L. A. Nagahara, T. Thundat, P. Mokarian-Tabari, H. Furukawa, A. Khosla, Review—Organic-Inorganic Hybrid Functional Materials: An Integrated Platform for Applied Technologies, *J. Electrochem. Soc.*, **165**, B3137- B3156, 2018.
2. C. Sanchez, B. Julian, P. Belleville, M. Popall, Applications of hybrid organic-inorganic nanocomposites, *J. Mater. Chem.*, 15, 3559–3592, 2005.
3. Y. Zhang, D. Jiang, Y. Wang, Y. Wang, T. C. Zhang, G. Xiang, Y.-X. Zhang, S. Yuan, Core-Shell Structured Magnetic γ-Fe_2O_3@PANI Nanocomposites for Enhanced As(V) Adsorption, *Ind. Eng. Chem. Res.*, **59**, 7554–7563, 2020.
4. H. Zhang, R. Zong, J. Zhao, Z.Zhu, Dramatic Visible Photocatalytic Degradation Performances Due to Synergetic Effect of TiO_2 with PANI, *Sci. Technol.*, **42**, 3803-3807, 2008.
5. B. Kuzmanović, Milica J. Vujković, N. Tomić, D. Bajuk-Bogdanović, V. Lazović, B. Sljukić, N. Ivanović, S. Mentus, The influence of oxygen vacancy concentration in nanodispersed nonstoichiometric $CeO_{2-\delta}$ oxides on the physico-chemical properties of conducting polyaniline/CeO_2 composites, *Electrochim. Acta*, **306**, 506-515, 2019.
6. S. Daikh, F. Z. Zeggai, A. Bellil, A. Benyoucef, Chemical polymerization, characterization and electrochemical studies of PANI/ZnO doped with hydrochloric acid and/or zinc chloride: differences between the synthesized nanocomposites, *J. Phys. Chem. Solids*, **121**, 78-84, 2018.
7. C. Bian, G. Xue, Nanocomposites based on rutile-TiO_2 and polyaniline, *Mater. Lett.*, **61**, 1299-1302, 2007.
8. G. Iinzhang, W. Shengying, Y. Wu, Z. Guohu, B. Lili, S. Li, Preparation and photocatalytic activity of PANI/TiO_2 composite film, *Rare Metals*, **26**, 1-7, 2007.
9. S. Min, F. Wang, Z. Kan, An investigation on synthesis and photocatalytic activity of polyaniline sensitized nanocrystalline TiO_2 composites, *J. Mater. Sci,*. **42**, 9966-9972, 2007.

10. H. Tai, Y. Jiang, G.g Xie, J. Yu, X. Chen, Z.Ying, Influence of polymerization temperature on NH_3 response of PANI/TiO_2 thin film gas sensor, *Sens. Actuators B*, **129**, 319-326, 2008.
11. M. B. Poudel, C. Yu, H. J. Kim, Synthesis of Conducting Bifunctional Polyaniline@Mn-TiO_2 Nanocomposites for Supercapacitor Electrode and Visible Light Driven Photocatalysis, *Catalysts*, **10**, 546, 2020.
12. S. Nasirian, H. M. Moghaddam, Hydrogen gas sensing based on polyaniline/anatase titania nanocomposite, *Int. J. Hydrog. Energy*, **39**, 630-642, 2014.
13. M. R. Nabid, M. Golbabaee, A. B. Moghaddam, R. Dinarvand, R. Sedghi, Polyaniline/TiO_2 Nanocomposite: Enzymatic Synthesis and Electrochemical Properties, *Int. J. Electrochem. Sci.*, **3**, 1117-1126, 2008.
14. R. Ganesan, A. Gedanken, Organic-inorganic hybrid materials based on polyaniline/TiO_2 nanocomposites for ascorbic acid fuel cell systems, *Nanotechn.*, **19**, 435709 (5pp), 2008.
15. A. Kremenović, M. Grujić-Brojčin, N. Tomić, V. Lazovic, D. Bajuk-Bogdanović, J. Krstić, M. Šćepanović, Size-strain line-broadening analysis of anatase/brookite (TiO_2)-based nanocomposites with carbon (C): XRPD and Raman spectroscopic analysis, *Acta Cryst.*, **B78**, 214-222, 2022.
16. M. Trchová, Z. Morávková, M. Bláha, J. Stejskal, Raman spectroscopy of polyaniline and oligoaniline thin films, *Electrochim. Acta*., **122**, 28-38, 2014.
17. P. Colomban, S. Folch, A. Gruger, Vibrational study of short-range order and structure of polyaniline bases and salts, *Macromol.*, **32**, 3080-3092, 1999.
18. G. Ćirić-Marjanović, M. Trchová, J. Stejskal, The chemical oxidative polymerization of aniline in water: Raman spectroscopy, *J. Raman Spetrosc.*, **39**, 1375-1387, 2008.
19. T. Ohsaka, F. Izumi, Y. Fujiki ,"Raman spectrum of anats, TiO_2", J. Raman Spectrosc. 7 (1978) 321-324.
20. M. Trchová, Z. Morávková, I. Šeděnková, J. Stejskal, Spectroscopy of thin polyanilin films deposited during chemical oxidation of aniline, *Chem. Pap.*, **66**, 415-445, 2012.
21. H. Lv, Y. Wang, L. Pan, L. Zhang, H. Zhang, L. Shang, H. Qu,N. Li, J. Zhao, Y. Li, Patterned polyaniline encapsulated in titania nanotubes for Electrochromism, *Phys. Chem. Chem. Phys.*, **20**, 5818-5826, 2018.
22. M. R. Nabid, M. Golbabaee, A. B. Moghaddam, R. Dinarvand, R. Sedghi, Polyaniline/TiO_2 Nanocomposite: Enzymatic Synthesis and Electrochemical Properties, *Int. J. Electrochem. Sci.*, **3**, 1117-1126, 2008.
23. R. Pauliukaite, C. M. A. Brett, A. P. Monkman, Polyaniline fibres as electrodes. Electrochemical characterisation in acid solutions, *Eelectrocim. Acta*, **50**, 159-167, 2004.
24. E. Song, J.-W. Choi, Conducting polyaniline nanowire and its applications in chemiresistive sensing, *Nanomater.*, **3**, 498-523, 2013.

Long-term air exposure surface modification-XPS first principle approach study

Ispitivanje promena na površini nakon dugotrajnog izlaganja vazduhu polazeći od prvih principa-XPS

Mirjana Medić Ilić[1,*], Bojana Kuzmanović[1], Bojana Paskaš Mamula[1], Katarina Batalović[1], Nenad Bundaleski[1,2]

[1]*Vinča Institute of Nuclear Sciences – National Institute of the Republic of Serbia, University of Belgrade, P.O. Box 522, 11001, Belgrade, Serbia*

[2]*CEFITEC, Faculdade de Ciências e Tecnologia – Universidade Nova de Lisboa, 2829-516 Caparica, Lisboa, Portugal*

[*]*mirjanamedic@vinca.rs*

Abstract

Within the scope of this paper, a potential impact of noble metal particles on the surface of N-TiO_2 and its catalytic properties is observed through correlation with contamination layer thickness. Owing to 'first principle' approach study, without additional experimental measurements or permanent damage to the surface of the samples, it is possible to obtain significant novel information based on a single measurement of the XPS spectra. Presented research demonstrated how the surface contamination layer in the case of samples based on N-TiO_2 is related to the nature of two studied noble metals, indicating that Pd might serve as an important co-modifier to suppress surface contamination.

Keywords: *X-ray Photoelectron Spectroscopy (XPS); surface structure; surface layers thicknesses; N-TiO_2*

Izvod

Kroz ovaj rad će biti sagledan uticaj čestica plemenitih metala na strukturu površine titanijum dioksida dopiranog azotom i katalitička svojstva kroz uticaj na debljinu sloja nečistoća. U ovakvom pristupu koji polazi od „prvih principa" je bez dodatnih eksperimentalnih merenja i trajnog oštećenja površine uzoraka moguće dobiti značajne nove informacije korišćenjem rezultata jednom izvedenog merenja rendgenskog fotoelektronskog spektra. Dobijeni rezultati ukazuju na to da promene na površini uzoraka na bazi N-TiO_2, do kojih dolazi zbog prisustva Pd, utiču na suzbijanje površinskih organskih nečistoća

Ključne reči: *Фотоелектронска спектроскопија рендгенским зрачењем (XPS); površinska struktura; debljina površinskih slojeva; N-TiO_2*

Introduction

The surface of materials plays a prominent role in heterogeneous catalysis. Oxidation and impurities formed during the synthesis and aging of the materials interfere with the material's functionality, and understanding all the factors that influence catalyst performance is therefore of high significance. In this paper, we consider attractive photocatalytic material, N-doped TiO_2 in order to examine whether the presence of surface deposited Pd and Pt affects the surface structure and, indirectly, its catalytic properties. All the samples presented in this paper have a non-uniform in depth surface structure, which is a characteristic of most samples in general. When we talk about X-ray Photoelectron Spectroscopy (XPS), there are several standard ways of the sample in-depth analysis. A commonly

used procedure is sputter depth profiling i.e. successive ion sputtering and acquiring of spectra [1], which makes a permanent change of the surface structure caused by ion bombardment thus afecting the experimental result. In order to perform analysis without surface damage, the AR–XPS technique can be used, but in practice, there are often limiting factors concerning the size of the sample and the roughness [2]. Non-uniformity of the surfaces, for instance due to long-term air exposure, and the need for detailed information concerning the sample surface motivated us to develop a model for quantitative analysis of in-depth non-uniform surfaces [3]. Here, the major idea was to reexamine the XPS data of N-TiO_2 based samples starting from the 'first principles', in order to reveal the details of the samples surface structure. Potential impact of metal particles on the changed surface structure is observed through correlation with impurity (contamination) layer thickness.

Experimental details

N-doped TiO_2 (N-TiO_2) was prepared via a solvothermal method, using urea (Acros Organics, purity 99%) as the dopant source and titanium(IV) isopropoxide (Acros organics, purity 98%) as titanium source (molar ratio of N/Ti was 10%). Noble metals were deposited at the surface of N-TiO_2 using photoreduction from the solution to reach 0.10wt% of Pt (N-TiO_2/Pt) and 0.05wt% of Pd (N-TiO_2/Pd) in the final samples. The solution was filtered, dried, and finally calcinated at 440 °C for one hour.

XPS analysis was carried out on a SPECS customized UHV surface analysis system with PHOIBOS 100 spectrometer for energy analysis, dual anode Al/Ag monochromatic source, and electron flood gun. XPS spectra were taken using a monochromatic Al Kα line (photon energy of 1486.74 eV) in FAT 40 mode with an energy step of 0.5 eV and dwell time of 0.2 s. The samples, in a powder form, have been supported on a copper adhesive tape and analysed 'as received'.

Experimental results and surface layer thickness calculation

Survey XPS spectra of all investigated samples are presented in Fig. 1, where the most prominent photoelectron lines are denoted. Characteristic O, C and Ti photoelectron lines are clearly visible in each spectra (Fig. 1), as well as the typical Pd photoelectron line (Fig. 1b). The nitrogen N 1s line with very low intensity was also detected during higher energy resolution measurements and a prolonged acquisition time, though not visible in the survey spectrum of each sample. It should be pointed out that the Pt 4f line is overlapping with the inelastic contribution of Ti 3s photoelectron line (Fig. 1c and 1d). The elemental surface compositions of investigated samples, determined from the intensities of the characteristic XPS lines, using the appropriate relative sensitivity factors [4], are given in Table 1.
Different chemical phases present at the surface can be well estimated based on chemical peak shifts of the photoelectron lines. The thickness of the oxide layer can be calculated from the previously proposed compositions of the bulk and oxide phase, using the experimental intensity ratio of the two line contributions [4], as long as all line components can be clearly distinguished. While in the case of the O 1s line of the sample N-TiO_2 (Fig. 1a), there are contributions of Ti-oxides [5] in the samples with Pd and Pt, this line contains additional components originating from these metals. At the same time, samples with photo-deposited Pd or/and Pt have the main photoelectron lines of Pd and Pt with very low intensity (Fig. 1b) that overlaps with other lines (Fig. 1c) or below the detection limit of the XPS instrument (Fig. 1d). Therefore, oxide layer thicknesses calculation wasn’t performed, but an equivalent approach was applied to obtain the contamination layer thicknesses.

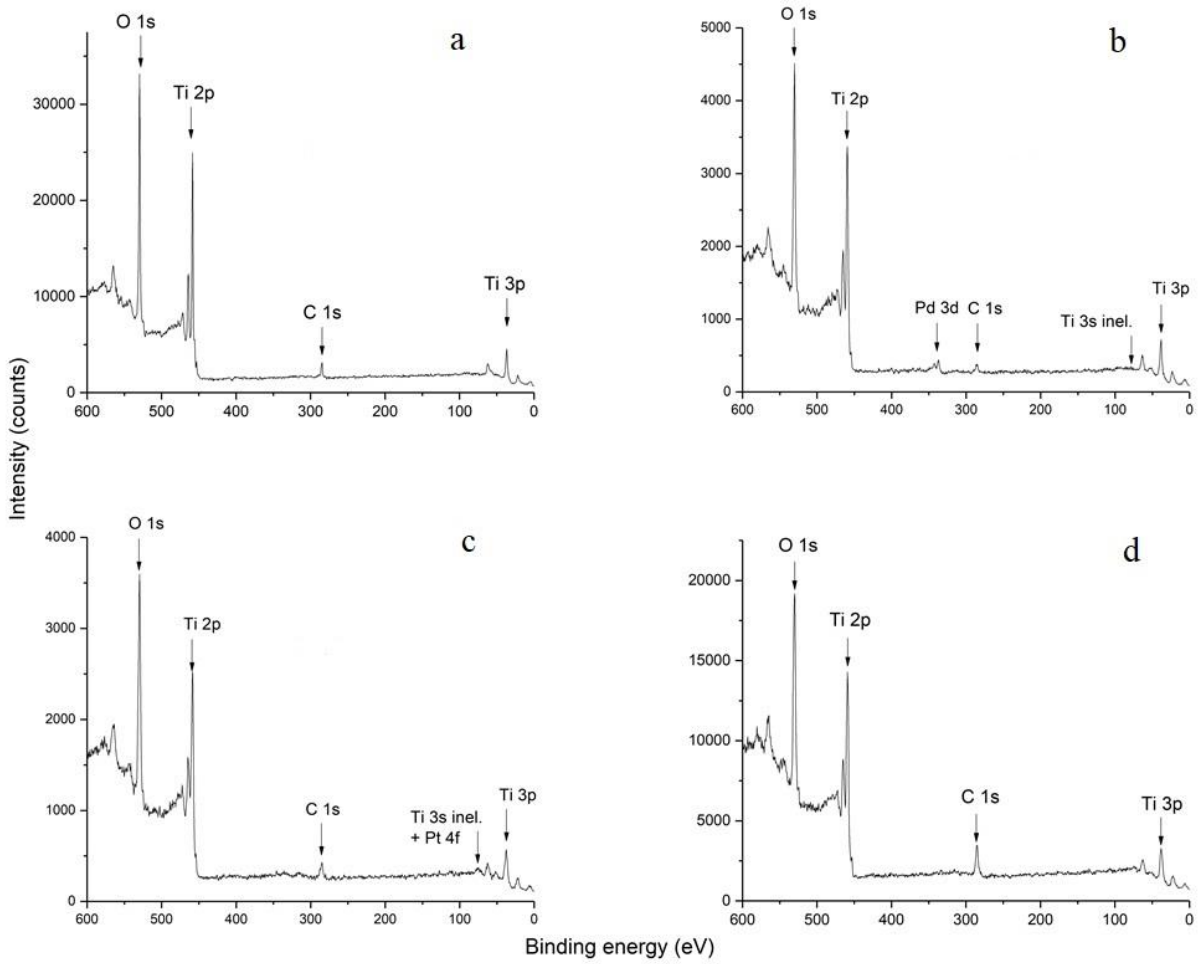

Figure 1. *Survey XPS spectra of as–received samples (a) N-TiO_2, (b) N-TiO_2/Pd, (c) N-TiO_2/Pt, and (d) N-TiO_2/Pd+Pt.*

In the further surface analysis of the tested samples, Ti 2p and Ti 3p lines (see Fig. 1) were selected as representative. The kinetic energies of these lines differ by more than 400 eV, and each has its own relative sensitivity factor, RSF. Since both lines originate from the same element, any of them could be used for quantitative analysis, but the result would be the same only if the surface is free of contamination. The difference between the obtained quantitative results comes from the layer of organic impurities, whose thickness can be determined precisely based on the intensity ratio of these lines. Intensity ratio, I_0(Ti 2p) / I_0(Ti 3p), is equal to the ratio of the corresponding relative sensitivity factors RSF(Ti 2p) / RSF(Ti 3p) only when the sample is homogeneous in depth. When the sample is covered with a contamination layer of thickness d, this ratio will be:

$$\frac{I_m(Ti\ 2p)}{I_m(Ti\ 3p)} = \frac{I_0(Ti\ 2p)}{I_0(Ti\ 3p)} \cdot \frac{A_T(Ti\ 2p)}{A_T(Ti\ 3p)} \qquad (1)$$

where $A_T(I) = \exp(-d/\lambda(I))$ is the corresponding attenuation factor [6] of the organic layer determined by the thickness of the layer *d* and the effective attenuation length λ. It can be easily shown that:

$$d = \frac{ln\left(\frac{I_m(Ti\ 2p)/I_m(Ti\ 3p)}{RSF(Ti\ 2p)/RSF(Ti\ 3p)}\right)}{\left(\frac{1}{\lambda(Ti\ 3p)} - \frac{1}{\lambda(Ti\ 2p)}\right)} \quad (2)$$

It should be noted that the thickness *d* corresponds only to the organic layer of the Ti-containing phase. In Table 1 we present the calculated thicknesses *d* with the composition results obtained using the RSF (i.e. assuming that the samples are uniform), revealing a considerably larger amount of organic impurities is present at the surface of the two samples containing Pt. This could be a consequence of the fact that the Pt on the surface acts as a catalyst for various reactions at the surface, among them also the oxidation of hydrocarbons [7].

Table 1. Surface composition based on relative sensitivity factors (RSF) and contamination layers thicknesses calculated using Equation 2.

Sample	Composition (%)					Contamination layer thickness (nm)
	C	N	O	Ti	Pd/Pt	
N-TiO_2	11.72	1.00	61.28	26.00	-	2.14
N-TiO_2/Pd	6.95	1.01	63.73	27.58	0.72	2.65
N-TiO_2/Pt	15.32	0.48	58.93	23.82	1.46	5.43
N-TiO_2/Pd+Pt	17.42	0.50	57.42	24.48	0.17 (Pt)	3.46

Considering that the matrix in all samples is the same (N-TiO_2), the contamination layer thicknesses are expected to be consistent with the C amount. Thereby, observed variations can be related to the presence of deposited Pt and Pd particles. Platinum creates favorable conditions for hydrocarbons contamination, which is in agreement with the experimentally determined increase in C amount of the N-TiO_2/Pt sample and especially N-TiO_2/Pd+Pt. On the other hand, the presence of Pd seems to 'clean' the surface. It is interesting to look into the differences in C quantity for N-TiO_2/Pt and N-TiO_2/Pd+Pt samples, and relate them to the thickness of the contamination layer. Since the highest amount of C is seen in N-TiO_2/Pd+Pt, where Pt is present in traces, there is a possibility that the hydrocarbons on the surface are laterally non-uniformly distributed. That way, it could be that C accumulates around the Pt and thus attenuates its signal. The small contamination layer thickness of 'only' 3.46 nm on the N-TiO_2 matrix with 17.42% C in the N-TiO_2/Pd+Pt sample, also supports this interpretation.

The main difference in the behavior of Pd and Pt as surface modifiers comes from the charge transfer trend, as shown in earlier DFT studies [8]. Charge transfer is from the surface to Pt, leaving some unoccupied N states near the Fermi level. Contrary, Pd donates charge to the surface, leading to the occupation of the previously empty N states. Therefore, for various molecular species adsorbed at the surface, Pt acts as a charge source. However, regarding the photocatalytic performance in the hydrogen generation reaction, it was shown that a combination of both metals on top of N-TiO_2 outperforms Pt/N-TiO_2 [5]. Our presented research is a certain supplement to these results, demonstrating how the surface contamination layer is also related to the nature of two studied noble metals and indicating that Pd might serve as an important surface co-modifier to reduce surface contamination.

Conclusion

The samples presented in this paper and the great majority of samples, in general, have in-depth non-uniform surface structure, which is especially present after long-term air exposure. Thus, an approach based on the 'first principles' was successfully applied to obtain the thicknesses of contamination layers. The major idea was to reexamine the XPS data of N-TiO2-based samples, in order to reveal the catalytic properties of noble metals and their potential impact on the samples' surface structure. A potential influence is observed through the correlation of surface composition and contamination layer thicknesses. While Pd might be an important co-modifier for reducing surface impurity formation, platinum creates favorable conditions for hydrocarbon contamination.

Acknowledgements

The funding for this research is provided by the Ministry of Science, Technological Development and Innovation of the Republic of Serbia, under Grant. No. 451-03-47/2023-01/200017.

References

1. J. F. Watts and J. Wolstenholme, *An Introduction to Surface Analysis by XPS and AES*,Wiley, 2003.
2. C. J. Powell, A. Jablonski, Progress in quantitative surface analysis by X-ray photoelectron spectroscopy: Current status and perspectives, *J. Electron Spectros. Relat. Phenomena*, **178–179**, 331–346, 2010.
3. N. Bundaleski, I. Radisavljević, N. Ivanović, Z. Rakočević, M. Medić Ilić, N. Romčević, O. M. N. D. Teodoro, Local, electronic and surface structure of multi-component Fe-doped CdTe(S) systems, *Surf. Sci.*, **681**, 76–86, 2019.
4. S. Hofmann, *Auger- and X-Ray Photoelectron Spectroscopy in Materials Science*, Springer, 2013.
5. K. Batalović, N. Bundaleski, J. Radaković, N. Abazović, M. Mitrić, R. A. Silva, M. Savić, J. Belošević-Čavor, Z. Rakočević, C. M. Rangel, Modification of N-doped TiO_2 photocatalysts using noble metals (Pt, Pd) – a combined XPS and DFT study, *Phys.Chem.Chem.Phys.*, **19**, 7062–7071, 2017.
6. C. J. Powell and A. Jablonski, Electron effective attenuation lengths for applications in Auger electron spectroscopy and X-ray photoelectron spectroscopy, *Surf. Interface Anal.*, **33**, 211–229, 2002.
7. M. Taleblou, M. F. Camellone, S. Fabris, S. Piccinin, Oxidation of Gas-Phase and Supported Pt Nanoclusters: An Ab Initio Investigation, *J. Phys. Chem. C*, **126**, 10880–10888, 2022.
8. K. Batalović, J. Radaković, N. Bundaleski, Z. Rakočević, I. Pašti, N. V. Skorodumova, C. M. Rangel, Origin of photocatalytic activity enhancement in Pd/Pt-deposited anatase N-TiO_2 – experimental insights and DFT study of the (001) surface, *Phys. Chem. Chem. Phys.*, **22**, 18536–18547, 2020.

DFT study of MgH_2 and AlH_3 hydrides doped with 3d transition metals

DFT studija MgH_2 i AlH_3 hidrida dopiranih 3d prelaznim metalima

Bojana Paskaš Mamula[1*], Milijana Dragojlović[2], Katarina Batalović[1], Bojana Kuzmanović[1], Mirjana Medić Ilić[1], Nikola Novaković[1]

[1]*Vinča Institute of Nuclear Sciences – National Institute of the Republic of Serbia, University of Belgrade, P.O. Box 522, 11001, Belgrade, Serbia*

[2]*Institute of Occupational Medicine – Military Medical Academy, Crnotravska st. No. 17, 11040 Belgrade, Serbia*

[*]*bpmamula@vin.bg.ac.rs*

Abstract

The electronic structures of lightweight binary hydrides MgH_2 and AlH_3 doped with 3d transition metals (TM=Sc, Ti, Mn, and Cu) were investigated using first-principles calculations. The influence of 3d states of TM was clearly visible from electronic structure calculations. Doping of these systems has a favorable influence on hydrogen desorption energies of both systems, decreasing it in the case of MgH_2 for all TM and increasing it in metastable AlH_3 when doped with Sc and Ti.

Keywords: *MgH_2; AlH_3; transition metal substitution; DFT; Hydrogen energy storage.*

Izvod

Elektronske strukture lakih binarnih hidrida MgH_2 i AlH_3 dopiranih 3d prelaznim metalima (PM=Sc, Ti, Mn i Cu) su ispitane primenom proračuna iz prvih principa. Na osnovu proračuna elektronske strukture jasno je vidljiv uticaj 3d stanja PM. Dopiranje ovih sistema ima povoljan uticaj na energije desorpcije vodonika oba sistema, smanjujući je u slučaju MgH_2 za sve PM i povećavajući je u metastabilnom AlH_3 kada se dopira sa Sc i Ti.

Ključne reči: *MgH_2; AlH_3; Supstitucija prelaznim metalom; DFT; Skladištenje energije vodonika.*

Introduction

Hydrogen has been recognized to have a large potential to be used as a fuel or energy vector. The first step for its practical application is its safe and efficient production and storage. Metal hydrides represent perspective systems for solid state hydrogen energy storage materials [1].

Lightweight binary hydrides MgH_2 and AlH_3, which are the subjects of research in this paper, have high volumetric hydrogen density (110 and 148 g H_2/L, respectively) and a gravimetric hydrogen density that exceeds 7.6% and 10 wt.%, respectively [2, 3]. Employing these systems as successful hydrogen storage materials is still hindered by obstacles concerning hydrogen adsorption/desorption kinetics, cycle life, and reaction thermodynamics of potential material candidates. Several different methods, i.e. nanostructuring by mechanical milling, the addition of transition metals (TM), their oxides and intermetallics can improve thermodynamic and kinetic properties [2, 4, 5]. This paper examines the influence of 3d transition metal substitution in MgH_2 and AlH_3 host matrix through results obtained from electronic structure calculations.

MgH_2 is a stable binary hydride with a rutile crystal structure with high hydrogen desorption temperature (447°C) and slow desorption kinetics. Doping of this hydride with transition metals was extensively studied by many authors [6-8] and a lowering of stability was reported. On the other hand,

α-AlH_3 is metastable at room temperature although the most stable among 8 different polymorphs that exist. In single-step reaction, it releases hydrogen at lower temperatures <100°C but the opposite direction – rehydrogenation is not possible under the same conditions. There are a few studies concerning investigations of the influence of dopants on stability and enhancement of some aspects of AlH_3 [9-11]. In this paper, we have selected to examine transition metals from the beginning (Sc, Ti), middle (Mn) and end of the 3d group (Cu), so we can trace impact of partially filled to almost filled 3d orbitals of TM on MgH_2 and AlH_3 host matrix.

Methods and calculation parameters

The calculations for pure MgH_2 (space group 136: $P4_2/mnm$) and its doped systems were performed using the full potential (linearized) augmented plane waves method with the addition of local orbitals (FP-LAPW+LO) implemented in WIEN2k software package [12]. RMTKmax parameter, which defines the size and completeness of the (L)APW basis set, is chosen to be 7.0 in all cases. The radii of MT-spheres were set to 1.6 bohr for all atoms. The exchange-correlation effects were included within the generalized gradient approximation (GGA). The supercell was constructed from 8 rutile MgH_2 unit cells in the 2x2x2 arrangement having 48 atoms in the primitive cell with one of the 16 Mg atoms substituted with a TM atom (see Fig. 1).

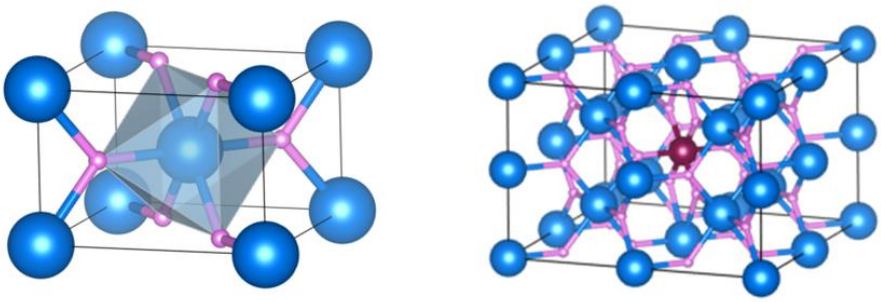

Figure 1. *MgH_2 unit cell (left) and primitive 2x2x2 supercell of MgH_2:TM systems (right).* ***Small pink spheres - H, blue spheres - Mg, maroon sphere - TM.***

Initial parameters for the supercell were obtained after full optimization of rutile MgH_2 unit cell parameters. After the substitution of the Mg atom by TM, relaxation of the structure has been performed by minimizing the forces acting on atoms while keeping the cell parameters fixed. The Brillouin zone sampling was performed using k points in the 3x3x4 arrangement.

The same method discussed previously was used to study the AlH_3 α-polymorph (space group 167: R-3C) and its electronic structure, adjusting the choice of parameters. The parameter RMTKmax was set to 5.00 while the radii of MT-spheres for Al and H were 1.75 bohr and 0.95 bohr, respectively. The sampling of the Brillouin zone was done using a 14×14×14 grid. To study TM substituted systems, supercells were constructed from AlH_3 unit cells in a 2x2x1 arrangement consisting of 96 atoms, with one of the 24 Al atoms replaced by a TM (see Fig. 2).

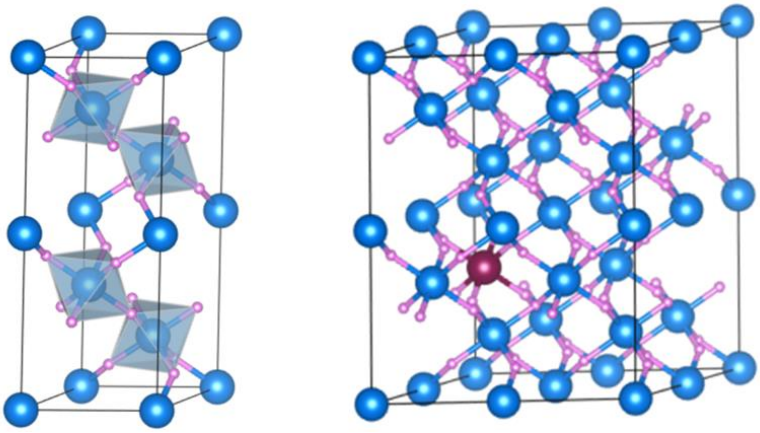

Figure 2. *AlH_3 unit cell (left) and primitive 2x2x1 supercell of AlH_3:TM systems (right)**.** Small pink spheres - H, blue spheres - Al, maroon sphere - TM.*

Due to the large number of atoms in the TM substitution of Al in α-AlH_3 systems, the investigation was done using the program package Quantum ESPRESSO [13]. The choice of this program package considerably reduced computational time for these systems retaining obtained accuracy from previously used software for calculations. Exchange-correlation interactions were treated by GGA of Perdew and Wang (PW91). The Kohn-Sham electronic orbitals are expanded on a plane-wave basis and set up to a kinetic energy cutoff of 37 Ry. The k-point sampling integration over the Brillouin zone is estimated using a 2×2×1 arrangement. Full relaxation of the pure AlH_3 and subsequent relaxation of the nearest dopant environment is done.

Results and discussion

Details of the electronic structure are presented through calculated total and atomic projected densities of states for pure MgH_2 and doped systems in Fig. 4. The first coordination of Mg atom consists of 6 H atoms that form octahedron, four are coplanar H atoms (denoted as H4) and two occupy remaining vertices (denoted as H2).

The most pronounced difference between pure and doped MgH_2 systems stems from narrow, well localized 3d states of the TM impurity. Going from the beginning to the end of the TM series, the charge increases from Sc to Cu, and 3d states shift towards lower energies together with the Fermi level [14]. From the bottom of the conduction band for the nearly empty band of Sc, states shift down to the energy gap for Ti and Mn, and reach the top of the valence band for the almost fully occupied bands of Cu. For Ti, Mn, and Cu two groups of peaks appear indicating crystal field splitting of their 3d states in an octahedral environment of H atoms. In the case of Cu impurity 3d state spreads over a broader energy range in the valence band and the localized peak of hybridized 3d state reaches the top of the valence band. The effects of hybridization and interaction of TM 3d states with the states of surrounding H atoms are visible in the valence band and the gap.

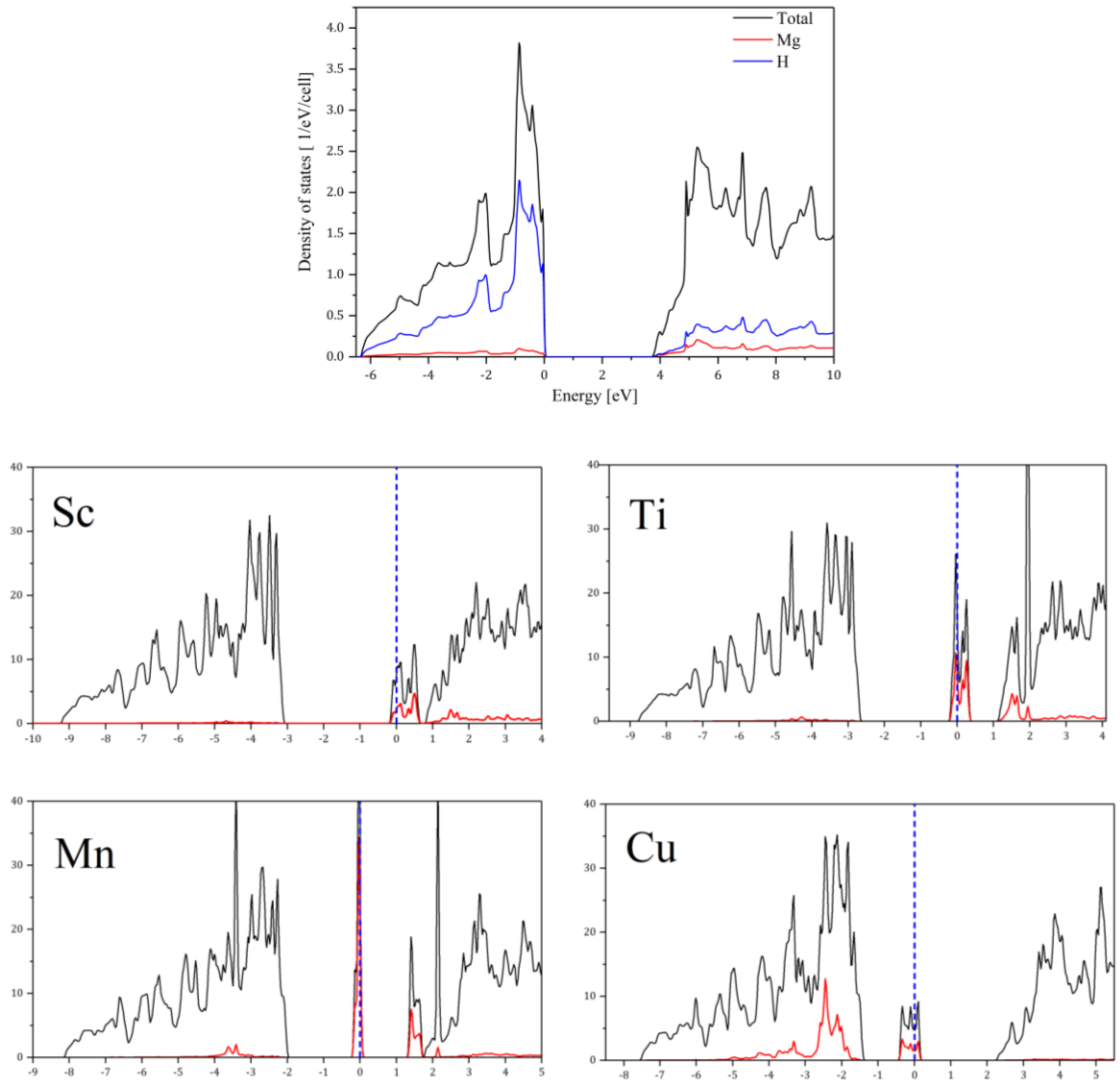

Figure 3. *(top) Total and atomic densities (Mg – blue and H-red) of states of MgH_2. (bottom) Total (black) and TM projected (red) densities of states of MgH_2:TM (TM= Sc, Ti, Mn, Cu). Fermi level is denoted with (blue) dashed vertical line.*

From these results, it is clear that TM impurities make an impact on the MgH_2 host matrix that can be observed on an electronic level (Fig. 3) and verified by calculated hydrogen desorption energies for these systems. The system for practical use as a hydrogen storage medium should have an enthalpy of formation between 20-50 kJ/molH_2 [15] to easily release H_2. In Table 1. desorption energies of pure MgH_2 and doped systems are presented. The observed values indicate that by inserting TM impurity, desorption energies decrease from Sc to Cu. Also, distances between TM and H atoms decrease, except Sc, leading to the assumption that TM from Ti to Cu bond stronger with H atoms from the first coordination and weaken the rest of the MgH_2 matrix.

Table 1. The shortest distances of Mg/TM from H atoms in the first coordination, total electronic energies, and dehydrogenation energies of pure and doped MgH_2. The grey fields refer to the MgH_2 compound, so the corresponding values are the Mg-H2 and Mg-H4 distances. *Experimental values [16]. **Experimental value [17].

TM	TM-H2[Å]	TM-H4[Å]	E[Ryd]	ΔE^{deh}[kJ/molH_2]
Mg	1.959 1.979*	1.944 1.980*	-403.037	71.98 74.06**
Sc	2.013	2.023	-7576.417	70.56
Ti	1.920	1.931	-7755.504	61.88
Mn	1.732	1.727	-8365.082	54.13
Cu	1.781	1.888	-9357.792	51.72

In Fig.4, densities of states for pure and doped AlH_3 are presented. 3d states of TM are present in the valence and conduction band and follow the same trend as in the case of MgH_2. The impact of the TM doping on AlH_3 is also verified in Table 2. by the values of calculated hydrogen desorption energies [18]. In the case of AlH_3 enthalpy of formation is too low, expressing the fact that this is a metastable system. Therefore doping with Sc and Ti rise stability is a favorable route to approach the range of stability for practical application.

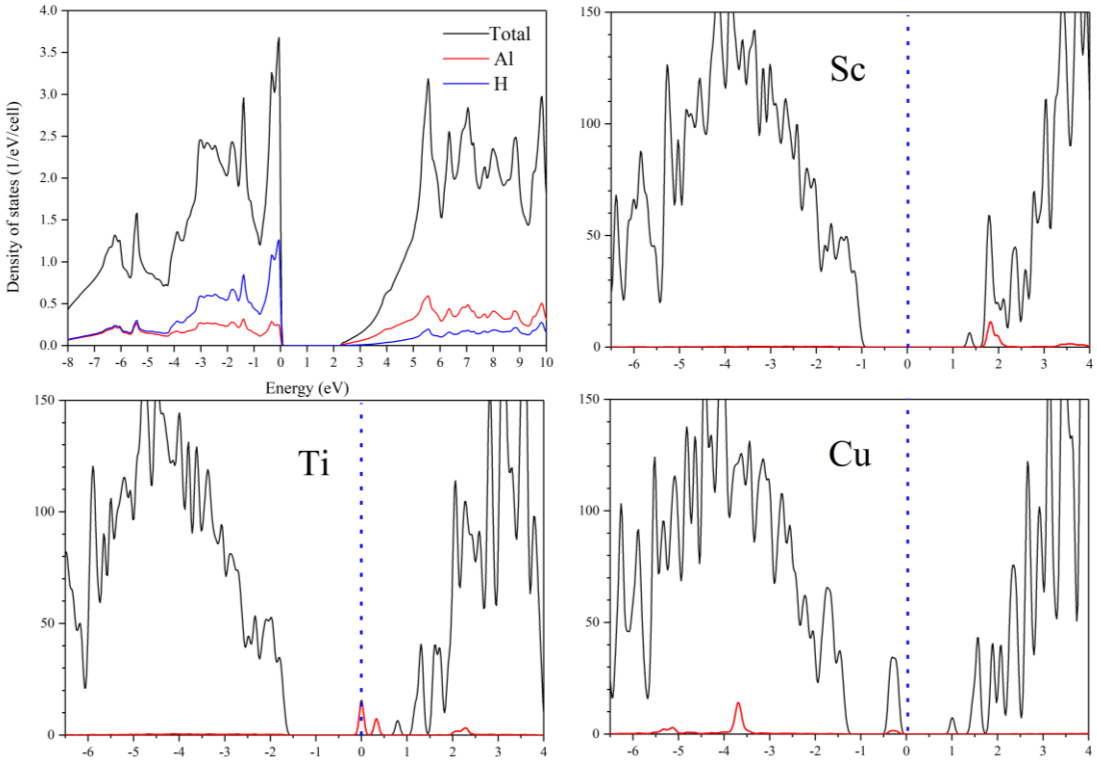

Figure 4. *(top-left)Total and atomic densities(Al –blue and H-red) of states of AlH_3. (top-right and bottom) Total (black) and TM projected (red) densities of states of AlH_3:TM (TM= Sc, Ti, Cu). Fermi level is denoted with (blue) dashed vertical line.*

Table 2. The shortest distances of Al/TM from H atoms in the first coordination, total electronic energies, and dehydrogenation energies of pure and doped AlH_3. The grey fields refer to the AlH_3 compound, so the corresponding values are the Al-H distances. *Experimental values [19]. **Experimental value [20].

TM	TM-H[Å]	E[Ryd]	ΔE^{deh}[kJ/molH_2]
Al*	1.717 1.715*	-489.1444	7.6 7.9**
Sc	1.858	-	14.8
Ti	1.804	-	12.3
Cu	1.646	-	1.4

It can be noted that TM-H distances increase for Sc and Ti-doped systems compared to the pure one, along with hydrogen desorption energy. In the case of Cu, desorption energy is even less than in pure AlH_3, so its influence is not beneficial to the system.

Conclusion

In this paper, we have observed the influence on the stability of 3d transition metal on binary hydrides MgH_2 and AlH_3. Our results obtained from electronic structure calculations imply that doping MgH_2 with TM decreases the stability of this system, making it more suitable for the hydrogen storage medium. Also, when doping AlH_3 with Sc and Ti, desorption energies increase. From these considerations, although these hydrides are opposite cases, doping with 3d transition metals brings them closer to achieving at least condition regarding stability when employing them as hydrogen storage materials.

Acknowledgments

The funding for this research is provided by the Ministry of Science, Technological Development and Innovation of the Republic of Serbia, under Grant. No. 451-03-47/2023-01/200017.

References

1. Boris P. Tarasov, Pavel V. Fursikov, Alexey A. Volodin et al. Metal hydride hydrogen storage and compression systems for energy storage technologies, International Journal of Hydrogen Energy, 46(25), 13647-13657, 2021.
2. Basile Galey, Aline Auroux, Sylviane Sabo-Etienne, et al., Improved hydrogen storage properties of Mg/MgH_2 thanks to the addition of nickel hydride complex precursors, International Journal of Hydrogen Energy, 44(54), 28848-28862, 2019.
3. J. Graetz, J.J. Reilly, V.A. Yartys, J.P. Maehlen, B.M. Bulychev, V.E. Antonov, B.P. Tarasov, I.E. Gabis, Aluminum hydride as a hydrogen and energy storage material: Past, present and future, Journal of Alloys and Compounds, 509(2), S517-S528, 2011.
4. H.Z. Yu, J.H. Dai, Y. Song, Catalytic effect of Ti and Ni on dehydrogenation of AlH_3: A first principles investigation, Applied Surface Science, 347, 139-146, 2015.
5. Liang G, Huot J, Boily S, Van Neste A, Schulz R. Catalytic effect of transition metals on hydrogen sorption in nanocrystalline ball milled MgH_2-Tm (Tm = Ti, V, Mn, Fe and Ni) systems. J Alloys Compd. 292, 247-52, 1999.
6. Dai JH, Song Y, Yang R. Intrinsic mechanisms on enhancement of hydrogen desorption from MgH_2 by (001) surface doping. Int J Hydrogen Energy; 36, 12939-49, 2011.

7. Dai JH, Song Y, Yang R. First principles study on hydrogen desorption from a metal (Al, Ti, Mn, Ni) doped MgH_2 (110) surface. J Phys Chem C; 114, 11328-34, 2010.
8. Er S, Tiwari D, de Wijs GA, Brocks G. Tunable hydrogen storage in magnesium-transition metal compounds: first principles calculations. Phys Rev B; 79(2), 024105-13, 2009.
9. J. Nisar, R. H. Scheicher, X. Peng, R. Ahuja Stability of ferromagnetic phase in Fe-doped AlH_3, EPL 85, 67006, 2009.
10. H. Z. Yu, J. H. Dai, Y. Song, Catalytic effect of Ti and Ni on dehydrogenation of AlH_3: A first principles investigation, Appl. Surf. Sci. 347, 139-146, 2015.
11. J. A. Teprovich, J. Zhang, H. Colón-Mercado, F. Cuevas, B. Peters, S. Greenway, R. Zidan, M Latroche, Li-Driven electrochemical conversion reaction of AlH_3, $LiAlH_4$, and $NaAlH_4$, J. Phys. Chem. C 119(9) 4666–4674, 2015.
12. Blaha P, Schwarz K, Madsen G, Kvasnicka D, Luitz J. WIEN2k, an augmented plane wave þ local orbitals program for calculating crystal properties. Austria: Karlheinz Schwarz, Techn. Universitet Wien; 2001, ISBN 3-9501031-1-2; 2001.
13. P. Giannozzi, S. Baroni, N. Bonini, et al. QUANTUM ESPRESSO: a modular and open-source software project for quantum simulations of materials, J. Phys.: Condens. Matter 21, 395502, 2009.
14. Bojana Paskaš Mamula, Jasmina Grbović Novaković, Ivana Radisavljević, Nenad Ivanović, Nikola Novaković. Electronic structure and charge distribution topology of MgH_2 doped with 3d transition metals. International Journal of Hydrogen Energy 39(11), 5874-5887, 2014.
15. J. Yang, A. Sudik, C. Wolverton, D. J. Siegel, High-capacity hydrogen storage materials: attributes for automotive applications and techniques for materials discovery, Chem. Soc. Rev. 39, 656–675, 2010.
16. F.H. Ellinger, C.E. Holley Jr, B.B. McInteer, D. Pavone, R.M. Potter, E. Staritzky et al. The Preparation and Some Properties of Magnesium Hydride. Journal of the American Chemical Society, 77, 2647-2648, 1955.
17. Crivello, JC., Dam, B., Denys, R.V. et al. Review of magnesium hydride-based materials: development and optimisation. Appl. Phys. A 122, 97, 2016.
18. M. Dragojlović, J.Radaković, K.Batalović, DFT study of crystal structure and electronic properties of metal-doped AlH3 polymorphs, International Journal of Hydrogen Energy 47, 6142-6153, 2022.
19. W. Turley, H.W. Rinn, The crystal structure of aluminum hydride, Inorg. Chem. 8(1), 18–22, 1969.
20. J. Liu, B. Xu, X. Wang, Preparation and thermal properties of aluminum hydride polymorphs, Vacuum 99, 127–134, 2014.

The Life of Humanity on an Environmentally Unstable Planet From the Aspect of Environmental Reality and Development

Božidarka Arsenović

"ORAO" AD for production and overhaul of Bijeljina; Republic of Srpska; Bosnia and Herzegovina

bokijevmejl@gmail.com

Abstract:

The ability of the human species to chart a much better future and move in that direction depends on her ability to accept very complex ideas and to break free from the once paralyzing state of international reality. It is known that sustainable development is an attractive goal that is not at all easy to realize, as well as that sustainable economic well-being requires controlled economic growth, but only on the condition that the depletion of natural resources and the destruction of life are prevented environment. In this sense, the research of the world economic field in the new millennium is approached.

In this regard, the aim of the titled work is to indicate a number of the most important issues from the framework of the conditions of living on an ecologically unstable planet from the aspect of humanitarian reality, given that it is realistic to assume that the next period will result in conflicts and even wars in the struggle for natural resources, in relation to the past times in which wars were fought and conflicts challenged for new ideological dominance and power.

Key words: Sustainable Development; environmental instability; human development

INTRODUCTION

Due to its importance, the first Earth Summit was held in Rio de Janeiro in 1992, and the second summit in Johannesburg in 2002, where the strategy was adopted and the road to good was laid out intentions and great expectations regarding the preservation of the environment. However, obligations and promises to preserve the ecology of the planet, at a time when the number of inhabitants on the planet is increasing they did not significantly improve the conditions and expectations regarding the country's basic ability to expand economic growth while at the same time supporting life [1,2].

The world's population is growing at a rate that threatens that human beings will have less and less food, forests are disappearing as well as fish stocks and the air and water on the planet are becoming more and more polluted, especially given the fact that global warming is increasingly exacerbating these alarming trends. In the postmodern environment, humanity behaves as if it is conducting a global experiment, in which, without sparing use of all natural resources, it produces, buys, uses and throws away trillions of different products (cars, used oil, tires, computers, batteries, plastic, leftover food, fertilizers, worn-out packaging, household appliances and devices...), thus directly affecting the environment and the entire ecosystem of the planet, turning the earth into a hot greenhouse, in which smog, acid rain, ozone hole reign, hazardous waste, waste water, and up to three plant and animal species are almost disappearing per day.

Human civilization is becoming more and more aware that there is no mechanism by which it could erase its previous and current unsustainable behavior towards the environment, which unfortunately often has fatal consequences, and that it must do everything to repair the damage done to the environment and prevent new negative impacts. The importance of environmental problems in the world is shown in table 1.

Table 1. *Importance of environmental problems in the world*

Environmental factors	Regions of the world						
	Africa	**Asia**	**Europe**	**Latin America**	**Northern America**	**West Asia**	**Polar regions**
City and ind. zones	2;B	1;A	1;B	1;A	1;B	1;A	2;D
Drinking water	1;A	1;A	1;B	2;A	1;B	1; A	3;B
Pollution atmosphere	2;B	1;A	1;B	1;A	2;B	2;B	4;B
Degradation land	1;A	1;A	2;B	1;A	3;C	1;A	3;B
Degradation the forest	1;A	1;A	2;B	1;A	3;B	3;A	4;D
Degradation marine zones	2;B	1;A	1;A	2;A	2;B	1;A	3;B
Violation biodiversity	2;A	1;A	2;A	2;A	2;B	2;A	2;B

Conditional tags:
Issues*: 1- critical, 2- important, 3- low priority, 4- irrelevant*
Trends: *A- increasing, B- relatively stable, C- declining, D- unknown*

The impact on the environment is carried out on several levels:
The base of the pyramid is represented by the individual, while the top is the social community in the global sense. The lowest level represents making simple, everyday decisions, such as that to recycle e.g. used can. Moving towards the top of the pyramid, it is observed that decisions adopted at the appropriate level influence decision-making within a higher level. That's it observe the following trends [3]:

- individual decisions are replaced by group ones,
- decisions become increasingly complex and cover a wider range of issues,
- the amount and quality of information needed for decision-making increases,
- short-term decisions evolve into long-term ones.

Decisions at both ends of the pyramid are mutually conditioned. Everyday choices to make on at the individual level, such as – *"Should I recycle this can?"* are based on a global basis decisions made, for example: - *"The global waste problem needs to be solved"*. As can be seen, the information generated at the top of the pyramid is politically oriented. The exits at the bottom of the pyramid, on the other hand, are oriented towards concrete action. There are many such examples that confirm how the cause-and-effect relationship works in practice (CO_2 emissions can be observed at every level of the pyramid).
The world is in a new energy crisis, while, however, we should not forget that the correlation between fuel use and economic development will continue to exist. The main reasons for improving energy efficiency can be seen in the shift towards higher-quality eco-fuels, changes in energy use relationships, where the dominant factor is the eco-quality of energy.
According to the popular theory of limited growth, according to which the world cannot go on indefinitely to increase its production possibilities, it is conditional on its being replaced by a password of sustainability, which specifically underlines that "constraint growth" is a general pattern in global ecology of all relationships and values between organisms and their environment on the planet. So, sustainable development means learning to live according to the pattern and rules in the interest of the country, but not to do so endangers its capital in order to enable the planet to continue

successfully provides general conditions of life that enable the realization of numerous other values such as which are economic and political freedoms or numerous other principles.

ENERGY DEVELOPMENT OF HUMANITY

The end of the 20th and the beginning of the 21st century is characterized by a turbulent development of technical and technological, telecommunication, information technology, space and nuclear development, along with huge pollution and the growth of hazardous waste. The damages, both ecologically and economically, are enormous.

Figure 1. *Inhumane investments – enormous financial resources*

Environmental problems were not given enough attention. With the expansion of the industrial growth enabled the penetration of the social system into the working and living environment. As a consequence Exceeding the endurance limits of the natural system was followed by an ecological flare-up crises. Numerous ecological debates show that the problem of environmental degradation must be solved be observed through a comprehensive treatment of the moral, legal, economic-political and technical-technological levels.

New species and large amounts of energy on the environment implied enormous problems which have been accumulating for the last two centuries. Like any human activity, the activities of the power industry and the oil industry affect the environment. The greatest pollution was recorded in the most industrialized and urban countries, which are the source and driving force of development [4]. The system of environmental degradation and pollution is proportional to the economic level development and industrialization, i.e. there is a clear cause-and-effect relationship between the state and development economy and environment. The second half of the 20th century and the beginning of the 21st century were characterized by accidents, which, due to their unfathomable scale and devastating consequences for humanity and the environment, were included in the category of environmental disasters. Availability and sufficiency of energy, especially oil and its energy acceptable prices resulted in humanity turning towards accelerated development and industrialization, without much thought about the implications for other sectors. Today, as never before, the stability of the ecology of the planet Earth has been disrupted, *"thanks to the activities carried out by the human species"*. This can be *"documented by specific indicators"*, which define the *"health of the planet"*, which is unfortunately deteriorating:

- global holocaust of all animal and plant species,
- destruction and disappearance of forests,
- disappearance of numerous species of fish,
- destruction of coral reefs,
- destabilization of biologically active substances,
- increase in antibiotic-resistant diseases,
- shortage of fresh water sources,
- pollution/contamination of all three resources (air, water, soil),
- the growing danger of chemicals,
- rapid deterioration/decline of biodiversity,
- dependence on pesticides and fertilizers,
- the increase of plant and animal species resistant to pesticides,
- addiction to "unhealthy forms" of energy,
- proliferation of weapons of mass destruction,
- destabilization of global weather patterns.

Throughout the world, there is an increasingly present necessity to respect eco requirements in sustainable development, with the adoption of environmental problems and needs, as key factors for the survival of civilization, as well as highlighting the awareness of human complicity in deterioration, which gives rise to new types of curriculum with ecological value attitudes. Successful application of eco management, i.e. of the concept of sustainable development will enable unhindered industrial growth, environmental quality, health, as well as harmonious life of present and future generations.

LEVEL OF HUMAN DEVELOPMENT AND HUMAN SECURITY

During the 70s of the 20th century, the humanistic dimension of development attracted attention for the first time more significant attention, partly as a response to the growing popularity of the theory at the time dependence [5,6], which was first made official by the statesmen of countries from the Global South, attributing poverty, exploitation, which is a consequence of the dependent relationship of underdeveloped countries in in relation to the so-called countries of the Global Rich North. With this attitude, supporters of the understanding of Fr basic human needs looked for new ways to assess the level of development not relying exclusively on economic findings and indicators, such as average ones personal income in one country, etc. [7].

The Human Development Index (HDI)[1] had the basic task of being used in comparative assessments of countries' ability to ensure the well-being of their inhabitants. HDI, according to the latest definition, has the tendency to include as many aspects of human development as possible in one unique, complex one index and in that way to value and rank achievements in the sphere of human development.

So far, there is no multiple index, or a detailed set of statistical values could accurately and present the degree of progress of human development. However, the human development index, as an assessment procedure, approaches that goal, measuring three dimensions of the development concept, length and health of life, level of education and height standard of living.

Therefore, the human development index is a many times more complex indicator than the index per capita income, because it also has the advantage of directing attention away from material things values on satisfying human needs. However, income is the main goal of human development, but it is not the main indicator of the overall quality of human life. Directing attention to the aspect of

[1]The human development index (HDI) refers to the length of life, literacy, the number of years of average education and the amount of average income in assessing the ability of the person concerned country to ensure the well-being and safety of all its inhabitants (Hoerder, Dirk, 2002)

human well-being, which is many times more comprehensive and wider than average personal income, and understanding income as a condition of a good standard of living, HDI it provides a more comprehensive picture of the quality of human life than just income. So, with this criteria, it is possible to establish a general view of the actual situation to what extent humanitarian aspirations advance or decline. In fact, this index represents value of a country and shows how far the country in question has progressed on the way to maximum possible value, and enables its comparison with other countries. With the help of the HDI, a detailed analysis of the extent to which personal well-being is provided in a country can be carried out. It means that these and other indicators raise more important questions about the relationship between national economic development and human development. Poor people and certain countries must accelerate the development of consumption, but that they do not have to do it in the same way as the rich and economically developed countries of the world do, so that the model of consumption that harms society and accentuates inequalities and poverty can be appropriately suspended or else, changed. The human goals of human development are very different and specific in different countries of the world. Why this is so is one of the most important questions. There we are obliged to analyze and consider several possible explanations. In this sense, it is not out of place to remind that the richest fifth of the planet's humanity, including rich minorities living in poor countries, consumed energy and resources at an enormously high consumption rate, so that providing a similar life for the rest of the population on earth would require resources for four planets large like Earth.

In the desire to reverse these global circumstances, over 180 countries of the world signed agreements on the protection of global resources in Johannesburg. However, there were no significant changes in terms commitment to the continuous development and preservation of the environment that could calm down existing conflicts between financial growth and environmental protection.

Economic and political preconditions of human development

Economic and political preconditions of human development A large number of factors affect the level of realization of humane human rights because the same they represent the basic thread and factor of quality life. Certainly the level of economic well-being and realization of political freedoms associated with the degree of democratic exercise authorities in the state, and the protection of civil rights, represent the basic determinant of human development. Therefore, in a state or region where democracy is realized in action, human rights and human development are also realized.

It is important to recall a number of countries in which democracy and political freedom exist and are realized. By comparing the appropriate criteria with different degrees of economic and political development in countries around the world, with grounded economic development, in which real democracy exists, and human and ecological development, or vice versa, in autocratic systems that do not respect the will of their people, human rights are diminished, human development stagnates and thus, at the same time, environmental protection is also marginalized.

It should be emphasized that in addition *to democracy*, *national and economic development* also contributes to human development and environmental protection, as well as that democracy in itself is not enough, although democratization supports the ecological and economic development of countries. However, in order to achieve the goals of human development that protect basic human rights, strategic ecological prosperity is also important.

Human and ecological development in the age of globalization

One of the basic characteristics of the current time of globalization is rapid transfer of global capital and investments across national borders that integrates the world economy.

The world economy, i.e. the appearance of the so-called a single global economy that transcends and integrates the main economic regions of the world should contribute to overcoming the chronic poverty faced by the majority of the world's population. Today there is a widely accepted notion

globalization as a worldwide process of converging income and lifestyle under the influence of everything
greater international flow of goods, money, capital and people, as powerful unifying factors, which represents greater economic openness of individual countries and parts of the world. That's it globalization is spreading to new regions and to a greater number of underdeveloped countries in the world. On the other hand, critics of globalization hold the view that globalization is to blame for the huge number of the population, the relative poverty of some in relation to others, and that the consequences of globalization will not be removed. Thus, on the other hand, the opponents see globalization as part of the problem and the cause of human misery and suffering, and not as a solution, and that globalization does not bring anything good to those sections of the population that need help the most.
Capital moves faster and more freely around the world, but at the same time it reaches the people and places where it is least abundant. Underdeveloped countries today represent a larger and more heterogeneous group compared to the period after the end of the Second World War, and globalization does not help them become more equal. The fact is that they cannot compete with the richest and that more and more people all over the planet are increasingly exposed to the laws of the global market, that is, most often only as permanent observers, but not participants. This means that the majority of the world's population is falling further and further behind economically.
In addition, we are witnessing the fact that the gap between the poor and the rich is growing, as well as that they pay a high price and promote the enrichment of the richest, and that they are in the process globalization workers marginalized. This brings humanity to numerous controversies around answers to the question *"does globalization bring blessing or misery"*.
In the 21st century, intensive action is needed at all levels - local, national, regional and international in the priority segment of environmental protection. It is realistic to assume that states that regulate the use of global common spaces in the 21st century will have far-reaching consequences for the environment and humanity. A very complex period begins, i.e. a time when ultimately decisions of crucial importance must be made because humanity has reached a critical historical point.

Picture 2. *How to preserve the beauty of this nature*

The path taken will determine the health of the planet for centuries to come. Exactly, because of such high stakes, in all parts, it is certainly a central question population, planet, environmental protection, technology policy and attitudes towards way of life, and this must be done simultaneously through global efforts.

CONCLUSION

Preservation of the environment is a civilizational obligation of mankind. In order to future generations developed and progressed, it is necessary to fundamentally change the attitude towards the environment.

At the center of global, national and ecological security research is man, as the essential subject of the phenomenon of human security. In the context of solving environmental problems, on an ecologically unstable planet, it is necessary to emphasize sustainable development as the most complex model, expressed through the "ecological paradigm", as a new philosophy of life, work and progress.

The ecological paradigm represents the strategy of the socio-ecological optimum, the basis of which *is the balance between man, society and nature*. It provides civilization with a roadmap for the transition from traditional, industrial to postmodern society through all segments of international politics.

LITERATURE

1. Allen, T. David.; Shonnard, R. David: Green engineering, Designing chemical processes with environmental awareness, PMF Sarajevo, 2009.
2. Aleksić S., Rakić R., Biočanin R. Energy efficiency in the function of preserving the quality of life middle, VIII Symposium *"MODERN TECHNOLOGIES AND ECONOMIC DEVELOPMENT"*, Leskovac, 2009.
3. Broadhead, Lee-Anne, International Environmental Politics: The Limits of Green diplomacy,Boulder, Colo: Lynne Rienner, 2003.
4. Biočanin R. Energy (in) efficiency in conditions globalization sustainable development, International scientific meeting *"RENEWABLE ENERGY SOURCES AND SUSTAINABLE DEVELOPMENT";* Banja Luka, 2011.
5. Bodiroža, Mladen, International Economics, International University of Travnik in Travnik, Faculty of Economics, 2012.
6. Hoerder, Dirk, Culturesd in Contact: *World Migrations in the Second Millenium*, Durham, N.C.: Duke University Press, 2002.
7. Klare, T. Michael, *Resource Wars: The New landscape of Global Conflict*, New York: Holtzbrinck Academie, 2002.

Procedures for preventing corrosion of welded joints

Procedure za sprečavanje korozije zavarenih spojeva

Srđan Bulatović[1*],Vujadin Aleksić[1], Bojana Zečević[2], Ognjen Ristić[1], Ana Maksimović[2]

[1] *Institute for testing of materials, Bulevar vojvode Mišića 43, Belgrade, Serbia*

[2] *Innovation Centre, Faculty of Technology and Metallurgy, Karnegijeva 4, Belgrade, Serbia*

[*] *srdjan.bulatovic@institutims.rs*

Abstract

This paper describes the procedures for preventing corrosion of welded joints. Also, a theoretical overview of the forms of corrosion that are most prevalent in welded joints is presented.
The concept of corrosion in welded joints is very pronounced in real conditions. Welded joints are inseparable joints that form an integral part of steel welded constructions. The internal energy increases during the fusion welding especially in the heat affected places around the welded joint, which become initiating spot of corrosion degradation. That is why it is of vital importance to focus on ways to increase the resistance of welded structures to the impact of corrosion.
Keywords: *corrosion, welded joints, corrosion resistance*

Izvod

U ovom radu opisane su procedure za sprečavanje pojave korozije zavarenih spojeva. Takođe, prikazan je teoretski osvrt na oblike korozije koje su najzastupljenije kod zavarenih spojeva.
Koncept korozije u zavarenim spojevima je veoma izražen u realnim uslovima. Zavareni spojevi su nerastavljivi spojevi koji čine sastavni deo čeličnih zavarenih konstrukcija. Unutrašnja energija se povećava tokom zavarivanja topljenjem, posebno na mestima pogođenim toplotom oko zavarenog spoja, koja postaju inicijalna tačka degradacije korozije. Zato je od velikog značaja posvetiti se načinima za povećanje otpornosti zavarenih konstrukcija na uticaj od korozije.
Ključne reči: *korozija, zavareni spojevi, koroziona otpornost*

Introduction

Looking around, corrosion can be seen everywhere. Its formation is a consequence of natural chemical processes of decomposition of various materials. Protection of materials from corrosion is most important in its initial phase (production phase), because prevention of potential damage is significantly more profitable than possible reparation. Since it is not possible to completely protect materials from corrosion, it is also important to restore and protect them when corrosion occurs. Corrosion is basically a physical-chemical interaction between the material and the environment, and it can be defined in several ways. The impact of corrosion is most often reflected in the erosion and destruction of the surface, whereby the properties of the material change, which leads to a weakening of the load-bearing capacity and functionality of the structure, that is, permanent damage to the function of the metal and the associated construction.
The effect of corrosion in welded joints is very prevalent in exploitation, because in the welded joint itself there are several zones that are susceptible to corrosion, that is, the separation of phases along the grain boundaries. As a result of welding, the base metal is overheated in the immediate vicinity of the weld metal, which causes chemical and structural changes in the crystal lattice in the overheated zone. Structural heterogeneity is a frequent cause of the local occurrence of various types of corrosion in a welded joint [1,2].
Corrosion processes are classified differently for identification of corrosion mechanisms and for preventing corrosion with appropriate corrosion protection agents as well as for predicting the

corrosion behavior of metallic materials under operating conditions. Therefore, according to the above, corrosion processes are divided according to the mechanism of action, according to the geometry of corrosion damage and according to corrosive environments [3].

Types of corrosion

According to the mechanism of process, corrosion is divided into two basic forms/types: chemical and electrochemical corrosion. Chemical corrosion occurs in non-electrolytes, while for electrochemical corrosion an electrolyte is necessary and occurs on metals, welded joints of metals and alloys, where the processes of oxidation-releasing electrons and reduction-receiving electrons take place. Electrochemical corrosion is very widespread because a large number of metal welded structures and plants are exposed to water, moist soil or humid atmosphere, for example ship structures. Seawater is the electrolyte that attacks the welded joint and causes problems and ship damage [3].

In the types of corrosion according to the geometry of corrosion damage, the most common is general corrosion, which is the most widespread and least dangerous form of corrosion because it includes the entire metal surface together with its welded joints and it is possible to predict the service life of the welded structure. General corrosion is characterized by a uniform reduction in the thickness of the metal and represents the depth of penetration into the metal over a certain period of time [1].

Also, in the types mentioned above includes galvanic corrosion and corrosion in the crevice. Galvanic corrosion represents electrochemical corrosion between two or more different metals with the presence of an electrolyte and a potential difference between the metals in contact. For contact corrosion to occur, it is necessary that there is a sufficient potential difference between the metals in contact. If the potential difference is higher, contact corrosion is more intense. Galvanic corrosion is often present in welded joints when the composition of the additional metal is different from the composition of the base metal due to the difference in electrochemical potentials. It is most common due to the reparation of HSLA steel because fusible electrodes made of austenitic stainless steel are used. This process brings the stainless steel, which behaves cathodically, into electrical contact with the HSLA steel. In the presence of a corrosive environment, hydrogen is formed on stainless steel, which causes the cracks initiation of HAZ HSLA steel. The difference in temperature coefficients of expansion of ferrite and austenite causes internal stresses in the welded joint, which can cause cracks [4,5].

Crevice corrosion-this type of corrosion occurs in crevices that are large enough for the liquid to penetrate and at the same time the crevices are small enough for the liquid to remain in them. The very appearance of this corrosion is related to the production technology and the design of the structure itself. It is most common in stainless steels that are found in still and slow-flowing seawater [6].

Pitting corrosion, in Figure 1, is present in stainless steels that are in water or an aggressive environment by forming pits [3]. It is especially prevalent in ships because their large surface area is in the water. This corrosion occurs in a local area of the metal surface and the remaining areas are not corroded or are slightly corroded.

In the case of welded joints, pits are often formed in places with a certain microstructure, that is, in places of metallurgical heterogeneity of the metal [4]. Chromium-depleted areas that form when austenitic stainless steel is heated to the sensitization temperature are susceptible to pitting. Pits can also form at austenite-ferrite phase boundaries in stainless steel welds.

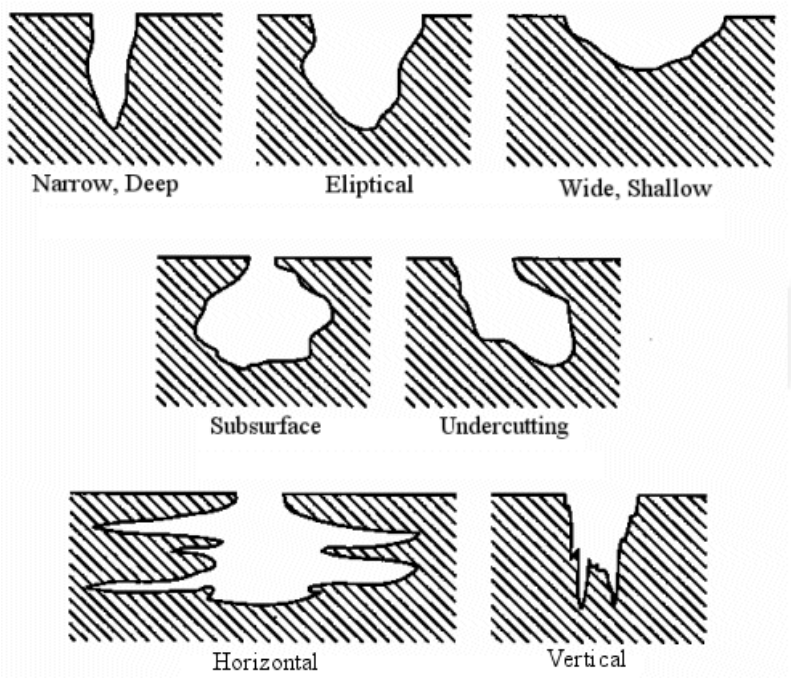

Figure 1. *Pitting corrosion according ASTM-G46 standard*

Stress corrosion and Hydrogen embrittlement

Along with the release of hydrogen at the top of the crack as a product of corrosion reactions, crack growth is accompanied by the process of local hydrogen embrittlement. At cracks, during welding, machining and places where inclusions disrupt the homogeneity of the surface, pitting corrosion occurs, Figure 2. It usually occurs in aqueous environments with the presence of ions that cause the fracture of alloys and stainless steels. Due to the influence of high voltages, welded metal joints can be exposed to stress corrosion. Residual stresses are proportional to the size of the weld metal, which directly depends on the heat input during welding. By means of heat treatment after welding and by making the weld metal smaller in size, stress corrosion cracking can be reduced [7]. Stress corrosion testing at a low tensile rate is performed by slowly increasing the load or strain. Samples that are in contact with a corrosive medium are tightened in a tear machine. The method is qualitative and is also used to determine the relative susceptibility of alloys and welded joints to stress corrosion. Its advantage is in the speed of obtaining results, the examination of one sample lasts from several hours to several days.

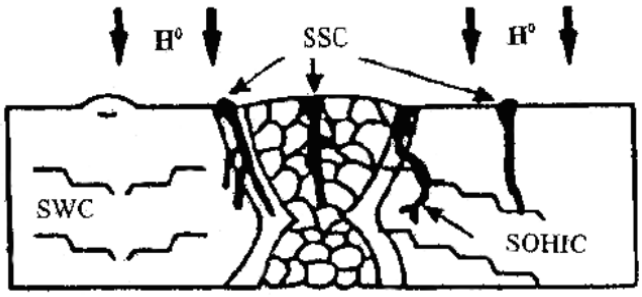

Figure 2. *Stress corrosion and Hydrogen embrittlement [7]*

Procedures for preventing corrosion of welded joints

Choosing the most fitting material and choosing the best construction solution of the machine part is one of the prior elements of anticorrosion protection of not only welded constructions. Further criterion of anticorrosion protection is the appropriate anticorrosion coating applied on the base material. There are distinguished two kinds of anticorrosion protections: organic and inorganic. The protective principle of organic coatings is to eliminate air humidity from the access to the base material. The quality of such a barrier is affected by many external factors. Inorganic coatings consist in nobleness of passivating metals comparing to the base material [8].
In general, there are several procedures to prevent corrosion of welded joints:
Correct choice of base metal and additional material-Careful selection of base metal and fusible electrode can reduce differences in the composition of the welded joint, that is, reduce the risk of galvanic corrosion.
Surface preparation-A properly selected surface cleaning procedure can reduce the occurrence of defects, which are often sites of corrosion attack in aggressive environments.
Weld Design-The weld metal should be low profile, with straight edges to prevent slag retention on the surface. An improperly designed welded joint can cause gaps in which electrolyte is retained, forming pits and corrosion in the crevice. Irregular shape of the weld metal can cause turbulent fluid flow in the pipes, i.e. the appearance of erosion corrosion.
Welding process-During welding, it is necessary to achieve a complete penetration, in order not to create a crevice under the weld metal. In multi-pass welding, slag should be removed after each pass. If welding under powder, the geometry of the welded joint must allow the removal of the powder because some of its constituents may be hydrophilic or corrosive.
Surface treatment of the welded joint-The best resistance to corrosion is achieved if the surface of the weld metal is smooth, evenly oxidized, without impurities. The roughness of the weld metal is usually reduced by subsequent grinding.
Protective surface coatings-When the difference in the composition of the welded joint can cause local corrosion, it is necessary to apply protective coatings. The protective coating should cover the weld metal and the base metal. Special surface preparation is necessary for applying protective coatings.
Heat Treatment-Post-weld heat treatment is often an effective way to increase the corrosion resistance of a welded joint. Thermal treatment achieves a reduction of internal stresses, which affect the growth of stress-corrosion cracks. Subsequent heat treatment (annealing) facilitates the removal of hydrogen from the welded joint and reduces the risk of hydrogen embrittlement. Subsequent heat treatment can also reduce differences in composition, which prevents the formation of microgalvanic couplings.
Preheating and intermediate heating-Application of preheating and intermediate heating can prevent hydrogen embrittlement of carbon and low alloy steels. Preventing gap formation. Proper selection of additional material, welding procedure and careful removal of slag after welding can avoid formation of gaps, i.e. local corrosion.
Removing the source of hydrogen-By carefully choosing a fusible electrode with a coating, drying it, as well as eliminating impurities and moisture from the surfaces to be welded, the risk of the appearance of hydrogen, i.e. hydrogen embrittlement (cold cracks), can be significantly reduced.

Increasing the resistance of welded joints from the aspect of corrosion

Figure 3 shows some of the characteristic forms of corrosion destruction of welded structures. For each form, there are procedures for assessing corrosion resistance as well as specific corrosion indicators [9].

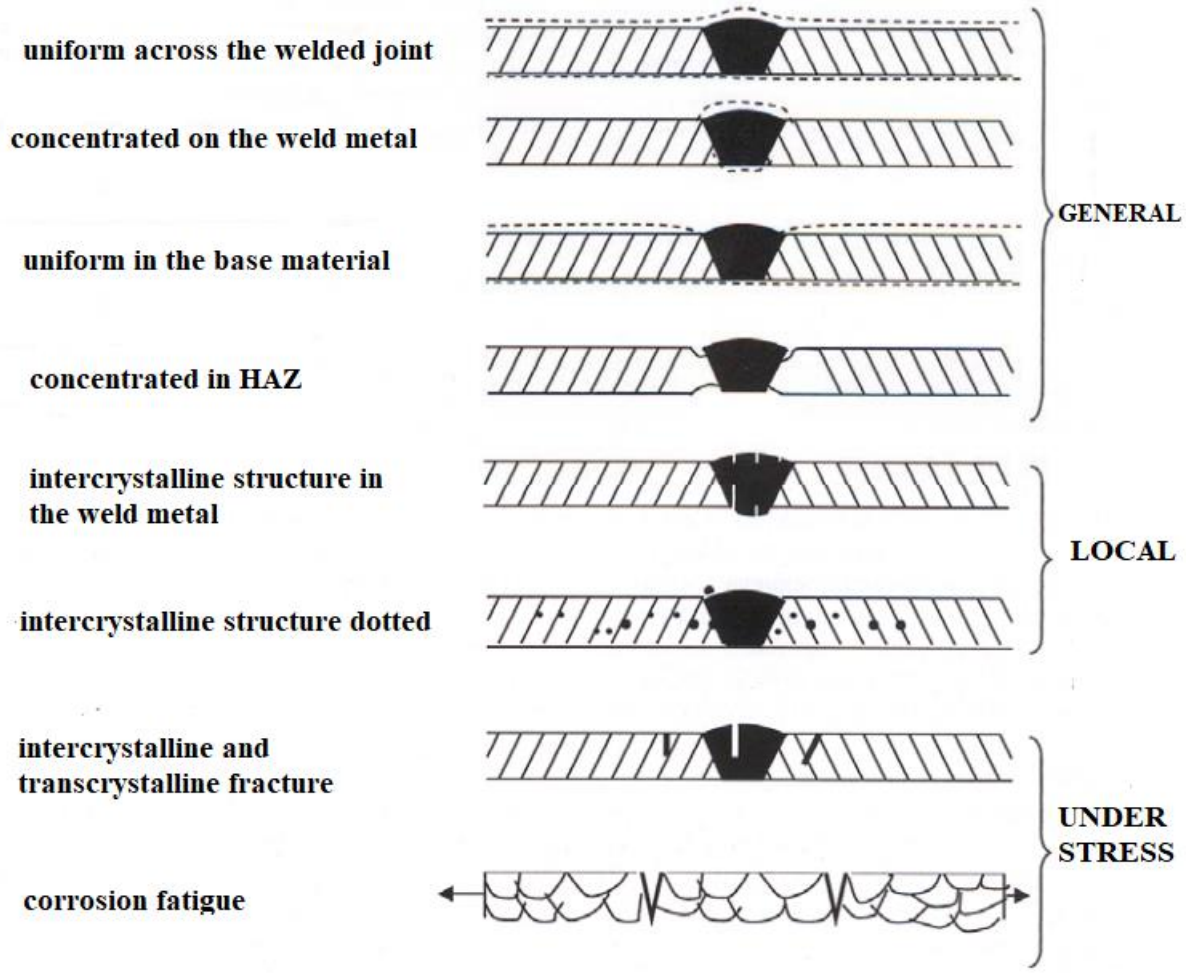

Figure 3. *Characteristic forms of corrosion destruction of welded structures [9,10]*

If the corrosion develops uniformly, the rate of destruction can be taken into account and the life of the structure can be determined in advance. This form of corrosion destruction is characteristic of most welded constructions made of structural steel in practice under ordinary conditions of exploitation, and refers to atmospheric corrosion, which mostly depends on meteorological conditions. it should be emphasized that it is very dangerous to concentrate general corrosion at the seam or in the heat-affected zone, which can lead to very quick destruction of the structure with relatively small mass losses.

Special forms of local corrosion are characteristic of welded joints of high-alloy steels and non-ferrous metal alloys. Spot corrosion is typical for electrochemically passive materials (chromium, aluminum, chrome-nickel steels).

Corrosion of welded joints due to the effect of stress is among the most dangerous in practice. During the hardening of the welded joint, high level residual stresses appear, which are often the cause of stress corrosion and corrosion fatigue. Due to stress, the speed of general metal corrosion increases in acidic environments, and very little in neutral ones. Stresses have little effect on general but increase local corrosion.

The resistance of welded structures against corrosion can be increased by various methods/procedures, divided into two methods [11]:

- reduction of chemical and structural inhomogeneity (choice of optimal composition and heat treatment of the base material before welding, selection of additional materials and construction of the welded joint with the aim of regulating the chemical composition of the material, regulation of the thermal cycle of welding and crystallization conditions, heat treatment after welding).

- improvement of the stress state (reduction of the stress value, regulation of the thermal cycle, no defects in the weld metal, removal of residual stresses).

Conclusion

Along with a brief review of the main divisions of corrosion in welded joints, the paper defines procedures for preventing corrosion of welded joints, by applying which we can ensure the integrity and life of welded structures. By reducing the inhomogeneity of the welded joint itself and less heat input in the welding zone, the service life of the welded structure is also extended and their reliability is increased. As a proposal for further research, it is necessary to emphasize the improvement of procedures for preventing corrosion and improving the resistance of welded joints to corrosion through the education of professional staff.

Acknowledgements

This research is supported by the Ministry of Education, Science and Technological Development of the Republic of Serbia (Contract No. 451-03-47/2023-01/ 200012).

References

1. B. V. Jegdić, B. M. Bobić, Corrosion of welded joints, *Structural integrity and life*, 7(2), 101-104, 2007.
2. A. Sedmak, V. Šijački-Žeravčić, A. Milosavljević, V. Đorđević, M. Vukićević, Mašinski materijali, drugi deo, Mašinski fakultet, Beograd, 2000.
3. K. Brzić, *Korozija i zaštita potonulih brodova*, Završni rad, Sveučilište u Zagrebu, Fakultet kemijskog inženjerstva i tehnologije, 2022.
4. A.Wahid, D.L. Olson, D.K. Matlock, Corrosion of Weldments, ASM Handbook, Welding, Brazing and Soldering, Ohio, 6, 1065-1069, 1997.
5. K.F. Krysiak, Corrosion of Weldments, ASM Handbook, Corrosion, Ohio, 13, 344-368, 1998.
6. K.A. Chandler, Marine and Offshore Corrosion, Butterworths, London, 1985.
7. R.H. Jones, Stress Corrosion Cracking, ASM Handbook, Corrosion, Ohio, 13, 145-163, 1998.
8. J. Votava, Protection of welded joints against corrosion degradation, *Acta universitatis Agriculturae et Silviculturae Mendelianae Brunensis*, **61(6)**, 1897-1904, 2013.
9. D. Seferijan, Metalurgija zavarivanja, prevod s francuskog, Građevinska knjiga, Beograd, 1979.
10. J. H. Garrett, The Action of weter on Lead, K.H. Lewis, London, 1991.
11. B.B. Pejović, M.V. Tomić, V.M. Mićić, M.G. Pavlović, O nekim načinima za povećanje otpornosti zavarenih konstrukcija sa aspekta korozionih razaranja, Zaštita materijala, 48(2), 11-16, 2007.

The Finite Element Method in the function of corrosion damage assessment of pipelines

Metoda konačnih elemenata u funkciji procene korozionog oštećenja cevovoda

Vujadin Aleksić[1*], Bojana Zečević[2], Srđan Bulatović[1], Ana Maksimović[2], Ljubica Milović[3]

[1]*Institute for testing of materials-IMS Institute, Bulevar vojvode Mišića 43, Belgrade, Serbia*

[2]*Innovation Centre of the Faculty of Technology and Metallurgy, Karnegijeva 4, Belgrade, Serbia*

[3]*University of Belgrade, Faculty of Technology and Metallurgy, Karnegijeva 4, Belgrade, Serbia*

[*]*vujadin.aleksic@institutims.rs*

Abstract

Pipelines, with specifics in design, construction, testing and safety requirements must be designed based on all relevant influences to ensure that they are safe during their working life. Allowable stresses must be limited by possible errors in working conditions, in order to completely eliminate the uncertainty arising from the production, the calculation model, the actual working conditions and the characteristics and behavior of the material. In the paper, on the example of modeling and calculation of the corrosion-damaged structure of the ammonia (NH3) transfer pipeline, a methodological approach to the calculation using the Finite Element Method (FEM), is shown, in accordance with the methods defined by the new and general approach to standardization and technical harmonization for pressure equipment (Pressure Equipment Directive - PED 97/23 EC). The paper uses advanced modeling techniques of corroded surfaces, based on FEM, with the aim of developing a procedure for assessing the residual strength of steel pipelines operating in the environmental conditions of the chemical products industry. The presentation of possible damages and consequences caused by the corrosion of steel pipelines in the chemical products industry is also given, and the possibility of taking measures to prevent such occurrences is discussed.

Keywords: *pipeline; corrosion-damage; measurement; corrosion assessment; FEM*

Izvod

Cevovodi, sa specifičnostima u projektovanju, izradi, ispitivanju i zahtevima u pogledu bezbednosti mora da budu projektovani na osnovu svih relevantnih uticaja kako bi se obezbedilo da budu bezbedni tokom radnog veka. Dozvoljena naprezanja moraju biti ograničena mogućim greškama u radnim uslovima, kako bi se potpuno eliminisala neizvesnost koja nastaje od proizvodnje, modela proračuna, stvarnih radnih uslova i karakteristika i ponašanja materijala. U radu je na primeru modeliranja i proračuna korozijom oštećene strukture cevovoda za pretakanje amonijaka (NH_3) prikazan metodološki pristup proračunu Metodom Konačnih Elemenata (MKE), a u saglasnosti sa metodama definisanim novim i opštim pristupom standardizaciji i tehničkom usaglašavanju za opremu pod pritiskom (Pressure Equipment Directive – PED 97/23 EC). U radu se koriste napredne tehnike modeliranja korodiranih površina, bazirane na MKE, sa ciljem razvoja procedure za procenu preostale čvrstoće čeličnih cevovoda koji rade u uslovima sredine industrije hemijskih proizvoda. Takođe je dat i prikaz mogućih oštećenja i posledica izazvanih korozijom čeličnih cevovoda u industriji hemijskih proizvoda, a razmotrena je i mogućnost preduzimanja mera da se takve pojave preventivno spreče.

Ključne reči: *cevovod; koroziono oštećenje; merenje; procena korozije; MKE*

Introduction

The steel pipelines of the chemical industry in Serbia are in a very bad condition due to irregular maintenance. Due to neglect, most of the steel pipelines need to be recovery due to significant corrosion damage. Before recovery, it is necessary to carry out a visual inspection and tests using non-destructive methods. Based on the obtained test results, it is necessary to make a report on the current state of the corrosion-damaged steel structure of the pipeline, and then begin the rehabilitation. The construction of steel pipelines depends on the working fluid for transport (flowing), working pressure and temperature, as well as operating conditions and working environment. Figure 1 shows constructions of steel spherical tanks and pipelines for pouring and filling in the chemical industry.

(a) spherical tanks *b) pipelines for streaming and filling*

Figure 1. *Steel constructions of spherical tanks and pipelines in the chemical industry are daily exposed to external and internal corrosion [1]*

Corrosion of steel pipeline elements in the chemical industry

Despite numerous protection methods due to the harsh environmental conditions in the chemical industry, corrosion of steel pipelines is inevitable. It occurs in different forms such as general corrosion with equal loss of wall thickness or pitting corrosion corresponding to a local reduction in wall thickness. In practice, it happens that the steel embedded in the pipeline corrodes partially or completely, reducing the cross-section and thus the load-bearing capacity of the structure. In more severe cases, an accident can occur with catastrophic consequences for production, facilities, means of production, devices and human lives. Such accidents result in pollution and harmful effects on flora and fauna, air, watercourses and groundwater. Drastic examples of corrosion degradation of steel pipeline structures in the chemical industry are shown in the photographs of Figure 2.

Figure 2. *Examples of corrosion damage to pipeline steel structures [1, 2]*

Corrosion manifests itself in the following way: the appearance of cracks, a decrease in strength, the appearance of swelling and loss of mass, corrosion spots and a weakening of the cross-section. Visual signs of destruction are: erosion, peeling and crumbling, crushing, softening, cracking, crystallization, appearance of "popcorn". Spot corrosion on parts of the structure that are exposed to tension is

particularly dangerous. Due to the reduction of the cross-section and the high degree of stress, occasional damage can lead to the formation of cracks and stress concentration [3].
The direct and indirect costs caused by corrosion in the chemical industry are enormous. In the USA, the total annual direct costs of corrosion in this industrial area are estimated at 1.7 billion dollars, which is about 8 percent of the total capital costs [4]. No calculations have been made of the indirect costs of stopping production due to failure or catastrophic destruction, but it is estimated that they are several times higher.

Characteristics of the corrosion environment in the assessment of corrosion damage of steel pipelines

The durability of steel for pipelines in the chemical industry depends on the characteristics of the corrosive environment and the ability to resist internal and external influences, the character and intensity of which depend on the conditions of exploitation of steel pipelines. The internal influence is reflected through the purpose and type of fluid in steel pipelines, which can be of different aggressiveness, toxicity and explosiveness, of different pressures, temperatures and flows. The external influence depends on the type, composition and temperature of the waste gases and air surrounding the objects in question, the speed, flow and pressure of the gases, as well as the powdery substances in the gas stream.
External influences also include: the chemical effect of water - the environment and substances dissolved in it, the alternating effect of temperature changes (which leads to expansion changes on steel), alternating wetting and drying of steel and the action of dissolved salts in contaminated water. The emission of harmful substances, which are almost always present in the surrounding atmosphere of the chemical industry, has a major impact. It contains gases O2, CO, CO2, SO2, NO, NO2, NOx, H2S, water vapor, as well as particles of solid substances such as KCl, K2SO4, (NH4)2SO4, CO(NH2)2. and others Also, the composition of waste gases and solid substances, their speed, flow and increased concentration affect the rate of corrosion and erosion of steel pipelines.

Production of steel pipelines

For the construction of steel pipelines, pipes of appropriate diameter and wall thickness are used, as well as various profiles in some of the qualities of general and fine-grained structural steel.
Steel pipelines made of steel elements require precision, great attention, trained and professional workforce during production. They are made by welding or joining pipe flanges of appropriate quality. They are equipped with appropriate equipment such as manometers, level gauges, safety valves, filling, emptying and overflowing valves, etc.
Depending on the aggressiveness of the transported fluid, steel pipelines are exposed to internal corrosion, that is, depending on the environmental conditions and the effect of external corrosion.
The side of steel pipelines that faces the sources of emissions of harmful substances, supported by air flow from that direction, is more exposed to corrosion due to the direct application of harmful substances to the structure of the steel pipeline. When there is poor air circulation, steel pipelines can be exposed to constant moisture, which, together with the emission of harmful substances, can be disastrous for the construction.

Testing and control using non-destructive methods

Steel pipelines in the chemical industry are subject to inspection, which means that before use they must be properly inspected in order to obtain a work permit. During exploitation, legally prescribed controls are also carried out in order to ensure safe and reliable operation of steel pipelines [3, 5].
All defects, whether built in or caused during the explosion, are examined in a certain period of time, which gives a realistic insight into the possible progression of damage, which directly affects the

reduction of the number of breakdowns and the planning of plant downtime, and thus a significant reduction total costs.
In order to avoid defects and ensure safe operation, corrosion should be detected, measured and assessed for the remaining strength of the corroded surface of the element and, based on the assessment, appropriate measures should be taken in order to eliminate harmful consequences and preserve the environment.
Before the inspection, it is necessary to familiarize yourself with the technical documentation of the steel structure of the pipeline in detail and to determine the critical elements and places that should be paid particular attention to during the inspection.
Control and tests should be documented with sketches and photographs for repeatability of tests and updating of files, i.e. the "passport" of the steel pipeline.
In order to assess the residual strength of corroded elements of steel pipelines using one of the existing methods, it is necessary to accurately measure the corrosion defect. The ultrasonic method with associated devices is currently the most widely used for testing corrosion damage on steel pipelines.
Test and control results are processed manually or automatically using computer programs. The programs can work in such a way that we provide them with data collected by the classic method of measuring the maximum depth of corrosion (that is, the minimum thickness of the pipe wall) or the program is integrated with a measuring instrument that scans the tested surface, and compares the obtained results with the standard prescribed acceptance criteria. As a result, we obtain, by classical calculation or automatically, the remaining strength of the tested steel pipeline, and based on it we determine the maximum permissible working pressure.

Methods for assessing corrosion damage of steel pipelines

There are various methods used to assess the residual strength of corroded pipes. Some of them are very simple and rely only on the length and depth of the fault, while others are much more complicated, based on finite element modeling (FEM).
ASME B31G [3] is one of the most widely accepted solutions for assessing corrosion damage in steel pipelines. The improvement of the method [6, 7] was achieved by introducing the damage factor, material load, detailed consideration of the form of damage using calculations. This method is included in the program known as RSTRENG (Remaining Strength of Corroded Pipe). ASME B31G and RSTRENG have found wide application in the assessment of corrosion damage of steel pipelines in industry.
The presented methods enable the assessment of longitudinally oriented corrosion defects. The role of transversely propagated faults is usually denied. For transversely oriented faults, Kastner's norm can be used for the decrease in plasticity at the point of the defect [8].
However, these criteria are too conservative when applied to damage to steel pipelines made of high resistance materials. Based on experimental observations, a specific finite element rulebook called PCORRC was developed, and solutions were proposed for the evaluation of pipes made of moderate to high strength steel based on a large series of FEM experiments and calculations.

Data for the calculation of corrosion damage of the steel pipe of the pipeline

The data required for the calculation of pipe corrosion damage, Fig. 3, using the RSTRENG method and MKE are as follows:

- ✓ Nominal value of the outer diameter of the pipe, D=125 mm;
- ✓ Nominal pipe wall thickness, t=5 mm;
- ✓ Maximum depth of corrosion damage, d=2 mm;
- ✓ Measured (longitudinal) length of corrosion damage, L_m=70 mm;

The pipe is made of steel with the following mechanical characteristics:

- ✓ Modulus of elasticity, E=211500 MPa;

- ✓ Poisson's coefficient, ν=0.3;
- ✓ Lower yield stress, S_{eH}=813.4 MPa;
- ✓ Tensile strength, S_M=854.8MPa.

The pipe is exposed to pressure during operation, P=60 MPa (N/mm^2).

Corrosion damaged pipe

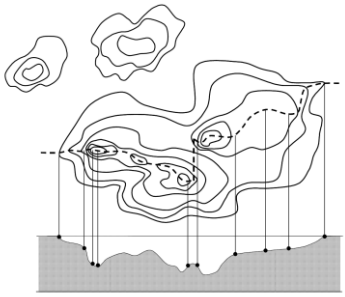

Irregular length, width and depth of a typical corrosion defect [9]

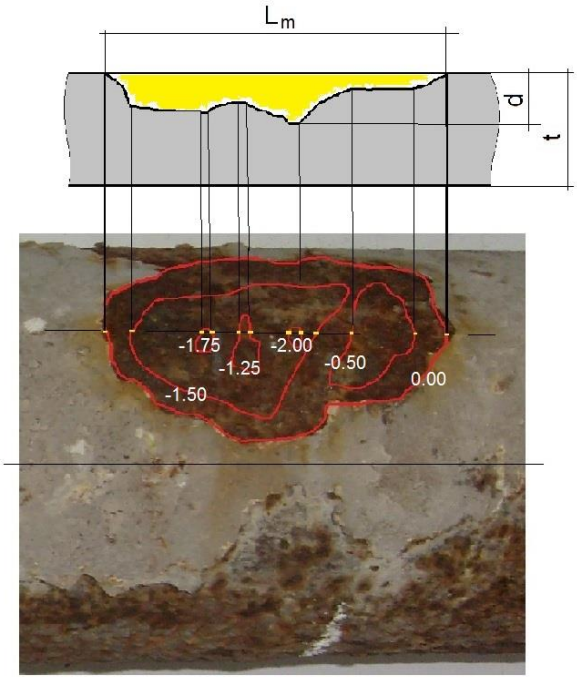

Measured values of asymmetric corrosion damage

***Figure 3.** Data for assessment of corrosion damage*

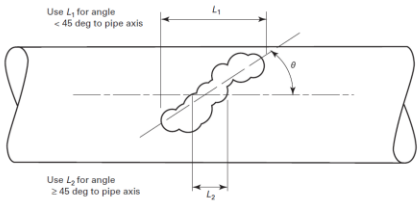

Orientation of corrosion damage

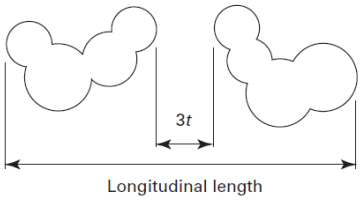

The influence of the distance between corrosion damages

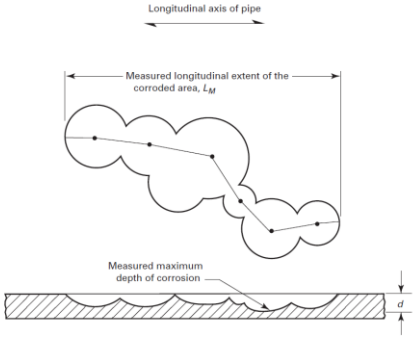

Measured values used for corrosion damage analysis

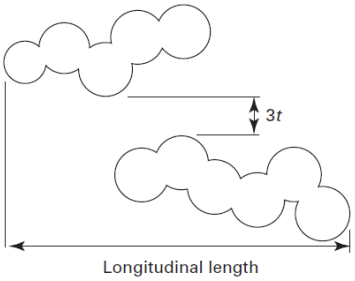

The influence of the distance between corrosion damages

***Figure 4.** Recommendations of standards for the assessment of corrosion damage [3]*

Determination of the maximum acceptable length of corrosion damage using the RSTRENG method

The depth of corrosion damage can be expressed as a percentage of the nominal value of the pipe wall thickness. When the corrosion depth of the part is greater than 10% or less than 80% of the nominal value of the pipe wall thickness, the length of the corrosion damage must not be greater than the value obtained by equation (1).

$$L = 1.12 \cdot B \cdot \sqrt{D \cdot t} \quad (1),$$

where: L - maximum permitted length of corrosion damage;
B - value determined using equation (2).
The maximum depth of corrosion damage is: d=2 mm, 40%=100·2/5.

$$B = \sqrt{\left(\frac{d/t}{1.1 \cdot \frac{d}{t} - 0.15}\right)^2 - 1} = \sqrt{\left(\frac{2/5}{1.1 \cdot \frac{2}{5} - 0.15}\right)^2 - 1} = 0{,}949998 \quad (2)$$

The maximum length of corrosion damage is:

$$L = 1.12 \cdot B \cdot \sqrt{D \cdot t} = 1.12 \cdot 0.949998 \cdot \sqrt{125 \cdot 5} = \mathbf{26.6\ mm}$$

Figure 5 shows the relationship between corrosion damage and the acceptance criteria for pipe corrosion damage. The criterion is that they should withstand a pressure equal to the lower yield stress SeL. The image represents a parabolic section of the corroded part where the value of the maximum depth of corrosion damage divided by the thickness of the pipe wall is shown on the y axis and on the x axis the length of the corrosion damage is given divided by the square root of the product of the pipe radius and pipe wall thickness.

$$\text{d/t}=\mathbf{0.400};\ \frac{L}{\sqrt{R \cdot t}} = \frac{26.6}{\sqrt{\frac{125}{2} \cdot 5}} = \mathbf{1.505} \quad (3)$$

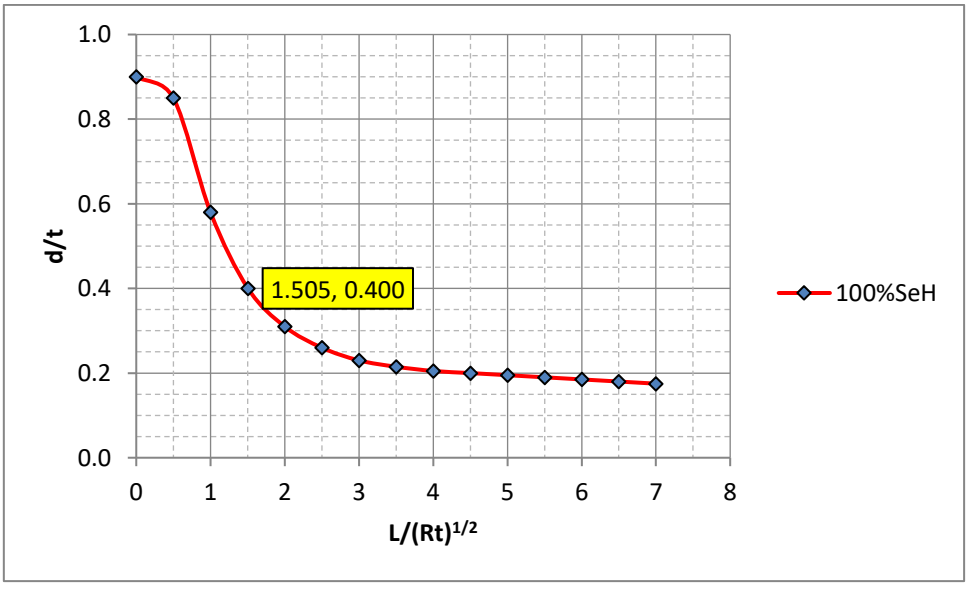

Figure 5. *Diagram for assessment of corrosion damage*

The coordinates of the point from equation (3) are located on the very line of the diagram, fig.5. Given that the actual measured length of corrosion damage is L=70 mm, the working pressure should be reduced or the pipe with corrosion damage should be replaced or repaired.
If the maximum measured depth of corrosion damage is greater than 10% of the nominal value of the pipe wall thickness and less than 80% of the nominal value of the pipe wall thickness, and the measured length of the corrosion damage is greater than the value determined based on equation 1, it is necessary to calculate:

$$P' = 1.1 \cdot P \left[\frac{1-\frac{2}{3}\cdot\left(\frac{d}{t}\right)}{1-\frac{2}{3}\left(\frac{d}{t\cdot\sqrt{A^2+1}}\right)} \right] \quad (4),$$

where: P' - maximum allowable pressure for Lm and cannot be greater than P;
P - determined pressure value in the pipe or:

$$P = 2 \cdot SeH \cdot t \cdot F \cdot \frac{T}{D} = 2 \cdot 813.4 \cdot 5 \cdot 1 \cdot \frac{1}{125} = \mathbf{65.1\ MPa} \quad (5),$$

where: F - corresponding factor from ASME B31.4 [10], ASME B31.8 [11];
T - corresponding temperature value based on the B31 rulebook (if not specified, T=1).

$$A = 0.893\left(\frac{L_m}{\sqrt{Dt}}\right) = 0.893\left(\frac{70}{\sqrt{125\cdot5}}\right) = 2.50 \quad (6)$$

For a depth of damage of 40% of the nominal thickness of the pipe wall, the maximum permitted length of corrosion damage of L=26.6 mm was calculated. This length of corrosion damage is smaller than the actual measured length of corrosion damage, which is L=70 mm, so it is necessary to calculate the maximum allowable pressure (P') of the corroded pipe for this case of damage and it is:

$$P' = 1.1 \cdot P \left[\frac{1-\frac{2}{3}\cdot\left(\frac{d}{t}\right)}{1-\frac{2}{3}\left(\frac{d}{t\cdot\sqrt{A^2+1}}\right)} \right] = 1.1 \cdot 65.1 \left[\frac{1-\frac{2}{3}\left(\frac{2}{5}\right)}{1-\frac{2}{3}\left(\frac{2}{2\sqrt{2.50^2+1}}\right)} \right] = \mathbf{3.9\ MPa} \quad (7)$$

Assessment of the residual strength of steel pipelines using the FEM

In order to assess the residual strength of steel pipelines using the FEM [2, 7], the processed test results can be implemented in the form of a model in one of the commercial programs for calculation using the FEM. Due to the asymmetry of corrosion damage, a part of the pipe with corrosion damage is modeled in an approximate shape to the actual shape (rectangular, elliptical, spherical...). The model is made by connecting isoparametric elements, and the number of elements depends on the size of the corrosion damage. It is necessary to represent the bottom of the damaged area with a sufficient number of elements determined by the previous section analysis. The inside of the model is subjected to operational, i.e., test pressure. Planes of symmetry are places where boundary conditions are set (displacements in certain planes are limited). Figure 6 shows the sequence of procedures before calculating the FEM of pipes with corrosion damage.
Figure 7 shows the calculation results of a pipe with asymmetric corrosion damage. The calculation was made for pressures in the pipe of 60 MPa (working pressure of an undamaged pipe), 3 MPa (calculated pressure according to ASME B31.G, and a pressure of 22 MPa which ensures the operation of the pipe with safety level 1, which means that the pressure in the pipe does not it must not exceed this value at any one time.

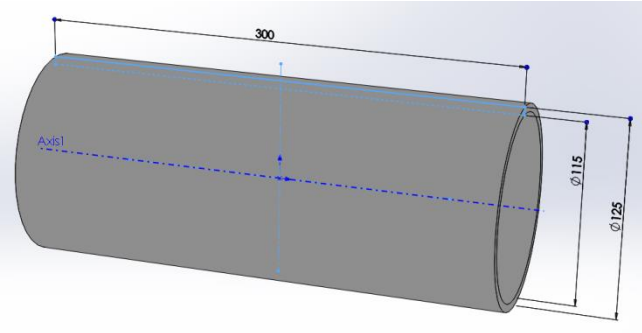

Pipe model without corrosion damage

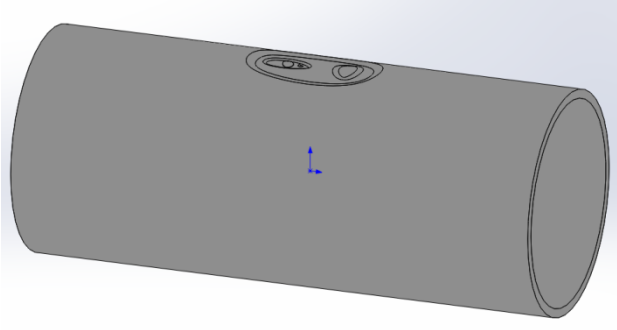

Pipe model with corrosion damage

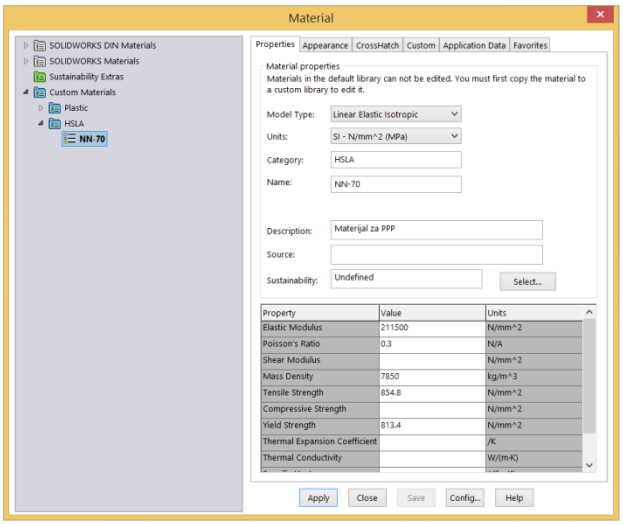

Pipe material data and boundary conditions

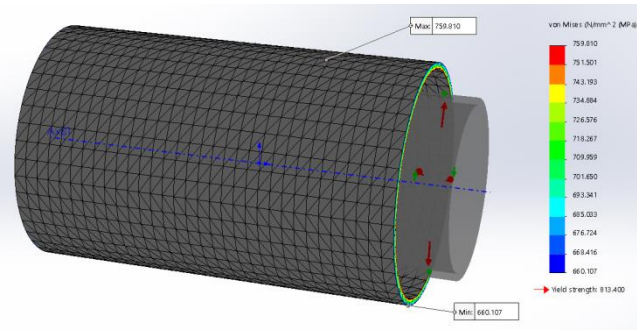

The Finite Element mesh on the pipe without corrosion damage and a pressure value of 60 MPa

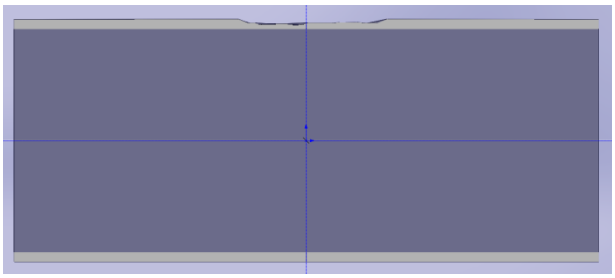

Cross-section of a pipe model with corrosion damage

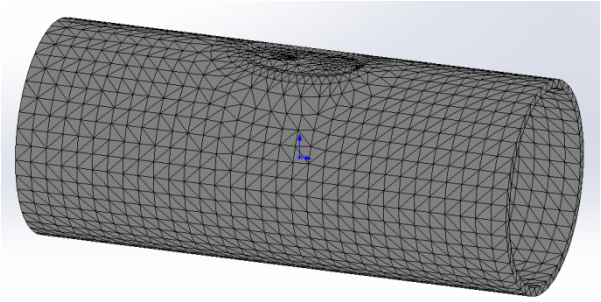

Finite Element mesh on a pipe with corrosion damage

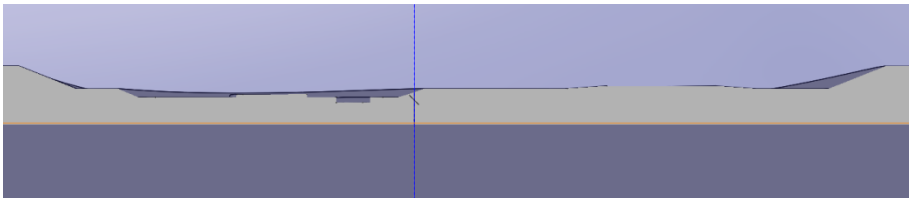

Section through the corrosion damage model

Figure 6. *Data entry for the calculation by the FEM of corrosion-damaged pipe of the pipeline*

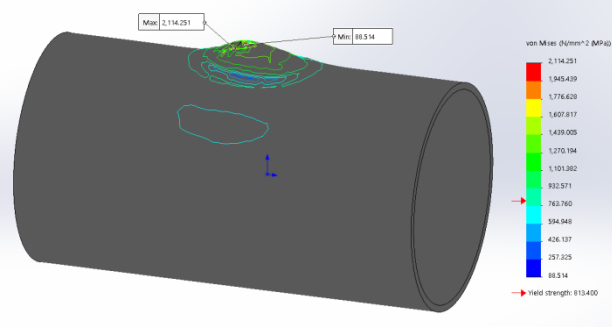

Distribution and stress values on pipes with corrosion damage for a pressure of 60 MPa

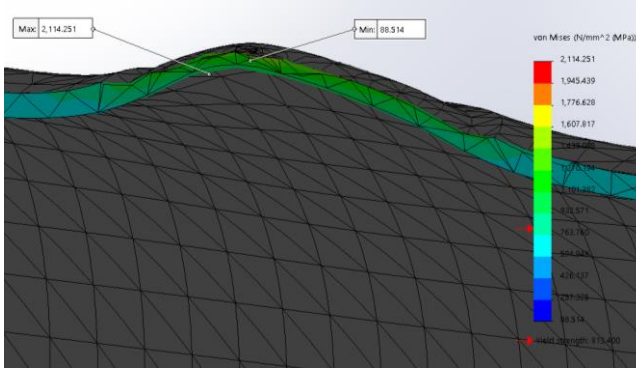

Section through the model of corrosion damage on a pipe loaded with a pressure of 60 MPa

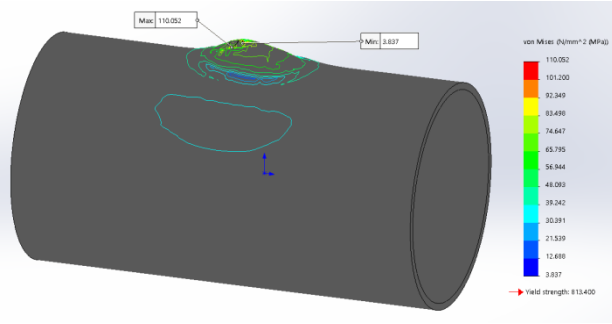

Distribution and stress values on pipes with corrosion damage for a pressure of 3 MPa

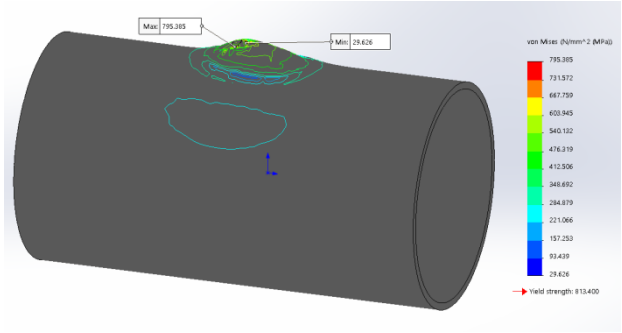

Distribution and stress values on pipes with corrosion damage for a pressure of 22 MPa

Figure 7. *Calculation by the FEM and stress distribution on the corrosion damage of pipeline pipe*

Measures to protect steel pipelines against corrosion

From the previous consideration of the danger of corrosion to which parts of the steel structure of the pipeline are exposed due to the action of various attacking agents, a number of corrosion protection measures are imposed even in the construction phase: the use of clean and uncorroded sheets, profiles and binding material with anti-corrosion protection done in workshop conditions, which immediately after installation, it should be properly protected on the construction site itself. In addition, before installation, the parts should be protected from the effects of any corrosive agent that could be found on the construction site. Preservatives that can be easily removed (oils, fats, non-drying agents) can significantly slow down the access of gaseous attack substances (hydrogen sulphide).

Modern protective coatings made of epoxy resin adhere very well to the surfaces of steel parts where cracks do not appear on elements exposed to tension almost to the limit of their strength.

Steel pipelines are subject to inspection, which means that before use they must be properly inspected in order to obtain a work permit. During exploitation, legally prescribed controls are also carried out in order to ensure safe and reliable operation of the steel pipeline.

In addition to proper and timely maintenance, it is also necessary to monitor corrosion processes during exploitation. These processes can be monitored directly or indirectly. Direct monitoring controls the condition of the steel surface and the aggressiveness of the environment surrounding the steel construction of the pipeline. Indirect monitoring involves measuring the corrosion effect on coupons made of the same type of material as the steel structure of the pipeline.

Even during the construction of steel pipelines, it is necessary to install sensors and measuring tapes to monitor changes in the aggressiveness of the environment, voltage and elongation of the responsible supporting parts of the steel pipelines, which would be in conjunction with a computer on which the received information would be processed and appropriate decisions would be made.

Conclusion

Corrosion damage, in which the bearing capacity of the section is reduced, greatly endangers the steel pipeline as a whole. Failure to comply with prescribed regular and emergency controls and inadequate maintenance can lead to destruction with catastrophic consequences.
Improper maintenance of steel pipelines from the aspect of corrosion protection entails very expensive repairs, so in this regard it is necessary to thoroughly investigate the issues of protection, durability and maintenance of steel pipelines and the possibility of monitoring corrosion aggression in exploitation. In this regard, it is necessary to assess the state, or the assessment of the remaining strength, of the steel pipeline threatened by corrosion after long-term use, which should be followed by certain tests using non-destructive methods, in order to determine the actual degree of damage to the vital parts of the structure. Control and testing by non-destructive methods of the corroded zones of the bearing elements of the steel construction of pipelines must be followed by control calculations using methods, standard and MKE, to assess the remaining strength of steel pipelines, with opinions and recommendations. In uncertain situations, calculations need to be confirmed by experimental analyses.
Control and testing by non-destructive methods must be preceded by the process of cleaning the steel structure of the pipeline (eg sandblasting), and immediately after the necessary interventions in terms of changing critical elements, anti-corrosion protection follows.

Acknowledgements

This work was supported by the Ministry of Science, Technological Development and Innovation of the Republic of Serbia (Contracts: No. 451-03-47/2023-02/200012 and No. 451-03-47/2023-01/200287).

References

1. V. Aleksić, Uzroci i posledice korozionih oštećenja čeličnih sfernih rezervoara i cevovoda u hemijskoj industriji, *XI YUCORR, Međunarodna konferencija, Saradnja istraživača različitih struka na području korozije, zaštite materijala i životne sredine*, Tara, 17. – 20.05.2009, 109–114.
2. V. Aleksić, Procena preostale čvrstoće metodom konačnih elemenata korozijom oštećenih čeličnih cevovoda u hemijskoj industriji, *I Međunarodni kongres, Inženjerstvo, materijali i menadžment u procesnoj industriji*, Jahorina, Republika Srpska, 14.10. – 16.10. 2009, CD, 98–102.
3. ASME B31G-2012 (Revision of ASME B31G-2009), *Manual for Determining the Remaining Strength of Corroded Pipelines*, Supplement to ASME B31 Code for Pressure Piping.
4. G. H. Koch et al, Corrosion costs and preventive strategies in the United States, *Publication No. FH WA-RD-01-156, CC Technologies*, Dublin, Ohio, March 2002.
5. Pressure Equipment Directive – PED 97/23/EC, 1997.
6. J. Kiefner, P. Vieth, Evaluating Pipe-1 New Method Corrects Criterion for Evaluating Corroded Pipe, *Oil & Gas Journal*, **6** August, 1990.
7. Tomasz Szary, *The Finite Element Method Analysis for Assessing the Remaining Strength of Corroded Oil Field Casing and Tubing*, Ph.D. dissertation, Der Fakultät für Geowissenschaften, Geotechnik und Bergbau der Technischen Universität Bergakademie, Freiberg, 2006.
8. W. Kastner el al., Critical Crack Sizes in Ductile Piping, *International Journal of Pressure Vessels and Piping*, **9**, 1981, 197-219.
9. A. Cosham, P. Hopkins, The Assessment of Corrosion in Pipelines – Guidance in the Pipeline Defect Assessment Manual (PDAM), *Pipeline Pigging and Integrity Management Conference*, 17-18th May 2004 – Amsterdam, The Netherlands, 1-31.
10. ASME B31.4-2002 (Revision of ASME B31.4-1998), *Pipeline Transportation System for Liquid Hydrocarbons and other Liquids*, ASME Code for Pressure Piping, B31.
    ASME B31.8-2014 (Revision of ASME B31.8-2012), *Gas Transsmision and Distribution Piping Systems*, ASME Code for Pressure Piping, B31.

In-situ hydrothermal synthesis of Pt/TiO2 nanocomposites for electrochemical applications

Milica Košević[1], Marija Mihailović[1,*], Vladimir Panić[1,2]

[1] *University of Belgrade- Institute of Chemistry, Technology and Metallurgy – National Institute of the Republic of Serbia, Njegoševa 12, 11000 Belgrade, Serbia*

[2] *Centre of Excellence in Environmental Chemistry and Engineering—ICTM, University of Belgrade,11000 Belgrade, Serbia*

[*] *marija.mihailovic@ihtm.bg.ac.rs*

Abstract

Pt/TiO_2 composites were synthesized by in situ hydrothermal oxido-reduction process between Ti^{3+} and $PtCl_6^{2-}$ ions at different temperatures, using H_2PtCl_6 and $TiCl_3$ solutions as precursors. Four different samples were prepared, with the projected mass loading of Pt in all composites at 50%. Two precursors out of four contained 10 mass% of commercial TiO_2 powder, and final Pt mass loading is adjusted with the quantity of $TiCl_3$ added. The morphology and composition of the synthesized Pt particles were examined by scanning electron microscopy/energy dispersive X-ray spectroscopy. Electrochemical properties of prepared material were checked by cyclic voltammetry (CV) and linear sweep voltammetry (LSV). Analysis of results obtained from the electrochemical measurements showed electrocatalytic response typical for Pt material. The highest currents in CV were registered for the composite synthesized at 100°C with 10 mass% of commercial TiO_2 powder, which was also found to exhibit the highest activity in ORR. These findings suggest that in situ oxido-reduction process was successfully employed for the synthesis of Pt/TiO_2 with the potential to be an efficient electrocatalysts for oxygen reduction reaction (ORR).

Keywords: *electrocatalysis; supported Pt nanoparticles; SEM images; EDX analysis.*

Introduction

In the world striving to reduce the carbon footprint, the evergrin theme became energy production, conversion and storage. For the reason of increasing demands for sustainable energy production and consumption, the fuel cell (FC) comprehensive investigations became the must [1–3]. Recent investigation activities are directed to FC reliability and durability [4,5]. Platinum nanoparticles deposited onto powdered carbon substrates are widely used electrocatalysts in FCs [6]. Carbon as electrocatalyst support has a low stability and low resistivity to corrosion [7-9]. These disadvantages can cause the decrease of the electrochemically active surface area [10–12]. Therefore, the development of alternative catalyst carriers is attracting attention. TiO_2 appears to be suitable replacement since it is at least of low cost and high stability [13, 14]. The synthesis of Pt/TiO_2 needs to be carefully tailored to meet the demands for promising electrocatalytic materials of the next generation, especially for the cathodic FC reactions [4]. It was found that TiO_2 enhances the Pt activity for oxygen reduction reaction (ORR), which is assigned to increased electron density on Pt due to partial charge transfer from oxide to metal nanoparticles [15-17].

In terms of catalysis, TiO_2 is generally known by its photocatalytic and photoelectrocatalytic activity [6,13], but it also found the application in electrocatalysis as a stabilizing component of the electro-active coatings of activated titanium anodes [18] and potentially interactive support for nanoparticular metallic electrocatalysts, e.g., Pt [19].

Experimental

Synthesis of the Pt/TiO2 composites

For the synthesis of Pt/TiO_2 composites, the solutions of $TiCl_3$ (12 mas % $TiCl_3$ in HCl from Sigma Aldrich) and H_2PtCl_6 (Sigma Aldrich, 8 wt. % in H_2O) were used as precursors. H_2PtCl_6 solution was diluted with water before the synthesis by mixing 25 mL H_2O with 1.071 mL H_2PtCl_6. $TiCl_3$ was used without dilution.

The composites were prepared using an in situ oxido-reduction process between Ti^{3+} and $PtCl_6^{2-}$ ions. Four different samples were synthesized, each with a projected mass loading of 50% Pt in the Pt/TiO_2 composite. The first step in each synthesis was to mix the H_2PtCl_6 precursor solution with water and stir the resulting solution. The temperature of the mixture was controlled using a bath, and when the desired synthesis temperature was reached, $TiCl_3$ was added all at once to the solution of water and H_2PtCl_6.

The conversion of the precursors was monitored by observing color changes. Specifically, the H_2PtCl_6 solution was yellow to orange due to the presence of $PtCl_6^{2-}$ ions. After the addition of $TiCl_3$, the solution became slightly milky due to hydrolysis of Ti^{3+} and a bit gray due to the reduction of $PtCl_6^{2-}$ ions. Ultimately, the solution turned black when $PtCl_6^{2-}$ ions were reduced to metallic Pt. When left overnight, a precipitate appeared.

Two of the four composites synthesized also contained 10% commercial TiO_2 *Degusa* powder. In these samples, 10% of the resulting TiO_2 was added to the water prior to the addition of the H_2PtCl_6 solution, and the remaining 90% of TiO_2 was added during the rest of the synthesis.

The synthesis temperature was maintained at 60°C for samples 1 and 4, and varied for samples 2 and 5. Sample 1 was prepared by adding 0.535 mL H_2PtCl_6 solution to 30 mL H_2O at room temperature, and then adding 0.350 mL $TiCl_3$ once the temperature reached 60°C. The resulting solution turned dark, indicating successful reduction of Pt^{4+} ions. The resulting precipitate was centrifuged, washed, and dried to prepare the composite for further electrochemical investigation.

Sample 2 was synthesized using the same procedure as Sample 1, except that the temperature was adjusted to 10°C. Sample 4 contained 10% commercial TiO_2 *Degusa* powder and was prepared by mixing 0.00228 g TiO_2 with 30 mL H_2O, dispersing it by ultrasound, and then adding 0.315 mL $TiCl_3$ solution once the temperature reached 60°C. Sample 5 was prepared in the same manner as Sample 4, but with a synthesis temperature of 100°C. Sample from synthesis 3 is omitted from this analysis, yet marks are retained so that it can be followed-up and compared in other related publications.

The resulting composites were collected in powder form by centrifugation and washing with water. Obtained powders were thermaly treated for 3 h in N_2 atmosphere at 160°C.

Syntheses parameteres are given in the Table 1.

Table 1. Parameters of the samples syntheses

Serial number of synthesis	Projected mass fraction of Pt in composite, %	Temperature of synthesis, °C	TiO_2 powder added in precursors mixture prior to synthesis, mas % of the total TiO_2	
1	50	60	/	
2	50	10	/	pH = 2,2
4	50	60	10	
5	50	100	10	

Electrochemical measurements

The electrochemical characterization of the Pt/TiO_2 composites synthesized in this study was carried out using cyclic voltammetry (CV) and linear polarization measurements (LSV) in a 1 M H_2SO_4 electrolyte. LSV and CV were performed at sweep rates of 1 and 50 mV s-1, respectively, and LSV measurements were conducted at 1500 rpm. The electrolyte was purged with N_2 (CV) or O_2 (LSV). All measurements were performed in a three-electrode cell with an Ag/AgCl reference electrode (all potentials in the paper are given in SCE scale) and platinum plate as a counter electrode on a Bio-Logic SP200 potentiostat/galvanostat (Bio-Logic SAS, Grenoble). The working electrode was prepared by dispersing 3 mg of powder in 1 mL distilled water and ultrasonically homogenizing it for 1 h (40 kHz, 70 W). The resulting suspension was deposited as a 0.31 mg cm-2 layer onto a glassy carbon electrode that served as a support and room-dried.

Results and disscusion

Figures 1-4 present results of Pt/TiO_2 composite samples examination by scanning electron microscopy (SEM) and energy dispersive X-ray spectroscopy (EDX). These SEM images reveal the size, shape, and distribution of the Pt particles supported on the TiO_2 surface. The Pt particles range in size from a few tens of nanometers to a few hundred nanometers, and their distribution vary depending on the synthesis method and/or parameters of the samples syntheses.

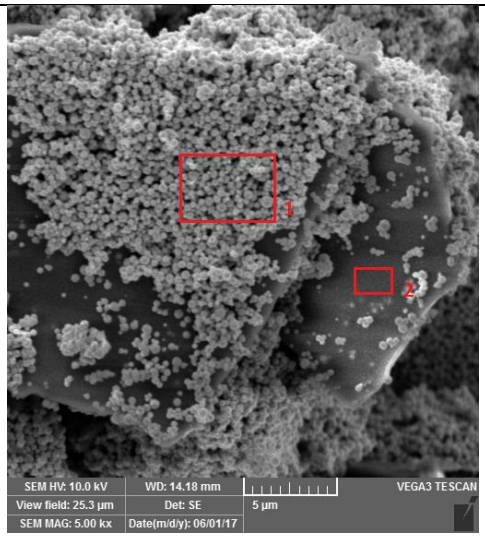

Area	Element, mas. %				
	Pt	Ti	O	C	Cl
1	92.2	/	2.3	5.6	/
2	19.7	46.9	27.0	/	10.3

Area	mol %				
	Pt	Ti	O	C	Cl
1	0.47	/	0.14	0.47	/
2	0.101	0.98	1.69	/	0.29

1. 100 mas. % Pt
2. 20 mas. % Pt

Figure 1. *SEM image and EDX analysis of Pt/TiO_2 sample 1 (synthesis T = 60°C, mas. % Pt = 50).*

Pt particles on the TiO_2 support exhibit tendencies to aggregate or form clusters. The clusters of fine Pt globules (pale areas in Fig.1) are unhomogenously dispersed over the TiO_2 surface. EDX analysis of area 1 on the Figure 1 reveals 92.2 mas.% Pt, without the presence of registered Ti, indicating that the layer of Pt clusters is thick enough not to detect the underlayer. However, the large dark-gray areas remained uncovered with Pt. These Pt aggregations influence the catalytic properties and overall performance of the material.

For the same SEM magnification, but the other synthesis condition, at the Figure 2, the Pt nanoparticles are seen to be homogenously distributed over the TiO_2 support, with some fine clusters as well as micro- and nano-sized pores. The EDX analysis shows that the Pt nanoparticles are not distributed in monolayer, since the Pt is registered in the pores, too (analysis ranging from 93.1 mas. % Pt to 100 mas. % Pt).

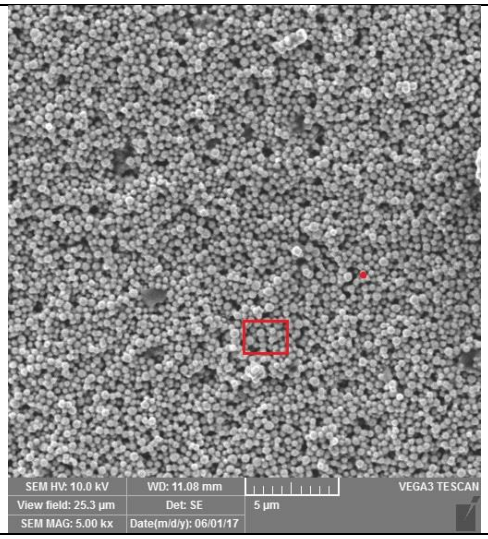

Element, mas. %				
	Pt	Ti	Cl	O
Surface	90.0	/	5.2	4.8
Point	87.7	3.9	4.3	4.0

Surface: 100 mas. % Pt
Point: 93.1 mas. % Pt

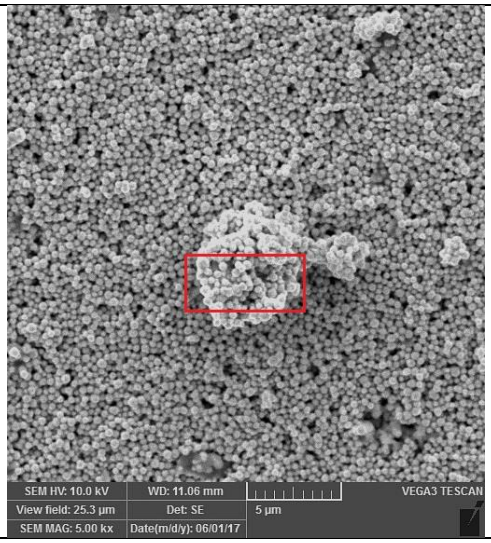

Element, mas. %			
Pt	Ti	Cl	O
87.8	3.9	4.3	4.0

93 mas. % Pt

Figure 2. *SEM image and EDX analysis of Pt/TiO₂ sample 2 (synthesis T=10°C, mas. % Pt = 50).*

Figure 3. presents SEM images of the sample 4, synthesized at 60°C, but with with the addition of commercial TiO_2 in the precursors mixture in the amount of 10 mas %. Here, the Pt particles size is not uniform as in figure 3, neither the EDX analysis of selected squared areas is homogenous as in previous case (here analysis ranging from 6.6 mas. % Pt, across 41.6 mas.% to 100 mas.% Pt), giving a combination of the fine particles surrounded by coarser globules and some clusters, and even inhomogenously scattered porosity is visible. The EDX analysis of pores clearly indicates Ti underneath.

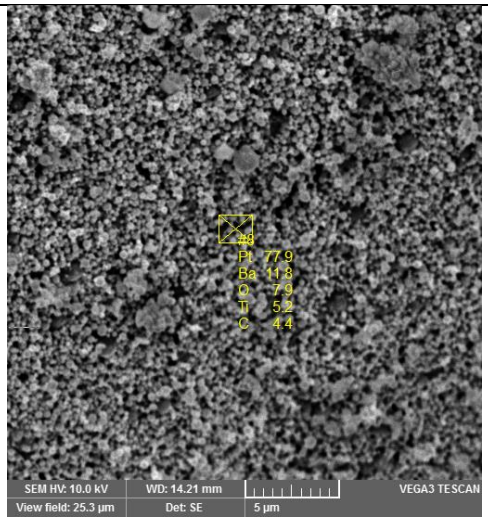

73.4 mas. % Pt

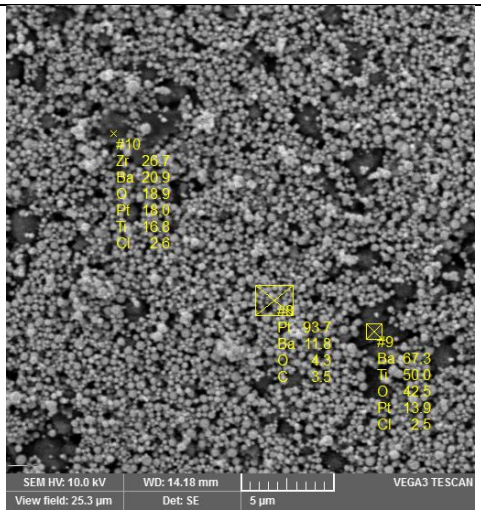

#8: 82.7 mas. % Pt
#9: 6.6 mas. % Pt
#10: 41.6 mas. % Pt

Figure 3. *SEM image and EDX analysis of Pt/TiO₂ sample 4 (synthesis T = 60°C, mas. % Pt = 50) with the addition of 10 mas % commercial TiO₂ in precursors mixture.*

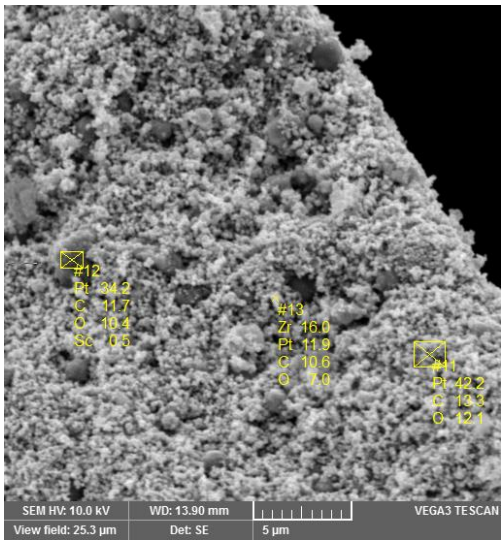

#11: 100 mas. % Pt
#12: 100 mas. % Pt
#13: 100 mas. % Pt

Figure 4. *SEM image and EDX analysis of Pt/TiO_2 sample 5 (synthesis T=100°C, mas. % Pt = 50) with the addition of 10 mas % commercial TiO_2 in precursors mixture.*

SEM image at Figure 4, for sample 5 from Table 1, reveals fine Pt nanoparticles with highly dispersed structure, obtained during synthesis at 100°C, with the addition of 10 mass % commercial TiO_2 in precursors mixture. The EDX analysis of all the selected areas gives 100 mass % Pt. The morphology of this highly dispersed appearance shows small scattered pores, formed in the bulk of the same material, also confirmed with EDX analysis of 100 mass % Pt.

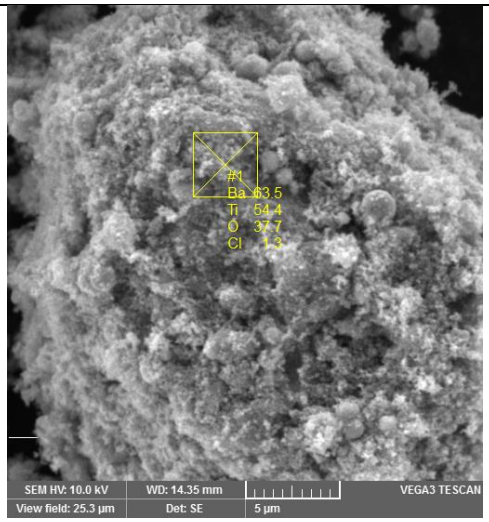

Figure 5. *SEM image and EDX analysis of the commercial TiO_2* **.**

The Figure 5 is given here for comparison of the commercial TiO_2 appearance, as well as for ensuring that what is marked with Ba is really Ti, while on the Figures 3 and 4 what is marked with Zr is actually Pt. Due to the overlapping the peaks of these elements, the marks on the images of the mentioned figures are marked incorrectly.

Analysing these SEM images, it can be concluded how well the Pt nanoparticles are dispersed or immobilized on the TiO_2 support. A good dispersion of Pt nanoparticles indicates a higher surface area available for catalytic reactions, what is further examined employing CV analysis.

Cyclic voltammograms and polarization curves obtained examinating of Pt/TiO_2 composites which are syntetized by mutual oxido-reduction of Pt^{4+} and Ti^{3+} are presented in Figure 6 and 7. The parameters of the synthesis are given in Table 1.

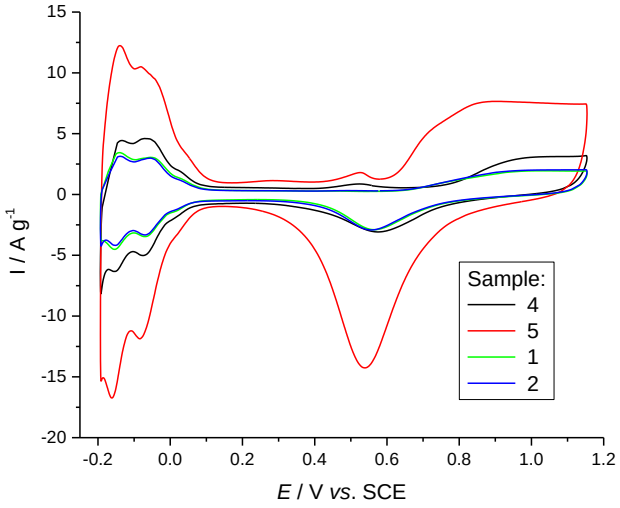

Figure 6. *Cyclic voltammograms of Pt/TiO_2 composites. Electrolyte: de-aerated 1M H_2SO_4, sweep rate 50 mV s^{-1}.*

For Pt/TiO_2 voltammograms in Figure 6, which are typical for nanostructured Pt in acid solution, it can be concluded that they are in accordance with the structure revealed on SEM images. The sample 5 (Fig. 6, Table 1), exhibited the best response, i.e., it has the largest electrochemically active surface area, which is direct consenquence of highly dispersed surface area available for electrochemical reactions, as can be seen on the SEM image presented in Figure 4. The CV regions around 0.6 V, typical for oxide formation/reduction and two well-developed peaks in hydrogen adsorption/desorption region can be noticed in the Figure 6.

Conversely, the cyclic voltammograms of samples 1, 2 and 4, Figure 6, gives a poor response what is the effect of the lower electrochemically active surface area. This could be due to a lower dispersion of Pt nanoparticles, the presence of agglomerates or incomplete coverage of Pt on the TiO_2 support, what is revealed on SEM images in Figures 1-3.

The quasi-steady-state polarization curves, Figure 7, provides the electrochemical performance of all the samples, presented in Table 1, and analysed on SEM images with EDX measurements. The highest electrocatalytic activity in the steady-state region, with respect to the applied potential, shows sample 5 (red line). The same is for anodic region, where processes like oxygen evolution reaction (OER) takes part, and the current density increases due to oxidation reactions occurring at the electrode surface.

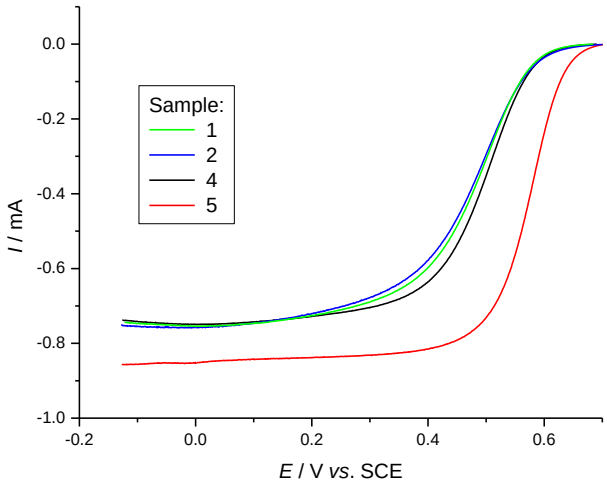

Figure 7. *Quasi-steady-state polarization curves of Pt/TiO_2 composites. Electrolyte: 1M H_2SO_4 purged with O_2, room temperature, 1500 rpm, sweep rate: 1 mV s^{-1}.*

It's worth mentioning that the highly dispersed structure is generally considered favorable for various catalytic reactions, not just the ORR. However, it's important to note that the synthesis at 100°C, with the addition of 10 mass % of commercial TiO_2 in precursors mixture contributed the catalytic activity of the specimen 5, which exhibited the best electrochemical performance.

Conclusion

In the highly dispersed structure, the Pt atoms are well-dispersed and maximize the exposure of active sites, leading to improved catalytic activity for the ORR. This high dispersion minimizes particle aggregation or clustering, which can limit the accessibility of reactants and hinder catalytic performance.

The highly dispersed structure offers several advantages for the ORR:

1. Enhanced mass transport: The presence of individual Pt atoms or small clusters ensures efficient mass transport of reactants (oxygen molecules) to the catalytic sites, promoting faster reaction kinetics.
2. Increased active surface area: The atomically dispersed Pt configuration provides a larger active surface area, allowing more oxygen molecules to interact with the catalyst and enhancing the overall catalytic activity.
3. Improved utilization of Pt: With highly dispersed Pt atoms, a smaller amount of Pt can achieve comparable or even superior catalytic performance compared to Pt nanoparticles with a higher loading. This can be advantageous from a cost and resource utilization perspective.

Achieving a highly dispersed Pt structure on the TiO_2 support often requires precise control over synthesis parameters such as temperature, precursor concentration, and reducing agents.

Acknowledgements

The authors wish to acknowledge the financial support from the Ministry of Education, Science and Technological Development of the Republic of Serbia [Grant No. 451-03-47/2023-01/200026].

References

1. B. Sørensen, *Hydrogen and Fuel Cells*, Emerging technologies and applications, 2nd ed., Academic Press, Oxford, 2012, 1–4.
2. P. P. Edwards, V. L. Kuznetsov, W. I. F. David, N. P. Brandon, *Energy Policy* 2008, **36**, 4356.
3. S. Shafiee, E. Topal, *Energy Policy* 2009, **37**, 181.
4. H. R. Colon-Mercado, B. N. Popov, Stability of platinum based alloy cathode catalysts in PEM fuel cells, *J. Power Sources*, 2006, **155**, 253-263.
5. A. Pozio, M. De Francesco, A. Cemmi, F. Cardellini, L. Giorgi, Comparison of high surface Pt/C catalysts by cyclic voltammetry, *J. Power Sources* 2002, **105**, 13
6. J. C. Meier, C. Galeano, I. Katsounaros, J. Witte, H. J. Bongard, A. A. Topalov, C. Baldizzone, S. Mezzavilla, F. Schüth, K. J. J. Mayrhofer, Design criteria for stable Pt/C fuel cell catalysts, *Beilstein J. Nanotechnol*. 2014, **5**, 44.
7. H. Li, R. Wang, R. Cao, Physical and electrochemical characterization of hydrous ruthenium oxide/ordered mesoporous carbon composites as supercapacitor, *Microporous Mesoporous Mater*. 2008, **11**, 32–38.
8. Y. Wang, Z. Wang, Y. Xia, An asymmetric supercapacitor using RuO_2/TiO_2 nano-tube composite and activated carbon electrodes, *Electrochim. Acta*, 2005, **50**, 5641–5646.
9. V. Panić, A. Dekanski, V. Mišković-Stanković, S. Milonjić, B. Nikolić, On the deactivation mechanism of RuO_2–TiO_2/Ti anodes prepared by the sol–gel procedure, *J. Electroanal. Chem.*, 2005, **579,** 67–76.
10. M. Chena, M. Wanga, Z. Yanga, X. Wanga, High performance and durability of order-structured cathode catalyst layer based on TiO2@PANI core-shell nanowire arrays, *Appl. Surf. Sci.* 2017, 406, 69.
11. J. Xu, M. Zhao, S. Yamaura, T. Jin, N. Asao, Core–shell Pd–P@Pt nanoparticles as efficient catalysts for electrooxidation of formic acid, *J. Appl. Electrochem*. 2016, 46, 1109.
12. B. Li, D. C. Higgins, Q. Xiao, D. Yang, C. Zhng, M. Cai, Z. Chen, J. Ma, The durability of carbon supported Pt nanowire as novel cathode catalyst for a 1.5 kW PEMFC stack, *Appl. Catal. B* 2015, **162**, 133.
13. A. Marcu, G. Toth, P. Pietrasz, J. Waldecker, C. R., Cathode catalysts degradation mechanism from liquid electrolyte to membrane electrode assembly, *Chim.* 2014, **17**, 752.
14. A. Sclafani, J. M. Herrmann, Comparison of the Photoelectronic and Photocatalytic Activities of Various Anatase and Rutile Forms of Titania in Pure Liquid Organic Phases and in Aqueous Solutions, *J. Phys. Chem.* 1996, **100**, 13655.
15. Y.-G. Wang, X.-G. Zhang, Preparation and electrochemical capacitance of RuO_2/TiO_2 nanotubes composites, *Electrochim. Acta*, 2004, **49,** 1957–1962.
16. C.C. Hu, K.H. Chang, M.C. Lin, Y.T. Wu, Design and tailoring of the nanotubular arrayed architecture of hydrous RuO2 for next generation supercapacitors, *Nano Lett.*, 2006, **6**, 2690–2700.
17. S. Stopić, B. Friedrich, M. Schroeder, T. Weirich, Synthesis of TiO2 core/RuO2 shell particles using multi step ultrasonic spray pyrolysis, Mater. Res. Bull. 48 (2013)
18. V. Panić, A. Dekanski, S. Milonjić, V. Mišković-Stanković, B. Nikolić, Electrocatalytic activity of sol-gel-prepared RuO_2/Ti anode in chlorine and oxygen evolution reactions, *Russ. J. Electrochem*. 2006, **42** 1055–1060.
19. S. Sharma, B. G. Pollet, Support materials for PEMFC and DMFC electrocatalysts—A review, *J. Power Sources*, 2012, **208**, 96.

SPONSORS

SPONZORI


INTERNATIONAL SOCIETY OF ELECTROCHEMISTRY
ISE

Кнеза Милоша 7
11000 Београд

Савез инжењера и техничара Србије

Union of Engineers and Technicians of Serbia

HELIOS INDUSTRIJSKI PREMAZI ZA METAL

ZAŠTITA METALA OD POVERENJA

Saradnjom sa našim timom dobijate pouzdanog partnera koji Vam pruža:

Stručno savetovanje i tehničku pomoć

Visok kvalitet gotovih proizvoda

Dinamiku isporuke saglasno potrebama i željama kupca

Mogućnost izrade različitih nijansi i kvaliteta premaza po zahtevu

Pomoć pri izradi i kontroli projektne dokumentacije u skladu sa EN ISO 12944

Helios Srbija a.d., Radovana Grkovića 24, 32300 Gornji Milanovac, Srbija
T +381 32 771 000, E metal@helios.rs, E info@helios.rs www.helios.rs

HELIOS


ikrolux
www.mikrolux.hr


TESCAN
PERFORMANCE IN NANOSPACE

Firestop®
INTERNACIONAL

Inovativni protivpožarni premazi za sigurnu budućnost

Kompanija **Firestop Internacional** je sa svojim brendom **FIRESTOP** izbor broj 1 na tržištu Srbije i regiona u oblasti ekspandujućih protivpožarnih premaza za zaštitu čelika i drveta.

U svom portfoliju ima i **Tinto color** osnovne i završne premaze za zaštitu metala, koji se mogu koristiti samostalno ili u sklopu Firestop sistema zaštite.

Korišćenjem ovog inovativnog sistema premaza postiže se kompletna antikorozivna i protivpožarna zaštita.

Firestop Internacional d.o.o.
Gavrila Principa 20, 22330 Nova Pazova
Tel. 022 321 030, 326 342, 323 134 / Fax. 022 325 002
office@internacional.rs / www.firestopinternacional.rs

Protection upgraded



Custom Made Chemical Specialities for Surface Treatment

- Optimal solutions for all key applications of surface finishing
  - **Industrial Parts Cleaning**
  - **Metal Pre-treatment**
  - **Functional and Decorative Electroplating**
- Worldwide representatives in more than 50 countries
- A company of Freudenberg Group since 2011

SurTec doo Serbia

sales.serbia@surtec.com
www.SurTec.com

Preljinska baluga bb
32000 Cacak, Srbija

Tel. +381 32 538 1569
Fax. +381 32 538 1569

Institut za preventivu

zaštitu na radu, protivpožarnu zaštitu i razvoj d.o.o.

21000 Novi Sad • Kraljevića Marka 11 • tel/fax: 021 / 420-571, 420-572, 420-573
institut@izp.rs • www.izp.rs

ATC 04-010 АКРЕДИТОВАНО СЕРТИФИКАЦИОНО ТЕЛО SRPS EN 45011:2004

ATC 06-013 АКРЕДИТОВАНА КОНТРОЛНА ОРГАНИЗАЦИЈА SRPS ISO/IEC 17020:2002

ATC 01-069 АКРЕДИТОВАНА ЛАБОРАТОРИЈА ЗА ИСПИТИВАЊЕ SRPS ISO/IEC 17025:2006

- bezbednost i zdravlje na radu
- zaštita od požara i eksplozije
- zaštita životne sredine
- tehnički pregledi objekata
- izrada projektno tehničke dokumentacije
- katodna zaštita
- akreditovana tela
- sertifikacija i ispitivanje opreme u "Ex" izvedbi


ELKER


EKO
zaštita

IPIN d.o.o.

institut za primijenjenu geologiju i vodoinženjering

ANTIKOROZIONA ZAŠTITA METALA - INDUSTRIJSKA POTROŠNJA

DEKORATIVA - ŠIROKA POTROŠNJA

HEMIPRODUKT
BOJE I LAKOVI

PREMAZI ZA METAL
PREMAZI ZA DRVO
RAZREĐIVAČI
PROGRAM ZA GRAĐEVINARSTVO

Hemiprodukt doo, Masarikova br. 1, 21000 Novi Sad, Srbija • hemiboje@gmail.com • www.hemiprodukt.co.rs
tel.: +381 21 2998 420, +381 21 2998 498, +381 60 531 7440, +381 60 531 8220, +381 60 531 5001, +381 63 531 724

ИНСТИТУТ ЗА ОПШТУ И ФИЗИЧКУ ХЕМИЈУ
INSTITUTE OF GENERAL AND PHYSICAL CHEMISTRY

ЕЛЕКТРОХЕМИЈСКО
ЦИНКОВАЊЕ

ПОВРШИНСКА ЗАШТИТА

СЗР ГАЛВА

Каменичка 26,
34000 Крагујевац
Тел/Факс: 034-63-63-297


Огранак ДРИНСКО-ЛИМСКЕ ХЕ